Tetrazine-Triggered Bioorthogonal Decaging Reactions for Prodrug Activation

Sarah Hannah Davies

Jesus College

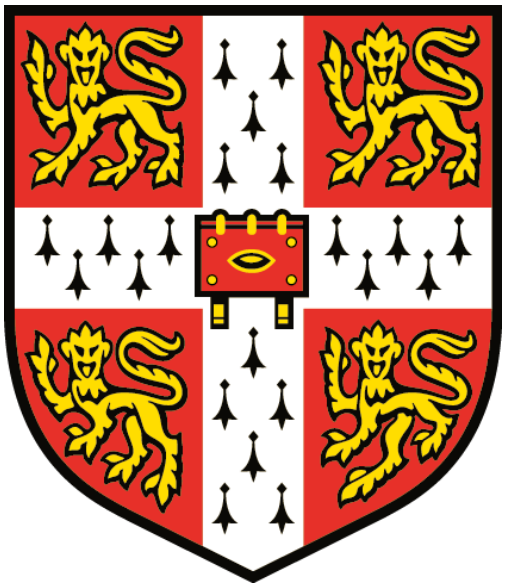

This thesis is submitted for the degree of Doctor of Philosophy

at the

University of Cambridge

April 2020

Declaration

This thesis is the result of my own work and includes nothing which is the outcome of work done in collaboration except as declared in the Preface and specified in the text. It is not substantially the same as any that I have submitted, or, is being concurrently submitted for a degree or diploma or other qualification at the University of Cambridge or any other University or similar institution except as declared in the Preface and specified in the text. I further state that no substantial part of my thesis has already been submitted, or, is being concurrently submitted for any such degree, diploma or other qualification at the University of Cambridge or any other University or similar institution except as declared in the Preface and specified in the text. It does not exceed the prescribed word limit for the Physics and Chemistry Degree Committee.

Sarah Hannah Davies

April 2020

Abstract

Tetrazine-Triggered Bioorthogonal Decaging Reactions for Prodrug Activation

Sarah H. Davies

Bioorthogonal decaging reactions have emerged as a promising strategy for the spatially and temporally controlled activation of proteins and drugs. The inverse electron-demand Diels-Alder (IEDDA) reaction between tetrazines and strained alkenes exhibits high reaction rates and selectivity and has been widely applied for the decaging of amine prodrugs. Although amines are common in small molecule drugs, decaging methods for other functional groups are required in order to develop a broadly applicable prodrug activation strategy that can be applied to a wider range of drugs and diseases. This thesis describes the application of the tetrazine-triggered IEDDA reaction to cleave protecting groups from carboxylic acid- and alcohol-containing molecules.

The first project relates to the development of both vinyl and *trans*-cyclooctene (TCO) protecting groups to mask a carboxylic acid-containing anti-inflammatory drug. In each case, the prodrug stability, reaction profile and kinetics of decaging were studied with a range of tetrazines. Whilst vinyl esters suffered from poor stability and release rates, rapid drug release (< 2 minutes) was achieved from a stable TCO prodrug. Importantly, decaging of a non-toxic TCO prodrug in live macrophages was demonstrated, resulting in the reinstation of the anti-inflammatory activity.

The second project describes methods to release alcohol-containing molecules via the TCO-tetrazine IEDDA reaction. Work towards three linkers (carbonate, ether and carbamate benzyl ether) is described. The carbamate benzyl ether linker was shown to be both synthetically accessible and stable, which was not the case for the other linkers. Therefore, the tetrazine-triggered decaging of a TCO-carbamate benzyl ether fluorophore was studied in detail. In addition, this reaction was shown to be compatible with living organisms through decaging of a prodrug in the presence of live cells.

Overall, the work presented here offers new methods for masking carboxylic acid and alcohol functionality that can be rapidly reinstated through tetrazine-triggered decaging.

List of Publications

- Bioorthogonal Decaging Reactions for Targeted Drug Activation. **Sarah Davies**†, Benjamin. J. Stenton† and Gonçalo J. L. Bernardes. *Chimia*, **2018**, *72*, 771–776.

Sections from this publication are included in Chapter 1

- Tetrazine-Triggered Release of Carboxylic-Acid-Containing Molecules for Activation of an Anti-inflammatory Drug. **Sarah Davies**†, Luxi Qiao†, Bruno L. Oliveira, Claudio D. Navo, Gonzalo Jiménez-Osés and Gonçalo J. L. Bernardes. *ChemBioChem*, **2019**, *20*, 1541-1546.

Sections from this publication are included in Chapter 2

- Development of a self-immolative linker for tetrazine-triggered release of alcohols in cells. **Sarah Davies**, Bruno L. Oliveira, and Gonçalo J. L. Bernardes. *Org. Biomol. Chem.*, **2019**, *17*, 5725-5730.

Sections from this publication are included in Chapter 3

† These authors contributed equally.

Acknowledgements

I would firstly like to thank Dr Gonçalo Bernardes for all his help and support over the past four years and for giving me the opportunity to work in his group. Since I joined the group, it has grown in size and we now have our own lab space, which would not have been possible without Gonçalo's hard work and commitment to the lab. I have really enjoyed the opportunity to work in the Bernardes group.

The projects I worked on during my PhD would not have been possible without help from other group members. I'd particularly like to thank Dr Bruno Oliveira for his excellent advice and guidance throughout my PhD. I am grateful for his positivity that kept me motivated through difficult times. A big thank you also to Lucy Qiao who worked on one of the projects with me. Without her hard work and input, the project would not have been completed as quickly. I would also like to acknowledge our collaborators Claudio Navo and Gonzalo Jiménez-Osés in Spain, who provided valuable contributions to this project.

I would also like to thank all the current and past members of the Bernardes group for providing a great atmosphere to work in. There have been so many people working in this group over the past four years and there are too many to acknowledge everyone individually here, but I have really enjoyed working alongside so many interesting people. Thank you for all the advice, pub trips and Christmas dinners- it's been really great getting to know you all.

Thank you to Nic, Naomi and Kevin for all the work they have done to keep the lab running efficiently. I would also like to take this opportunity to acknowledge the NMR staff for providing a great service, as well as the Mass spectrometry and the MPACC team for their help. Thank you to the Ley group for sharing the Whiffen lab with us for the first 2 years of my PhD and to all the members of the Whiffen (Ley group and Phipps group) for being so friendly and helpful- it was great sharing a lab with you.

A huge thank you to Libby Brown, Lavinia Dunsmore, Hannah Kiely-Collins and Barbara Bernardim for proof-reading various sections of this thesis. I am very grateful to my Viva examiners Dr Anthony Coyne and Professor Sander van Kasteren for an interesting discussion about my work. Finally, I would like to thank my family and Dimitri Sideris for their continual support.

Abbreviations

°C	degrees Celsius
δ	chemical shift in ppm
µ	micro
ν	stretching frequency
λ	wavelength
7-HC	7-hydroxycoumarin
Å	angstrom
Ac	acetyl
ADC	antibody-drug conjugate
ADEPT	antibody-directed enzyme prodrug therapy
Alloc	allyoxycarbonyl
ANOVA	analysis of variance
aq	aqueous
Ar	aryl
ASAP	atmospheric solids analysis probe
ATR	attenuated total reflectance
ax	axial
BARAC	biarylazacyclooctynone
BCN	bicyclo[6.1.0]nonyne
Boc	*tert*-butoxycarbonyl
BODIPY	boron-dipyrromethane
br	broad (spectral)
Bu	butyl
cal	calorie(s)
calc.	calculated
CBT	2-cyanobenthothiazole
cis-CO	*cis*-cyclooctene
Cit	citrulline
CLIPTAC	click-formed proteolysis targeting chimera
COSY	correlation spectroscopy
CPT	camptothecin
CuAAC	copper-catalysed azide-alkyne cycloaddition
d	doublet (spectral)

dd	double doublet (spectral)
DABCO	1,4-diazabicyclo[2.2.2]octane
DBU	diazabicyclo[5.4.0]undec-7-ene
decomp.	decomposition
DFO	deferoxamine
DIAD	diisopropyl azodicarboxylate
DIBAC	dibenzo-aza-cyclooctyne
DIBO	dibenzocyclooctyne
DiCl-Tz	3,6-di-2-chloro-1,2,4,5-tetrazine
DIFO	difluorinated cyclooctyne
DiMe-Tz	3,6-di-2-methyl-1,2,4,5-tetrazine
dioxo-TCO	7-methoxy-1, 3-dioxacyclo-oct- 5(*E*)-ene
DIPEA	*N*,*N*-diisopropylethylamine
DiPy-Tz	3,6-di-2-pyridyl-1,2,4,5-tetrazine
DMAP	4-(*N*,*N*-dimethylamino)pyridine
DMEM	Dulbecco's Modified Eagle's Medium
DMF	dimethlyformamide
DMSO	dimethyl sulfoxide
DNA	deoxyribonucleic acid
DOTA	dodecane tetraacetic acid
Dox	doxorubicin
d-TCO	dioxolane-fused *tran*s-cyclooctene
EC_{50}	half maximal effective concentration
ELISA	enzyme-linked immunosorbent assay
em	emission
ENR	enol-acyl carrier protein reductase
eq	equatorial
equiv.	equivalent
ESI	electrospray ionisation
EWG	electron-withdrawing group
ex	excitation
Fab	antigen-binding fragment
FBS	fetal bovine serum
FI	fluorescence intensity

FLD	fluorescence detector
FT	fourier transform
g	gram(s)
GFP	green fluorescent protein
h	hour(s)
HER2	human epidermal growth factor receptor 2
HG-II	Hoveyda-Grubbs 2nd generation catalyst
HMBC	heteronuclear multiple bond correlation
HOMO	highest occupied molecular orbital
HPLC	high-performance liquid chromatography
HRMS	high-resolution mass spectrometry
HSQC	heteronuclear single quantum correlation
Hz	hertz
ICPr	3-isocyanopropyl
IC_{50}	half maximal inhibitory concentration
IEDDA	inverse electron-demand Diels-Alder
IgG	Immunoglobulin G
int	intermediate
IR	infrared
J	coupling constant
k_{obs}	observed rate constant
k_2	second order rate constant
L	litre(s)
LB	Lysogeny broth
LC-MS	liquid chromatography-mass spectrometry
LPS	lipopolysaccharide
LUMO	lowest unoccupied molecular orbital
m	multiplet (spectral), meter(s), milli, medium (spectral)
M	molar
max	maximum
Me	methyl
MePy-Tz	3-methyl-6-(pyridin-2'-yl)-1,2,4,5-tetrazine
min	minute(s)
miRNA	micro ribonucleic acid

MMAE	Monomethylauristatin E
Mol	mole(s)
Mol%	mole fraction
Mp	melting point
Ms	methylsulfonyl
m/z	mass-to-charge ratio
n	nano
NAD(P)-H	nicotinamide adenine dinucleotide (phosphate)
NaPi	sodium phosphate buffer
n.d.	not determined
NMR	nuclear magnetic resonance
NP	nanoparticle
ns	not significant
NSAID	non-steroidal anti-inflammatory drug
o-	*ortho*-
OD_{600}	optical density at 600 nm
ONB	*ortho*-nitrobenzyl
O/N	overnight
oxasilaTCO	*trans*-oxasilacycloheptene
oxTCO	oxazolone-fused *trans*-cyclooctene
oxoTCO	*trans*-5-oxocene
p-	*para*-
PABC	*p*ara-aminobenzyl carbamate
PBS	phosphate-buffered saline
PEG	polyethylene glycol
PET	positron-emission tomography
petrol	petroleum ether
PGE2	prostaglandin E2
Ph	phenyl
ppm	part(s) per million
Proc	propargyloxycarbonyl
PROTAC	proteolysis targeting chimera
Py	pyridine
q	quartet (spectral)

qNMR	quantitative nuclear magnetic resonance
R	undefined substituent
RCM	ring closing metathesis
RDS	rate-determining step
R_f	retention factor
RNA	ribonucleic acid
rt	room temperature
s	singlet (spectral), second(s), strong (spectral)
sat.	saturated
SAM-TCO	sulfenic acid modifying *trans*-cyclooct-4-en-1-ol
scFv	single-chain variable fragment
siRNA	small interfering ribonucleic acid
Si-TCH	*trans*-1-sila-4-cycloheptene
soln.	solution
S_N2	substitution nucleophilic second order
S_N2'	nucleophilic conjugate substitution
SPAAC	strain-promoted azide-alkyne cycloaddition
SPECT	single photon emission computed tomography
s-TCO	strained *trans*-cyclooctene
t	time, triplet (spectral)
$t_{1/2}$	half-life
T	temperature
t-	*tert*-
TBS	*tert*-butyl dimethylsilyl
TCH	*trans*-cycloheptene
TCO	*trans*-cyclooctene
TCO-OH	*trans*-cyclooct-2-en-1-ol
4-TCO-OH	*trans*-cyclooct-4-en-1-ol
Tf	trifluoromethane sulfonyl
THF	tetrahydrofuran
TLC	thin-layer chromatography
TMSBr	bromotrimethylsilane
TMTH	3,3,6,6-tetramethylthiacycloheptyne
TON	turnover number

Trx	Thioredoxin
Ts	toluenesulfonyl (tosyl)
TS	transition state
Tz	tetrazine
TzMe	tetrazylmethyl
Ub	Ubiquitin
UHPLC	ultra high performance liquid chromatography
UV	ultraviolet
Val	valine
vs	*versus*
w	weak (spectral), weight

Contents

Chapter 1

Introduction

This chapter contains work from the following publication:

Bioorthogonal Decaging Reactions for Targeted Drug Activation. **Sarah Davies**†, Benjamin. J. Stenton† and Gonçalo J. L. Bernardes. *Chimia*, **2018**, *72*, 771–776.

† These authors contributed equally.

1.1 Bioorthogonal ligation reactions

1.1.1 Bioorthogonal chemistry

Bioorthogonal reactions are chemical reactions that can be carried out in living systems, without affecting any native biological processes.[1] Therefore, an essential requirement is that the reaction is highly selective and no cross reactivity is observed with biomolecules. In addition, the reaction must have a fast rate under physiological conditions (aqueous media, 37 °C, near physiological pH) and at the low reactant concentrations (typically ≤ μM) that are required for use in biological systems.[2] The reagents and products should be both thermally and metabolically stable to enable accurate study of the biomolecule. Furthermore, the reagents and by-products should be non-toxic to cells. However, in practice, most reported bioorthogonal reactions do not fulfil all these criteria (often they suffer from slow reaction rates, stability or toxicity issues) and more work is required in order for their full potential to be realised.

Bioorthogonal chemistry arose from the need for suitable methods to label and study biomolecules in their native biological environment. Previous methods for labelling proteins relied on the use of monoclonal antibodies and genetically encoded fluorescent proteins. However, the large size of these biological moieties can drastically alter the properties of the molecule being studied. In addition, they cannot always be used to study intracellular processes or non-protein biomolecules such as lipids, glycans and metabolites.[1,2] The development of bioorthogonal chemistry offers a widely applicable strategy for the labelling and studying of biomolecules. It involves incorporating a small, abiotic, bioorthogonal handle into a molecule of interest, which can then react with a probe containing the

complementary bioorthogonal functional group (**Scheme 1**).[1,3] Since being first described in 2003 by Professor Carolyn Bertozzi,[4] several biorthogonal ligation reactions (in which a bond is formed between two reactants) have been reported.[3,5–12]

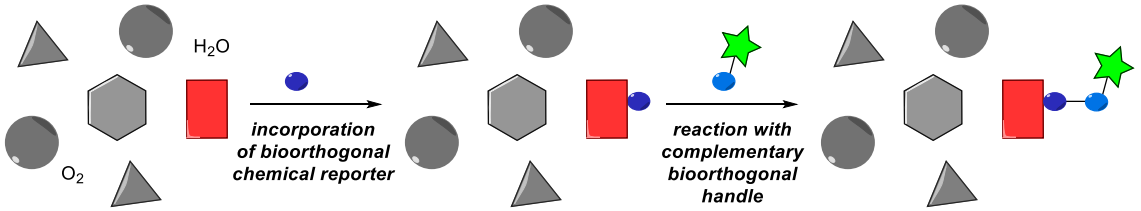

Scheme 1. Schematic representation of the bioorthogonal labelling strategy. A chemical reporter (dark blue circle) is incorporated into the target biomolecule (red rectangle). This is labelled with a probe (green star) containing the complementary bioorthogonal handle (light blue circle).

Bioorthogonal reactions may be initiated using either a photo- or chemical- (metal or small organic molecule) trigger. This thesis will primarily focus on the use of small molecule, chemical-triggered bioorthogonal reactions that have been applied in mammalian cells or higher organisms.

1.1.2 Small molecule-triggered ligation reactions

The term "bioorthogonal" was first used to describe a Staudinger ligation reaction between a glycoprotein containing a metabolically-incorporated azide handle and fluorescent phosphine probes.[4,13] The classical Staudinger reduction results in an aza-ylide, which is susceptible to hydrolysis.[14,15] However, incorporating an electrophilic methyl ester into the phosphine probe prevents hydrolysis of the aza-ylide and instead, intramolecular cyclisation results in the formation a stable carbamate bond (**Scheme 2**).

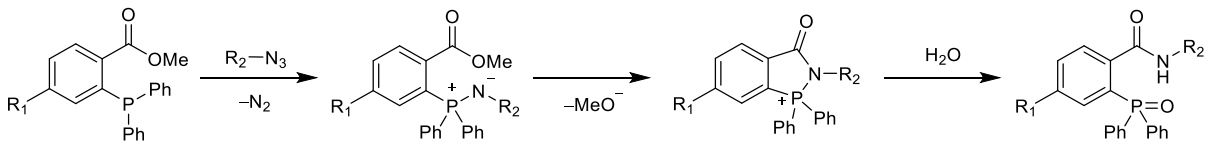

Scheme 2. Staudinger ligation reaction.

Disadvantages of this reaction include slow kinetics (k_2 = 2.5 x 10^{-3} M^{-1} s^{-1}) and the oxidation of phosphines by air and metabolic enzymes. Unfortunately, attempts to enhance the rate-determining step (RDS, nucleophilic attack of the phosphine onto the azide)[16] through using electron-rich phosphines, resulted in increased deactivation of the phosphine through oxidation.[5] However, despite these drawbacks, the Staudinger ligation was successfully used to label cell surface

glycoproteins in living mice.[17] Mice were injected with azide-containing sugars, which were metabolically incorporated onto the surface of splenocyte cells. This was followed by injection of a phosphine probe and *ex vivo* analysis which confirmed that the Staudinger ligation had occurred in the mice. On the other hand, a pretargeting strategy utilising the Staudinger ligation in tumour-bearing mice was unsuccessful.[18] A radiolabelled phosphine probe was administered after accumulation of an antibody-azide conjugate at the tumour. No Staudinger reaction occurred *in vivo* due to the formation of a side product, which could not be identified.

Further developments led to the traceless Staudinger ligation in which the acyl group is connected to the phosphine via a cleavable linker.[19,20] Attack of the aza-ylide nitrogen results in linker cleavage and removal of the phosphine oxide from the ligation product. This traceless Staudinger reaction has been used to install diazirines into a molecule of interest (through incorporation of an azide and reaction with a phosphine-diazirine probe),[21] as well as for peptide bond synthesis.[22]

Azides are appealing handles for bioorthogonal chemistry since they are small, abiotic, non-toxic and inert to biological systems (they can be reduced by thiols, however, this does not normally occur under physiological conditions).[1] In addition to their electrophilic nature, they are 1,3-dipoles and can undergo [3+2] cycloadditions with alkynes to generate stable triazoles.[23] However, activation of the alkyne is required in order for the reaction to proceed at physiological temperature. Several activation methods exist, including the use of a Cu(I) catalyst, which will be discussed in more detail in section 1.1.3. Alternatively, a strain-promoted azide-alkyne cycloaddition (SPAAC) utilises ring strain to activate the alkyne (**Scheme 3**).[24]

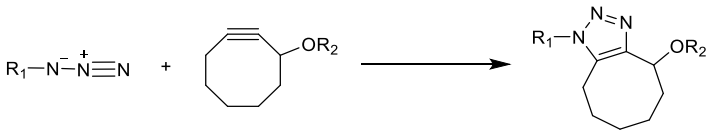

Scheme 3. Strain-promoted azide-alkyne cycloaddition (SPAAC).

Although the SPAAC (k_2 = 1.2 x 10^{-3} M^{-1} s^{-1}) is slower than the Staudinger ligation, the rate can be enhanced by modifying the cyclooctyne with electron-withdrawing groups (EWGs). Difluorinated cyclooctyne (DIFO) exhibits a second order rate constant one order of magnitude higher than cyclooctyne (**Figure 1**).[25] Although DIFO is synthetically challenging,[25,26] it has been utilised for imaging glycans in zebrafish embryos.[27] In an alternative strategy, the reaction rate was accelerated by increasing ring strain (**Figure 1**).[28] This was achieved by either fusing additional rings to cyclo-octyne (dibenzocyclooctyne (DIBO),[29] dibenzo-aza-cyclooctyne (DIBAC),[30] biarylazacyclooctynone

(BARAC),[31] bicyclo[6.1.0]nonyne (BCN)[32]) or by decreasing ring size (3,3,6,6-tetramethylthiacycloheptyne, (TMTH, **1**)).[33]

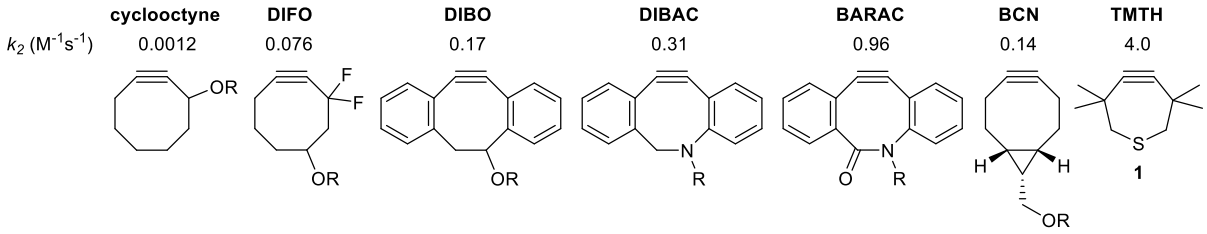

Figure 1. Selection of cyclooctyne derivatives and their second order rate constants for SPAAC.

Cycloaddition reactions constitute a large section of the bioorthogonal repertoire due to their high selectivity and their orthogonality to biological systems. The cycloaddition of cyclooctyne derivatives with nitrones,[34,35] nitrile oxides[36] and diazo groups[37] have also been reported. However, cyclooctyne is not truly bioorthogonal as it can react with biological nucleophiles including thiols.[38,39]

Azides also react with oxonorbornadiene to give a stable triazole product (**Scheme 4**).[40] The reaction proceeds via a regioselective [3+2] cycloaddition, followed by a retro Diels-Alder reaction and elimination of furan (**2**). Oxonorbornadienes are synthetically accessible, but the reaction suffers from slow rates ($k_2 = 10^{-4}\,M^{-1}\,s^{-1}$).

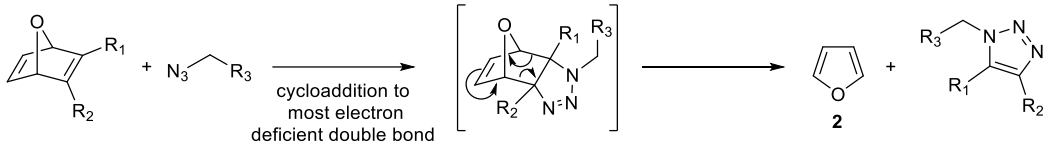

Scheme 4. [3+2] cycloaddition of an azide with oxonorbornadiene.

The inverse electron-demand Diels-Alder (IEDDA) reaction (**Scheme 5**) between a strained alkene, *trans*-cyclooctene (TCO), and a tetrazine is one of the fastest reported biorthogonal reactions to date.[41] As a result, the reaction has been extensively studied and several dienes and dienophiles have been explored. This reaction will be discussed in detail in section 1.2.

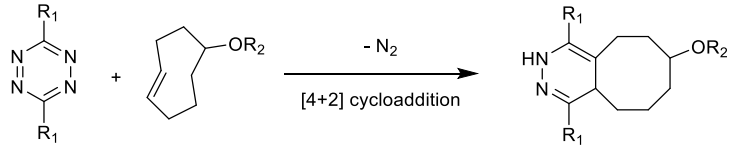

Scheme 5. IEDDA reaction between a tetrazine and TCO. Discussed in more detail in section 1.2.

Tetrazines also undergo [4+1] cycloadditions with tertiary isonitriles ($k_2 = 0.58\,M^{-1}\,s^{-1}$), which, after retro Diels-Alder reaction, result in stable imine complexes (**Scheme 6**).[42] Asymmetric tetrazines

bearing an EWG and a bulky *t*-Bu substituent were shown to react preferentially with isonitriles over strained alkenes/alkynes, with accelerated reaction rates (k_2 = 57 M^{-1} s^{-1}).[43]

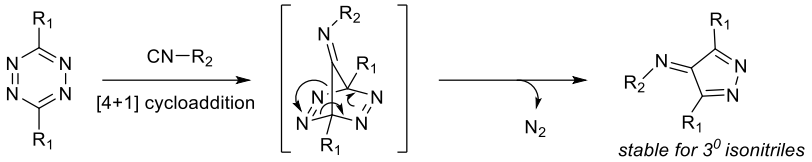

Scheme 6. [4+1] cycloaddition of tetrazines with tertiary isonitriles.

Aldehydes and ketones were some of the first bioorthogonal handles to be explored since they can be easily incorporated into biomolecules. They are small, mild electrophiles and undergo condensation reactions with hydrazines and hydroxylamines to generate Schiff bases that are stabilised by the alpha effect (**Scheme 7**).[44] The reaction of an aldehyde with hydrazine was applied to assemble a drug from inactive precursors in live cells several years before the term bioorthogonal had been introduced.[45] Typically the second order rate constant is 10^{-4} M^{-1} s^{-1} and aniline catalysts have been shown to increase the rate up to 170 M^{-1} s^{-1}.[46,47] Although reaction with lysine is possible, the equilibrium in water favours the carbonyl, meaning negligible formation of the Schiff base occurs.[48] These reactions are more suited for extracellular applications where the optimum pH for the reaction (pH 5–6) can be achieved. In addition, the reactive handles are not abiotic and intracellular aldehyde and ketone metabolites (e.g. free sugars, pyruvate) may interfere with the reaction.

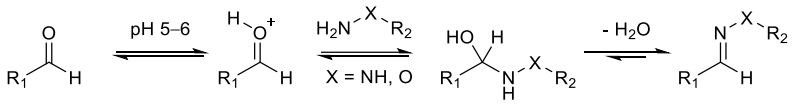

Scheme 7. Condensation of aldehydes with hydrazines and hydroxylamines under acidic pH.

An alternative aldehyde condensation based on a Pictet-Spengler reaction has also been reported.[49,50] This reaction results in C–C bond formation through condensation of an aldehyde with a tryptamine, followed by intramolecular cyclisation (**Scheme 8**).

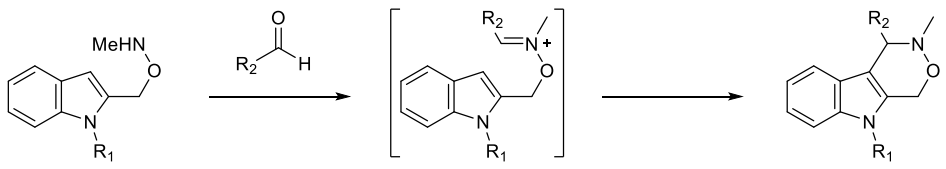

Scheme 8. Aldehyde condensation based on a Pictet-Spengler reaction.

In another example of a condensation reaction, 2-cyanobenzothiazole (CBT, **3**) reacts rapidly with 1,2-aminothiols (k_2 = 10 M^{-1} s^{-1}, **Scheme 9**).[51] However, since 1,2-aminothiols form adducts with cellular metabolites, the reaction is more suitable for *in vitro* applications. [52]

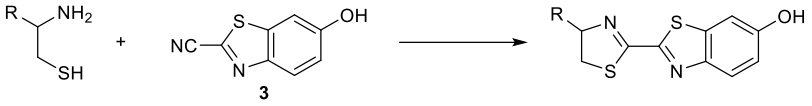

Scheme 9. Condensation of CBT (**3**) with 1,2-aminothiols.

1.1.3 Metal-triggered ligation reactions

Examples of metal-mediated bioorthogonal reactions[53] include palladium-catalysed cross-couplings,[54] ruthenium-catalysed olefin metatheses[55] and the copper-catalysed azide-alkyne cycloaddition (CuAAC),[56,57] commonly referred to as the click reaction (**Scheme 10**).

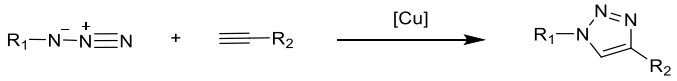

Scheme 10. Copper-catalysed azide-alkyne cycloaddition (CuAAC).

The [3+2] cycloadditon between an azide and terminal alkyne, as mentioned previously, was first carried out under physiological conditions through activation of a terminal alkyne with a Cu (I) catalyst.[56,57] This CuAAC or click reaction, occurred with high regioselectivity and reaction rate (25 times faster than the Staudinger ligation and 6 orders of magnitude higher than in the absence of a Cu catalyst), making it particularly useful for studying biomolecules that are present in low concentrations.[1,56] However, the toxicity of the metal catalyst limits the CuAAC to labelling experiments, as harmful effects are often observed even with low concentrations of Cu(I) and short exposure times.[5,58] Ligands that stabilise Cu (I) and prevent toxicity through the formation of reactive oxygen species have been developed, allowing its use to be extended to glycan labelling in zebra fish embryos.[59] Other methods of overcoming the toxicity of the catalyst include the development of metal-organic nanoparticles (NPs)[60] and heterogeneous Cu NPs.[61] Non-toxic Cu NPs were used to generate a triazole-containing anti-cancer drug in cells from two inactive precursors.[61]

Despite the toxicity of Cu, the CuAAC is still widely used for labelling and analysis due to its fast reaction rate, the small size of both handles and the commercial availability of a wide range of alkynes and azides.[8] It is commonly utilised in affinity based protein profiling, in which an azide-modified covalent inhibitor is added to cells and covalently binds to the target enzyme.[62,63] This is followed by

labelling with an alkyne affinity probe (fluorophore/biotin) and analysis.[64–66] Phosphine affinity probes have also been used to label an alkyne via the Staudinger ligation.[67] Photoaffinity labelling can be used to extend this approach to non-covalent enzyme inhibitors (**Scheme 11**).[66] A probe containing both an alkyne and a photoreactive group, such as a diazirine, is added to cells and allowed to bind to the target protein. UV light then triggers a reaction which covalently links the probe to the target. This can then be labelled via CuAAC with an azide affinity probe.

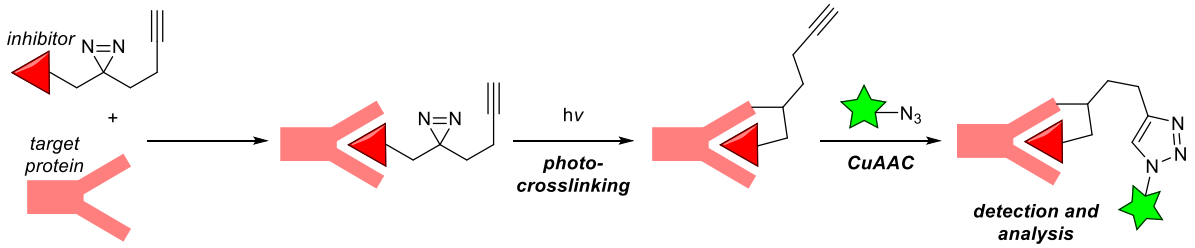

Scheme 11. Affinity based protein profiling. Photocrosslinking is used to stabilise the interaction between a non-covalent inhibitor and a target protein. CuAAC is then applied to label the protein-inhibitor complex for analysis.

Ru-catalysed cross metathesis has been reported for C–C bond formation on proteins containing *S*-allyl-cysteine[55] or *Se*-allyl-seleno cysteine[68] residues (**Scheme 12a**). Alternative C–C bond forming reactions based on Pd cross coupling have also been reported. Using a Pd(II) catalyst, modification of proteins in bacterial cells by a Cu-free Sonogashira cross-coupling was demonstrated.[69,70] In addition, intracellular assembly of an anti-cancer agent (PP-121 (**6**)) was achieved through a Pd-catalysed Suzuki-Miyaura cross coupling reaction (**Scheme 12b**).[71]

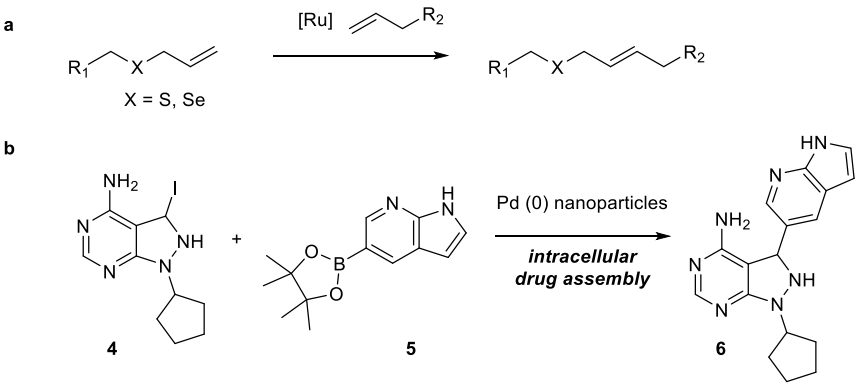

Scheme 12. Metal catalysed C–C bond formation reactions. **a.** Ruthenium-catalysed olefin metathesis **b.** Example of intracellular formation of anti-cancer drug PP-121 (**6**) by Pd-catalysed cross coupling.

Gold(I) chloride complexes have been reported for intramolecular hydroarylation reactions in cells, leading to formation of fluorophore **8** (**Scheme 13**).[72] This reaction was carried out in cells in parallel

to Ru catalysed deallylation (discussed in section 1.3.3), representing the first example of two orthogonal, metal-triggered bioorthogonal reactions occurring simultaneously.

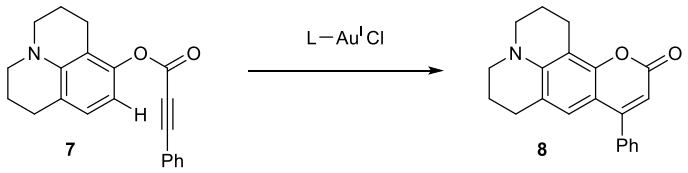

Scheme 13. Gold-catalysed intramolecular hydroarylation.

1.1.4 Photo-triggered ligation reactions

The tetrazole-alkene photo-catalysed cycloaddition[73] is an example of a photo-triggered reaction. Upon treatment with UV light (302 nm), the tetrazole undergoes cycloreversion and elimination of nitrogen to produce a nitrile imine that then undergoes spontaneous [3+2] cycloaddition with an alkene (**Scheme 14**). Nitrile imines are highly reactive 1,3-dipoles that must be generated *in situ*. The use of light to trigger the reaction offers a method to spatio-temporally control the initiation of the reaction.[74] Additional advantages include the simple synthesis of tetrazoles, the high yield and regioselectivity of the reaction and the formation of fluorescent products that enables easy tracking.[3] The reaction was applied to modify alkene-containing proteins in mammalian[75] and bacterial cells.[76] However, the toxicity associated with the use of UV light limits the application of this reaction. Reports of tetrazoles that can be activated with long wave radiation (365 nm) have been described in an effort to reduce photo-toxicity.[77] Another disadvantage is that the reaction of tetrazoles with tryptophan and thiols has been observed.[78]

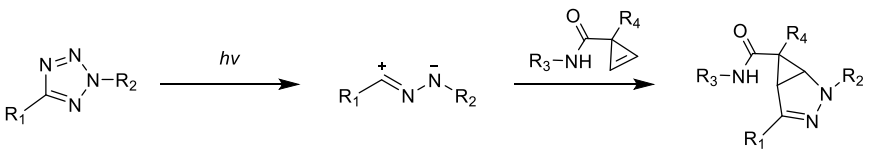

Scheme 14. Photo-triggered tetrazole-alkene reaction.

Photo-induced versions of small molecule-triggered ligation reactions have also been reported. For example, photo-triggered dehydration of an *o*-naphthalene quinone precursor **9** generates reactive intermediate **10** that undergoes Diels-Alder reaction with vinyl ethers (**Scheme 15a**).[79] A photo-induced SPAAC reaction was also developed by masking the alkyne as cyclopropenone (**Scheme 15b**).[80] Upon application of a photo-trigger, the alkyne is generated *in situ* and reaction with azides occurs.

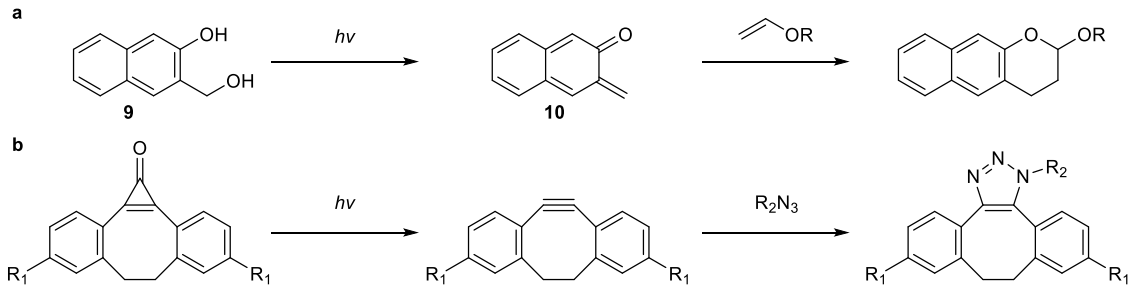

Scheme 15. Photo-triggered versions of ligation reactions. **a.** the Diels-Alder reaction **b.** the SPAAC.

1.1.5 Conclusion

Second order rate constants of ligation reactions are significantly lower than the formation of an antibody-antigen complex (k_2 = 0.1–3 x 10^6 M^{-1} s^{-1}).[81] However, the reaction handles are more cell permeable and compatible with biological systems. Despite the discovery of several bioorthogonal reactions (**Scheme 16**), all of them still suffer from limitations meaning that there is not one perfect bioorthogonal reaction. Therefore, the ideal reaction depends on the nature of the specific application and even those with severe limitations have proved useful in chemical biology. For example, the Staudinger reaction, which suffers from slow reaction rates, is often used for *in vivo* labelling as the reaction is highly selective and virtually no background labelling occurs in fluorescent studies.[8]

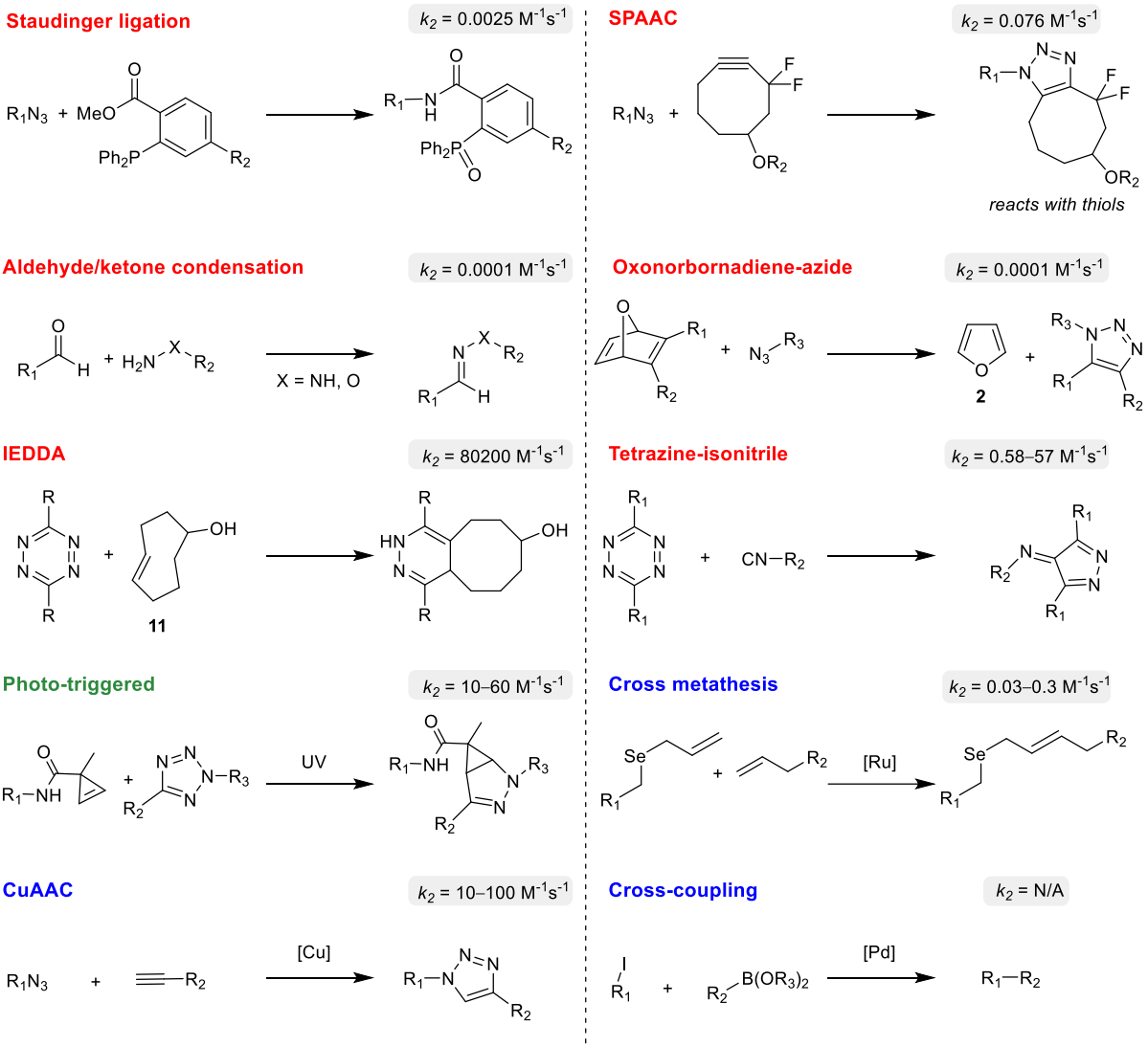

Scheme 16. Overview of some of the most common bioorthogonal ligation reactions and their typical second order rate constants.

Bioorthogonal ligation reactions have also been applied for dual labelling experiments, which utilise two orthogonal ligation reactions for the simultaneous labelling of two different biomolecules.[82–84] Recently a one-pot triple labelling experiment was performed, in which three proteins, modified with either an azide, a non-sterically hindered tetrazine or a *t*-Bu-tetrazine, underwent selective reaction with a corresponding modified-fluorophore (DIBAC, TCO or isonitrile, respectively).[43] No cross-labelling was observed by in-gel fluorescence, demonstrating the orthogonality of these three bioorthogonal reactions. Bioorthogonal ligation reactions have emerged as a useful strategy for labelling and studying biomolecules and by combining multiple orthogonal reactions, the power of this approach can be further increased.

1.2 The IEDDA reaction between tetrazines and alkenes

1.2.1 Mechanism

The reaction of tetrazines with alkenes was first reported in 1959[85] and highlights the fact that most bioorthogonal reactions existed well before they were used for biological applications.[86] Its fast reaction rate (1000 times faster than the Cu click reaction) and high selectivity at low concentrations give it potential for *in vivo* applications.[41,87] On the other hand, the normal electron-demand Diels-Alder reaction requires dienophiles (for example, maleimides) that are also Michael acceptors. This means that the dienophile can react with biological nucleophiles, such as thiols.[88,89]

The IEDDA reaction is a [4+2] cycloaddition between an electron-poor diene and an electron-rich dienophile that forms a highly strained bicyclic intermediate. This then eliminates nitrogen in a retro [4+2] cycloaddition to give a 4,5-dihydropyridazine which either isomerises to a 1,4-dihydropyridazine or is oxidised to a pyridazine (**Scheme 17**).[12,90] The kinetics of the reaction depend on several factors including electronics, ring strain, stereochemistry and solvent effects.[12]

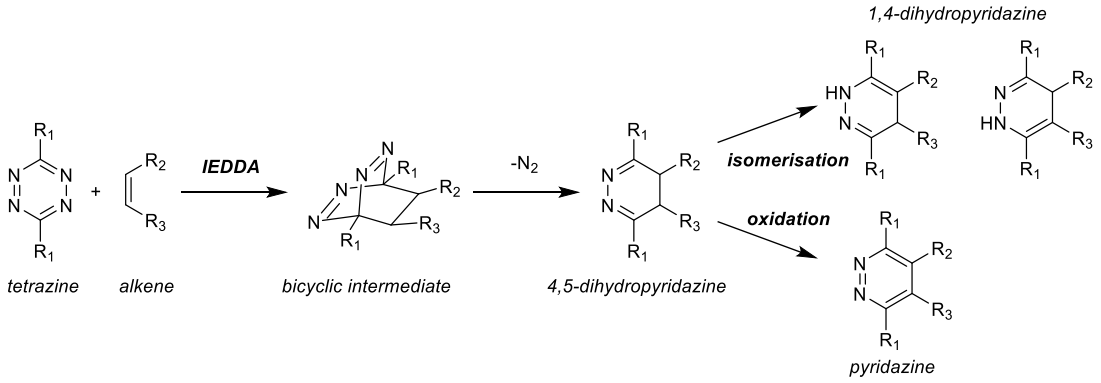

Scheme 17. IEDDA reaction between a tetrazine and an alkene.

A faster rate can be achieved by utilising electron-withdrawing substituents on the diene (to lower the LUMO energy) and electron-donating groups on the dienophile (to increase the HOMO energy), thereby decreasing the HOMO-LUMO energy gap.[12] For this reason, tetrazines are more reactive than triazines, which have attracted significantly less attention as bioorthogonal reagents due to their lower reaction rates (10^5 times slower than tetrazines).[91] EWGs on the tetrazine can enhance the rate,[92] however there is a balance between reactivity and stability. Several tetrazines bearing strong EWGs (**12** and **13**) are unstable under aqueous conditions.[41] For this reason diaryl tetrazines, such as **14** and **15**, are often used since they offer both moderate reactivity and stability (**Figure 2**).[41]

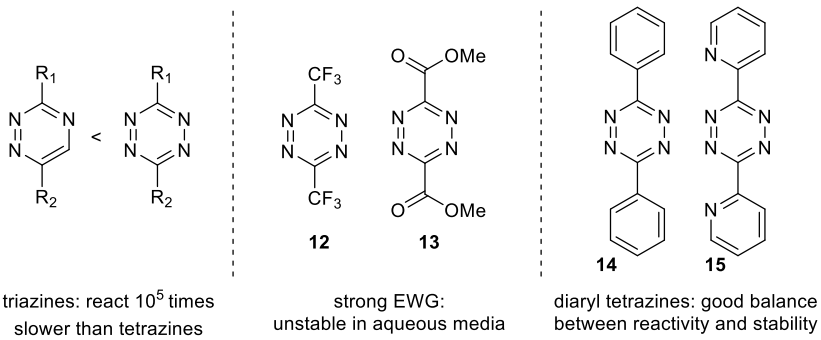

Figure 2. Electronic effects of the diene.

Ring strain was shown to have a larger effect on raising the energy of the HOMO than electronic effects. Sauer and co-workers showed that smaller, more strained rings exhibited faster rates (cyclopropene > cyclobutene > cyclopentene > cyclohexene > *cis*-cyclooctene (*cis*-CO)).[93] However, TCO (**16**) adopts a crown conformation[94,95] in which the double bond is twisted (**Figure 3**), creating a highly strained system with a high energy HOMO,[96] making it 7 orders of magnitude more reactive than the *cis*-isomer.[41] In fact, the rate constant for TCO is 28 times that of cyclopropene for the reaction with tetrazine **13** in dioxane at 20 °C.[93] The rapid reaction between 3,6-di-2-pyridyl-1,2,4,5-tetrazine (DiPy-Tz, **15**) and TCO (k_2 = 1140 $M^{-1} s^{-1}$ in MeOH, 25 °C) proceeds, without catalysis, in both organic solvents and water, with a high tolerance to a range of functional groups.[97] Unfortunately the ring strain in TCO makes it unstable with respect to isomerisation ($t_{1/2}$ = 3.26 h in mouse serum).[98]

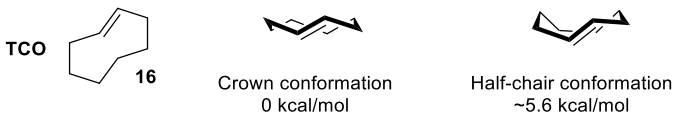

Figure 3. TCO adopts the lower energy crown conformation. The highly strained double bond makes it very reactive.

Stereochemistry also influences the rate and the axial isomer of functionalised TCO (TCO-OR, k_2 = 8.02 x 10^4 $M^{-1} s^{-1}$ in 100% water) undergoes cycloaddition with tetrazines approximately 4 times faster than the equatorial isomer (k_2 = 2.26 x 10^4 $M^{-1} s^{-1}$, **Figure 4**),[97] possibly due to transannular interactions destabilising the axial isomer.[98]

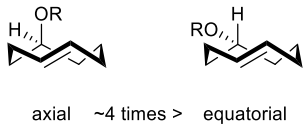

Figure 4. The axial isomer reacts approximately 4 times faster with tetrazines than the equatorial isomer.

As well as different cycloaddition rates, the axial and equatorial isomers of *trans*-cyclooct-4-en-1-ol (4-TCO-OH, **11**) were also shown to have different rates of tautomerisation. The axial isomer of 4-TCO-OH reacts with DiPy-Tz to produce fluorescent 1,4-dihydropyridazine and the 4,5-dihydropyridazine is not observed.[92] It is proposed that the rapid tautomerisation occurs as a result of neighbouring group participation of the OH group. Indeed, removal of the OH (e.g. in a TCO-carbamate) prevents the rapid formation of the 1,4-dihyropyridazine. On the other hand, the equatorial isomer was shown to rapidly form the non-fluorescent 4,5-dihydropyridazine, which then slowly isomerises ($t_{1/2}$ = 2 h) to the 1,4-tautomer through addition of water followed by dehydration.[92] After tuning the tetrazine substituents, reaction with either the axial or equatorial isomer resulted in fluorescent products with different emission wavelengths, due to the formation of different tautomers.[99]

Sterics on the tetrazine have also been shown to affect the rate of cycloaddition. Mono-substituted tetrazines can react faster than di-substituted tetrazines, even those containing a strong EWG.[91,100,101] In addition, 1,2,4,5-tetrazine displayed higher reactivity than 3,6-dimethyl-1,2,4,5-tetrazine (DiMe-Tz) in some cases.[102] However, slightly altering the substituents can alter the energy of the LUMO and cause the reaction to proceed via the normal Diels-Alder reaction.[102]

Finally, water enhances the rate due to the hydrophobic effect (k_2 = 2000 M^{-1} s^{-1} in 10% H_2O/MeOH and k_2 = 1400 M^{-1} s^{-1} in MeOH).[97] In aqueous conditions, hydrophobic reagents are forced together in order to maximise hydrophobic-hydrophobic interactions and to minimise their contact with hydrophilic water molecules. This increases the effective concentration of the reagents and accelerates the rate. It is also proposed that water stabilises the activated complex by coordination.[103] H-bonding to the tetrazine can also occur, which lowers the LUMO in a similar way to the presence of EWGs.[103,104]

1.2.2 Alternative dienophiles

In attempts to further enhance the reactivity of TCO, several derivatives have been reported (**Figure 5**). Strained *trans*-cyclooctene[105] (s-TCO, **17**) and dioxolane-fused *trans*-cyclooctene[97] (d-TCO, **18**) are more reactive than TCO as the *cis*-fused rings force cyclooctene to adopt the higher energy half-chair conformation.[105,106] s-TCO with an attached PEG linker (**24**) is water soluble and its reaction with a tetrazine (k_2 = 3.30 x 10^6 M^{-1} s^{-1} in water, **Table 1**, **Entry 2**) is 160 times greater than TCO.[97] However, s-TCO is even more unstable than TCO and is easily isomerised in the presence of thiols.[105] This can be prevented by complexation with $AgNO_3$, which increases the stability and enables it to be stored for a long period of time. This complex can be used directly in cells without the need for prior removal

of $AgNO_3$.[107] d-TCO (**18**) exhibits a good balance between reactivity and stability. It is more reactive (k_2 = 3.66 x 10^5 M^{-1} s^{-1} in water, **Table 1**, **Entry 3**) than TCO but, unlike s-TCO, it is stable to isomerisation (> 97% remaining after 4 days in human serum).[97] This increased stability is due to the presence of electron-withdrawing oxygen groups that make the double bond less reactive. d-TCO also has the additional advantage of being easier to prepare than s-TCO.

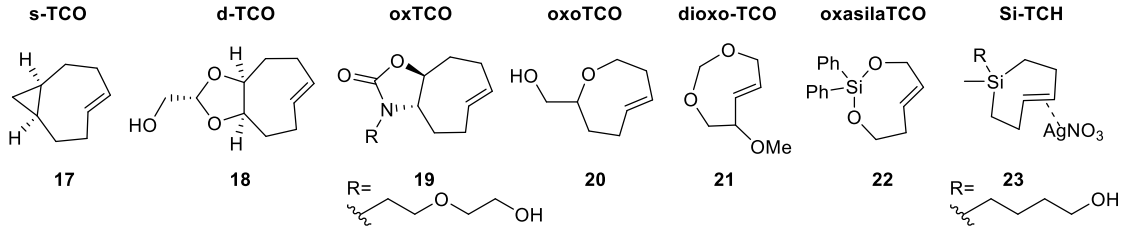

Figure 5. Structures of TCO derivatives: s-TCO[105] (**17**), d-TCO[97] (**18**), oxazolone-fused *trans*-cyclooctene[108] (oxTCO, **19**), oxoTCO[109] (**20**), 3-dioxacyclo-oct-5(*E*)-ene[110] (dioxo-TCO, **21**), *trans*-oxasilacycloheptene[111,112] (oxasilaTCO, **22**) and Si-TCH[113] (**23**).

As well as conformationally strained derivatives, heterocyclic versions of TCO (**20–23**) have also been reported (**Figure 5**).[109–113] One example is the rationally designed *trans*-5-oxocene (oxoTCO, **20**), which was proposed to be more reactive than TCO due to increased angle strain as a result of short C–O bond lengths.[109] oxoTCO (**20**) was shown to be synthetically accessible from 7 high-yielding steps. However, the desired axial *trans*-isomer could not be easily separated from the equatorial isomer and, therefore, further studies were carried out using a mixture of diastereomers. oxoTCO (**20**) reacts rapidly with tetrazines (k_2 = 9.5 x 10^4 M^{-1} s^{-1}, 1:2.2 axial:equatorial diastereomeric mixture) and showed similar stability to d-TCO. Unlike TCO, it has the advantage of being highly hydrophilic and cell permeable, enabling it to enter *E. coli* cells overexpressing a tetrazine-modified green fluorescent protein (GFP). The fluorescence of GFP is quenched by the tetrazine and is restored upon reaction with oxoTCO. Other heterocyclic derivatives (**19**, **21**, **22**) also proved to be hydrophilic and more reactive than TCO.[108,110–112]

Finally, stable $AgNO_3$ complexes of *trans*-cycloheptene (TCH) and *trans*-1-sila-4-cycloheptene (Si-TCH, **23**) have also been reported (**Figure 5**).[113] TCH is highly unstable and can only be isolated through trapping or complexation with metals.[114] Si-TCH offers additional stability as a result of decreased ring strain[115,116] (C–Si bonds are longer that C–C bonds) and even metal-free Si-TCHs show good stability in solution.[113] The decomplexation of $AgNO_3$ occurs *in situ* in cell media due to the presence of NaCl and reaction of decomplexed Si-TCH with a tetrazine is the fastest bioorthogonal reaction to date (k_2 = 1.1 x 10^7 M^{-1} s^{-1} in 90% H_2O/MeOH). This reaction was applied to protein labelling in live cells. Although all these derivatives offer advantages in rate and hydrophilicity, they have not been

widely utilised, and TCO is likely to remain the reagent of choice until other derivatives become commercially available or improved syntheses are reported.

In addition to TCO derivatives, a wide variety of other dienophiles have been reported (**Table 1**). It should be noted that a direct comparison of the reaction rates in **Table 1** is not reliable, since they are reported in different solvent systems. The fact that there is no standard solvent system for studying bioorthogonal reaction kinetics is a limitation of the field. Since the percentage of aqueous solvent and the presence of buffers has a large effect on the rate, a more useful approach would be for all reactions to be reported in the same solvent system. This would enable quantitative comparison of the reaction rates. However, the data in **Table 1** still provides an approximate idea of the order of magnitude of the rates. It is also important to note that when reactions are carried out *in vivo,* lower concentrations of reagent are utilised to minimise toxicity and therefore the rate will be slower than *in vitro*. The kinetics of bioorthogonal reactions are usually only studied *in vitro*. An exception is the reaction of s-TCO with a GFP-tetrazine, which was also studied *in cellulo*. It displayed a second order rate constant of 72000 $M^{-1} s^{-1}$ *in cellulo* compared to 87000 $M^{-1} s^{-1}$ in phosphate-buffered saline (PBS) at 21 °C.[117]

All dienophiles suffer from slower reaction rates than 4-TCO-OH (**11**, **Table 1**, **Entry 1**). For example cyclopropene[101] (**25**, **Table 1**, **Entry 4**) and norbornene[86] (**26**, **Table 1**, **Entry 5**) react rapidly with tetrazines and demonstrate a good balance between reactivity and stability. However, TCO (**11**, **Table 1**, **Entry 1**) is significantly more reactive and, unlike norbornene (**26**) and cyclopropene (**25**), can even react with the less reactive triazines.[118] Other examples of dienophiles include N-acylazetine[119] (**Table 1**, **Entry 6**), BCN[120] (**27**, **Table 1**, **Entry 7**), vinyl boronic acids[121] (**Table 1**, **Entry 8**) and primary alkenes[122,123] (**28**, **29**, **Table 1**, **Entries 9 and 10**). Although these dienophiles are significantly less reactive than TCO, there are cases where they are more suitable than TCO. For example, they are less hydrophobic than TCO and their smaller size allows them to be easily incorporated into biomolecules.

Table 1. Typical second order rate constants observed with selected dienophiles. Adapted from Oliveira *et. al.*[12]

Entry	Dienophile	Typical k_2 ($M^{-1} s^{-1}$)	Aqueous solvent %
1	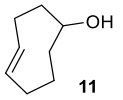 **11**	22,600 (eq)[97] 80,200 (ax)	100
2	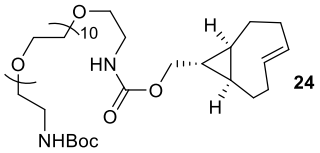 **24**	3300000[97]	100
3	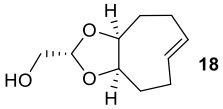 **18**	366,000 (syn)[97] 318,000 (anti)	100
4	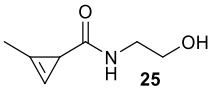 **25**	2.3[101]	50
5	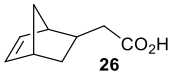 **26**	1.9[86]	100
6	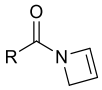	0.39[119]	88
7	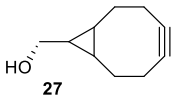 **27**	1245[120]	45
8	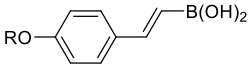	27[121]	100
9	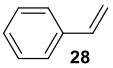 **28**	0.05[122]	50
10	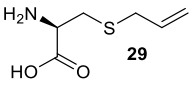 **29**	0.002[123]	50

1.2.3 Applications of IEDDA ligation reaction

Bioorthogonal ligation reactions have been widely used for the labelling and studying of biomolecules such as proteins, lipids and glycans.[124] The first use of the IEDDA reaction for protein labelling was reported in 2008 by Fox and co-workers.[41] Thioredoxin (Trx), which has a single, solvent-exposed disulfide in the active site, was labelled by site-selective chemical conjugation to TCO via a maleimide-carbamate linker (**30**). This was followed by reaction with DiPy-Tz (**15**) which gave **31** in 100% conversion within 5 min (**Scheme 18**).[41]

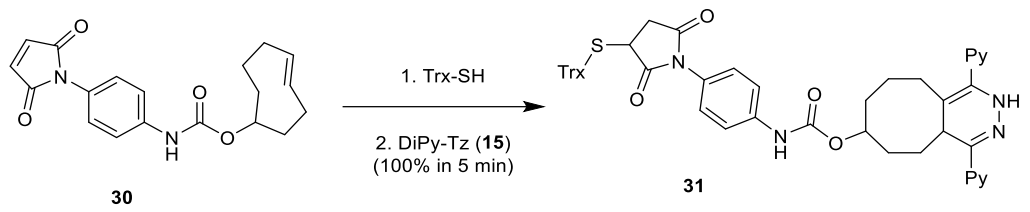

Scheme 18. Application of the IEDDA reaction for protein labelling.

Site-specific labelling of recombinant proteins in live *E. coli* cells was achieved through genetic encoding of a tetrazine-containing unnatural amino acid, followed by reaction with s-TCO.[117,125] A second order rate constant of 72500 M^{-1} s^{-1} was observed in cells, confirming the suitability of this reaction for *in vivo* applications.[117]

Other bioorthogonal handles, including TCO,[120,126] norbornene,[126,127] BCN,[120,128] and cyclopropene[75] have been site-specifically incorporated into proteins through genetic code expansion.[129] Reaction of a genetically incorporated TCO handle with fluorogenic tetrazines was used to image intracellular proteins and observe the intracellular localisation and trafficking of a membrane-associated protein.[130] Imaging of endogenous kinases in live cells was also demonstrated through the subsequent addition of a TCO-modified inhibitor followed by a tetrazine-fluorophore.[131]

A selective method for labelling proteins that are produced at a specific developmental stage in a certain tissue was developed.[132] By using genetic code expansion, cyclopropene handles were selectively incorporated into proteins synthesised in germ cells in the ovaries of *Drosophila melanogaster*. Reaction with a labelled tetrazine (fluorophore/biotin) then enabled imaging/identification of the proteins. The small size of cyclopropene is advantageous, as it does not perturb the structure and function of the protein.

The IEDDA reaction has been applied for super resolution imaging of cytoskeleton[133] and intracellular proteins.[133,134] In a first example, site-specific labelling of proteins with BCN/TCO-modified amino acids through genetic encoding was followed by reaction with a tetrazine fluorophore.[133] In another example, a Click-PAINT strategy was described, in which the incorporated TCO reacts with a tetrazine-DNA conjugate, followed by a fluorophore linked to the complementary DNA sequence. This strategy, based on DNA-PAINT, was used to label intracellular proteins of low abundance.[134]

An appealing method for protein labelling is disulfide rebridging or stapling (the insertion of a chemical motif between the two sulfides, **Scheme 19a**). Since all IgG antibodies contain four disulphide bonds, stapling is a general strategy for antibody modification that offers a high degree of control. This is not the case for other modification methods, for example lysine modification, where the number of

reactive sites is much higher and varies between antibodies. Stapling can result in increased protein stability and cell permeability[124] and it has been used to site-selectively install tetrazines into peptides, proteins and antibodies. In a key example, Trx was reacted with 3,6-di-2-chloro-1,2,4,5-tetrazine (DiCl-Tz, **32**) to produce a stapled tetrazine handle (**Scheme 19b**).[135] The authors claim that this is advantageous as it enables selective incorporation of a tetrazine into proteins, which can then either be labelled through reaction with a dienophile or removed by photolysis. However, the resulting tetrazine showed poor reactivity (Trx-Tz was labelled by reaction with a BCN fluorophore (10 equiv.) for 10 days) and removal of the tetrazine staple by photolysis resulted in loss of protein activity. Therefore, the utility of this tetrazine stapling method is debatable. Recently, the incorporation of a tetrazine through an allyl sulfone handle (**33**) was reported (**Scheme 19c**).[136] The resulting tetrazine was highly reactive and reacted in near-quantitative yield with TCO-probes within 0.5 h. This approach enables rapid labelling of antibodies via the TCO-tetrazine reaction. Importantly, in both cases the protein conjugates were shown to be stable and the secondary structure was not affected by stapling.

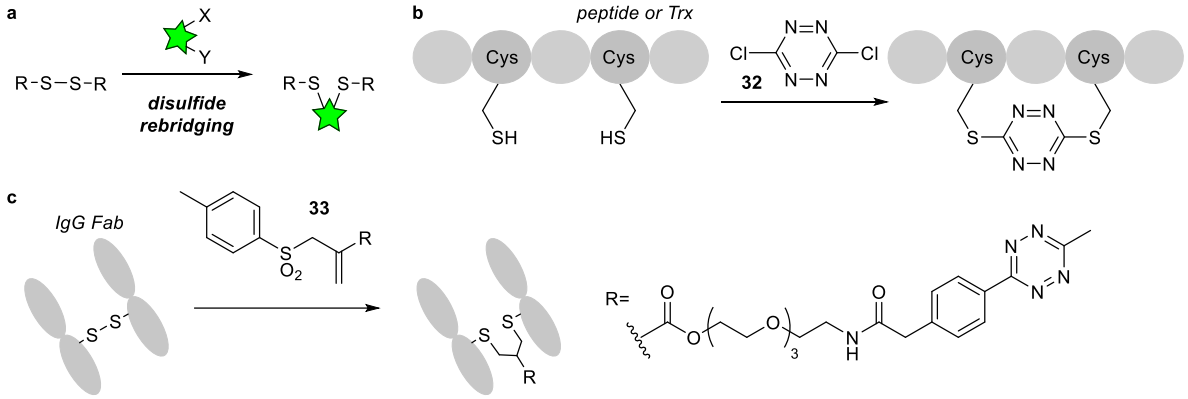

Scheme 19. Disulfide rebridging. **a.** Insertion of chemical motif between two sulfides. **b.** Stapling with DiCl-Tz (**32**) introduces a tetrazine with poor reactivity towards dienophiles. **c.** Allyl sulfone handle (**33**) to incorporate a highly reactive tetrazine.

The IEDDA reaction can also be used for the identification of bioactive targets of small molecule drugs. Cells are incubated with a TCO-modified drug, followed by addition of a tetrazine-biotin conjugate and proteomic analysis.[137] The IEDDA reaction resulted in more efficient labelling than both the CuAAC and the SPAAC. In addition, a modular strategy involving co-incubation of the TCO-modified drug with the unmodified drug, followed by addition of a tetrazine-fluorophore was used to determine the target occupancy of the underivatised drug at subcellular resolution.[137]

The IEDDA reaction has also been used to detect post-translational modifications in live cells. Sulfenic acid modifying *trans*-cyclooct-4-en-1-ol (SAM-TCO) probes react selectively with sulfenic acids to form thiiranium ions, which then undergo transannular attack by the axial hydroxyl group and

thioetherification to from stable adducts (**Scheme 20**).[138] Methods for detecting sulfenic acids involve addition of a probe, followed by cell lysis and detection of the modified sulfenic acids. However, cell lysis can result in oxidation of thiols to sulfenic acids, which can then react with the probe. An advantage of the SAM-TCO probes is that tetrazines can be added to cells before lysis to quench any unreacted probe and to prevent further labelling occurring during the lysis step. In addition, the probes are small, cell permeable and a proteomic method utilising SAM-TCO-alkyne probes, was able to detect significantly more proteins than previously reported probes.

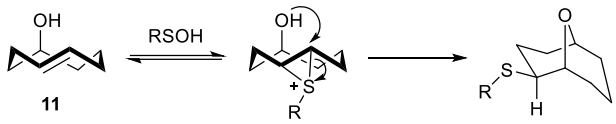

Scheme 20. SAM-TCO probes for detecting endogenous sulfenic acids.

Tetrazines have been shown to quench the fluorescence of an attached fluorophore, which can be successfully turned on after IEDDA reaction.[92] Highly specific fluorogenic tetrazine probes for the detection and imaging of DNA/miRNA in live cells have also been developed.[139,140] Antisense oligonucleotide probes containing a fluorogenic tetrazine and either a benzonorbornadiene[139] or cyclopropene,[140] undergo a template driven reaction in the presence of the specific complementary strand (**Scheme 21**). Binding to the template strand brings the tetrazine and dienophile into close proximity and increases their effective concentration, resulting in rapid reaction and production of a fluorescent signal. This approach is highly specific and can detect a single base mismatch.

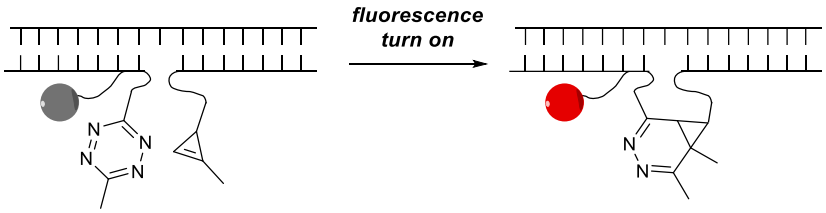

Scheme 21. Detection of specific DNA sequences in live cells through a template driven IEDDA reaction.

In addition to the use of ligation reactions for the labelling and tracking of biomolecules in biological systems,[141] several alternative applications have been reported. These include hydrogel[142,143] and polymer[144,145] synthesis, delivering NPs to target cells[12,146] and proteolysis targeting chimera (PROTAC) assembly in live cells.[147] A click-formed proteolysis targeting chimera (CLIPTAC) strategy was developed, in order to overcome the poor solubility and cell permeability of high molecular weight PROTACs.[147] A TCO-modified ligand for the protein of interest, followed by a tetrazine-thalidomide (E3 ligase recruiting ligand) conjugate were sequentially added to cells and demonstrated improved cell permeability. Upon intracellular formation of a CLIPTAC, the E3 ligase and protein are brought into

close proximity, which enables ubiquitination and proteasomal degradation of the target protein (**Scheme 22**).

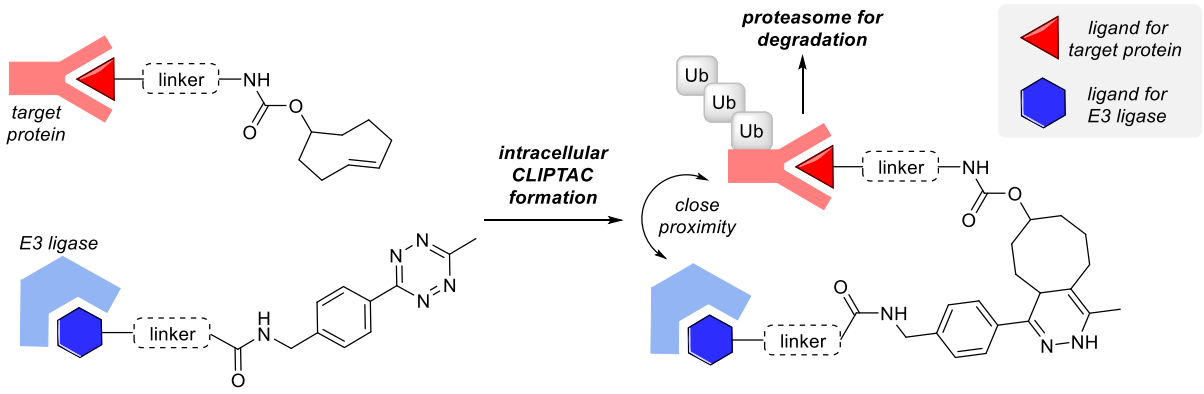

Scheme 22. CLIPTAC formation in live cells brings an E3 ligase into close proximity with the target protein, resulting in ubiquitination and proteasomal degradation of the target.

Preparation of radioactive probes for nuclear imaging can be achieved through bioorthogonal ligation of a radioactive nuclei to a targeting molecule. Due to the short half-life of the radionuclide, the rapid clearance of small molecules and the low target expression *in vivo*, the preparation must be rapid and efficient. Therefore, the TCO-tetrazine IEDDA reaction has been applied for *in vivo* imaging and pretargeting applications.[148,149]

Rossin *et al.* reported the first TCO-tetrazine pretargeting strategy for nuclear imaging.[150] Mice bearing colon cancer xenografts were injected with a TCO-CC49 antibody against TAG72, which is overexpressed in several solid tumours. After 24 h, 3.4 equiv. of an ^{111}In-dodecane tetraacetic acid (DOTA)-tetrazine conjugate was injected, and localisation of radioactivity at the tumour was observed by single photon emission computed tomography (SPECT) imaging. However, a low tumour-to-blood ratio resulted from reaction with excess TCO in circulation. In addition, TCO was slowly inactivated *in vivo*. It was later shown that shortening the linker length reduced TCO deactivation by Cu-containing proteins[98] and that less hydrophobic TCO tags improved tumour uptake and *in vivo* stability.[151]

As well as radiolabelling with metals, the TCO-tetrazine reaction has been used to rapidly generate ^{18}F probes. ^{18}F-labelling of TCO was achieved in 71% after 15 min and reaction with a tetrazine occurred in quantitative yield within 10 seconds.[152] Reaction of ^{18}F-TCO with a tetrazine, conjugated to either a peptide[153] or a small molecule inhibitor,[154] resulted in positron-emission tomography (PET) probes that demonstrated good tumour uptake. Additional probes were generated from reaction of tetrazines with ^{18}F-labelled norbornene,[155] s-TCO,[156] d-TCO[157] and oxoTCO.[158] The highest tumour-to-background ratio was observed with oxoTCO due to rapid clearance as a result of its hydrophilic

nature. Dextran polymers have also been shown to improve labelling though increasing *in vivo* circulation time of the radioactive isotope.[159]

Initially, tetrazines were found to be unstable to ^{18}F labelling conditions. However, since then, several robust methods for generating ^{18}F-Tz compounds have been reported.[160–162] Additionally, tetrazine derivatives of other radionuclides have been reported for *in vivo* labelling, including ^{177}Lu-Tz,[163] ^{64}Cu-Tz,[164] ^{99m}Tc-Tz,[165] ^{68}Ga-Tz[166] and even ^{11}C[167] which has a half-life of only 20.3 minutes. Tetrazines linked to various chelating groups (DOTA for chelating ^{64}Cu and deferoxamine (DFO) for chelating ^{89}Zr) have also been used to label a norbornene-modified antibody.[168] Finally, by reaction of TCO-modified Trastuzumab with a fluorogenic chelate tetrazine (Tz-DFO-BODIPY), multimodal imaging of HER2 positive tumours was achieved.[169]

Antibody-drug conjugates (ADCs) often suffer from heterogeneity due to a lack of control of both the site and number of modifications. However, incorporation of a bioorthogonal handle into the antibody enables controlled conjugation[170] and there are currently several bioorthogonally-prepared ADCs in clinical trial.[171] Furthermore, the first clinical trials of utilising bioorthogonal chemistry in humans are currently underway for the treatment of pancreatic ductal adenocarcinoma.[171] After pretargeting with a TCO-modified antibody (5B1), ^{64}Cu-Tz will be added to radiolabel the antibody at the tumour site and enable PET imaging. This strategy was demonstrated to be more efficient than direct administration of a radiolabelled antibody in mice, likely because the radioactive probe is only administered after clearance of excess antibody.[170] The fact that this radiolabelling strategy based on the IEDDA reaction is currently in clinical trials, highlights the significant progress that has been made in the field of bioorthogonal chemistry.

1.2.4 Conclusion

The IEDDA reaction between a tetrazine and TCO is one of the fastest and most selective bioorthogonal reactions reported to date. As a result, it has attracted a lot of attention and has been utilised for a diverse range of applications beyond the typical labelling of biomolecules. The significant amount of work done in this area has led to this reaction reaching clinical trials. However, the full potential of the TCO-tetrazine reaction is still unknown and it is envisaged that further clinical trials will follow. In addition, it is likely that the applications of this reaction will continue to increase as a wider range of tetrazine and TCO reagents become commercially available.

1.3 Bioorthogonal decaging reactions for prodrug activation

1.3.1 Prodrug activation

Conventional chemotherapy involves injection of an active drug, which then circulates around the body and binds to the intended target. The lack of specificity for the target tissue results in toxic side effects, which restrict the maximum dose that can be administered. This means treatment often fails as a sufficiently high drug concentration at the target site cannot be achieved.

A prodrug is an inactive form of a drug, in which a functional group essential for the activity of the drug has been masked with a protecting group. By selectively activating the prodrug at the target site, for example at a tumour, it is possible to reduce unwanted side effects that occur as a result of off-target interactions with healthy cells (**Scheme 23**). Therefore, this enables higher doses to be administered, improving the efficacy of the drug. Prodrugs can also be used to improve the pharmacokinetics of the drug, for example the solubility and cell permeability.

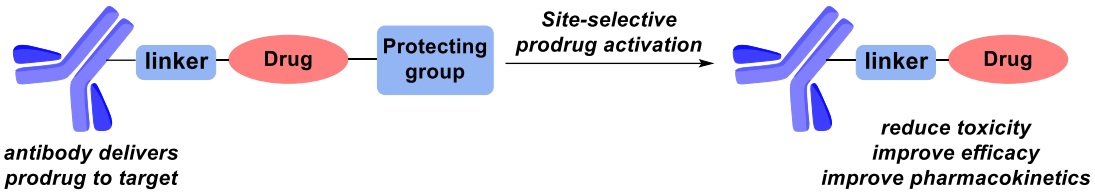

Scheme 23. Prodrug activation.

Prodrugs are commonly activated by endogenous factors in target cells, such as a difference in pH[172] or the overexpression of an enzyme[173–176] compared to healthy cells. Other examples of prodrug activation have been reported that exploit levels of H_2O_2,[177] glutathione[178] and thiols.[179] However, endogenous activation often suffers from low selectivity because the difference, for example in enzyme expression, between target and healthy cells is usually small. In order to increase specificity, an exogenous enzyme can be installed at the target site through the use of an antibody-enzyme conjugate.[180] Antibody-directed enzyme prodrug therapy (ADEPT) results in site-selective, extracellular release of a small molecule drug, which can then diffuse through the tumour and kill cancer cells (**Scheme 24a**). However, immunogenicity of the exogenous enzyme prevents treatment being repeated. An alternative strategy to increase the specificity of endogenous activation is to use ADCs containing cleavable linkers, such as acid labile hydrazones, disulfides and enzymatically cleavable linkers (**Scheme 24a**).[181] For example, the commonly used valine-citrulline-*p*-aminobenzyl carbamate (Val-Cit-PABC) linker is a peptide linker that releases the payload through 1,6-elimination following protease cleavage by Cathepsin B (**Scheme 24b**).[182] Disadvantages of antibody-directed

approaches include the rapid mutation of antigens that generates resistance,[183] hydrolysis of the linker that leads to non-specific drug release and high ADC heterogeneity.[184]

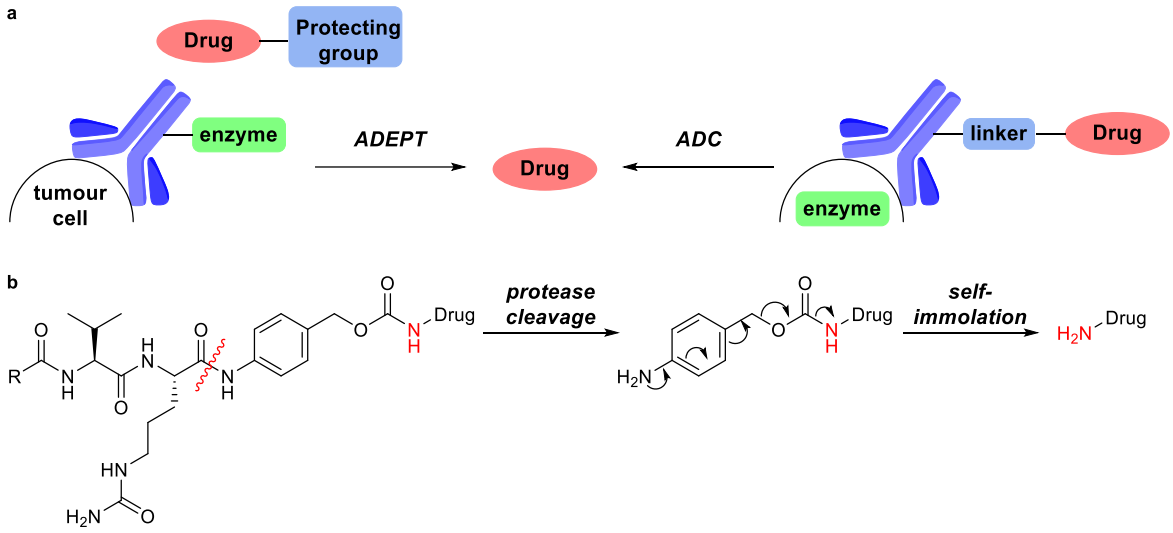

Scheme 24. Antibody-directed approaches for site-specific drug release. **a.** Antibody-enzyme conjugates catalyse extracellular prodrug activation and ADCs are cleaved by intracellular enzymes upon internalisation. **b.** mechanism of cleavage of a Val-Cit-PABC linker commonly used in ADCs.

A new class of bioorthogonal reactions has been developed in which a bond is broken to release a molecule of interest.[185–188] These bioorthogonal decaging reactions provide a method to activate prodrugs with a high level of control and selectivity, and are, therefore, appealing for site-selective therapies. Like ligation reactions, many decaging reactions have been reported that involve light, metal or small molecule triggers. Several of these will be discussed here, with a focus on chemical-triggered reactions that have been used for prodrug activation.

1.3.2 Photo-triggered decaging reactions

In a photo-triggered decaging reaction, a protecting group absorbs photons and is transferred to an excited state, where it undergoes a reaction to release the molecule of interest. UV-triggered decaging of *o*-nitrobenzyl (ONB) ether protecting groups has been widely explored (**Scheme 25**).[189,190] However, UV light (350–365 nm) suffers from issues of cytotoxicity and poor tissue penetration, limiting its use *in vivo*.

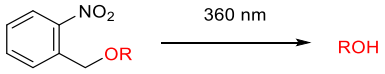

Scheme 25. UV-triggered decaging of ONB ethers.

Using light of a lower energy and longer wavelength (near-IR, 650–900 nm) is appealing as it offers increased tissue penetration and low toxicity in comparison to UV radiation. Near-IR light was used to decage a prodrug consisting of a cyanine fluorophore connected to an alcohol-containing drug (hydroxy-cyclofen) in mammalian cells (**Scheme 26**).[191] Upon irradiation with near-IR light, photooxidative C–C bond cleavage occurs, followed by hydrolysis to release an amine. This then undergoes intramolecular cyclisation to release the alcohol. This near-IR cyanine-based cleavable linker has been incorporated into an ADC and the intrinsic fluorescence of the cyanine caging group was used to demonstrate good *in vivo* stability and high tumour uptake.[192] Further work resulted in a second generation ADC with improved stability, a longer wavelength absorbance maximum and a more potent duocarmycin payload, which resulted in a significant decrease in tumour size and increased survival of the mice after a single dose.[193]

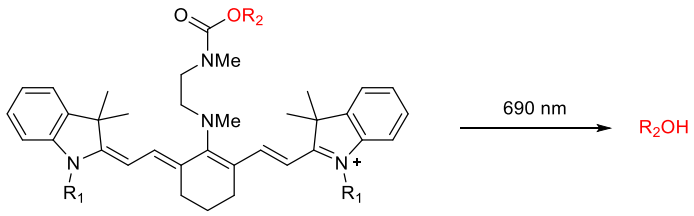

Scheme 26. Near-IR-cyanine-based cleavable linker for protecting alcohols.

A photo-triggered Ru-catalysed azide reduction has been described in which a catalytically active Ru species is generated upon treatment with visible light.[194] The reduction of azides that were connected to self-immolative linkers, was applied to release fluorophores in living cells (**Scheme 27**).[195,196] The reduction of aromatic azides to amines in mammalian cells has also been reported through the use of iron catalysts.[197]

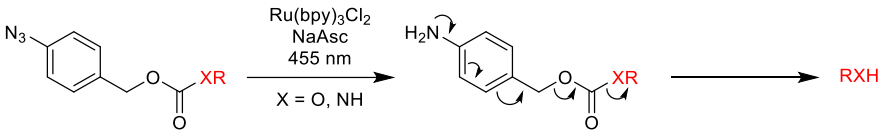

Scheme 27. Visible light-triggered reduction of azides followed by 1,6-elimination to release fluorophore in cells.

1.3.3 Metal-triggered decaging reactions

Metal-triggered bioorthogonal decaging reactions have been widely explored,[198,199] with the most extensively studied metal being palladium. In 2014 Chen and co-workers reported the first use of palladium for specific protein activation in cells.[200] Palladium catalysts were used to deprotect a propargyl-carbamate-lysine that was genetically incorporated into the protein of interest (**Scheme 28a**). The same group also reported palladium-catalysed protein activation in cells through removal of an allene-protected tyrosine residue (**Scheme 28b**).[201]

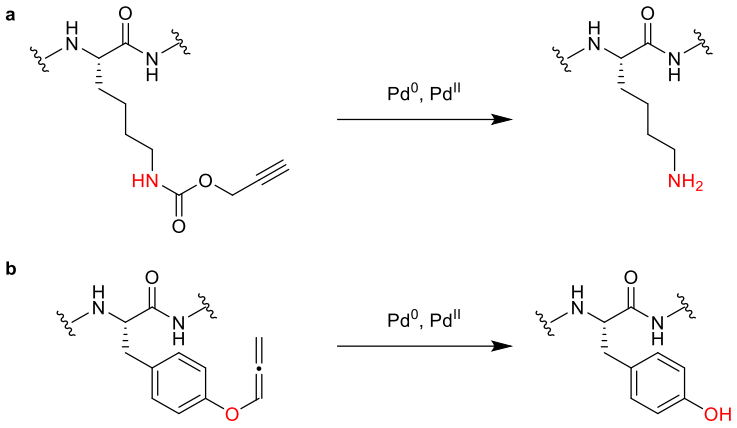

Scheme 28. Palladium-triggered decaging for the activation of proteins in cells. **a.** removal of a propargyl-carbamate protecting group from a lysine residue. **b.** removal of an allene protecting group from a tyrosine residue.

In 2014 Weiss *et al.* reported one of the first uses of bioorthogonal decaging for prodrug activation.[202] A biocompatible palladium resin was used to cleave a propargyl group from a 5-fluorouracil prodrug (**34**) *in vitro* (**Scheme 29**). In addition, fluorescence recovery was performed *in vivo* for the imaging of zebrafish embryos.

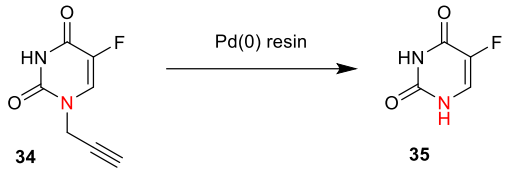

Scheme 29. Palladium-triggered activation of a 5-fluorouracil prodrug (**34**).

The same group then reported several carbamate prodrugs of gemcitabine which could also be activated using palladium-mediated decaging.[203] The most successful carbamate protecting group tested was *N*-propargyloxycarbonyl (*N*-Proc) which resulted in the greatest amount of free drug release, and therefore cytotoxicity, in cells (**Scheme 30a**). In addition, the activation of *N*-Proc-rhodamine in zebrafish embryos was shown by fluorescence to occur locally at the site of the

palladium resin. Palladium-catalysed depropargylation to release Floxuridine, a cytotoxic anti-cancer drug, under hypoxic conditions in cells has also been reported (**Scheme 30b**).[204]

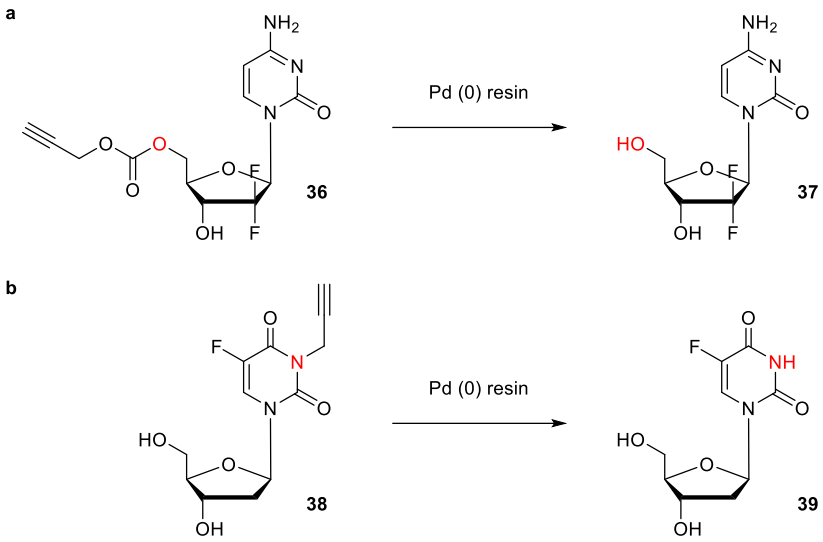

Scheme 30. Palladium-triggered release of anti-cancer drugs. **a.** Activation of *N*-Proc-gemcitabine prodrug **36**. **b.** activation of propargyl-floxuridine prodrug **38**.

Palladium-mediated decaging has also been extended to the release of hydroxamic acid functional groups. Successful activation of Vorinostat (**43**), a histone deacetylase, was achieved in cells using palladium-catalyzed depropargylation to release phenol **41** which then undergoes 1,6-elimination to release the alcohol of the hydroxamic acid group (**Scheme 31**).[205]

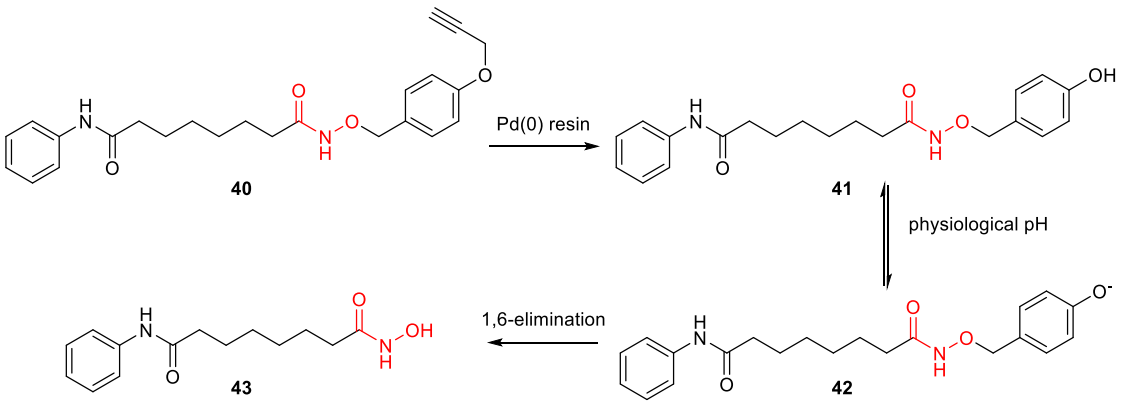

Scheme 31. Release of hydroxamic acid-containing drug, Vorinostat (**43**): palladium-catalysed depropargylation is followed by 1,6-elimination of a 4-hydroxybenzyl group.

In addition to palladium, ruthenium decaging[206] has also been used for prodrug activation. Meggers developed organometallic ruthenium (IV) catalysts for decaging of *N*-allyoxycarbonyl (*N*-Alloc) protected amines (**Scheme 32**).[207] These catalysts were highly cell permeable and exhibited high turnover numbers (TONs) of up to 270 cycles in the presence of thiols at millimolar concentrations.

Thiols usually result in deactivation of metal catalysts, however, the authors propose that in this case the biological nucleophiles reduce the Ru (IV) complex to the catalytically active Ru (II) species. Catalytic activation of doxorubicin (Dox) was achieved in the cytoplasm of HeLa cells, which resulted in apoptosis.

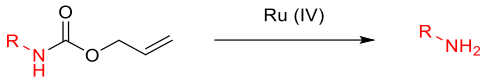

Scheme 32. Ruthenium-triggered removal of an *N*-Alloc protecting group from amines.

Recently, a bioorthogonal decaging method based on ring-closing metathesis (RCM) was reported.[208] This "close-to-release" strategy involves ruthenium-catalysed RCM followed by 1,4-elimination, driven by formation of an aromatic compound. Treatment of several diolefinic esters with Hoveyda-Grubbs 2nd generation catalyst (HG-II) resulted in the release of carboxylic acids, although mostly with yields of < 50% (**Scheme 33**). Examples include release of nicotinic acid (**44**, an NAD(P)-H precursor) and valproic acid (**45**, an antineuroleptic drug).

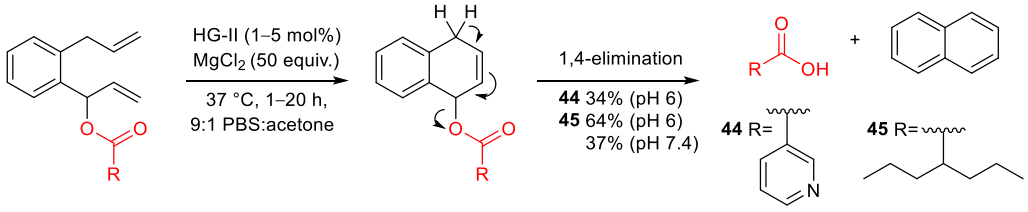

Scheme 33. Close-to-release decaging strategy involving RCM followed by 1,4-elimination: decaging of an ester linker to release carboxylic acids **44** and **45**.

It was also shown that analogous ether, carbonate and carbamate linkers could be decaged to release alcohols or amines, respectively. However, lower yields (often < 20%) and TONs were observed than from the ester linker with similar catalyst loading. Although the decaging of esters and ethers occurred in the presence of serum, mammalian cells and in the periplasm of *E. coli*, reduced yields and catalyst TONs were observed. For example, with 5 mol% HG-II in the presence of HeLa cells in DMEM (10% FBS), which are representative of standard cell culture conditions, ether decaging resulted in 27% of free alcohol with a low TON of 5. This is likely due to Ru catalyst deactivation by reaction with glutathione.[209] However, it is possible to improve the stability of the catalyst towards biological nucleophiles by altering the ligands.[207]

An example of gold-mediated decaging has also been reported.[210] Gold is known to coordinate preferentially to alkynes, however, it also has a high affinity for thiols. The authors proposed that by using solid-supported gold NPs, reaction with large thiol-containing biomolecules could be prevented

whilst allowing deprotection of small molecule drugs in biological systems. The decaging of three alkyne-protected cancer drugs (vorinostat, 5-fluorouracil and doxorubicin) using heterogeneous gold NPs was demonstrated in live cells (**Scheme 34**). This was also the first bioorthogonal decaging reaction to be carried out in the brain of zebrafish embryos. Intracranial activation of a caged rhodamine was achieved, highlighting the potential of gold-mediated decaging reactions *in vivo*.

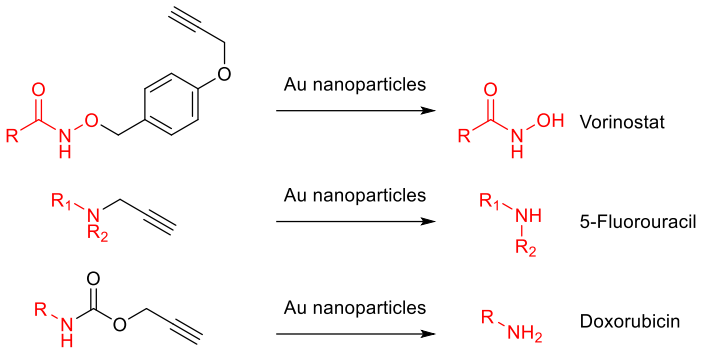

Scheme 34. Gold-triggered decaging of alkyne-protected anticancer drugs.

In the area of drug activation, metal-triggered decaging has mainly been used to cleave monofunctional protecting groups from anticancer prodrugs. Recently, our group reported a bifunctional thioether propargyl carbamate linker for palladium-mediated drug release (**Scheme 35**).[211] The thioether group was shown to bind to palladium and direct the decaging. After demonstrating palladium-triggered drug release from a PEGylated doxorubicin prodrug in live cells, the application was extended to the development of a palladium-activated ADC (**46**). Doxorubicin (**48**) was connected to a nanobody targeted to the HER2 antigen via the bifunctional thioether propargyl carbamate linker. The ADC (**46**) proved stable and thioether-directed palladium-triggered decaging in cells was achieved using non-toxic concentrations of palladium.

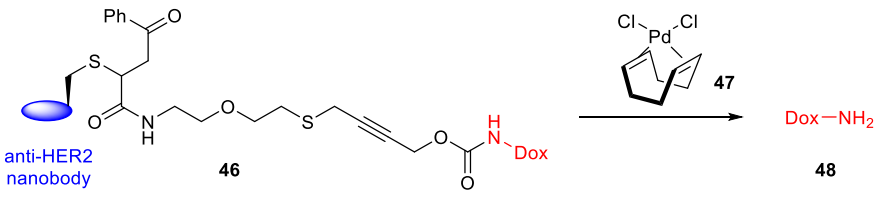

Scheme 35. Palladium-triggered release of doxorubicin (**48**) from an ADC (**46**).

Performing metal-triggered decaging reactions *in vivo* poses several challenges such as ensuring efficient cellular uptake of the catalyst at the target organ and avoiding loss of catalytic activity through reaction with thiols and intracellular proteins.[212] However, methods for the effective, intracellular delivery of palladium *in vivo* have been developed, including metal NPs,[213,214] NPs entrapped in microspheres[199,215] and metal complexes.[216] For example, cell-penetrant Pd NPs have

been shown to accumulate at the tumour site in mice and catalyse the activation of a doxorubicin prodrug, resulting in inhibited tumour growth and increased survival of the mice.[213] Linking metal complexes to cancer-targeting cyclic peptides is another strategy to generate efficient internalisation at the desired site.[216] Pd-NP functionalised microspheres that were linked to a cancer targeting cyclic peptide were shown to selectively and rapidly enter glioblastoma cells. They successfully catalysed the simultaneous intracellular decaging of a 5-fluorouracil prodrug and the synthesis of PP-121 (**6**) via Suzuki-Miyaura cross coupling.[217] This dual anti-cancer drug-formation strategy resulted in increased therapeutic effect compared to either strategy alone.

The development of optimised, biocompatible palladium devices for *in vivo* catalysis has been reported.[218] These Pd NP-functionalised polymers were inserted directly into the tumour in murine models of prostate cancer by ultrasound-guided injection. It was observed that after being in the tumour for 3 weeks, the catalytic activity remained the same as that of a newly installed Pd device, showing that the device was resistant to the deactivating effect of thiols and proteins. This study highlights the potential for metal-catalysed decaging reactions in localised prodrug activation therapy. Metal-triggered ligation reactions are unlikely to occur *in vivo* due to the small probability of 3 components coming together at sufficient concentration to react. However, for decaging reactions, only two components (the caged molecule and the metal trigger) need to be in close proximity for the reaction to occur. Therefore, the potential for metal triggered decaging is much greater than for ligation reactions.

1.3.4 Small molecule-triggered decaging reactions

Decaging reactions that do not involve a tetrazine have been reported. For example, the SPAAC was successfully transformed into a cleavage reaction by linking an azide to a self-immolative linker (**Scheme 36**).[219] Azide **49** undergoes a [1+3] cycloaddition with TCO (**16**) to form unstable triazoline **50** which decomposes to form imine **51**. Hydrolysis of the imine is followed by self-immolation of the PABC linker to release an amine. This was applied to decage a prodrug in cells and had a similar rate constant to the SPAAC ligation (k_2 = 0.027 M^{-1} s^{-1} in 50% MeCN/PBS for the cycloaddition). Azide **49** could also be reduced by phosphines (via a Staudinger reaction) to form aniline **52** directly, which then underwent 1,6-elimination to release doxorubicin (**48**).[220]

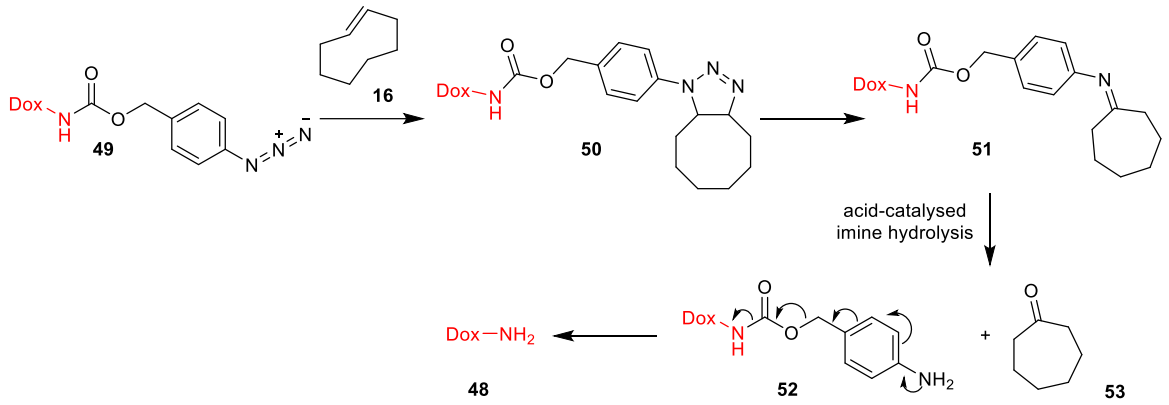

Scheme 36. Strain promoted 1,3-dipolar cycloaddition of TCO (**16**) and an azido-PABC linker for the activation of a doxorubicin prodrug (**49**).

The Staudinger reaction was also adapted for decaging and applied to activate a doxorubicin prodrug (**Scheme 37**).[221] By modifying the phosphine with a phenyl carbamate substituent, the aza-ylide undergoes intramolecular cyclisation and cleaves the carbamate bond. The resulting intermediate then undergoes 1,6-elimination to release doxorubicin (**48**).

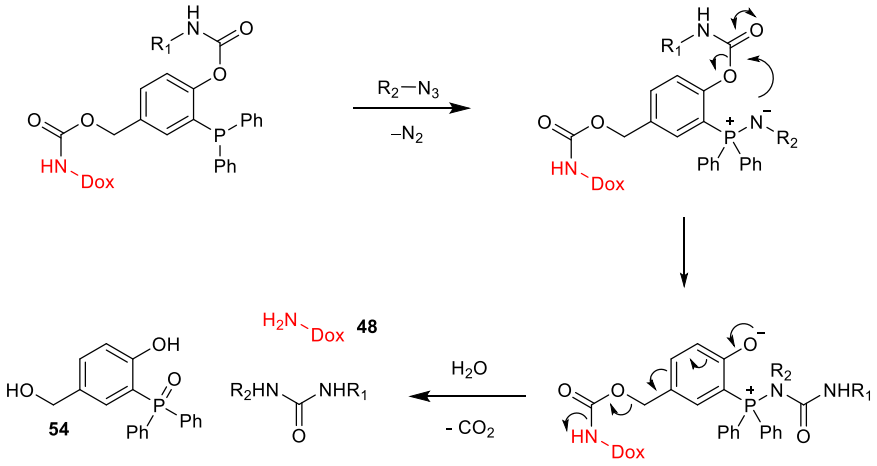

Scheme 37. The Staudinger ligation was adapted for decaging by connecting the phosphine to a phenyl carbamate.

A decaging reaction between iminosyndones and strained alkynes has also been reported.[222] The reaction proceeds via a [3+2] dipolar cycloaddition, followed by a retro Diels-Alder reaction to release a free amine (**Scheme 38**). A second order rate constant of 0.18 $M^{-1} s^{-1}$ was observed with BCN (**27**), which could be increased up to 29 $M^{-1} s^{-1}$ by using the more strained alkyne TMTH (**1**).

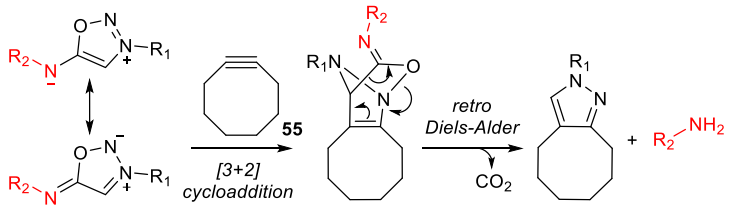

Scheme 38. Cyclooctyne-triggered decaging of aminosyndones to release amines.

Most decaging reactions are modified forms of ligation reactions, in which the intermediate that forms upon ligation is unstable and therefore undergoes rearrangement followed by subsequent elimination. Other examples of bioorthogonal cleavage reactions that are not based on the ligation reactions have been reported, such as the reaction of *N*-oxides with boron reagents (**Scheme 39**).[223]

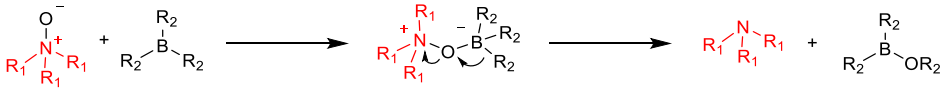

Scheme 39. Decaging of *N*-oxides with boron reagents.

Although several bioorthogonal decaging reactions have been reported, they have not been widely utilised. This is likely due to the fact that they suffer from slow reaction rates and the reagents undergo oxidation (Staudinger) or react with biological nucleophiles (SPAAC). Therefore, they cannot compete with the rapid IEDDA reaction for *in vivo* and cellular applications.

1.3.5 TCO-tetrazine IEDDA decaging

Small molecule triggers are advantageous over metal/photo-triggers since they provide a controlled, non-invasive method that does not require the use of a catalyst. The Robillard group showed that the IEDDA reaction could be adapted for fast decaging by placing an alcohol substituent in the allylic position of TCO, where it is appropriately placed to eliminate upon tautomerisation of the 4,5-dihydropyridazine (**Scheme 40**).[224]

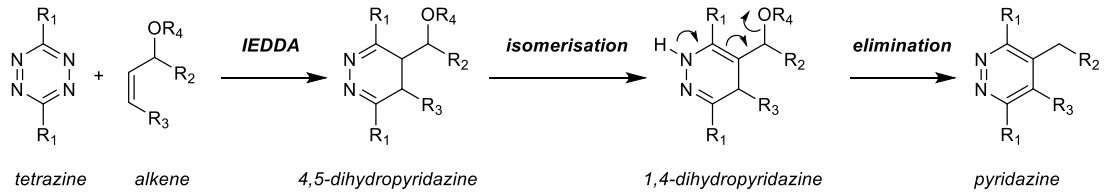

Scheme 40. IEDDA decaging reaction between a tetrazine and alkene.

This reaction was applied to decage a TCO-carbamate-Dox prodrug (**56**) *in vitro* through a click-to-release strategy (**Scheme 41**).[224] The axial isomer reacted 16 times faster with DiPy-Tz (**15**,

k_2 = 57.7 $M^{-1} s^{-1}$ in MeCN) than the equatorial (k_2 = 0.37 $M^{-1} s^{-1}$), which was attributed to the sterically hindered approach of the tetrazine to the equatorial isomer. Despite this fast rate of cycloaddition, only 7% free doxorubicin was released after 3 h. 3-methyl-6-(pyridin-2'-yl)-1,2,4,5-tetrazine (MePy-Tz) and DiMe-Tz resulted in much faster release rates (55% complete in 3 min and 79% complete in 16 min, respectively) even though the cycloaddition step was an order of magnitude slower. The prodrug (**56**) showed significantly reduced toxicity in A431 tumour cells (EC_{50} = 3.834 µM) compared to the parent drug (EC_{50} = 0.037 µM) and a combination of the prodrug and DiMe-Tz almost completely restored cytotoxicity (EC_{50} = 0.049 µM).[224]

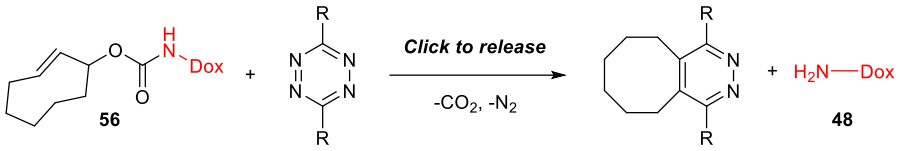

Scheme 41. Click to release strategy for activation of a TCO-carbamate-Dox prodrug (**56**) *in vitro*.

The IEDDA decaging reaction consists of two steps: a cycloaddition followed by an elimination step. Initial studies showed that DiPy-Tz resulted in a fast cycloaddition, but negligible drug release occurred. On the other hand, DiMe-Tz resulted in the highest percent of drug release even with a slow rate of cycloaddition. The effect of tetrazine substituents was then studied and it was shown that EWGs enhance the rate of cycloaddition but hinder the rate of elimination (due to the formation of a stable cycloaddition intermediate).[225] Therefore, a non-EWG is required for efficient elimination and optimised, asymmetric tetrazines bearing one EWG and one small alkyl non-EWG were reported (**Figure 6**). Asymmetric tetrazine **57** showed the highest decaging efficiency *in vitro* while **58** performed better in cells (90% decaging in 4 min), likely due to the poor membrane permeability of the OH group in **57** reducing the decaging efficiency in cells).

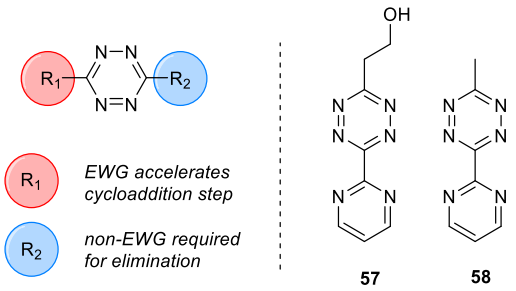

Figure 6. Electronic effects of tetrazine substituents on the rate of decaging.

TCO-tetrazine decaging often results in incomplete release and detailed studies concluded that this was due to the formation of a dead-end tricyclic product as a result of cyclisation of the carbamate amine onto the tetrazine (**Scheme 42**).[226] This dead-end pathway could be completely prevented by utilising a tertiary amine, however, it is not always practical to modify the N on the drug.

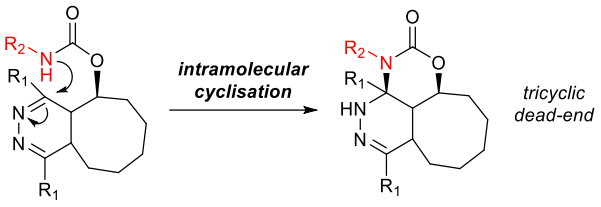

Scheme 42. Formation of a dead-end tricyclic product results in incomplete release.

The same study showed that the decaging is pH dependent, with higher rates and yields of release observed at acidic pH. Since the click reaction is rapid, it is likely that the pH affects the rate of the tautomerisation step. An alternative to lowering the pH of the reaction is to use carboxylic acid-functionalised tetrazines such as **59**, which provide a nearby proton source and accelerate the rate of tautomerisation. In addition, complete release was observed as rapid tautomerisation disfavours the dead-end cyclisation.

Asymmetric tetrazines can react with functionalised TCO in two orientations: head-to-head or head-to-tail (**Scheme 43**). The click orientation favours a particular isomerisation pathway due to assisted H transfer from the vicinal carboxylic acid. It was shown that the head-to-head isomer preferentially forms the releasing isomer, whereas the head-to-tail isomer favours formation of the non-releasing isomer.[226]

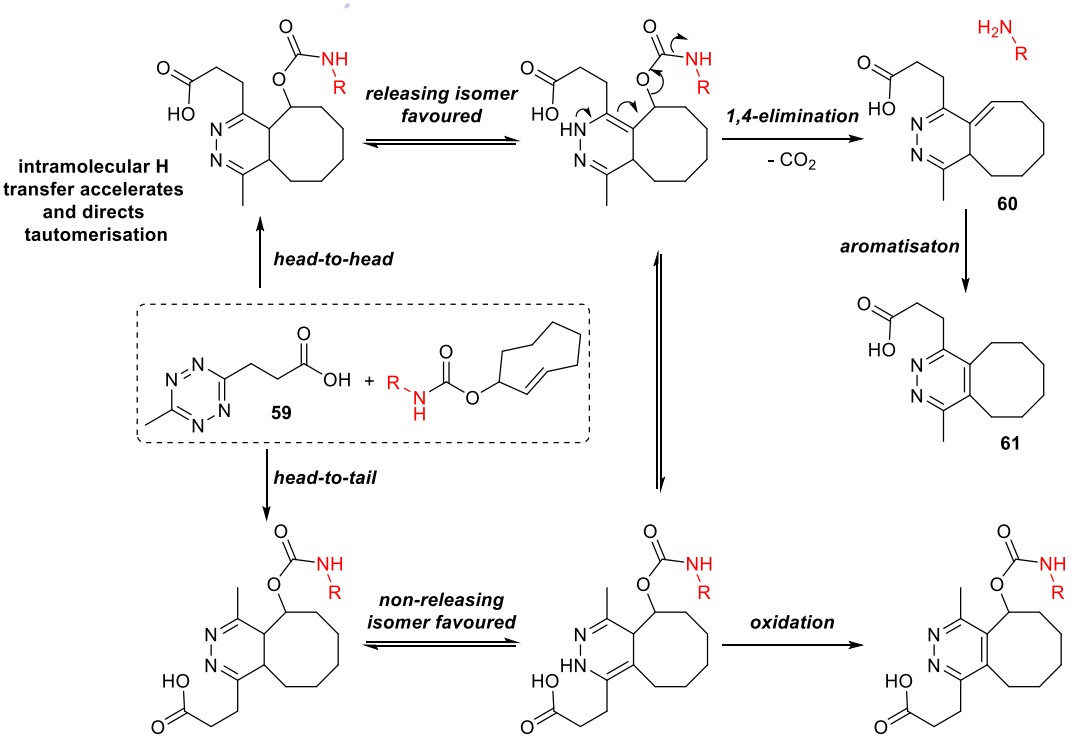

Scheme 43. Mechanistic studies of the TCO-tetrazine decaging reaction found that carboxylic acid-functionalised tetrazine **59** enhanced the rate of tautomerisation and drug release.

Following on from this, the group of van Kasteren reported a class of amino-ethyl functionalised tetrazines (**62** and **64**) that give rapid and pH independent release.[227] Under the biologically relevant pH range (pH 3.5–7.5), the amino ethyl group is protonated and can function as an intramolecular proton source, enhancing the rate of tautomerisation. In addition, it can also catalyse the elimination step through close proximity to either the dihydropyridazine or the carbamate (**Scheme 44**). It was demonstrated that the presence of an aminoethyl group leads to a 4-fold increase in elimination rate when compared to the carboxylic acid group and this can be increased a further 4.4-fold by the presence of EWGs.

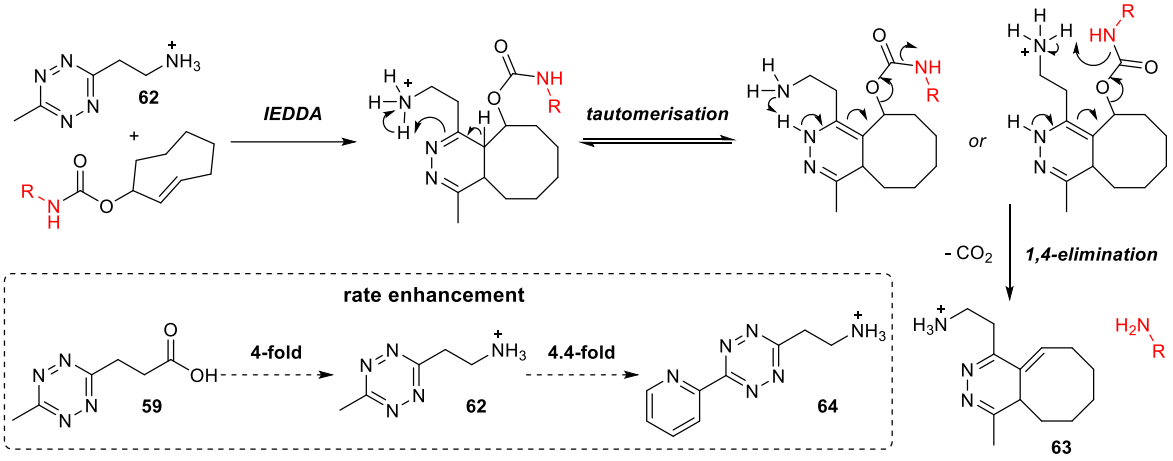

Scheme 44. Aminoethyl-functionalised tetrazines for rapid and pH independent elimination.

1.3.6 Applications of TCO-tetrazine IEDDA decaging

Mejia-Oneto reported a 'catch and release' strategy for controlled tissue-specific drug release from a TCO-carbamate-Dox (**56**) *in vivo* (**Scheme 45**).[228] This method involves installing a tetrazine-modified hydrogel at the site of the tumour in mice, followed by intravenous injection of prodrug **56** (75 times less active against HT1080 cells than doxorubicin (**84**)), which circulates around the body. When close to the hydrogel, the bioorthogonal reaction occurs (the 'catch' step), which traps and concentrates the prodrug at the site of the tumour. Tautomerisation and release of the active drug then occurs. This method was applied to mice bearing xenograft soft tissue sarcoma tumours and tumour remission occurred in 50% of cases, with fewer side effects observed compared to standard doxorubicin treatment. This approach has also been applied to the concentration and activation of systemically administered antibiotic prodrugs *in vivo*.[229] The presence of multiple tetrazines on the hydrogel enabled the activation of several doses of prodrug. However, since this method requires instalment of a hydrogel at the target site, it is mainly limited to the treatment of resectable tumours.

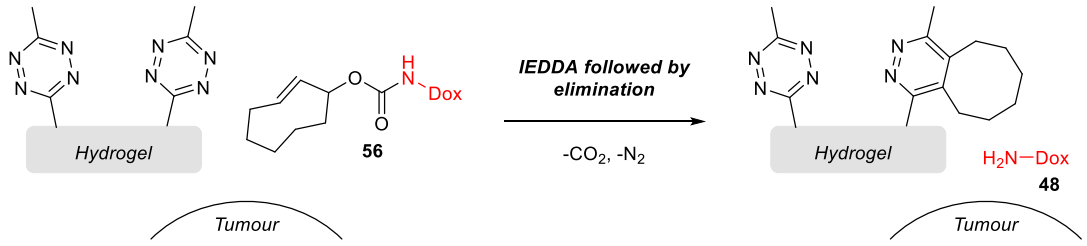

Scheme 45. Catch and release strategy for tissue-specific prodrug activation *in vivo*.

In an alternative strategy, the Robillard group developed an ADC containing a bifunctional TCO linker (**65**) that enabled targeted drug release in mice (**Scheme 46**).[230] The TCO-carbamate prodrug was attached to an antibody via functionalisation of TCO with an activated succinimidyl ester. When reacted with a tetrazine ≈ 65% decaging was observed after 2 minutes in PBS, and ≈ 25% in mouse serum. Isomerisation of the *trans*-alkene in the TCO-carbamate prodrug occurs in biological systems due to the presence of copper ions. Importantly, this does not lead to off-target drug release. However, it limits the utility of the hydrogel approach as deactivation of the prodrug may occur before it can reach the tetrazine-modified hydrogel. On the other hand, the ADC displayed good stability *in vivo* with a half-life almost identical to the free antibody, due to steric hindrance preventing this deactivating isomerisation from occurring.[98] This highlights the fact that the ADC affects the stability and reactivity of the caging group. Importantly, when applied to a tumour xenograft in mice, the ADC showed excellent tumour uptake and reaction occurred with a radiolabelled tetrazine. It was shown that good levels of free doxorubicin were retained in the tumour, however it was not shown that this resulted in tumour shrinkage or increased survival of the mice. Although this was a huge breakthrough as the first example of ADC activation using metal-free bioorthogonal chemistry, there are still several factors which limit its widespread application, including the challenging 11-step synthesis (which requires a specialised UV-irradiation under flow).[230]

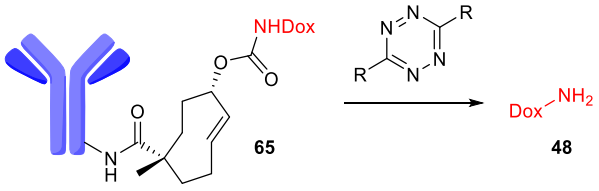

Scheme 46. 1st generation ADC (**65**) containing a bifunctional TCO linker than can be cleaved upon reaction with a tetrazine to release the free drug.

Following on from this, the Robillard group reported the first example of therapy using bioorthogonal decaging in tumour-bearing mice.[231] An ADC (**66**) consisting of a cytotoxic payload, monomethyl auristatin E (MMAE, **67**), conjugated to the cysteine residues in a diabody via a bifunctional TCO linker, was developed for targeting non-internalising receptors (**Scheme 47**). Near-quantitative drug release

was achieved by the use of new tetrazine derivatives. It was found that installing a DOTA chelate on the tetrazine reduced the rate of clearance and, therefore, increased the decaging yield. It also enabled direct imaging of the tetrazine trigger, which was used to show that a good distribution occurred throughout the tumour. The ADC showed selective uptake in the tumour and fast blood clearance. Importantly, a potent therapeutic effect was observed in two mouse xenograft models. In the same models, an analogous ADC bearing the Val-Cit linker that is cleaved intracellularly by proteases failed to control tumour growth. This work expands the scope of ADCs to non-internalising receptors and, therefore, the range of solid tumours that can be treated using ADC therapy. It also highlights the potential of small molecule-triggered decaging reactions for therapeutics.

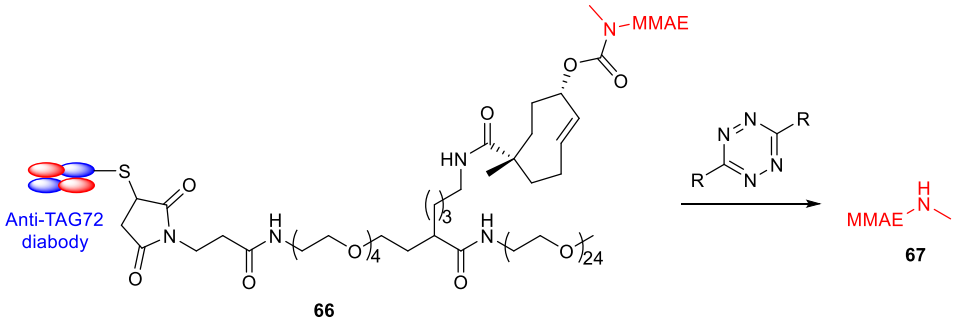

Scheme 47. 2nd generation ADC (**66**) containing a bifunctional TCO linker. *In vivo* decaging resulted in tumour shrinkage.

Recently, Robillard reported a reverse strategy in which TCO is used as the activator to trigger release from tetrazine methylene-carbamate linkers (**Scheme 48**).[232] Upon IEDDA cycloaddition, a 4,5-dihydropyridazine is formed, which selectively tautomerises to the 2,5-isomer. This then undergoes 1,4-elimination to release the amine. Previously, the reactivity of TCO was reduced due to the requirement of an allylic substituent bearing the payload.[224] Additionally, in a pretargeting strategy, the targeting moiety must be stable, which prevents the use of more reactive s-TCO derivatives. Since the trigger has a shorter exposure to *in vivo* conditions, the stability requirements are not as strict. Therefore, it was proposed that by using TCO as the trigger, the reaction rate could be increased through the use of more reactive TCOs (unsubstituted TCO (**16**) and s-TCO (**17**)).[232] Indeed, reaction in 25% MeCN/PBS with TCO (**16**) was 5 times faster (k_2 = 287 M^{-1} s^{-1}, for the cycloaddition) than tetrazine-triggered cleavage of a TCO-carbamate (k_2 = 57.7 M^{-1} s^{-1}). By using s-TCO, a rate (k_2 = 23800 M^{-1} s^{-1}) 3 orders of magnitude higher than the TCO-carbamate was achieved. However, the reaction displayed much slower release kinetics ($t_{1/2}$ = 20 h in 25% MeCN/PBS and it was predicted to be complete in < 3h in aqueous conditions).

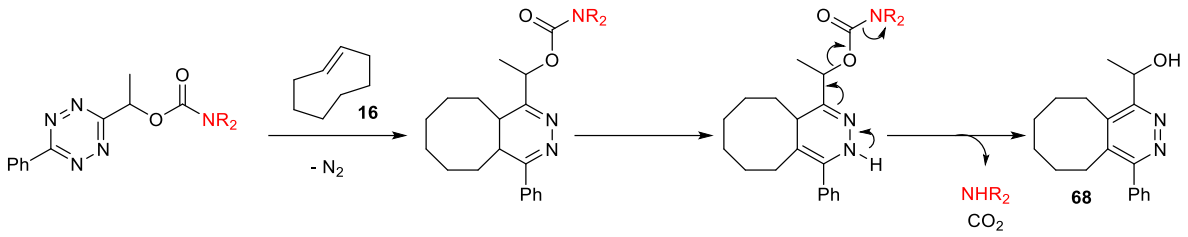

Scheme 48. TCO-triggered cleavage of tetrazine methylene-carbamate linkers.

An ADC (**69**) containing a cleavable tetrazine linker was synthesised and reacted with TCO (**16**) or s-TCO (**17**) in PBS to give decaging yields of 90% and 63%, respectively (**Scheme 49**).[232] Treatment of the ADC with a DOTA-PEG-s-TCO conjugate in human colorectal cancer cells resulted in reinstation of the cytotoxicity upon release of **67**. At low concentrations in PBS, 37 °C, the cycloaddition reaction of the Tz-ADC with DOTA-PEG-s-TCO was complete within 1 min, whereas under identical conditions, the previously reported reaction of TCO-ADC and DOTA-Tz had a half-life of 3 h. Pretargeting strategies often require a large excess of the activator. However, in this case the high rate of cycloaddition enables lower doses to be used. Finally, tetrazine linkers are easier to synthesise than TCO linkers, which makes this strategy more widely applicable. Tetrazine protecting groups hold great potential and may offer improved cycloaddition kinetics and ADC stability compared to TCO.

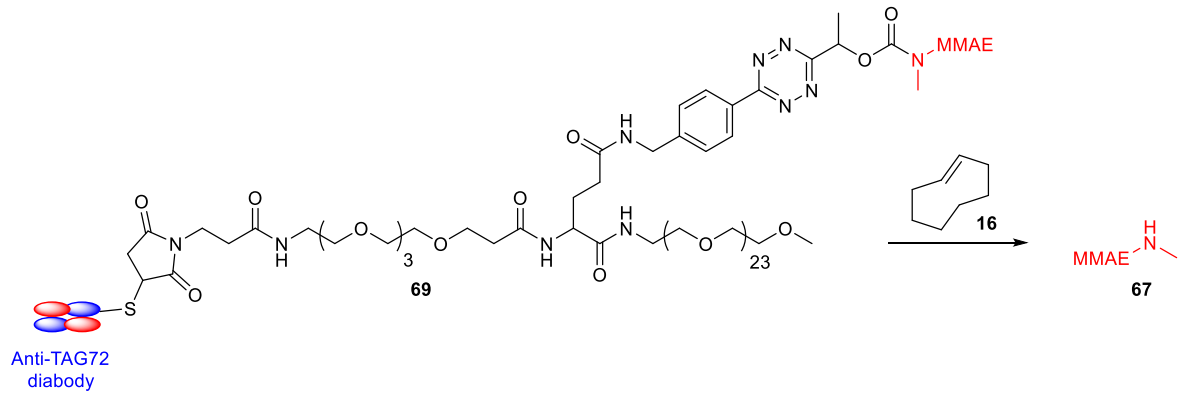

Scheme 49. ADC containing a cleavable tetrazine linker that released the active drug **67** upon reaction with TCO.

An alternative method for spatiotemporally controlled prodrug activation was achieved by using an enzyme, that is overexpressed in cancer cells, to trigger supramolecular self-assembly.[233] This resulted in accumulation of the tetrazine trigger inside cancer cells and when treated with a TCO-Dox prodrug (**56**), tumour inhibition in mice was achieved. In another example, image-guided prodrug activation has been achieved through the use of magnetic iron oxide NPs modified with both tetrazine and a fluorophore.[234] After fluorescent imaging to confirm accumulation of the NPs inside breast cancer cells, TCO-Dox prodrug **56** was added to trigger release of the active drug. Finally, a TCO-

thiocarbamate has also been described for the release of carbonyl sulfide, which is converted to H_2S by carbonic anhydrase.[235]

The TCO-tetrazine reaction has also been utilised for controlling cell function, such as the chemically-controlled activation of protected enzymes.[236,237] The activity of the enzyme was masked through genetic incorporation of TCO-caged lysine and it was then demonstrated that reaction with a tetrazine successfully restored the catalytic activity of the enzyme in mammalian cells[236,237] and mice.[237] In a second example, the controlled activation of T-cells was demonstrated both *in vitro* and *in vivo*.[238] Epitopes that are essential for T-cell activation were caged by modification of a key lysine residue with *cis*-CO, TCO or bifunctional TCO protecting groups. Upon addition of a tetrazine the free lysine was released from the TCO protecting groups, which enabled epitope recognition and T-cell activation. A bifunctional TCO protecting group containing an additional polar group resulted in the highest solubility and decaging yield. In another case, siRNA molecules were inactivated by conjugation to NPs through a bifunctional TCO linker.[239] After accumulation in cells, addition of a tetrazine resulted in linker cleavage and activation of siRNA, leading to RNA interference and gene silencing in cells.

Alternative applications include cell-selective proteome labelling.[240] This is achieved by using an antibody-tetrazine conjugate to target specific cells, followed by addition of a TCO-protected nucleoside puromycin. Upon IEDDA decaging at the target site, the TCO protecting group is removed, enabling incorporation of puromycin into protein synthesis. In a heterogeneous cell mixture, labelling was only observed in cells expressing the antigen. The TCO-tetrazine reaction has also been applied to the High-Performance Liquid Chromatography (HPLC)-free synthesis of RNA.[241] This method incorporates a cleavable TCO linker in the final coupling step, enabling selective trapping of the product onto tetrazine-modified agarose after cleavage from the solid support. By using a tetrazine that results in slow elimination, all by-products can be filtered from the resin before the TCO group is cleaved to generate the desired product.

1.3.7 Other tetrazine-triggered decaging reactions

Other examples of tetrazine-mediated IEDDA decaging have been reported, for example, the vinyl ether-tetrazine reaction for the release of alcohols.[242–244] Our group applied this to the decaging of a vinyl ether-duocarmycin prodrug (**70**) in live cells (**Scheme 50**).[242] This reaction is considerably slower than the TCO-tetrazine reaction (k_2 = 5.37 x 10^{-4} M^{-1} s^{-1} in 10% H_2O/DMF for the cycloaddition step) and the RDS was shown to be the initial cycloaddition step, the opposite of the TCO-carbamate IEDDA reaction.[224]

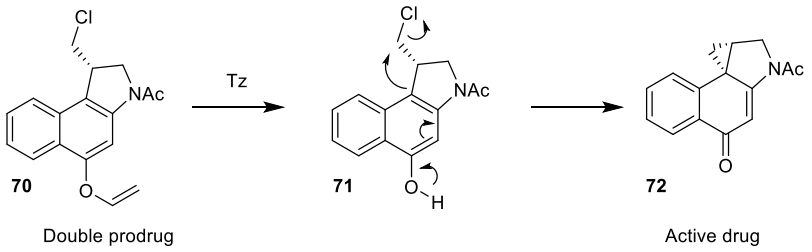

Scheme 50. Tetrazine-triggered decaging of a vinyl ether-duocarmycin prodrug.

The vinyl ether handle has also been connected to a self-immolative linker and applied to the tetrazine-triggered release of doxorubicin (**48**) via remote functional group activation followed by 1,6-elimination (**Scheme 51**).[243] Although the reaction of **73** with tetrazines suffers from a slow reaction rate, it has expanded the scope of functional groups that can be used in bioorthogonal chemistry. Following on from this work, vinylboronic acids (**75**) showed a slight improvement in reaction rate (k_2 = 3.3 x 10^{-3} M^{-1} s^{-1} in 25% PBS/MeOH) compared to vinyl ethers.[245] In this case, it is essential that the tetrazine contains substituents that can coordinate to boron (for example, pyridyl).

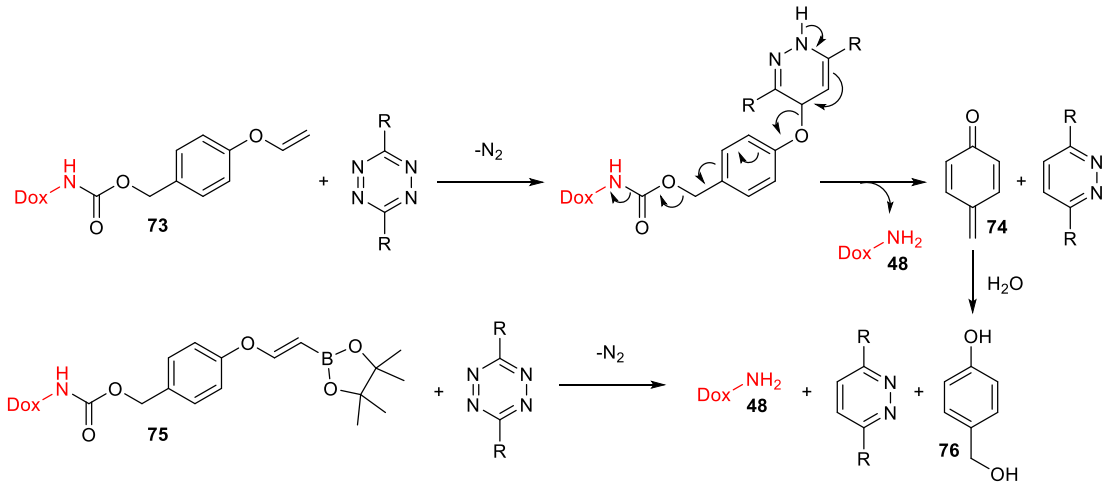

Scheme 51. Tetrazine-triggered decaging of vinyl ether **73** and vinylboronic acid **75** self-immolative linkers to release doxorubicin (**48**).

Tetrazines have also been used for the cleavage of a benzonorbornadiene protecting group from amines (**Scheme 52**). Although this reaction is also significantly slower than the TCO-carbamate reaction (k_2 = 0.028 M^{-1} s^{-1} in 10% H_2O/DMSO for the cycloaddition step), it offers other advantages, such as the simple synthesis of the benzonorbornadiene probes and the high stability of the probe under physiological conditions.[246]

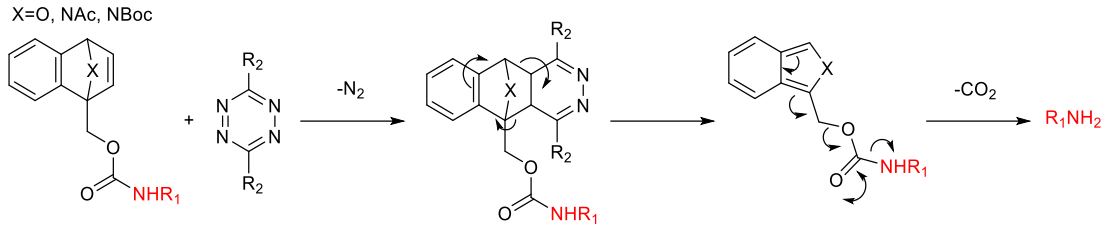

Scheme 52. Benzonorbornadiene reaction with tetrazines for the release of primary amines.

Recently, 3-isocyanopropyl (ICPr) protecting groups have been cleaved by reaction with tetrazine, resulting in the release of drugs containing amines (doxorubicin and mitomycin C), alcohols (SN-38) and thiols (mercaptopurine) *in vitro* (**Scheme 53**).[247] The isocyano group undergoes a [4+1] cycloaddition with the tetrazine to generate a pyrazole-imine intermediate which is then hydrolysed to a 3-oxypropyl species. β-elimination then occurs to release the molecule of interest and acrolein (**77**), a highly toxic compound, which may be a limitation of this reaction. Advantages include fast kinetics, near-quantitative yields and the synthetic ease of the protecting group. This reaction holds great potential as the isonitrile group is much smaller and more hydrophilic than TCO, potentially making it a more useful bioorthogonal handle. Tetrazine-modified beads were then implanted in zebrafish embryos and the release of mexiletine (a voltage-gated sodium channel blocker) was successfully shown to cause a decrease in heart rate.

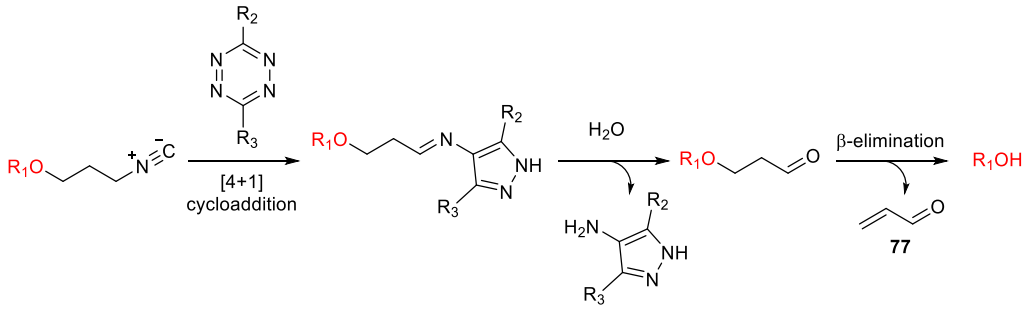

Scheme 53. Tetrazine-triggered decaging of isonitriles to release a free alcohol.

The use of tetrazines as protecting groups has also been reported. In an early example, a pyridazine microRNA 21 inhibitor (**80**) was masked as a tetrazine (**78**) and reaction with a vinyl prodrug (**79**) of camptothecin (CPT, **81**) resulted in dual drug release (**Scheme 54**).[248] An increased cytotoxic effect was observed in live cells compared to activation of either prodrug individually.

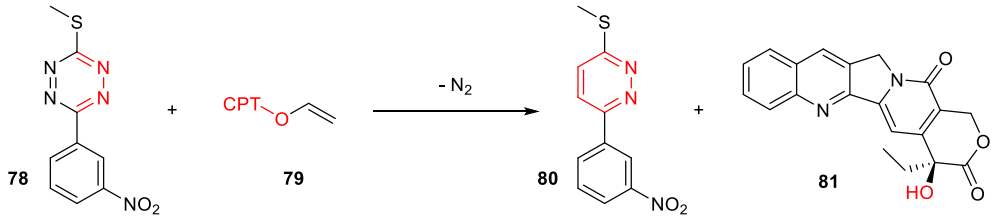

Scheme 54. Prodrug-prodrug activation strategy for dual drug release.

Tetrazylmethyl (TzMe)-based protecting groups that react with isonitriles in near-quantitative yield to release amines and alcohols have also been reported (**Scheme 55**).[249] It was shown that reaction with other alkenes, such as TCO and cyclopropene, resulted in low release yields. By reacting a TzMe-protected fluorescein with an ICPr-protected resorufin, the release of two fluorophores was achieved by a single bioorthogonal decaging reaction. Most reported examples of dual release rely on the use of two orthogonal reactions. However, this approach requires four reagents, which would be challenging *in vivo*. The ability to release two molecules from a single reaction is more useful and may enable the controlled release of synergistic drug combinations.

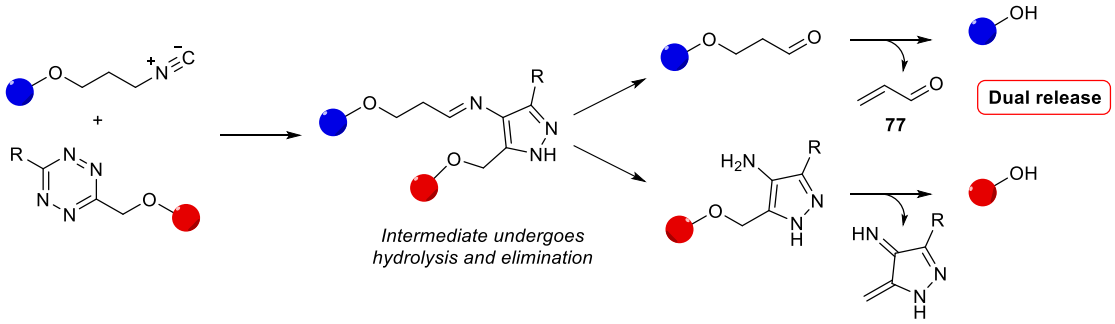

Scheme 55. Dual release from a single bioorthogonal reaction between TzMe-groups and ICPr handles.

In another example of tetrazines being used as protecting groups, Tz-Dox prodrugs were selectively decaged in mitochondria through the use of concentration-dependent chemistry.[250] The reaction involved tetrazine-cyclooctyne ligation, followed by lactonisation and elimination of the free drug (**Scheme 56**). This is a unique example that utilises rationally designed chemistry to remove a tetrazine protecting group from a drug. Both the Tz-prodrug (**82**) and the cyclooctyne trigger were connected to triphenylphosphonium (TPP), which is known to be enriched in mitochondria. In circulation, both reactants are present in low concentrations and no decaging occurs. After enrichment in the mitochondria, reactant concentration is enhanced and site-selective drug delivery occurs. Since this targeting approach relies on small molecules, it has the advantage of being able to target subcellular compartments.

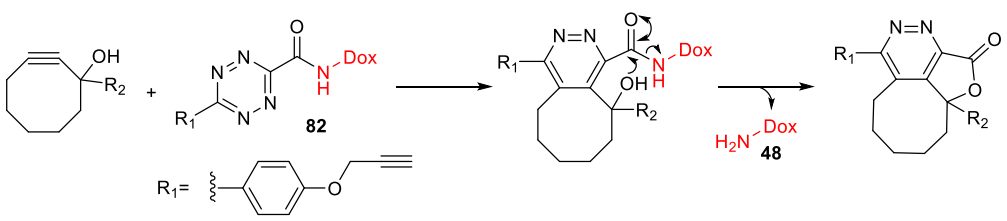

Scheme 56. Cyclooctyne-triggered removal of tetrazine protecting groups for activation of a doxorubicin prodrug.

1.3.8 Project aims

The development of bioorthogonal decaging reactions has provided methods for site-specific drug release, which offer a greater degree of control compared to prodrug activation by endogenous factors. The IEDDA reaction demonstrates particularly high selectivity and fast kinetics and, for these reasons, it remains the bioorthogonal reaction of choice. Its *in vivo* application for the release of amine containing drugs has been described above and this highlights the therapeutic potential for bioorthogonal bond-cleavage chemistry. However, further work is required to make this strategy more widely applicable by increasing the number of targets, antibodies and payloads that can be used. In addition, the pharmacokinetics of the current bioorthogonal reactions need improving. Due to the need for the selective accumulation and reactivity of the two components at the desired tissue, the reagent stability, as well as the reaction kinetics and selectivity, must be extremely high. Additionally, the reagents should be easy to synthesise in order to enable the widespread use of the reaction. All approaches to date have some issues and therefore, the aim of this PhD was to investigate alternative mechanisms and approaches using the IEDDA reaction.

Bioorthogonal decaging reactions have mainly been limited to the release of amines with some examples of alcohol release also reported. Although amines are common in small molecule drugs, they are not always present. In addition, the amine may not be vital for the function of the drug meaning that chemical modification at this site does not lead to reduced activity. In order to develop a broadly applicable prodrug activation strategy, the bioorthogonal toolkit needs to be extended to encompass a wider range of functional groups. The aim of this PhD was to extend the IEDDA reaction to the release of alcohol and carboxylic acid functional groups in order to increase the range of drugs that can be used in this strategy (**Scheme 57**). Chapter 2 will cover the application of the IEDDA reaction to the release of carboxylic acids and chapter 3 will cover the release of alcohols.

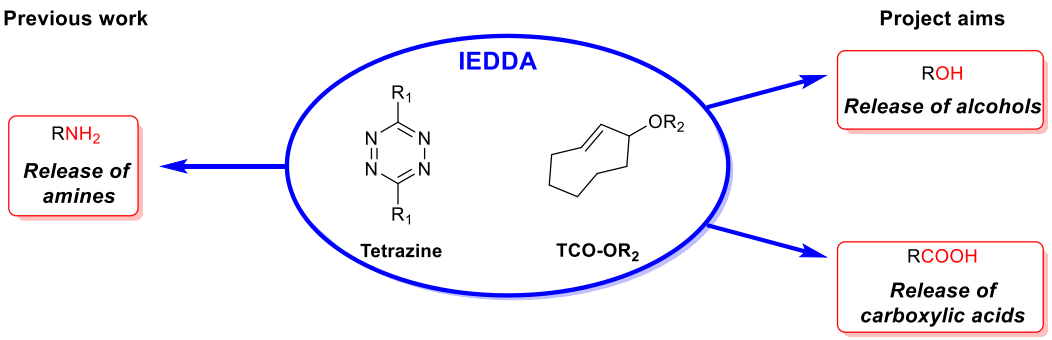

Scheme 57. Project aims: to extend the IEDDA reaction to the release of alcohol and carboxylic acid functional groups.

1.4 References for Chapter 1

[1] J. A. Prescher, C. R. Bertozzi, *Nat. Chem. Biol.* **2005**, *1*, 13–21.

[2] C. R. Bertozzi, *Acc. Chem. Res.* **2011**, *44*, 651–653.

[3] R. K. V. Lim, Q. Lin, *Chem. Commun.* **2010**, *46*, 1589–1600.

[4] H. C. Hang, C. Yu, D. L. Kato, C. R. Bertozzi, *Proc. Natl. Acad. Sci.* **2003**, *100*, 14846–14851.

[5] E. M. Sletten, C. R. Bertozzi, *Angew. Chem. Int. Ed.* **2009**, *48*, 6974–6998.

[6] X. Chen, Y. W. Wu, *Org. Biomol. Chem.* **2016**, *14*, 5417–5439.

[7] K. Lang, J. W. Chin, *ACS Chem. Biol.* **2014**, *9*, 16–20.

[8] D. M. Patterson, L. A. Nazarova, J. A. Prescher, *ACS Chem. Biol.* **2014**, *9*, 592–605.

[9] H. Wu, N. K. Devaraj, in *Inverse Electron-Demand Diels–Alder Bioorthogonal React.*, Springer, Switzerland, **2016**, pp. 109–130.

[10] E. M. Sletten, C. R. Bertozzi, *Acc. Chem. Res.* **2011**, *44*, 666–676.

[11] C. S. McKay, M. G. Finn, *Chem. Biol.* **2014**, *21*, 1075–1101.

[12] B. L. Oliveira, Z. Guo, G. J. L. Bernardes, *Chem. Soc. Rev.* **2017**, *46*, 4895–4950.

[13] E. Saxon, C. R. Bertozzi, *Science* **2000**, *287*, 2007–2010.

[14] Y. G. Gololobov, L. F. Kasukhin, *Tetrahedron* **1992**, *48*, 1353–1406.

[15] H. Staudinger, J. Meyer, *Helv. Chim. Acta* **1919**, *2*, 619–635.

[16] F. L. Lin, H. M. Hoyt, H. Van Halbeek, R. G. Bergman, C. R. Bertozzi, *J. Am. Chem. Soc.* **2005**, *127*, 2686–2695.

[17] J. A. Prescher, D. H. Dube, C. R. Bertozzi, *Nature* **2004**, *430*, 873–877.

[18] D. J. Vugts, A. Vervoort, M. Stigter-Van Walsum, G. W. M. Visser, M. S. Robillard, R. M. Versteegen, R. C. M. Vulders, J. D. M. Herscheid, G. A. M. S. Van Dongen, *Bioconjug. Chem.* **2011**, *22*, 2072–2081.

[19] E. Saxon, J. I. Armstrong, C. R. Bertozzi, *Org. Lett.* **2000**, *2*, 2141–2143.

[20] B. L. Nilsson, L. L. Kiessling, R. T. Raines, *Org. Lett.* **2000**, *2*, 1939–1941.

[21] A. M. Ahad, S. M. Jensen, J. C. Jewett, *Org. Lett.* **2013**, *15*, 5060–5063.

[22] A. Tam, R. T. Raines, *Methods Enzymol.* **2009**, *462*, 25–44.

[23] R. Huisgen, *Angew. Chem. Int. Ed.* **1963**, *2*, 565–598.

[24] N. J. Agard, J. A. Prescher, C. R. Bertozzi, *J. Am. Chem. Soc.* **2004**, *126*, 15046–15047.

[25] J. M. Baskin, J. A. Prescher, S. T. Laughlin, N. J. Agard, P. V. Chang, I. A. Miller, A. Lo, J. A. Codelli, C. R. Bertozzi, *Proc. Natl. Acad. Sci.* **2007**, *104*, 16793–16797.

[26] J. A. Codelli, J. M. Baskin, N. J. Agard, C. R. Bertozzi, *J. Am. Chem. Soc.* **2008**, *130*, 11486–11493.

[27] S. T. Laughlin, J. M. Baskin, S. L. Amacher, C. R. Bertozzi, *Science* **2008**, *320*, 664–667.

[28] C. P. Ramil, Q. Lin, *Chem. Commun.* **2013**, *49*, 11007–11022.

[29] X. Ning, J. Guo, M. A. Wolfert, G.-J. Boons, *Angew. Chem. Int. Ed.* **2008**, *47*, 2253–2255.

[30] M. F. Debets, S. S. Van Berkel, S. Schoffelen, F. P. J. T. Rutjes, J. C. M. Van Hest, F. L. Van Delft, *Chem. Commun.* **2010**, *46*, 97–99.

[31] J. C. Jewett, E. M. Sletten, C. R. Bertozzi, *J. Am. Chem. Soc.* **2010**, *132*, 3688–3690.

[32] J. Dommerholt, S. Schmidt, R. Temming, L. J. A. Hendriks, F. P. J. T. Rutjes, J. C. M. van Hest, D. J. Lefeber, P. Friedl, F. L. van Delft, *Angew. Chem. Int. Ed.* **2010**, *49*, 9422–9425.

[33] G. de Almeida, E. M. Sletten, H. Nakamura, K. K. Palaniappan, C. R. Bertozzi, *Angew. Chem. Int. Ed.* **2012**, *51*, 2443–2447.

[34] X. Ning, R. P. Temming, J. Dommerholt, J. Guo, D. B. Ania, M. F. Debets, M. A. Wolfert, G. J. Boons, F. L. Van Delft, *Angew. Chem. Int. Ed.* **2010**, *49*, 3065–3068.

[35] C. S. McKay, J. A. Blake, J. Cheng, D. C. Danielson, J. P. Pezacki, *Chem. Commun.* **2011**, *47*, 10040–10042.

[36] B. C. Sanders, F. Friscourt, P. A. Ledin, N. E. Mbua, S. Arumugam, J. Guo, T. J. Boltje, V. V. Popik, G. J. Boons, *J. Am. Chem. Soc.* **2011**, *133*, 949–957.

[37] N. A. McGrath, R. T. Raines, *Chem. Sci.* **2012**, *3*, 3237–3240.

[38] K. E. Beatty, J. D. Fisk, B. P. Smart, Y. Y. Lu, J. Szychowski, M. J. Hangauer, J. M. Baskin, C. R. Bertozzi, D. A. Tirrell, *ChemBioChem* **2010**, *11*, 2092–2095.

[39] B. Amgarten, R. Rajan, N. Martínez-Sáez, B. L. Oliveira, I. S. Albuquerque, R. A. Brooks, D. G. Reid, M. J. Duer, G. J. L. Bernardes, *Chem. Commun.* **2015**, *51*, 5250–5252.

[40] S. S. van Berkel, A. (Ton) J. Dirks, M. F. Debets, F. L. van Delft, J. J. L. M. Cornelissen, R. J. M. Nolte, F. P. J. T. Rutjes, *ChemBioChem* **2007**, *8*, 1504–1508.

[41] M. L. Blackman, M. Royzen, J. M. Fox, *J. Am. Chem. Soc.* **2008**, *130*, 13518–13519.

[42] H. Stöckmann, A. A. Neves, S. Stairs, K. M. Brindle, F. J. Leeper, *Org. Biomol. Chem.* **2011**, *9*, 7303–7305.

[43] J. Tu, D. Svatunek, S. Parvez, A. C. Liu, B. J. Levandowski, H. J. Eckvahl, R. T. Peterson, K. N. Houk, R. M. Franzini, *Angew. Chem. Int. Ed.* **2019**, *58*, 9043–9048.

[44] E. G. Sander, W. P. Jencks, *J. Am. Chem. Soc.* **1968**, *90*, 6154–6162.

[45] D. Rideout, *Science* **1986**, *233*, 561–563.

[46] A. Dirksen, T. M. Hackeng, P. E. Dawson, *Angew. Chem. Int. Ed.* **2006**, *45*, 7581–7584.

[47] A. Dirksen, S. Dirksen, T. M. Hackeng, P. E. Dawson, *J. Am. Chem. Soc.* **2006**, *128*, 15602–15603.

[48] W. P. Jencks, *J. Am. Chem. Soc.* **1959**, *81*, 475–481.

[49] P. Agarwal, R. Kudirka, A. E. Albers, R. M. Barfield, G. W. de Hart, P. M. Drake, L. C. Jones, D. Rabuka, *Bioconjug. Chem.* **2013**, *24*, 846–851.

[50] P. Agarwal, J. Van Der Weijden, E. M. Sletten, D. Rabuka, C. R. Bertozzi, *Proc. Natl. Acad. Sci.* **2013**, *110*, 46–51.

[51] G. Liang, H. Ren, J. Rao, *Nat. Chem.* **2010**, *2*, 54–60.

[52] D. P. Nguyen, T. Elliott, M. Holt, T. W. Muir, J. W. Chin, *J. Am. Chem. Soc.* **2011**, *133*, 11418–11421.

[53] M. Yang, J. Li, P. R. Chen, *Chem. Soc. Rev.* **2014**, *43*, 6511–6526.

[54] S. V. Chankeshwara, E. Indrigo, M. Bradley, *Curr. Opin. Chem. Biol.* **2014**, *21*, 128–135.

[55] Y. A. Lin, J. M. Chalker, N. Floyd, G. J. L. Bernardes, B. G. Davis, *J. Am. Chem. Soc.* **2008**, *130*, 9642–9643.

[56] C. W. Tornøe, C. Christensen, M. Meldal, *J. Org. Chem.* **2002**, *67*, 3057–3064.

[57] V. V. Rostovtsev, L. G. Green, V. V. Fokin, K. B. Sharpless, *Angew. Chem. Int. Ed.* **2002**, *41*, 2596–2599.

[58] F. Wolbers, P. ter Braak, S. Le Gac, R. Luttge, H. Andersson, I. Vermes, A. van den Berg, *Electrophoresis* **2006**, *27*, 5073–5080.

[59] D. Soriano Del Amo, W. Wang, H. Jiang, C. Besanceney, A. C. Yan, M. Levy, Y. Liu, F. L. Marlow, P. Wu, *J. Am. Chem. Soc.* **2010**, *132*, 16893–16899.

[60] Y. Bai, X. Feng, H. Xing, Y. Xu, B. K. Kim, N. Baig, T. Zhou, A. A. Gewirth, Y. Lu, E. Oldfield, et al., *J. Am. Chem. Soc.* **2016**, *138*, 11077–11080.

[61] J. Clavadetscher, S. Hoffmann, A. Lilienkampf, L. Mackay, R. M. Yusop, S. A. Rider, J. J. Mullins, M. Bradley, *Angew. Chem. Int. Ed.* **2016**, *55*, 15662–15666.

[62] L. I. Willems, H. S. Overkleeft, S. I. Van Kasteren, *Bioconjug. Chem.* **2014**, *25*, 1181–1191.

[63] S. I. van Kasteren, B. I. Florea, H. S. Overkleeft, *Activity-Based Protein Profiling: From Chemical Novelty to Biomedical Stalwart*, Humana Press Inc., New York, **2017**.

[64] K. T. Barglow, B. F. Cravatt, *Nat. Methods* **2007**, *4*, 822–827.

[65] A. E. Speers, G. C. Adam, B. F. Cravatt, *J. Am. Chem. Soc.* **2003**, *125*, 4686–4687.

[66] A. E. Speers, B. F. Cravatt, *Chem. Biol.* **2004**, *11*, 535–546.

[67] H. Ovaa, P. F. Van Swieten, B. M. Kessler, M. A. Leeuwenburgh, E. Fiebiger, A. M. C. H. Van den Nieuwendijk, P. J. Galardy, G. A. Van der Marel, H. L. Ploegh, H. S. Overkleeft, *Angew. Chem. Int. Ed.* **2003**, *42*, 3626–3629.

[68] Y. A. Lin, O. Boutureira, L. Lercher, B. Bhushan, R. S. Paton, B. G. Davis, *J. Am. Chem. Soc.* **2013**, *135*, 12156–12159.

[69] J. Li, S. Lin, J. Wang, S. Jia, M. Yang, Z. Hao, X. Zhang, P. R. Chen, *J. Am. Chem. Soc.* **2013**, *135*, 7330–7338.

[70] N. Li, R. K. V. Lim, S. Edwardraja, Q. Lin, *J. Am. Chem. Soc.* **2011**, *133*, 15316–15319.

[71] E. Indrigo, J. Clavadetscher, S. V. Chankeshwara, A. Lilienkampf, M. Bradley, *Chem. Commun.* **2016**, *52*, 14212–14214.

[72] C. Vidal, M. Tomás-Gamasa, P. Destito, F. López, J. L. Mascareñas, *Nat. Commun.* **2018**, *9*, 1913.

[73] Y. Wang, C. I. Rivera Vera, Q. Lin, *Org. Lett.* **2007**, *9*, 4155–4158.

[74] A. Herner, Q. Lin, *Top. Curr. Chem.* **2016**, *374*, 1.

[75] Z. Yu, Y. Pan, Z. Wang, J. Wang, Q. Lin, *Angew. Chem. Int. Ed.* **2012**, *51*, 10600–10604.

[76] W. Song, Y. Wang, J. Qu, Q. Lin, *J. Am. Chem. Soc.* **2008**, *130*, 9654–9655.

[77] Y. Wang, W. J. Hu, W. Song, R. K. V. Lim, Q. Lin, *Org. Lett.* **2008**, *10*, 3725–3728.

[78] R. Rakhit, R. Navarro, T. Wandless, *Chem. Biol.* **2014**, *21*, 1238–1252.

[79] S. Arumugam, V. V. Popik, *J. Am. Chem. Soc.* **2011**, *133*, 15730–15736.

[80] A. A. Poloukhtine, N. E. Mbua, M. A. Wolfert, G. J. Boons, V. V. Popik, *J. Am. Chem. Soc.* **2009**, *131*, 15769–15776.

[81] C. A. K. Borrebaeck, A. C. Malmborg, C. Furebring, A. Michaelsson, S. Ward, L. Danielsson, M. Ohlin, *Bio/Technology* **1992**, *10*, 697–698.

[82] I. Nikić, T. Plass, O. Schraidt, J. Szymanski, J. A. G. Briggs, C. Schultz, E. A. Lemke, *Angew. Chem. Int. Ed.* **2014**, *53*, 2245–2249.

[83] X. Zhang, T. Dong, Q. Li, X. Liu, L. Li, S. Chen, X. Lei, *ACS Chem. Biol.* **2015**, *10*, 1676–1683.

[84] Q. Li, T. Dong, X. Liu, X. Lei, *J. Am. Chem. Soc.* **2013**, *135*, 4996–4999.

[85] R. A. Carboni, R. V. Lindsey, *J. Am. Chem. Soc.* **1959**, *81*, 4342–4346.

[86] N. K. Devaraj, R. Weissleder, S. A. Hilderbrand, *Bioconjug. Chem.* **2008**, *19*, 2297–2299.

[87] X. Fan, J. Li, P. R. Chen, *Natl. Sci. Rev.* **2017**, *4*, 300–302.

[88] A. D. De Araújo, J. M. Palomo, J. Cramer, M. Köhn, H. Schröder, R. Wacker, C. Niemeyer, K. Alexandrov, H. Waldmann, *Angew. Chem. Int. Ed.* **2005**, *45*, 296–301.

[89] A. D. De Araújo, J. M. Palomo, J. Cramer, O. Seitz, K. Alexandrov, H. Waldmann, *Chem. - A Eur. J.* **2006**, *12*, 6095–6109.

[90] D. L. Boger, *Chem. Rev* **1986**, *86*, 781–793.

[91] J. Balcar, G. Chrisam, F. X. Huber, J. Sauer, *Tetrahedron Lett.* **1983**, *24*, 1481–1484.

[92] A. Vázquez, R. Dzijak, M. Dračínský, R. Rampmaier, S. J. Siegl, M. Vrabel, *Angew. Chem. Int. Ed.* **2017**, *56*, 1334–1337.

[93] F. Thalhammer, U. Wallfahrer, J. Sauer, *Tetrahedron Lett.* **1990**, *31*, 6851–6854.

[94] N. L. Allinger, J. T. Sprague, *J. Am. Chem. Soc.* **1972**, *94*, 5734–5747.

[95] R. D. Bach, U. Mazur, I. Hamama, S. K. Lauderback, *Tetrahedron* **1972**, *28*, 1955–1963.

[96] K. J. Shea, J. S. Kim, *J. Am. Chem. Soc.* **1992**, *114*, 4846–4855.

[97] A. Darko, S. Wallace, O. Dmitrenko, M. M. Machovina, R. A. Mehl, J. W. Chin, J. M. Fox, *Chem. Sci.* **2014**, *5*, 3770–3776.

[98] R. Rossin, S. M. van den Bosch, W. ten Hoeve, M. Carvelli, R. M. Versteegen, J. Lub, M. S. Robillard, *Bioconjug. Chem.* **2013**, *24*, 1210–1217.

[99] S. J. Siegl, J. Galeta, R. Dzijak, A. Vázquez, M. Del Río-Villanueva, M. Dračínský, M. Vrabel, *ChemBioChem* **2019**, *20*, 886–890.

[100] M. R. Karver, R. Weissleder, S. A. Hilderbrand, *Bioconjug. Chem.* **2011**, *22*, 2263–2270.

[101] J. Yang, Y. Liang, J. Šečkutė, K. N. Houk, N. K. Devaraj, *Chem. - A Eur. J.* **2014**, *20*, 3365–3375.

[102] J.-E. Hoffmann, T. Plass, I. Nikić, I. V. Aramburu, C. Koehler, H. Gillandt, E. A. Lemke, C. Schultz, *Chem. - A Eur. J.* **2015**, *21*, 12266–12270.

[103] Ale Meijer, A. Sijbren Otto, J. B. F. N. Engberts, *J. Org. Chem* **1998**, *63*, 8989–8994.

[104] J. W. Wijnen, S. Zavarise, J. B. F. N. Engberts, M. Charton, *J. Org. Chem.* **1996**, *61*, 2001–2005.

[105] M. T. Taylor, M. L. Blackman, O. Dmitrenko, J. M. Fox, *J. Am. Chem. Soc.* **2011**, *133*, 9646–9649.

[106] R. D. Bach, *J. Am. Chem. Soc.* **2009**, *131*, 5233–5243.

[107] H. E. Murrey, J. C. Judkins, C. W. am Ende, T. E. Ballard, Y. Fang, K. Riccardi, L. Di, E. R. Guilmette, J. W. Schwartz, J. M. Fox, et al., *J. Am. Chem. Soc.* **2015**, *137*, 11461–11475.

[108] E. Kozma, I. Nikić, B. R. Varga, I. V. Aramburu, J. H. Kang, O. T. Fackler, E. A. Lemke, P. Kele, *ChemBioChem* **2016**, *17*, 1518–1524.

[109] W. D. Lambert, S. L. Scinto, O. Dmitrenko, S. J. Boyd, R. Magboo, R. A. Mehl, J. W. Chin, J. M. Fox, S. Wallace, *Org. Biomol. Chem.* **2017**, *15*, 6640–6644.

[110] H. Jendralla, *Tetrahedron* **1983**, *39*, 1359–1363.

[111] K. Tomooka, S. Miyasaka, S. Motomura, K. Igawa, *Chem. - A Eur. J.* **2014**, *20*, 7598–7602.

[112] J. Santucci, J. R. Sanzone, K. A. Woerpel, *European J. Org. Chem.* **2016**, *2016*, 2933–2943.

[113] Y. Fang, H. Zhang, Z. Huang, S. L. Scinto, J. C. Yang, C. W. Am Ende, O. Dmitrenko, D. S. Johnson, J. M. Fox, *Chem. Sci.* **2018**, *9*, 1953–1963.

[114] F. Carey, R. J. Sundberg, *Advanced Organic Chemistry: Part A: Structure and Mechanisms*, Springer Science & Business Media, **2013**.

[115] A. Krebs, K.-I. Pforr, W. Raffay, B. Thölke, W. A. König, I. Hardt, R. Boese, *Angew. Chem.* **1997**, *109*, 159–161.

[116] T. Shimizu, K. Shimizu, W. Ando, *J. Am. Chem. Soc.* **1991**, *113*, 354–355.

[117] R. J. Blizzard, D. R. Backus, W. Brown, C. G. Bazewicz, Y. Li, R. A. Mehl, *J. Am. Chem. Soc.* **2015**, *137*, 10044–10047.

[118] D. N. Kamber, Y. Liang, R. J. Blizzard, F. Liu, R. A. Mehl, K. N. Houk, J. A. Prescher, *J. Am. Chem. Soc.* **2015**, *137*, 8388–8391.

[119] S. B. Engelsma, L. I. Willems, C. E. van Paaschen, S. I. van Kasteren, G. A. van der Marel, H. S. Overkleeft, D. V. Filippov, *Org. Lett.* **2014**, *16*, 2744–2747.

[120] K. Lang, L. Davis, S. Wallace, M. Mahesh, D. J. Cox, M. L. Blackman, J. M. Fox, J. W. Chin, *J. Am. Chem. Soc.* **2012**, *134*, 10317–10320.

[121] S. Eising, F. Lelivelt, K. M. Bonger, *Angew. Chem. Int. Ed.* **2016**, *55*, 12243–12247.

[122] U. Rieder, N. W. Luedtke, *Angew. Chem. Int. Ed.* **2014**, *53*, 9168–9172.

[123] B. L. Oliveira, Z. Guo, O. Boutureira, A. Guerreiro, G. Jiménez-Osés, G. J. L. Bernardes, *Angew. Chem. Int. Ed.* **2016**, *55*, 14683–14687.

[124] N. Martínez-Sáez, S. Sun, D. Oldrini, P. Sormanni, O. Boutureira, F. Carboni, I. Compañón, M. J. Deery, M. Vendruscolo, F. Corzana, et al., *Angew. Chem. Int. Ed.* **2017**, *56*, 14963–14967.

[125] J. L. Seitchik, J. C. Peeler, M. T. Taylor, M. L. Blackman, T. W. Rhoads, R. B. Cooley, C. Refakis, J. M. Fox, R. A. Mehl, *J. Am. Chem. Soc.* **2012**, *134*, 2898–2901.

[126] T. Plass, S. Milles, C. Koehler, J. Szymański, R. Mueller, M. Wießler, C. Schultz, E. A. Lemke, *Angew. Chem. Int. Ed.* **2012**, *51*, 4166–4170.

[127] K. Lang, L. Davis, J. Torres-Kolbus, C. Chou, A. Deiters, J. W. Chin, *Nat. Chem.* **2012**, *4*, 298–304.

[128] A. Borrmann, S. Milles, T. Plass, J. Dommerholt, J. M. M. Verkade, M. Wießler, C. Schultz, J. C. M. van Hest, F. L. van Delft, E. A. Lemke, *ChemBioChem* **2012**, *13*, 2094–2099.

[129] K. Wang, A. Sachdeva, D. J. Cox, N. W. Wilf, K. Lang, S. Wallace, R. A. Mehl, J. W. Chin, *Nat. Chem.* **2014**, *6*, 393–403.

[130] T. Peng, H. C. Hang, *J. Am. Chem. Soc.* **2016**, *138*, 14423–14433.

[131] K. S. Yang, G. Budin, T. Reiner, C. Vinegoni, R. Weissleder, *Angew. Chem. Int. Ed.* **2012**, *51*, 6598–6603.

[132] T. S. Elliott, F. M. Townsley, A. Bianco, R. J. Ernst, A. Sachdeva, S. J. Elsässer, L. Davis, K. Lang, R. Pisa, S. Greiss, et al., *Nat. Biotechnol.* **2014**, *32*, 465–472.

[133] C. Uttamapinant, J. D. Howe, K. Lang, V. Beránek, L. Davis, M. Mahesh, N. P. Barry, J. W. Chin, *J. Am. Chem. Soc.* **2015**, *137*, 4602–4605.

[134] I. Nikić, G. Estrada Girona, J. H. Kang, G. Paci, S. Mikhaleva, C. Koehler, N. V. Shymanska, C. Ventura Santos, D. Spitz, E. A. Lemke, *Angew. Chem. Int. Ed.* **2016**, *55*, 16172–16176.

[135] S. P. Brown, A. B. Smith, *J. Am. Chem. Soc.* **2015**, *137*, 4034–4037.

[136] L. Xu, M. Raabe, M. M. Zegota, J. C. F. Nogueira, V. Chudasama, S. L. Kuan, T. Weil, *Org. Biomol. Chem.* **2020**, *18*, 1140–1147.

[137] A. Rutkowska, D. W. Thomson, J. Vappiani, T. Werner, K. M. Mueller, L. Dittus, J. Krause, M. Muelbaier, G. Bergamini, M. Bantscheff, *ACS Chem. Biol.* **2016**, *11*, 2541–2550.

[138] S. L. Scinto, O. Ekanayake, U. Seneviratne, J. E. Pigga, S. J. Boyd, M. T. Taylor, J. Liu, C. W. Am Ende, S. Rozovsky, J. M. Fox, *J. Am. Chem. Soc.* **2019**, *141*, 10932–10937.

[139] H. Wu, B. T. Cisneros, C. M. Cole, N. K. Devaraj, *J. Am. Chem. Soc.* **2014**, *136*, 17942–17945.

[140] J. Šečkute, J. Yang, N. K. Devaraj, *Nucleic Acids Res.* **2013**, *41*, e148.

[141] N. K. Devaraj, R. Weissleder, *Acc. Chem. Res.* **2011**, *44*, 816–827.

[142] H. Zhang, K. T. Dicker, X. Xu, X. Jia, J. M. Fox, *ACS Macro Lett.* **2014**, *3*, 727–731.

[143] K. T. Dicker, J. Song, A. C. Moore, H. Zhang, Y. Li, D. L. Burris, X. Jia, J. M. Fox, *Chem. Sci.* **2018**, *9*, 5394–5404.

[144] H. Zhang, W. S. Trout, S. Liu, G. A. Andrade, D. A. Hudson, S. L. Scinto, K. T. Dicker, Y. Li, N. Lazouski, J. Rosenthal, et al., *J. Am. Chem. Soc.* **2016**, *138*, 5978–5983.

[145] S. Liu, H. Zhang, R. A. Remy, F. Deng, M. E. Mackay, J. M. Fox, X. Jia, *Adv. Mater.* **2015**, *27*, 2783–2790.

[146] J. B. Haun, N. K. Devaraj, S. A. Hilderbrand, H. Lee, R. Weissleder, *Nat. Nanotechnol.* **2010**, *5*, 660–665.

[147] H. Lebraud, D. J. Wright, C. N. Johnson, T. D. Heightman, *ACS Cent. Sci.* **2016**, *2*, 927–934.

[148] L. Qiu, W. Mao, H. Yin, H. Tan, D. Cheng, H. Shi, *Contrast Media Mol. Imaging* **2019**, 9182476.

[149] R. Rossin, M. S. Robillard, *Curr. Opin. Chem. Biol.* **2014**, *21*, 161–169.

[150] R. Rossin, P. Renart Verkerk, S. M. van den Bosch, R. C. M. Vulders, I. Verel, J. Lub, M. S. Robillard, *Angew. Chem. Int. Ed.* **2010**, *49*, 3375–3378.

[151] R. Rossin, S. M. J. van Duijnhoven, T. Läppchen, S. M. van den Bosch, M. S. Robillard, *Mol. Pharm.* **2014**, *11*, 3090–3096.

[152] Z. Li, H. Cai, M. Hassink, M. L. Blackman, R. C. D. Brown, P. S. Conti, J. M. Fox, *Chem. Commun.* **2010**, *46*, 8043–8045.

[153] R. Selvaraj, S. Liu, M. Hassink, C. W. Huang, L. P. Yap, R. Park, J. M. Fox, Z. Li, P. S. Conti, *Bioorganic Med. Chem. Lett.* **2011**, *21*, 5011–5014.

[154] T. Reiner, E. J. Keliher, S. Earley, B. Marinelli, R. Weissleder, *Angew. Chem. Int. Ed.* **2011**, *50*, 1922–1925.

[155] J. C. Knight, S. Richter, M. Wuest, J. D. Way, F. Wuest, *Org. Biomol. Chem.* **2013**, *11*, 3817–3825.

[156] M. Wang, D. Svatunek, K. Rohlfing, Y. Liu, H. Wang, B. Giglio, H. Yuan, Z. Wu, Z. Li, J. Fox, *Theranostics* **2016**, *6*, 887–895.

[157] E. M. F. Billaud, S. Belderbos, F. Cleeren, W. Maes, M. Van De Wouwer, M. Koole, A. Verbruggen, U. Himmelreich, N. Geukens, G. Bormans, *Bioconjug. Chem.* **2017**, *28*, 2915–2920.

[158] M. Wang, R. Vannam, W. D. Lambert, Y. Xie, H. Wang, B. Giglio, X. Ma, Z. Wu, J. Fox, Z. Li, *Chem. Commun.* **2019**, *55*, 2485–2488.

[159] N. K. Devaraj, G. M. Thurber, E. J. Keliher, B. Marinelli, R. Weissleder, *Proc. Natl. Acad. Sci.* **2012**, *109*, 4762–4767.

[160] J. Zhu, S. Li, C. Wängler, B. Wängler, R. B. Lennox, R. Schirrmacher, *Chem. Commun.* **2015**, *51*, 12415–12418.

[161] O. Keinänen, X.-G. Li, N. K. Chenna, D. Lumen, J. Ott, C. F. M. Molthoff, M. Sarparanta, K. Helariutta, T. Vuorinen, A. D. Windhorst, et al., *ACS Med. Chem. Lett.* **2016**, *7*, 62–66.

[162] M. Rashidian, L. Wang, J. G. Edens, J. T. Jacobsen, I. Hossain, Q. Wang, G. D. Victora, N. Vasdev, H. Ploegh, S. H. Liang, *Angew. Chem. Int. Ed.* **2016**, *55*, 528–533.

[163] R. Rossin, T. Läppchen, S. M. Van Den Bosch, R. Laforest, M. S. Robillard, *J. Nucl. Med.* **2013**, *54*, 1989–1995.

[164] B. M. Zeglis, K. K. Sevak, T. Reiner, P. Mohindra, S. D. Carlin, P. Zanzonico, R. Weissleder, J. S. Lewis, *J. Nucl. Med.* **2013**, *54*, 1389–1396.

[165] A. Yazdani, H. Bilton, A. Vito, A. R. Genady, S. M. Rathmann, Z. Ahmad, N. Janzen, S. Czorny, B. M. Zeglis, L. C. Francesconi, et al., *J. Med. Chem.* **2016**, *59*, 9381–9389.

[166] H. L. Evans, Q. D. Nguyen, L. S. Carroll, M. Kaliszczak, F. J. Twyman, A. C. Spivey, E. O. Aboagye, *Chem. Commun.* **2014**, *50*, 9557–9560.

[167] C. Denk, D. Svatunek, S. Mairinger, J. Stanek, T. Filip, D. Matscheko, C. Kuntner, T. Wanek, H. Mikula, *Bioconjug. Chem.* **2016**, *27*, 1707–1712.

[168] B. M. Zeglis, P. Mohindra, G. I. Weissmann, V. Divilov, S. A. Hilderbrand, R. Weissleder, J. S. Lewis, *Bioconjug. Chem.* **2011**, *22*, 2048–2059.

[169] L. G. Meimetis, E. Boros, J. C. Carlson, C. Ran, P. Caravan, R. Weissleder, *Bioconjug. Chem.* **2016**, *27*, 257–263.

[170] P. Agarwal, C. R. Bertozzi, *Bioconjug. Chem.* **2015**, *26*, 176–192.

[171] M. Peplow, *Nat. Biotechnol.* **2019**, *37*, 835–837.

[172] X. He, J. Li, S. An, C. Jiang, *Ther. Deliv.* **2013**, *4*, 1499–1510.

[173] Y. Zheng, B. Yu, Z. Li, Z. Yuan, C. L. Organ, R. K. Trivedi, S. Wang, D. J. Lefer, B. Wang, *Angew. Chem. Int. Ed.* **2017**, *56*, 11749–11753.

[174] C. Perez, K. B. Daniel, S. M. Cohen, *ChemMedChem* **2013**, *8*, 1662–1667.

[175] A. J. Wiemer, D. F. Wiemer, *Top. Curr. Chem.* **2015**, *360*, 115–160.

[176] J. R. Hamilton, J. Trejo, *Annu. Rev. Pharmacol. Toxicol.* **2017**, *57*, 349–373.

[177] G. Saravanakumar, J. Kim, W. J. Kim, *Adv. Sci.* **2017**, *4*, 1600124.

[178] J. F. Quinn, M. R. Whittaker, T. P. Davis, *Polym. Chem.* **2017**, *8*, 97–126.

[179] A. Al-Nahain, S. Y. Lee, I. In, K. D. Lee, S. Y. Park, *Int. J. Pharm.* **2013**, *450*, 208–217.

[180] S. K. Sharma, K. D. Bagshawe, *Adv. Drug Deliv. Rev.* **2017**, *118*, 2–7.

[181] J. D. Bargh, A. Isidro-Llobet, J. S. Parker, D. R. Spring, *Chem. Soc. Rev.* **2019**, *48*, 4361–4374.

[182] S. O. Doronina, B. E. Toki, M. Y. Torgov, B. A. Mendelsohn, C. G. Cerveny, D. F. Chace, R. L. DeBlanc, R. P. Gearing, T. D. Bovee, C. B. Siegall, et al., *Nat. Biotechnol.* **2003**, *21*, 778–784.

[183] D. M. Collins, B. Bossenmaier, G. Kollmorgen, G. Niederfellner, *Cancers (Basel).* **2019**, *11*, 394.

[184] A. M. Wu, P. D. Senter, *Nat. Biotechnol.* **2005**, *23*, 1137–1146.

[185] N. K. Devaraj, *ACS Cent. Sci.* **2018**, *4*, 952–959.

[186] J. Li, P. R. Chen, *Nat. Chem. Biol.* **2016**, *12*, 129–137.

[187] X. Ji, Z. Pan, B. Yu, L. K. De La Cruz, Y. Zheng, B. Ke, B. Wang, *Chem. Soc. Rev.* **2019**, *48*, 1077–1094.

[188] J. Tu, M. Xu, R. M. Franzini, *ChemBioChem* **2019**, *20*, 1615–1627.

[189] Y. V. Il'ichev, M. A. Schwörer, J. Wirz, *J. Am. Chem. Soc.* **2004**, *126*, 4581–4595.

[190] A. Patchornik, B. Amit, R. B. Woodward, *J. Am. Chem. Soc.* **1970**, *92*, 6333–6335.

[191] A. P. Gorka, R. R. Nani, J. Zhu, S. Mackem, M. J. Schnermann, *J. Am. Chem. Soc.* **2014**, *136*, 14153–14159.

[192] R. R. Nani, A. P. Gorka, T. Nagaya, H. Kobayashi, M. J. Schnermann, *Angew. Chem. Int. Ed.* **2015**, *54*, 13635–13638.

[193] R. R. Nani, A. P. Gorka, T. Nagaya, T. Yamamoto, J. Ivanic, H. Kobayashi, M. J. Schnermann, *ACS Cent. Sci.* **2017**, *3*, 329–337.

[194] Y. Chen, A. S. Kamlet, J. B. Steinman, D. R. Liu, *Nat. Chem.* **2011**, *3*, 146–153.

[195] K. K. Sadhu, T. Eierhoff, W. Römer, N. Winssinger, *J. Am. Chem. Soc.* **2012**, *134*, 20013–20016.

[196] K. K. Sadhu, E. Lindberg, N. Winssinger, *Chem. Commun.* **2015**, *51*, 16664–16666.

[197] P. K. Sasmal, S. Carregal-Romero, A. A. Han, C. N. Streu, Z. Lin, K. Namikawa, S. L. Elliott, R. W. Köster, W. J. Parak, E. Meggers, *ChemBioChem* **2012**, *13*, 1116–1120.

[198] P. K. Sasmal, C. N. Streu, E. Meggers, *Chem. Commun.* **2013**, *49*, 1581–1587.

[199] R. M. Yusop, A. Unciti-Broceta, E. M. V. Johansson, R. M. Sánchez-Martín, M. Bradley, *Nat. Chem.* **2011**, *3*, 239–243.

[200] J. Li, J. Yu, J. Zhao, J. Wang, S. Zheng, S. Lin, L. Chen, M. Yang, S. Jia, X. Zhang, et al., *Nat. Chem.* **2014**, *6*, 352–361.

[201] J. Wang, S. Zheng, Y. Liu, Z. Zhang, Z. Lin, J. Li, G. Zhang, X. Wang, J. Li, P. R. Chen, *J. Am. Chem. Soc.* **2016**, *138*, 15118–15121.

[202] J. T. Weiss, J. C. Dawson, K. G. Macleod, W. Rybski, C. Fraser, C. Torres-Sánchez, E. E. Patton, M. Bradley, N. O. Carragher, A. Unciti-Broceta, et al., *Nat. Commun.* **2014**, *5*, 3277.

[203] J. T. Weiss, J. C. Dawson, C. Fraser, W. Rybski, C. Torres-Sánchez, M. Bradley, E. E. Patton, N. O. Carragher, A. Unciti-Broceta, *J. Med. Chem.* **2014**, *57*, 5395–5404.

[204] J. T. Weiss, N. O. Carragher, A. Unciti-Broceta, *Sci. Rep.* **2015**, *5*, 9329.

[205] B. Rubio-Ruiz, J. T. Weiss, A. Unciti-Broceta, *J. Med. Chem.* **2016**, *59*, 9974–9980.

[206] C. Streu, E. Meggers, *Angew. Chem. Int. Ed.* **2006**, *45*, 5645–5648.

[207] T. Völker, F. Dempwolff, P. L. Graumann, E. Meggers, *Angew. Chem. Int. Ed.* **2014**, *53*, 10536–10540.

[208] V. Sabatino, J. G. Rebelein, T. R. Ward, *J. Am. Chem. Soc.* **2019**, *141*, 17048–17052.

[209] M. Jeschek, R. Reuter, T. Heinisch, C. Trindler, J. Klehr, S. Panke, T. R. Ward, *Nature* **2016**, *537*, 661–665.

[210] A. M. Pérez-López, B. Rubio-Ruiz, V. Sebastián, L. Hamilton, C. Adam, T. L. Bray, S. Irusta, P. M. Brennan, G. C. Lloyd-Jones, D. Sieger, et al., *Angew. Chem. Int. Ed.* **2017**, *56*, 12548–12552.

[211] B. J. Stenton, B. L. Oliveira, M. J. Matos, L. Sinatra, G. J. L. Bernardes, *Chem. Sci.* **2018**, *9*, 4185–4189.

[212] J. G. Rebelein, T. R. Ward, *Curr. Opin. Biotechnol.* **2018**, *53*, 106–114.

[213] M. A. Miller, B. Askevold, H. Mikula, R. H. Kohler, D. Pirovich, R. Weissleder, *Nat. Commun.* **2017**, *8*, 15906.

[214] G. Y. Tonga, Y. Jeong, B. Duncan, T. Mizuhara, R. Mout, R. Das, S. T. Kim, Y. C. Yeh, B. Yan, S. Hou, et al., *Nat. Chem.* **2015**, *7*, 597–603.

[215] A. Unciti-Broceta, E. M. V. Johansson, R. M. Yusop, R. M. Sánchez-Martín, M. Bradley, *Nat. Protoc.* **2012**, *7*, 1207–1218.

[216] E. Indrigo, J. Clavadetscher, S. V. Chankeshwara, A. Megia-Fernandez, A. Lilienkampf, M. Bradley, *Chem. Commun.* **2017**, *53*, 6712–6715.

[217] J. Clavadetscher, E. Indrigo, S. V. Chankeshwara, A. Lilienkampf, M. Bradley, *Angew. Chem. Int. Ed.* **2017**, *56*, 6864–6868.

[218] T. L. Bray, M. Salji, A. Brombin, A. M. Pérez-López, B. Rubio-Ruiz, L. C. A. Galbraith, E. E. Patton, H. Y. Leung, A. Unciti-Broceta, *Chem. Sci.* **2018**, *9*, 7354–7361.

[219] S. S. Matikonda, D. L. Orsi, V. Staudacher, I. A. Jenkins, F. Fiedler, J. Chen, A. B. Gamble, *Chem. Sci.* **2015**, *6*, 1212–1218.

[220] R. van Brakel, R. C. M. Vulders, R. J. Bokdam, H. Grüll, M. S. Robillard, *Bioconjug. Chem.* **2008**, *19*, 714–718.

[221] M. Azoulay, G. Tuffin, W. Sallem, J. C. Florent, *Bioorganic Med. Chem. Lett.* **2006**, *16*, 3147–3149.

[222] S. Bernard, D. Audisio, M. Riomet, S. Bregant, A. Sallustrau, L. Plougastel, E. Decuypere, S. Gabillet, R. A. Kumar, J. Elyian, et al., *Angew. Chem. Int. Ed.* **2017**, *56*, 15612–15616.

[223] J. Kim, C. R. Bertozzi, *Angew. Chem. Int. Ed.* **2015**, *54*, 15777–15781.

[224] R. M. Versteegen, R. Rossin, W. ten Hoeve, H. M. Janssen, M. S. Robillard, *Angew. Chem. Int. Ed.* **2013**, *52*, 14112–14116.

[225] X. Fan, Y. Ge, F. Lin, Y. Yang, G. Zhang, W. S. C. Ngai, Z. Lin, S. Zheng, J. Wang, J. Zhao, et al., *Angew. Chem. Int. Ed.* **2016**, *55*, 14046–14050.

[226] J. C. T. Carlson, H. Mikula, R. Weissleder, *J. Am. Chem. Soc.* **2018**, *140*, 3603–3612.

[227] A. J. C. Sarris, T. Hansen, M. A. R. de Geus, E. Maurits, W. Doelman, H. S. Overkleeft, J. D. C. Codée, D. V. Filippov, S. I. van Kasteren, *Chem. – A Eur. J.* **2018**, *24*, 18075–18081.

[228] J. M. M. Oneto, I. Khan, L. Seebald, M. Royzen, *ACS Cent. Sci.* **2016**, *2*, 476–482.

[229] M. Czuban, S. Srinivasan, N. A. Yee, E. Agustin, A. Koliszak, E. Miller, I. Khan, I. Quinones, H. Noory, C. Motola, et al., *ACS Cent. Sci.* **2018**, *4*, 1624–1632.

[230] R. Rossin, S. M. J. van Duijnhoven, W. ten Hoeve, H. M. Janssen, L. H. J. Kleijn, F. J. M. Hoeben, R. M. Versteegen, M. S. Robillard, *Bioconjug. Chem.* **2016**, *27*, 1697–1706.

[231] R. Rossin, R. M. Versteegen, J. Wu, A. Khasanov, H. J. Wessels, E. J. Steenbergen, W. Ten Hoeve, H. M. Janssen, A. H. A. M. Van Onzen, P. J. Hudson, et al., *Nat. Commun.* **2018**, *9*, 1484.

[232] A. Van Onzen, R. M. Versteegen, F. J. M. Hoeben, I. A. W. Filot, R. Rossin, J. Wu, P. J. Hudson, H. M. Janssen, M. Robillard, **2019**, DOI 10.26434/chemrxiv.11383659.v1.

[233] Q. Yao, F. Lin, X. Fan, Y. Wang, Y. Liu, Z. Liu, X. Jiang, P. R. Chen, Y. Gao, *Nat. Commun.* **2018**, *9*, 5032.

[234] I. Khan, P. F. Agris, M. V. Yigit, M. Royzen, *Chem. Commun.* **2016**, *52*, 6174–6177.

[235] A. K. Steiger, Y. Yang, M. Royzen, M. D. Pluth, *Chem. Commun.* **2017**, *53*, 1378–1380.

[236] J. Li, S. Jia, P. R. Chen, *Nat. Chem. Biol.* **2014**, *10*, 1003–1005.

[237] G. Zhang, J. Li, R. Xie, X. Fan, Y. Liu, S. Zheng, Y. Ge, P. R. Chen, *ACS Cent. Sci.* **2016**, *2*, 325–331.

[238] A. M. F. van der Gracht, M. A. R. de Geus, M. G. M. Camps, T. J. Ruckwardt, A. J. C. Sarris, J. Bremmers, E. Maurits, J. B. Pawlak, M. M. Posthoorn, K. M. Bonger, et al., *ACS Chem. Biol.* **2018**, *13*, 1569–1576.

[239] I. Khan, L. M. Seebald, N. M. Robertson, M. V. Yigit, M. Royzen, *Chem. Sci.* **2017**, *8*, 5705–5712.

[240] S. Du, D. Wang, J. S. Lee, B. Peng, J. Ge, S. Q. Yao, *Chem. Commun.* **2017**, *53*, 8443–8446.

[241] E. Agustin, P. N. Asare Okai, I. Khan, M. R. Miller, R. Wang, J. Sheng, M. Royzen, *Chem. Commun.* **2016**, *52*, 1405–1408.

[242] E. Jiménez-Moreno, Z. Guo, B. L. Oliveira, I. S. Albuquerque, A. Kitowski, A. Guerreiro, O. Boutureira, T. Rodrigues, G. Jiménez-Osés, G. J. L. Bernardes, *Angew. Chem. Int. Ed.* **2017**, *56*, 243–247.

[243] K. Neumann, S. Jain, A. Gambardella, S. E. Walker, E. Valero, A. Lilienkampf, M. Bradley, *ChemBioChem* **2017**, *18*, 91–95.

[244] H. Wu, S. C. Alexander, S. Jin, N. K. Devaraj, *J. Am. Chem. Soc.* **2016**, *138*, 11429–11432.

[245] L. P. W. M. Lelieveldt, S. Eising, A. Wijen, K. M. Bonger, *Org. Biomol. Chem.* **2019**, *17*, 8816–8821.

[246] M. Xu, J. Tu, R. M. Franzini, *Chem. Commun.* **2017**, *53*, 6271–6274.

[247] J. Tu, M. Xu, S. Parvez, R. T. Peterson, R. M. Franzini, *J. Am. Chem. Soc.* **2018**, *140*, 8410–8414.

[248] K. Neumann, A. Gambardella, A. Lilienkampf, M. Bradley, *Chem. Sci.* **2018**, *9*, 7198–7203.

[249] J. Tu, D. Svatunek, S. Parvez, H. J. Eckvahl, M. Xu, R. T. Peterson, K. N. Houk, R. M. Franzini, *Chem. Sci.* **2019**, *11*, 169–179.

[250] Y. Zheng, X. Ji, B. Yu, K. Ji, D. Gallo, E. Csizmadia, M. Zhu, M. R. Choudhury, L. K. C. De La Cruz, V. Chittavong, et al., *Nat. Chem.* **2018**, *10*, 787–794.

Chapter 2

Decaging TCO-esters for the release of carboxylic acids

This chapter is based on the following publication and all figures are adapted from the published manuscript:

Tetrazine-Triggered Release of Carboxylic-Acid-Containing Molecules for Activation of an Anti-inflammatory Drug. **Sarah Davies**†, Luxi Qiao†, Bruno L. Oliveira, Claudio D. Navo, Gonzalo Jiménez-Osés and Gonçalo J. L. Bernardes. *ChemBioChem*, **2019**, *20*, 1541-1546.

† These authors contributed equally. Density functional theory calculations were performed by Claudio Navo and Gonzalo Jiménez-Osés.

2.1 Introduction

Bioorthogonal decaging reactions have mainly been limited to the release of amine- or alcohol-containing anticancer drugs. Although these groups are common in small molecule drugs, they are not always present and they may not be essential for the function of the drug. Therefore, we aimed to develop bioorthogonal decaging reactions for the release of non-steroidal anti-inflammatory drugs (NSAIDs), an important class of drugs that contain a carboxylic acid group essential for their activity. It was proposed that chemically masking the carboxylic acid as an ester would result in a prodrug and the activity could then be restored upon decaging of the ester. The IEDDA reaction between a tetrazine and an alkene was chosen as the decaging strategy due to its high selectivity and reaction rate. In this chapter, both the vinyl handle and TCO handle were investigated as potential protecting groups for carboxylic acids (**Scheme 58**).

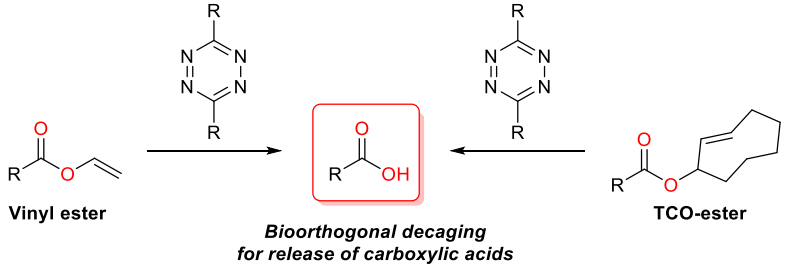

Scheme 58. Project aims: release of carboxylic acid-containing molecules from IEDDA tetrazine-triggered decaging of vinyl esters and TCO-esters.

In the course of this work, the release of carboxylic acids from TCO-esters was reported by the group of Robillard.[1] TCO-esters **83** and **85** were decaged in 25% acetonitrile/PBS to release model compounds benzoic acid (**84**) and 3-phenylpropionic acid (**86**) (**Scheme 59**). However, the reported TCO-protected carboxylic acids proved highly unstable (≈ 90% fragmentation in 50% mouse serum at 37 °C). Therefore, no further studies of TCO-esters were reported.

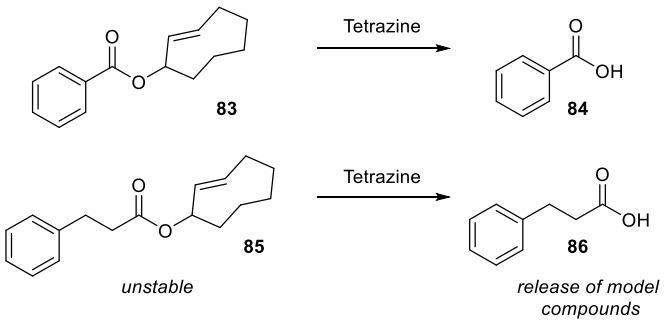

Scheme 59. Reported cleavage of TCO-esters to release model compounds containing carboxylic acids.[1]

2.2 Vinyl esters

2.2.1 Preliminary studies and reagent synthesis

Initially, we investigated the protection of carboxylic acids with the vinyl handle. A model system was designed to confirm if the IEDDA reaction could be extended to the release of carboxylic acids from vinyl esters. Vinyl 3-phenylpropanoate (**87**) was synthesised in 46% yield from commercially available **86** according to the procedure by Krejzová *et al*.[2] (**Scheme 60**).

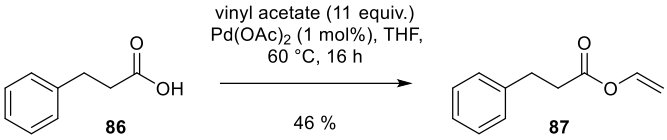

Scheme 60. Installation of the vinyl handle on model compound **86**.

Next the decaging of model compound **87** was attempted using the commercial DiPy-Tz (**15**), following the procedure by Jiménez-Moreno *et al.*[3] After 16 h, a 2:1 ratio of starting material:product was observed by ^{1}H NMR. Carboxylic acid **86** and the pyrizidine side product (**88**) were isolated in 28% and 31% yields, respectively (**Scheme 61**).

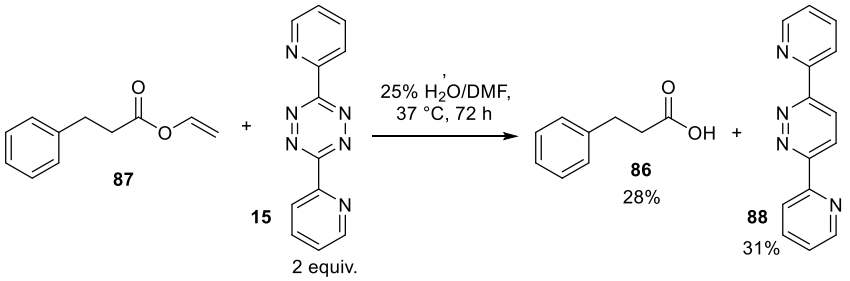

Scheme 61. Decaging of model compound **87** upon reaction with tetrazine **15**.

After confirming that carboxylic acids could be released from vinyl esters upon IEDDA reaction, several tetrazines were selected for further studies (**Figure 7**). The nature of the substituents on the tetrazine core affects the stability and solubility of the tetrazine, along with the rate of IEDDA reaction. As mentioned in the introduction, the rate of decaging of a TCO-carbamate was enhanced with asymmetric tetrazines containing both an EWG and a small alkyl group.[4] This is due to the fact that EWGs accelerate the cycloaddition step, whereas small, non-bulky groups increase the rate of the elimination step. Tetrazine **58** was chosen as it resulted in the fastest rate of decaging in cells with the analogous TCO-carbamate.[4] The less electron deficient tetrazine **89** was also selected in order to assess the effect of electron withdraw substituents on the tetrazine core. Another asymmetric tetrazine (**89**) bearing a H atom substituent was chosen to determine the effect of sterics. In addition, symmetrical tetrazines **15** and **91** were chosen for comparison. **15** is a commercially available, electron deficient tetrazine, whereas **91** has previously been shown to result in high release yields.[1]

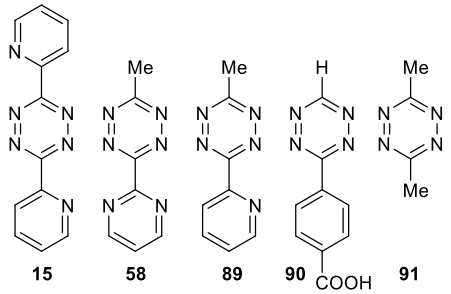

Figure 7. Tetrazines chosen for this study.

Asymmetric tetrazines **58** and **89** were synthesised in 27% and 18% yields, respectively, according to the procedure by Fan *et al.*[4] (**Scheme 62**). Tetrazines **90** and **91** were prepared by other members of the Bernardes group (Ester Jiménez-Moreno and Russel Guo, respectively).

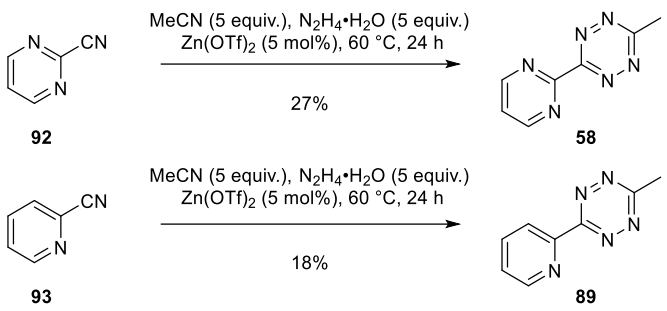

Scheme 62. Synthesis of asymmetric tetrazines **58** and **89**.

2.2.2 Kinetic and stability studies

Next, the kinetics of decaging were assessed. Computational studies (carried out by our collaborators Claudio Navo and Gonzalo Jiménez-Osés at the University of La Rioja) on the reaction between vinyl acetate (**94**) and DiPy-Tz (**15**) predicted that the first cycloaddition step was rate determining (**Figure 8**).

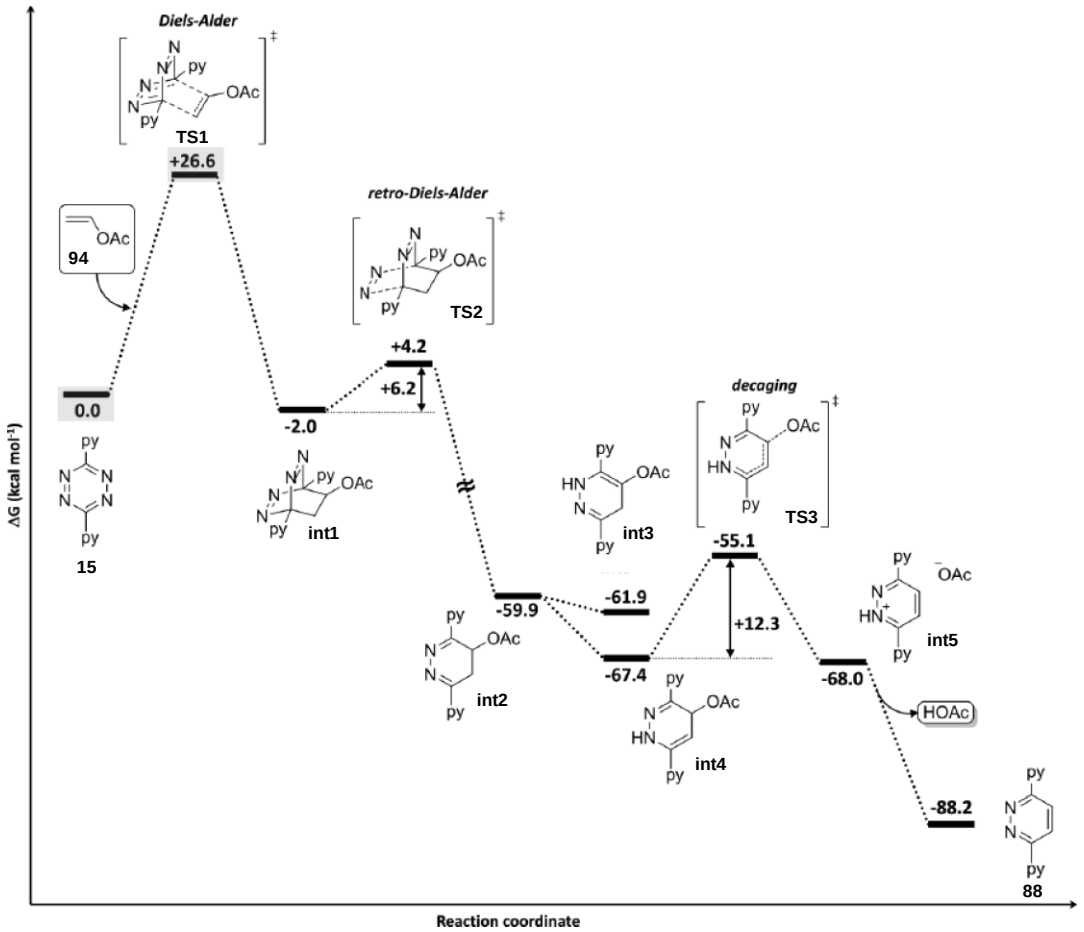

Figure 8. Minimum energy pathway for the reaction of vinyl acetate (**94**) with tetrazine **15** calculated with PCM_{H2O}/M06-2X/6-31+G(d,p). The RDS is the cycloaddition step.

This was also confirmed by ^{1}H NMR. The reaction between tetrazine **15** and **87** (4 equiv.) in 90% DMSO-D_6/D_2O was followed over time and no peaks were observed in the region 2.5–6 ppm that could be attributed to the intermediates (**Figure 9**). This supports the prediction that the cycloaddition is rate-limiting and, once it occurs, a fast elimination step affords the decaged product.

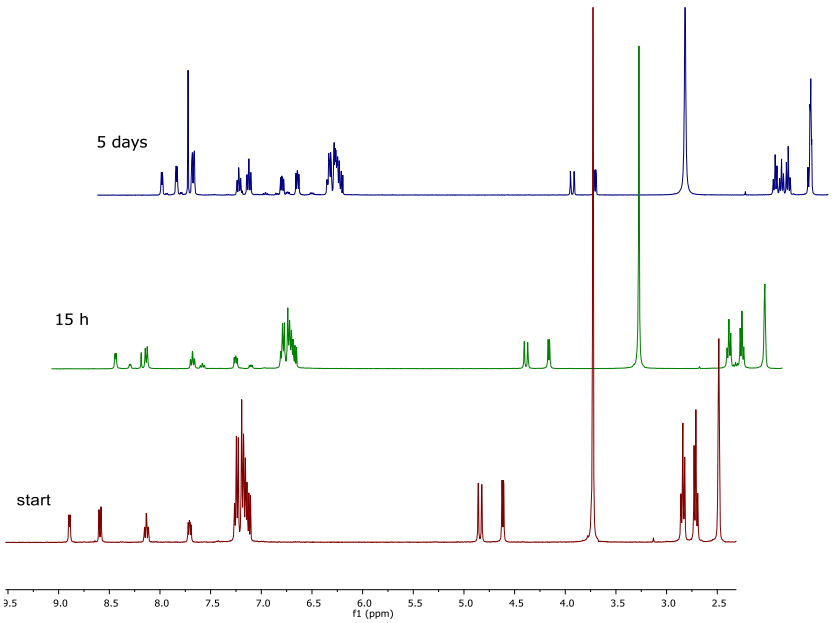

Figure 9. ^{1}H NMR studies to monitor the reaction of **87** with tetrazine **15**.

It was also predicted that the tetrazines should show similar reactivity, with the exception of DiMe-Tz (**91**) which was expected to be the least reactive (**Table 2**).

Table 2. Theoretical relative reaction rates and observed experimental second order rate constants for the rate-limiting cycloaddition step between vinyl acetate and tetrazines **15**, **58**, **89**, **90**, **91**. n.d.= not determined.

Tetrazine	Theoretical relative reaction rate ($M^{-1}\,s^{-1}$)	Rate Constant, k_2 ($M^{-1}\,s^{-1}$)	R^2
15	1	$(1.70 \pm 0.05) \times 10^{-4}$	0.9973
58	0.2	$(2.15 \pm 0.62) \times 10^{-4}$	0.9975
89	0.6	$(4.93 \pm 0.17) \times 10^{-5}$	0.9963
90	0.1	$(2.81 \pm 0.05) \times 10^{-4}$	0.9990
91	1×10^{-4}	n.d.	n.d.

Initially we aimed to measure the overall rate of the reaction by following the release of the carboxylic acid. To that purpose we sought a carboxylic acid-containing fluorescent molecule whose fluorescence

is quenched (or shifted to a different wavelength) when it is caged. First, coumarin-3-carboxylic acid (**95**) was converted into vinyl ester **96** using the previously described palladium coupling[2] (**Scheme 63**). The fluorescence of both the caged and free acid were then compared. However, unfortunately there was no quenching of the fluorescence (λ_{ex} = 300 nm, λ_{em} = 430 nm). This suggests that the carboxylic acid functional group does not contribute to the fluorescence, despite being directly conjugated to the fluorophore.

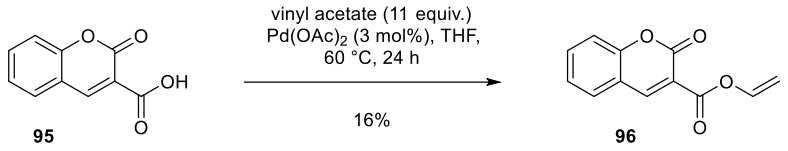

Scheme 63. Synthesis of vinyl-protected coumarin **96**. Converting the carboxylic acid to the vinyl ester did not quench the coumarin fluorescence.

In another attempt, 7-hydroxycoumarin-3-carboxylic acid (**100**) was synthesised by formation of ester **99** followed by base hydrolysis (**Scheme 64**).

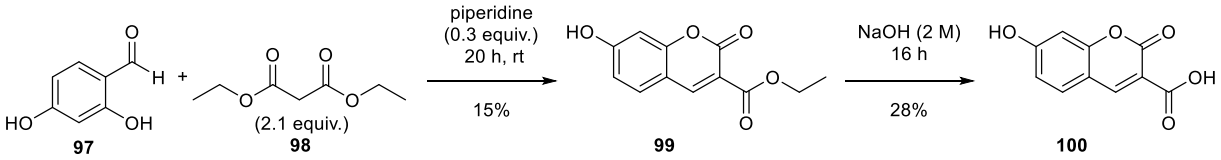

Scheme 64. Synthesis of 7-hydroxycoumarin-3-carboxylic acid (**100**).

Next, reaction of **100** with vinyl acetate resulted in the doubly caged coumarin **101**. Selective decaging of the alcohol group, using 4 M HCl produced vinyl-protected coumarin **102** (**Scheme 65**).

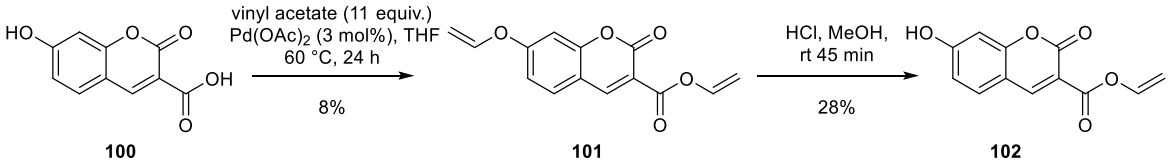

Scheme 65. Synthesis of vinyl-protected coumarin **102**.

Subsequent studies of the fluorescent properties of coumarin **102** showed that its fluorescence (λ_{ex} = 340 nm, λ_{em} = 450 nm) was not quenched. However, it possesses an additional excitation wavelength (λ_{ex} = 420 nm, λ_{em} = 450 nm) that **100** does not have. This means it is possible to monitor the consumption of **102** by measuring the decrease in fluorescence at λ_{ex} = 420 nm. However, it is not possible to detect formation of product **100** upon decaging.

Therefore, we decided to follow the kinetics by monitoring the decrease in absorption of the tetrazine in the visible region. This gives the rate of the IEDDA cycloaddition, which, as previously demonstrated, is the RDS. Therefore, since the subsequent steps are much faster, we can assume that the rate of the cycloaddition step is the same as the overall reaction rate.

The kinetics of the cycloaddition were experimentally determined with these tetrazines and commercially available vinyl propionate (**103**) under pseudo-first order conditions (**Scheme 66**, **Figure 10**).

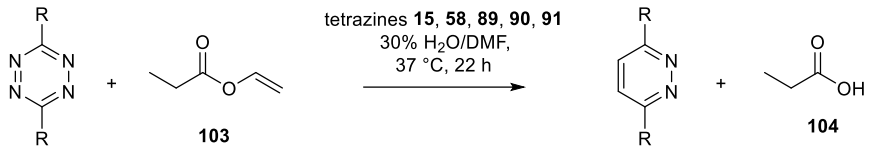

Scheme 66. Reaction of tetrazines **15**, **58**, **89**, **90**, **91** (2 mM) with vinyl propionate (**103**, 150–350 mM).

Briefly, each tetrazine was reacted with an excess of vinyl propionate (75–175 equiv.) in 30% H_2O/DMF at 37 °C and the decrease in tetrazine absorbance at 530 nm was measured over 22 h (**Figure 11**). This experiment was performed by Luxi Qiao. The observed rate constants (k_{obs}) were obtained by fitting the data to an exponential one-phase decay equation ($Y = (Y_0 - \text{Plateau})e^{(-kX)} + \text{Plateau}$). Finally, for each tetrazine, k_{obs} was plotted against concentration of vinyl propionate (**103**) and the second order rate constant, k_2, was found from the gradient (**Figure 10**, **Table 3**). The fastest rate occurred with tetrazine **90**, a mono-substituted tetrazine bearing a moderately electron-withdrawing benzoic acid group.

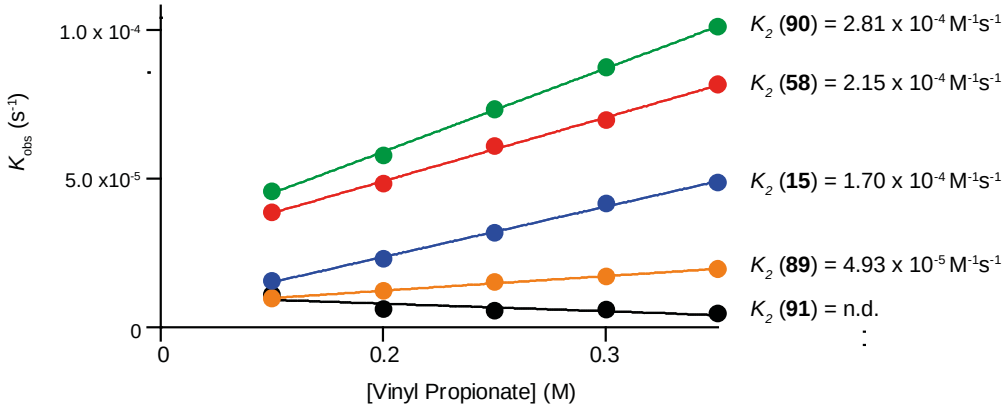

Figure 10. Kinetics of the cycloaddition step for the reaction of vinyl propionate with tetrazines **15**, **58**, **89**, **90**, **91**. K_2 was obtained from the gradient of plots of k_{obs} *vs* vinyl propionate concentration. Experiment performed by Luxi Qiao.

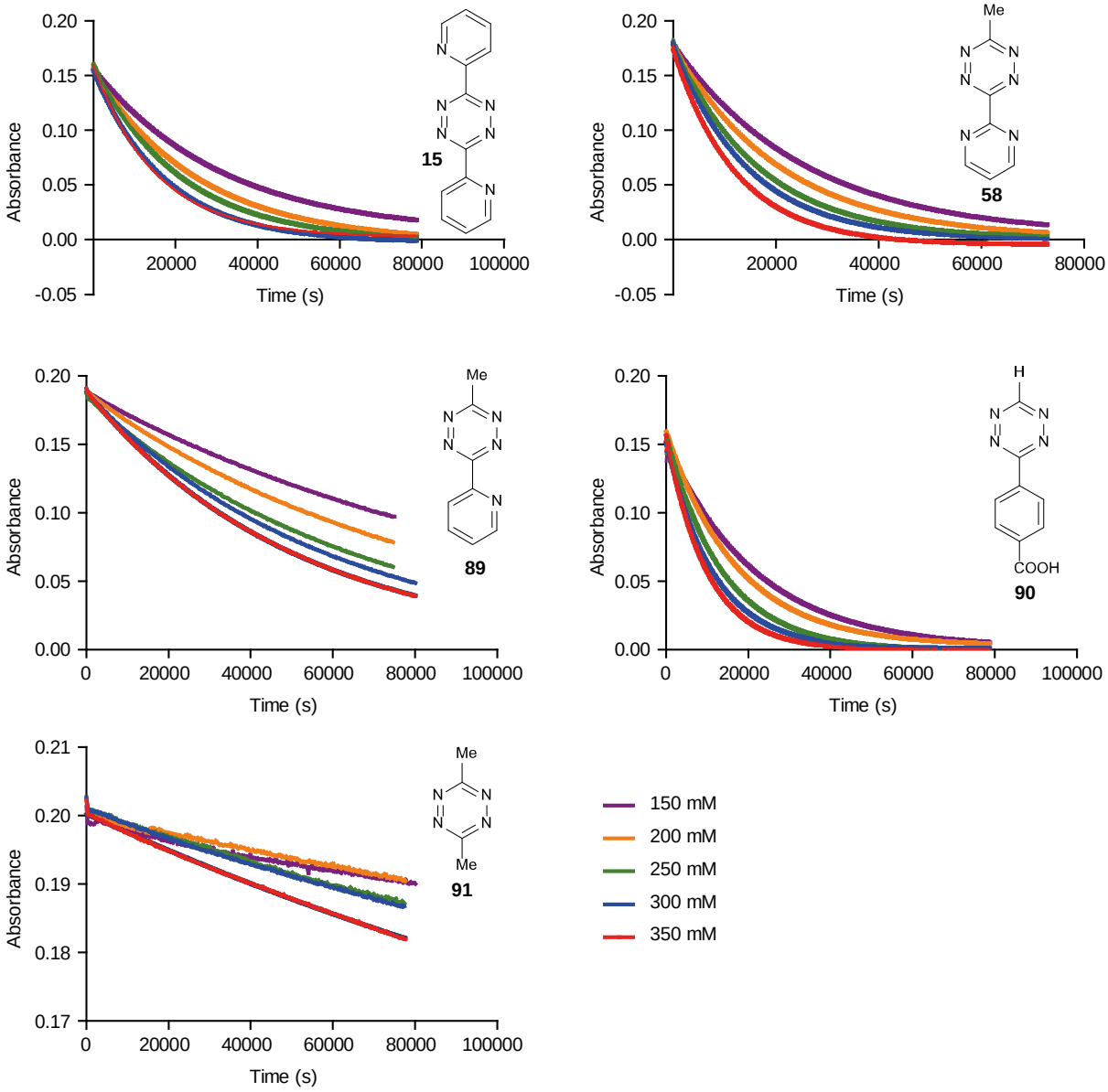

Figure 11. Plots of absorbance (530 nm) *vs* time for reaction of tetrazines **15**, **58**, **89**, **90**, **91** (2 mM) with vinyl propionate (150–350 mM) in 30% H_2O/DMF at 37 °C. The data were fitted to an exponential one-phase decay equation $Y = (Y_0 - \text{Plateau})e^{(-kX)} + \text{Plateau}$. Each measurement was repeated three different times. Experiment performed by Luxi Qiao.

Next, the stability of tetrazines **15**, **58**, **89**, **90**, **91** was assessed in 50% DMSO/H_2O by monitoring the UV absorbance at 530 nm (**Figure 12**). Tetrazine **15** showed moderate stability ($t_{1/2}$ = 15.8 h) and tetrazine **58** was the most unstable ($t_{1/2}$ = 5.7 h). Tetrazines **89**–**91** proved highly stable (≈ 85–90% intact after 24 h).

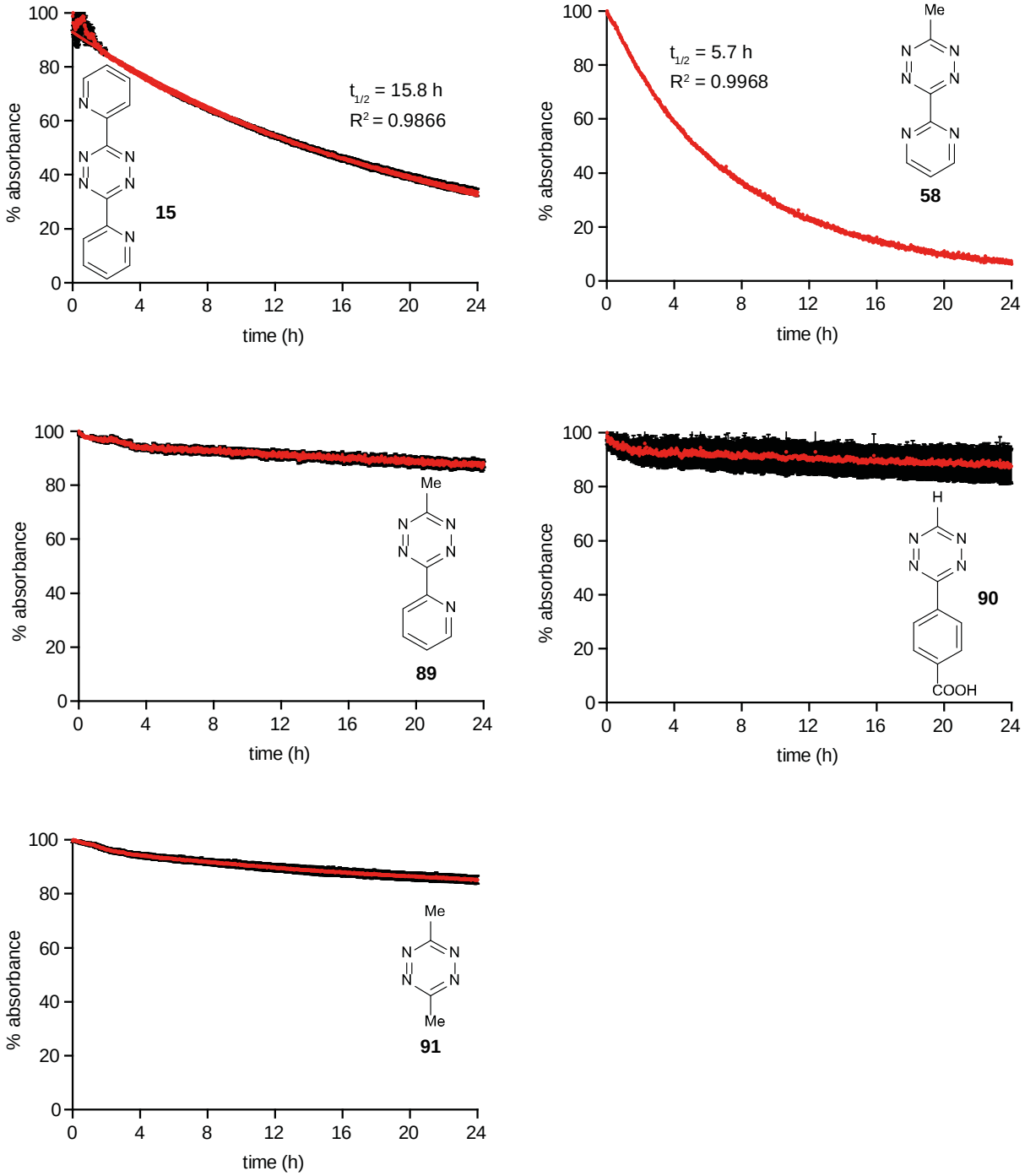

Figure 12. Stability of tetrazines **15**, **58**, **89**, **90**, **91** in 50% DMSO/H_2O. Decay of the UV absorbance of the tetrazines at 530 nm was followed over 24 h at 37 °C. The data for tetrazines **15** and **58** were fitted to an exponential one-phase decay equation $Y = (Y_0 - \text{Plateau})e^{(-kX)} + \text{Plateau}$. Each experiment was performed in triplicate and repeated two independent times.

The biological stability of tetrazine **90** was then assessed by Luxi Qiao and it proved to be stable in PBS pH 7.4, cell culture media (DMEM + 10% FBS) and 10% human plasma for at least 24 h (**Figure 13**). Therefore, tetrazine **90** was chosen for further studies.

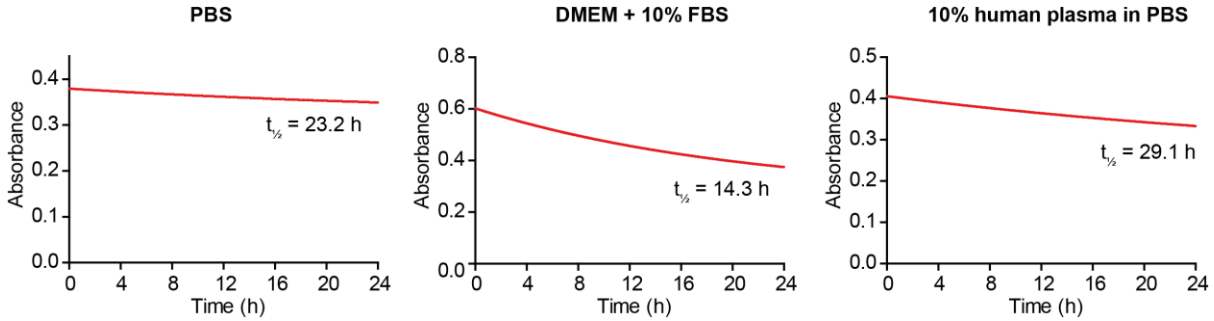

Figure 13. Stability of tetrazine **90** in PBS, DMEM + 10% FBS and 10% human plasma/PBS. Decay of the UV absorbance of the tetrazine at 530 nm was followed over 24 h at 37 °C. This experiment was performed by Luxi Qiao.

After the initial studies on the model compounds, we next synthesised a vinyl-protected prodrug. Ketoprofen (**105**) is a NSAID with a chiral centre. Although it is used as a racemate, the anti-inflammatory activity of ketoprofen mainly resides with the S-enantiomer. While the R-enantiomer is approximately 100 to 1000 times less potent than the S-enantiomer as a cyclooxygenase inhibitor, research has shown that the R-enantiomer is still important in that it contributes to the analgesic effect of ketoprofen.[5] We started by converting ketoprofen (**105**) into vinyl ester **106** using palladium coupling (**Scheme 67**).[2]

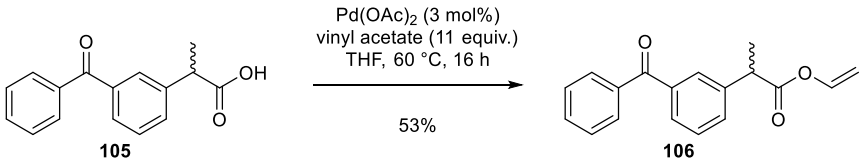

Scheme 67. Synthesis of vinyl-protected ketoprofen (**106**). This experiment was performed by Luxi Qiao.

The stability of vinyl ester **106** was then assessed using HPLC. It proved stable in PBS, however, limited stability was observed in 10% human plasma ($t_{1/2}$ = 12 min) and DMEM + 10% FBS ($t_{1/2}$ = 4 h, **Figure 14**). This is likely because the vinyl group does not provide steric protection of the ester group from nucleophilic attack and subsequent hydrolysis. This fact, along with the slow rate of reaction (approximately 20% of free drug observed after 24 h with 30 equiv. of tetrazine, **Figure 15**) resulted in the vinyl handle being abandoned, as its use for *in vivo* applications would be rather limited.

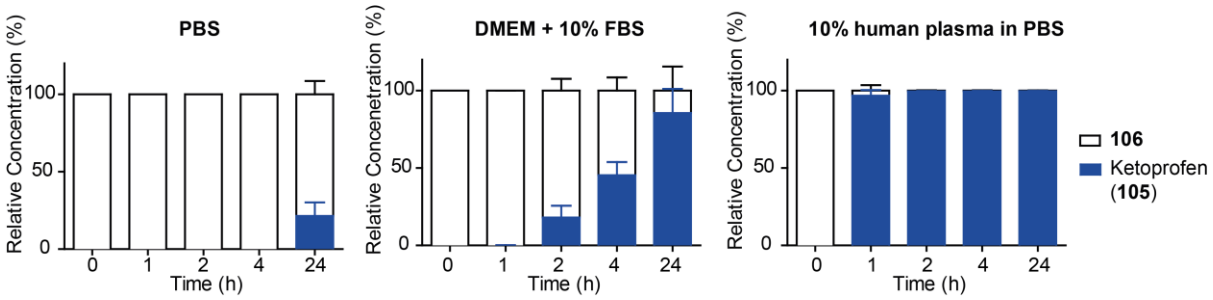

Figure 14. Stability of vinyl-ketoprofen (**106**) in PBS, DMEM + 10% FBS, and 10% human plasma/PBS assessed by HPLC. This experiment was performed by Luxi Qiao.

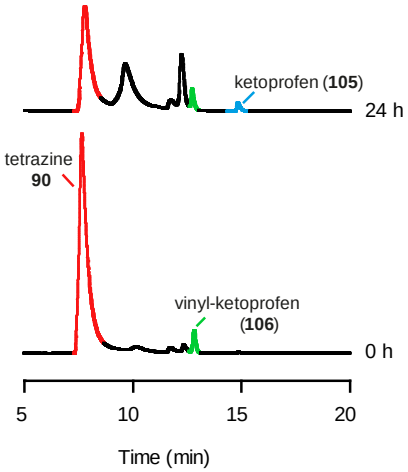

Figure 15. HPLC traces of decaging of vinyl-ketoprofen (**106**) upon reaction with 30 equiv. tetrazine **90**. Traces shown at time 0 h and after 24 h of reaction. This experiment was performed by Luxi Qiao.

2.3 TCO-esters

2.3.1 Computational studies

Next, we decided to investigate TCO as a caging group to render ketoprofen inactive. A more reactive alkene was necessary in order to make this a rapid, useful bioorthogonal cleavage reaction. Quantum mechanical calculations (carried out by our collaborators Claudio Navo and Gonzalo Jiménez-Osés at the University of La Rioja) suggested that the RDS depends on the nature of the tetrazine substituents. Hence, while the initial cycloaddition step is rate-limiting for DiMe-Tz (**91, Figure 16**), for DiPy-Tz (**15**) the allylic elimination step (decaging) is rate-limiting (**Figure 17**). Of note, the calculations reproduced the experimentally observed trend of axial-TCO being slightly more reactive than its equatorial isomer. Irrespective of which step determines the reaction rate, all reactions involving TCO acetate (**107**) were calculated to be much faster than those with vinyl acetate (**94**, **Table 3**).

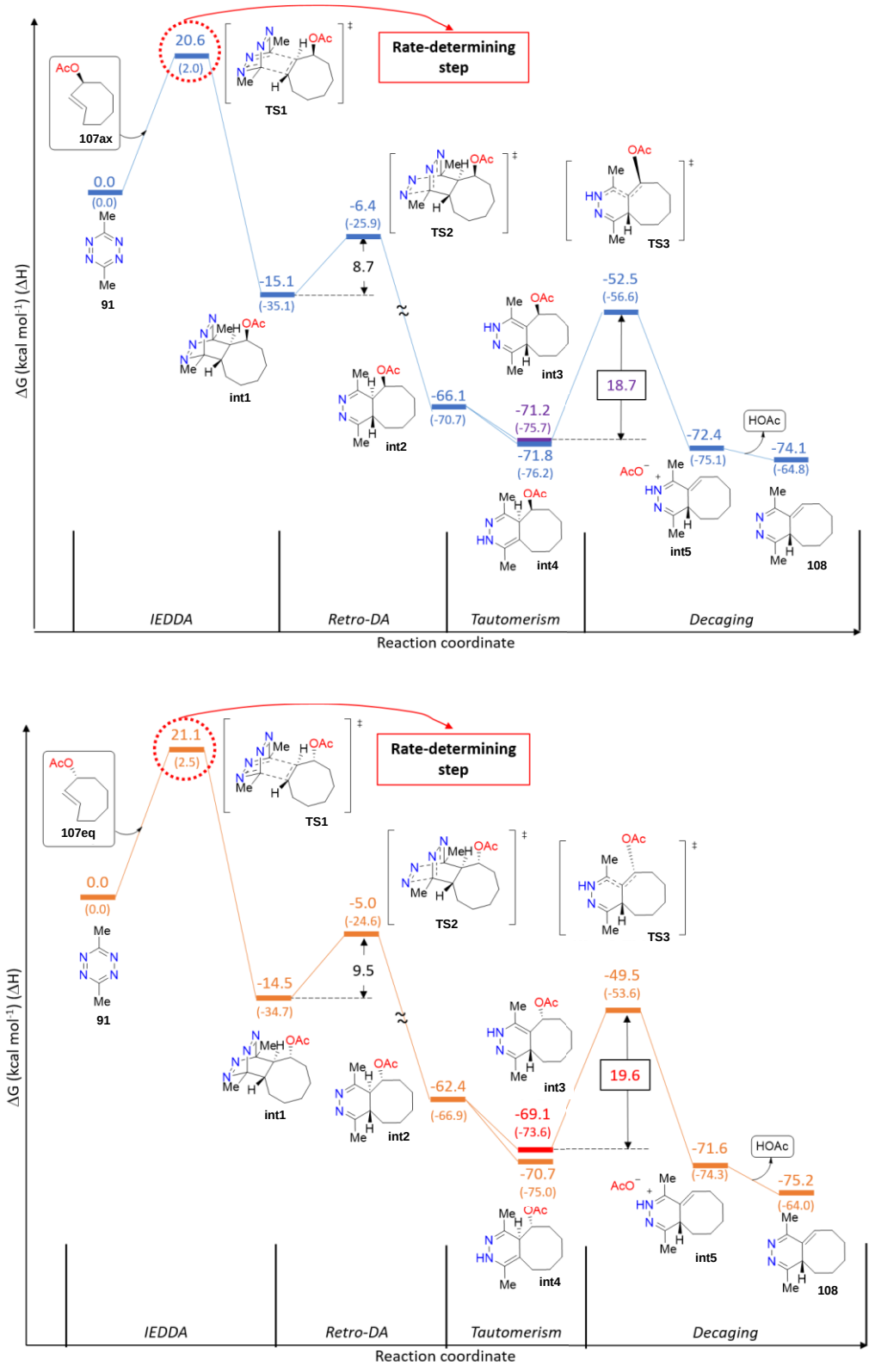

Figure 16. Minimum energy pathway for the reaction of TCO **107ax** (top, blue) and **107eq** (bottom, orange) with tetrazine **91** calculated with PCM_{H2O}/M06-2X/6-31+G(d,p). The RDS is the IEDDA cycloaddition step, the reaction being slightly more favorable for **107ax**. Experiment performed by Claudio Navo and Gonzalo Jiménez-Osés.

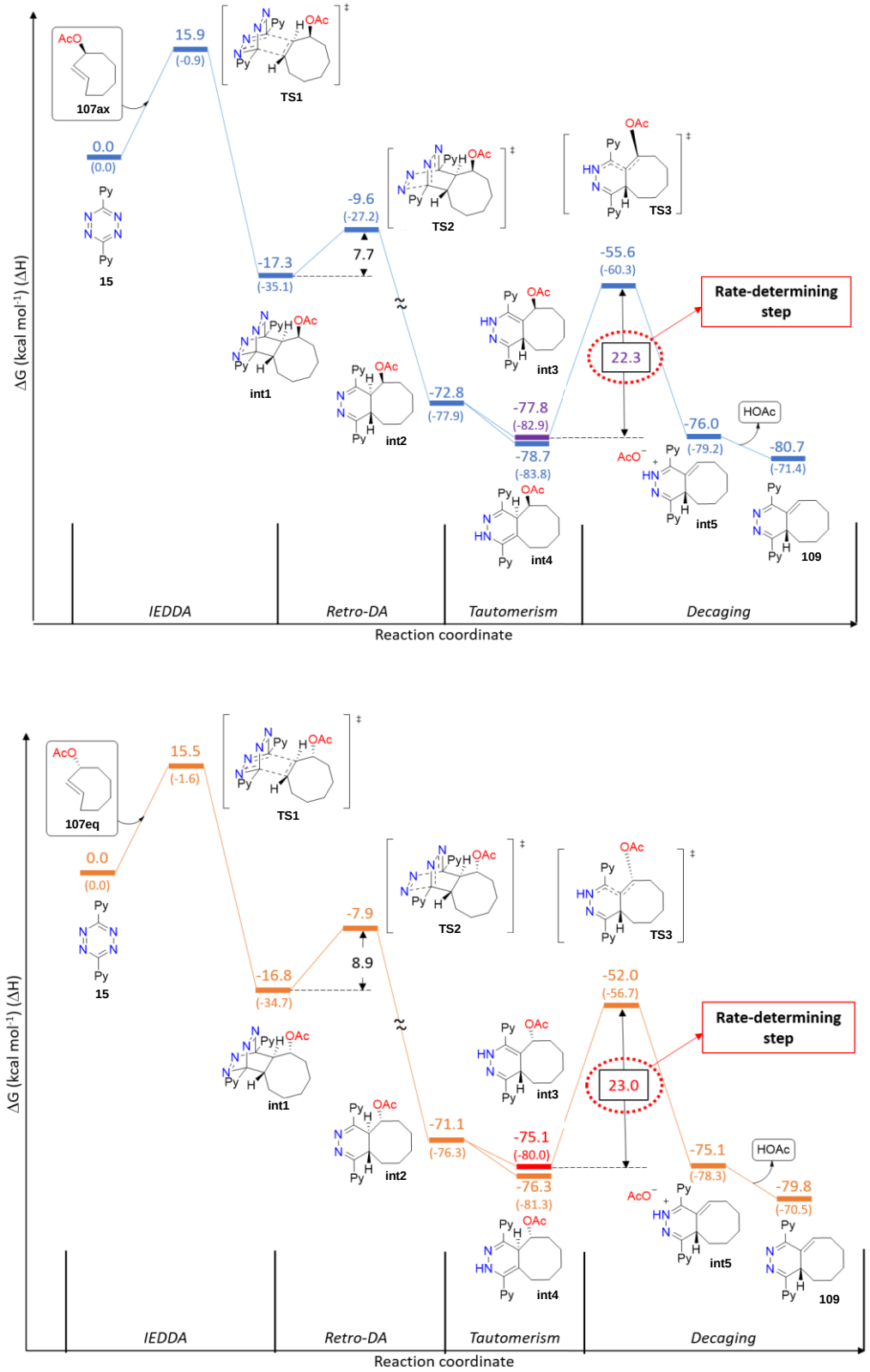

Figure 17. Minimum energy pathway for the reaction of TCO **107ax** (top, blue) and **107eq** (bottom, orange) with tetrazine **15** calculated with PCM_{H2O}/M06-2X/6-31+G(d,p)**.** The RDS is the elimination of the acetate group, the reaction being slightly more favorable for **107ax**. Experiment performed by Claudio Navo and Gonzalo Jiménez-Osés.

Table 3. Activation barriers for the RDS of the reaction of vinyl acetate (**94**) and either the axial or the equatorial isomer of TCO acetate (**107ax** or **107eq**) with either DiPy-Tz (**15**) or DiMe-Tz (**91**).

Caging group	Tetrazine	$\Delta G^{\ddagger}$ (kcal mol^{-1})
Vinyl	DiPy-Tz (**15**)	26.6
TCOax	DiPy-Tz (**15**)	22.3
TCOeq	DiPy-Tz (**15**)	23.0
Vinyl	DiMe-Tz (**91**)	31.8
TCOax	DiMe-Tz (**91**)	20.6
TCOeq	DiMe-Tz (**91**)	21.1

2.3.2 Synthesis of TCO-esters

Based on the promising computational predictions, we started by synthesising a *cis*-CO-protected ester, in order to assess both the synthetic feasibility and the stability of the ester bond. First, *cis*-cycloocten-1-ol (**111**) was synthesised according to the reported procedure (**Scheme 68**).[6]

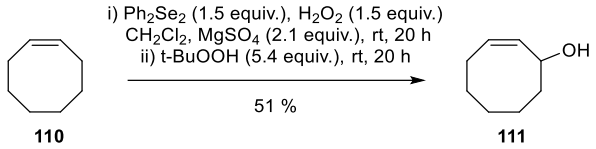

Scheme 68. Synthesis of *cis*-cycloocten-1-ol (**111**).

Next, *cis*-CO-protected ketoprofen (**113**) was synthesised in 75% yield (**Scheme 69**) and, unlike the vinyl ester, proved to be stable in cell media, PBS pH 7.4, and 10% plasma (only 5% free drug was observed after 24 h, **Figure 18**). This study was performed by Luxi Qiao.

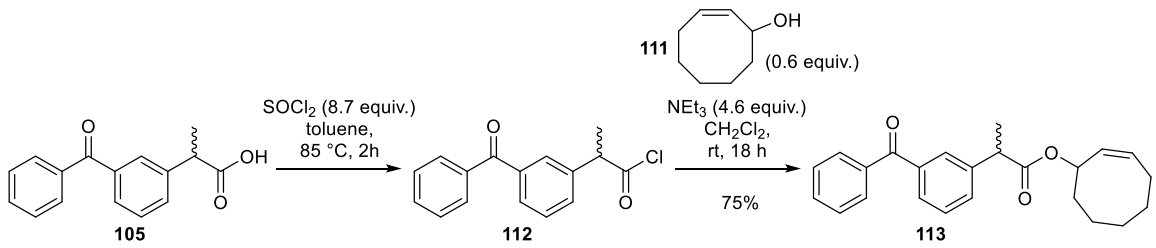

Scheme 69. Synthesis of *cis*-cyclooctene-protected ketoprofen (**113**), by Luxi Qiao.

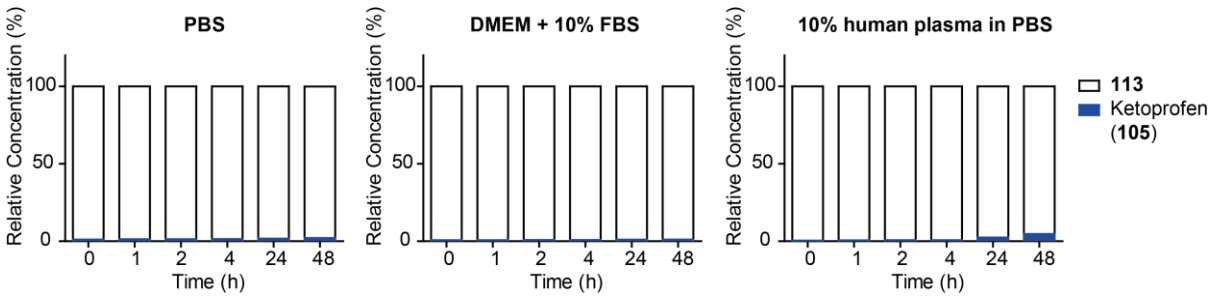

Figure 18. Stability of *cis*-cyclooctene-ketoprofen (**113**) in PBS, DMEM + 10% FBS and 10% human plasma/PBS assessed by HPLC by Luxi Qiao.

We propose that this increase in stability is due to the increased steric hindrance at the ester bond due to the TCO handle compared with the vinyl handle. It appears that significant steric hindrance is required on both sides of the ester bond and the ester proves unstable if either the protecting group (vinyl handle) or the active molecule (in the case of the TCO-esters reported by Robillard)[1] are not sterically bulky. In the case of **113**, a stereocentre α to the ester bond provides steric protection on one side, as does TCO on the other.

With these results in hand, we decided to further evaluate the TCO-ester for bioorthogonal IEDDA decaging. When incorporating TCO into compounds, it is common to synthesise the *cis*-product and then convert this to the *trans*-isomer using photochemical isomerisation under flow.[7] The reaction mixture is irradiated with UV light, which causes isomerisation of the *cis* double bond. It is then pumped through a column containing silver nitrate-coated silica. The *trans*-isomer selectively binds to silver nitrate and is removed from the equilibrium, while the *cis*-isomer returns to the flask where it is isomerised again. When isomerisation is complete, the *trans*-isomer is obtained by extraction from the silica using ammonium hydroxide, followed by extraction into organic solvent. This results in two isomers of functionalised TCO (axial and equatorial), which it is not always possible to separate using column chromatography. This photochemical isomerisation method is very low yielding[1] and is not always suitable for the final step in syntheses that require a large amount of valuable drug. Ketoprofen contains a benzophenone group, which is a widely used photo-crosslinking reagent. This means that the usual photochemical isomerisation method is unsuitable for this compound.[8] Therefore, in both projects we decided to start from the commercially available *trans*-cyclooct-2-en-1-ol (TCO-OH, axial isomer, purchased from Sirius Fine Chemicals). Repeating the synthesis with *trans*-cyclooct-2-en-1-ol resulted in the desired product **114**, with approximately 50% of the *trans* double bond isomerising to the *cis*-form (**113**, **Scheme 70**).

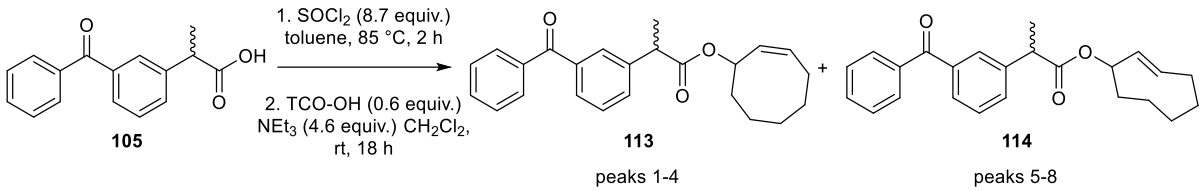

Scheme 70. Synthesis of TCO-protected ketoprofen resulted in 84% yield of the product as a mixture of *cis*-(**113**) and *trans*-isomers (**114**) (NMR ratio 51:49 *cis*:*trans*). Experiment performed by Luxi Qiao.

This highlights a common problem with synthesising TCO-functionalised molecules. The double bond in TCO is highly strained and therefore highly reactive, which makes it incompatible with several reaction conditions, such as the halide ions used in the formation of the acyl chloride intermediate. This can result in partial isomerisation to the *cis*-isomer, which is 7 orders of magnitude less reactive than the *trans*-isomer.[9] In addition to the modes of chirality on the *cis*- and *trans*-isomers of the TCO protecting group, ketoprofen also has a chiral centre. Indeed, using thionyl chloride as an activating agent we observed the formation of 8 diastereomers by HPLC (**Figure 19**) from the *cis*-and *trans*-isomers of TCO and the chiral centre of the protected ketoprofen.

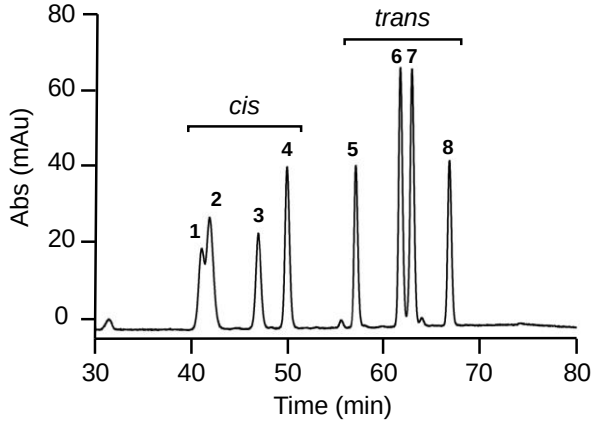

Figure 19. Separation of the 8 product diastereomers using chiral HPLC, by Luxi Qiao.

Using chiral HPLC we were able to separate each diastereomer, analyse them by NMR and characterise the four *trans*-isomers as enantiomeric pairs of either the axial (**114ax**) or equatorial (**114eq**) isomer (**Figure 20**). Since the axial TCO-isomer has previously been shown to have different reaction rates than the equatorial isomer, each enantiomeric pair of axial and equatorial isomers were combined. Both the axial and equatorial isomers of the prodrug were tested in further experiments.

We demonstrated a method of separating isomers of TCO and successfully overcame the isomerisation problem commonly experienced in syntheses using TCO, even in the challenging case of having an additional chiral centre in the drug. Now, although a low yield may be obtained, it is possible

to subject TCO to reaction conditions that readily cause isomerisation and still obtain the pure *trans*-isomer.

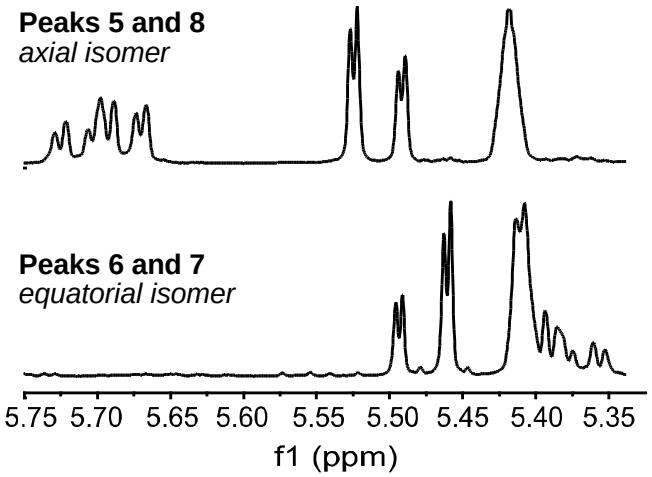

Figure 20. Alkene region from ^{1}H NMR spectra of *trans*-isomers of TCO-ketoprofen (**114**), after separation by HPLC by Luxi Qiao.

2.3.3 Studies of TCO-esters

The reaction of TCO ketoprofen (**114**, axial and equatorial isomers) with various tetrazines in the presence of an internal standard (benzoic acid) was then studied by HPLC (**Scheme 71**). Considering the fast kinetics observed for the decaging, an excess of free TCO-OH was added to quench the reaction at various time points. Liquid Chromatography-Mass Spectrometry (LC-MS) analysis of the quenched solution showed similar reaction profiles and decaging yields for both isomers of **114** with tetrazine **90** (**Figure 21**). Therefore, other tetrazines were tested with only the axial isomer of **114**.

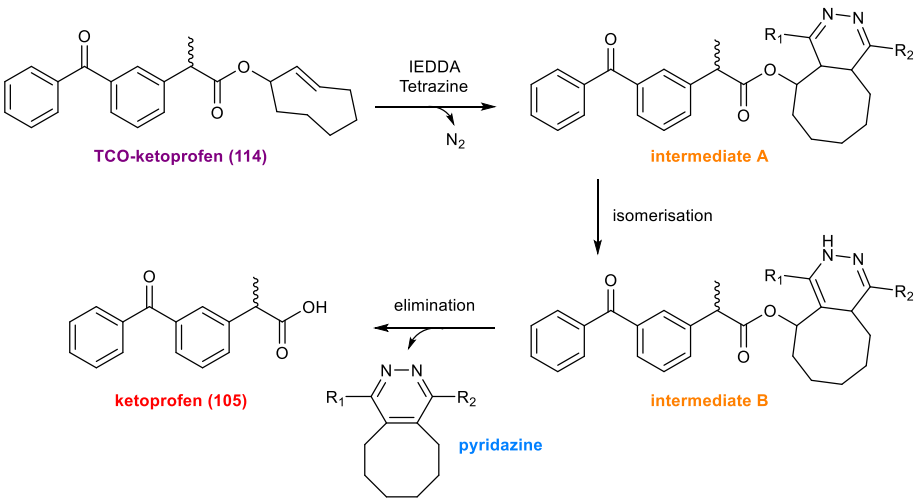

Scheme 71. Reaction of TCO-ketoprofen (**114**) with tetrazines **15**, **58**, **89**, **90**, **91** monitored by LC-MS.

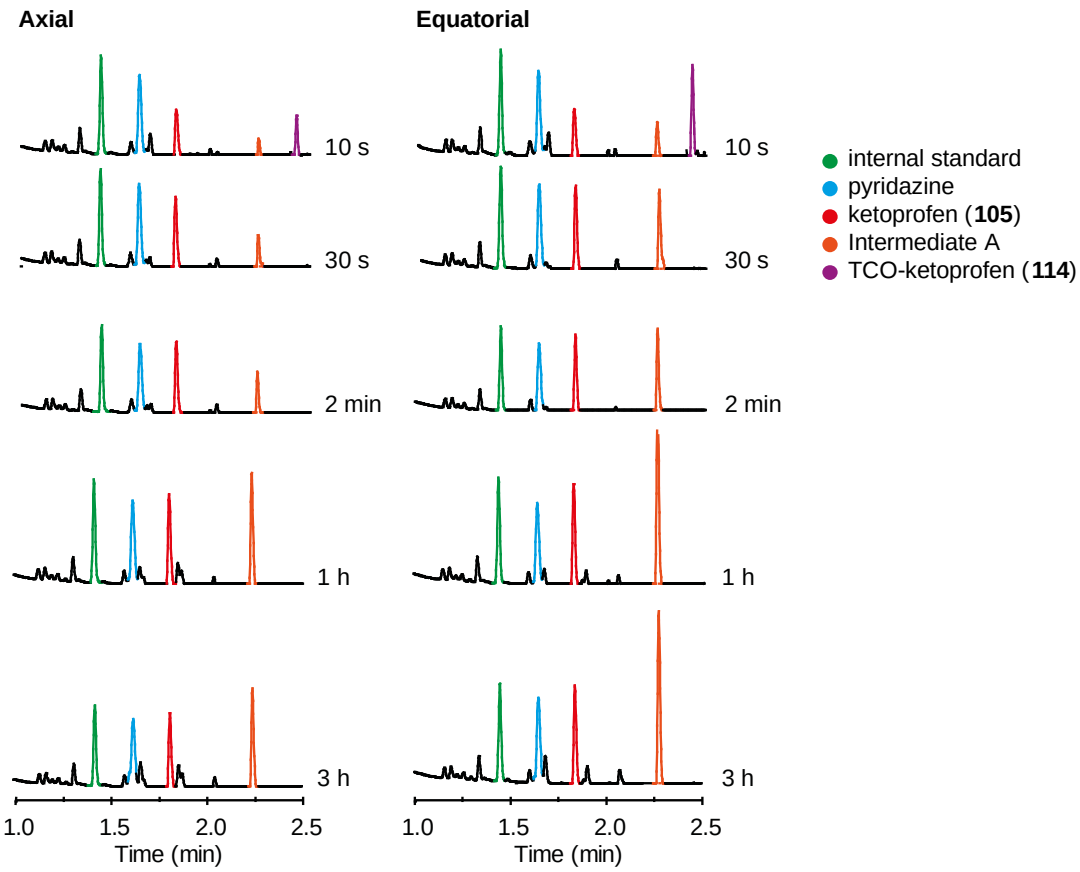

Figure 21. Reaction of TCO-ketoprofen (**114ax** and **114eq**) with tetrazine **90**, monitored by LC-MS at 10 s, 30 s, 2 min, 1 h and 3 h time points. Both axial and equatorial isomer showed similar reaction profiles and decaging yields (axial: 25%, equatorial: 24%).

The reaction of TCO-ketoprofen (**114ax**) was then also studied with tetrazines **15**, **89**, and **91** (tetrazine **58** was not chosen due to its high instability compared to other tetrazines, **Figure 12**). For tetrazines **15**, **89** and **90**, TCO-ketoprofen (**114ax**) is consumed within 30 seconds and after 2 minutes the change in the amount of ketoprofen (**105**) is negligible (**Figure 22**), which is in good agreement with the low activation barriers predicted computationally. The observed accumulation of dihydropyridazine intermediate(s) A/B demonstrates our prediction (for tetrazine **15**, **Figure 17**) that elimination of the carboxylate is the RDS. Also in agreement with computational predictions, tetrazine **91** showed a different reaction profile (**Figure 22**). In this case, no significant amount of long-lived intermediate was observed, indicating that the elimination is much quicker and therefore, for this tetrazine, it is the cycloaddition step which is rate-limiting. This is also confirmed by the much slower disappearance of TCO-ketoprofen (**114ax**) and the corresponding formation of ketoprofen (**105**), (incomplete after 2 min).

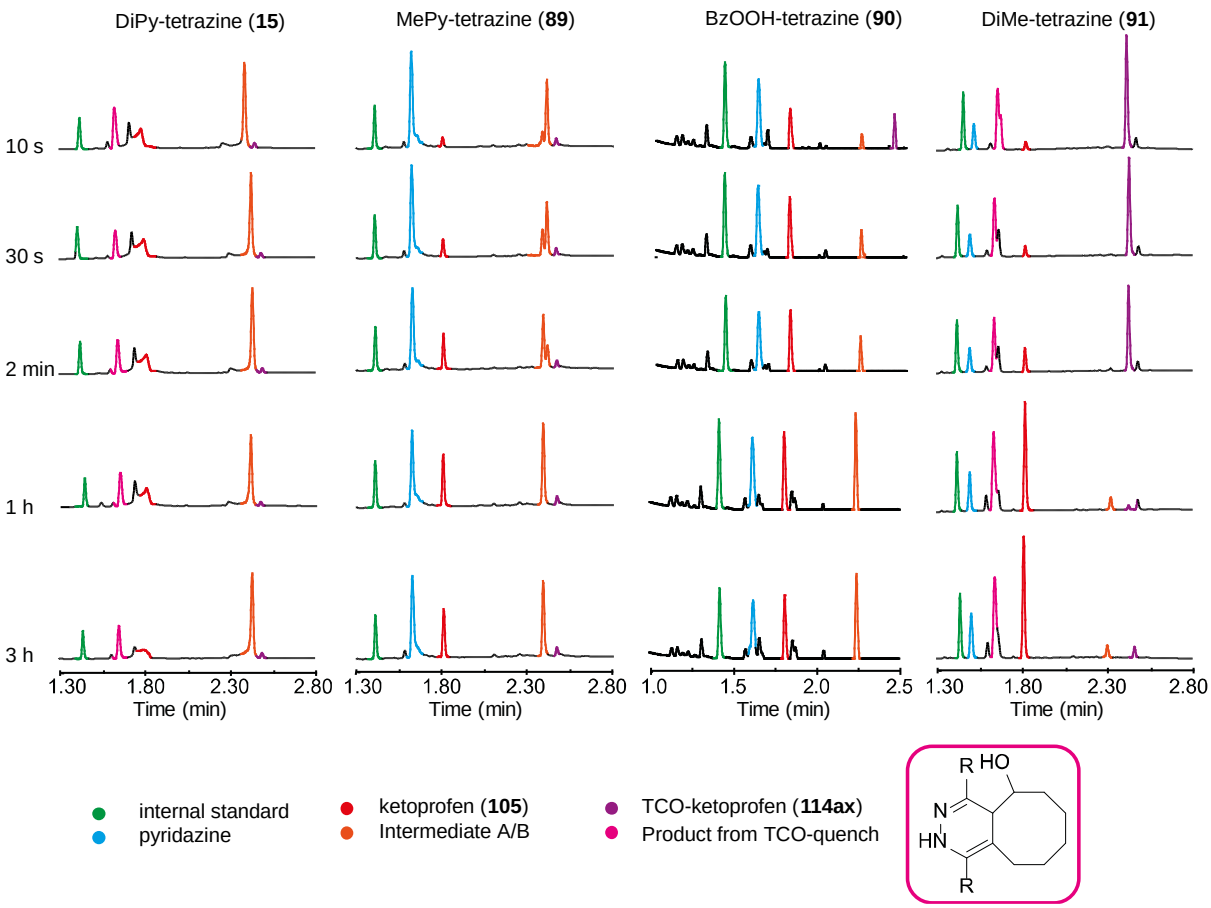

Figure 22. Reaction of TCO-ketoprofen (**114ax**) and tetrazines **15**, **89**, **90**, **91** monitored by LC-MS at 10 s, 30 s, 2 min, 1 h and 3 h time points. For tetrazine **89** the product from the quenching reaction with TCO (not shown), has the same retention time as the pyridazine by-product.

It is also important to note that the three tetrazines with the same RDS all show comparable decaging yields (≈ 25%, **Figure 23**). Interestingly, Tetrazine **91**, which showed no reaction with vinyl ketoprofen, gives a decaging yield double that of the other tetrazines (54%). This highlights the fact that different tetrazines are optimal for different decaging reactions.

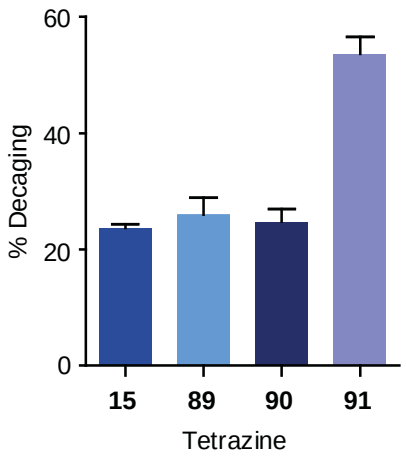

Figure 23. Decaging yields after 3 h assessed by HPLC with benzoic acid as an internal standard.

Next, the effect of water content and pH on decaging yield were assessed. Tetrazine **89** was chosen as a representative example of tetrazines **15**, **89** and **90**. It was shown that the reaction yield increased from 26% (0% water) to 33% (75% water). However, no increase in yield was observed by the addition of 1% formic acid (**Figure 24, Figure 25**).

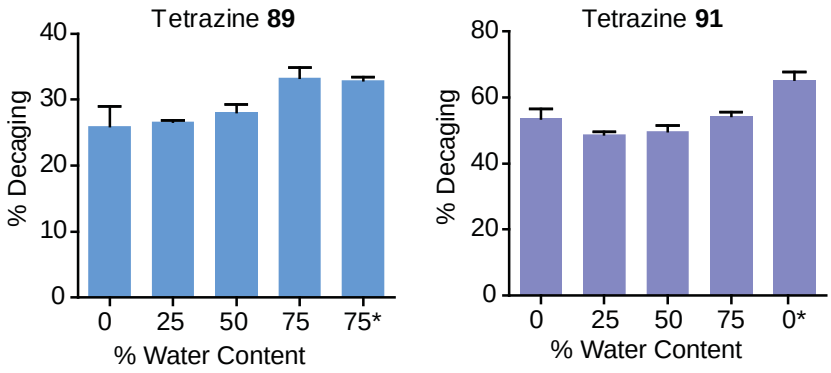

Figure 24. Effect of water content and the addition of 1% formic acid on the decaging yield for reaction of **114ax** with tetrazines **89** and **91**, which both have a different RDS. * + 1% Formic acid.

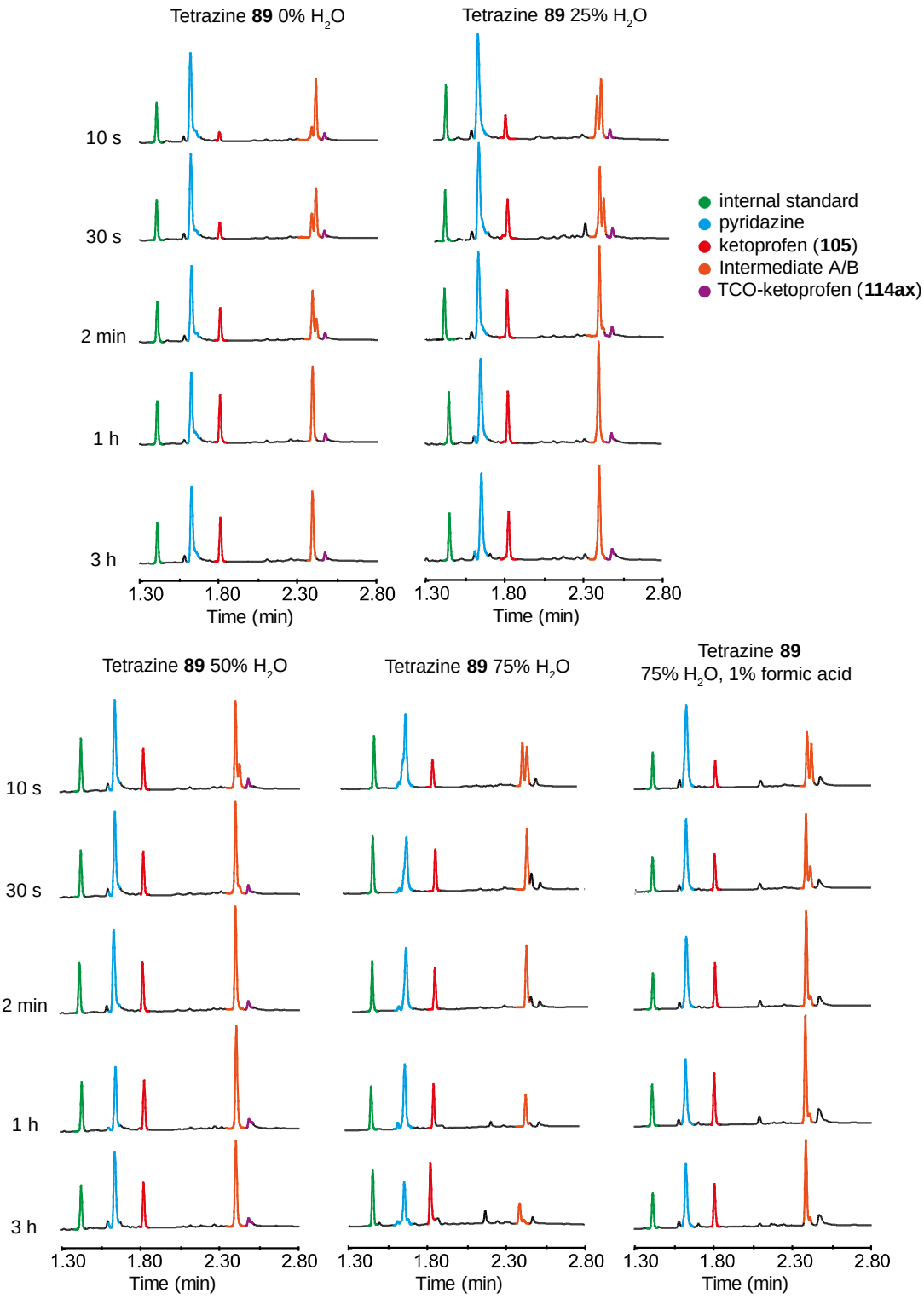

Figure 25. Effect of water content and addition of 1% formic acid on the decaging reaction of TCO-ketoprofen (**114ax**) and tetrazine **89** monitored by LC-MS at 10 s, 30 s, 2 min, 1 h and 3 h time points. The product from the quenching reaction with TCO (not shown), has the same retention time as the pyridazine by-product.

Conversely, tetrazine **91** showed no increase in yield upon increasing water concentration. However, the yield was increased to 65% by the addition of 1% formic acid (**Figure 24, Figure 26**).

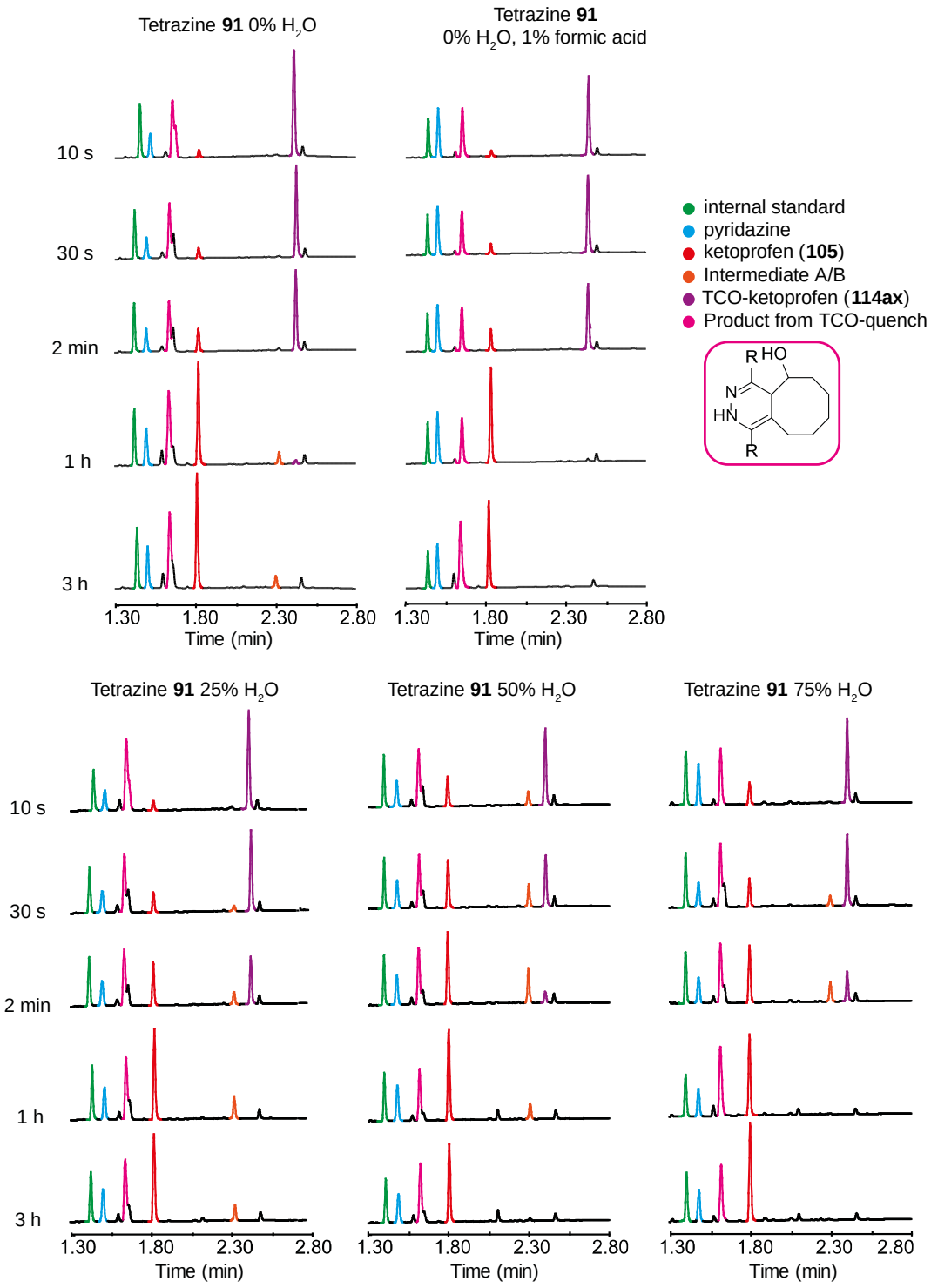

Figure 26. Effect of water content and addition of 1% formic acid on the decaging reaction of TCO-ketoprofen (**114ax**) and tetrazine **91** monitored by LC-MS at 10 s, 30 s, 2 min, 1 h and 3 h time points.

This study highlights the importance of optimising the tetrazine for each reaction, as the tetrazine substituents can alter the RDS of the reaction, resulting in different kinetics and yields of decaging.

2.3.4 Live cell studies

The promising stability and decaging results prompted us to further evaluate the application of this strategy in live cell studies. Using the macrophage cell line RAW264.7 (ATCC® T1B-71), we started by establishing non-toxic concentrations of each compound. The toxicity of tetrazines **89**–**91** were assessed using the CellTiter-Blue cell viability assay (**Figure 27**) and tetrazines **89** and **91** proved toxic to macrophages even at low concentrations (≈ 70–80% viability at 5 µM). In addition, the volatility of tetrazine **91** made it impractical for use in cell experiments, despite this tetrazine resulting in a higher decaging yield by LC-MS. Further studies were carried out using tetrazine **90** as it proved to be non-toxic at high concentrations (≈ 90% viability at 148 µM).

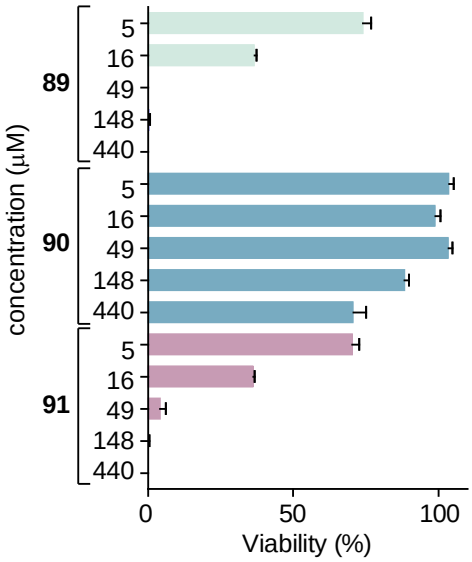

Figure 27. Representative toxicity data in RAW264.7 cells (ATCC® T1B-71) for tetrazines **89**–**91**. Compounds were dissolved in DMSO and added to cells in technical triplicates. Final concentration of DMSO in each well was < 0.5%. The experiment was performed 3 independent times and similar results were obtained each time.

Next, the toxicity of ketoprofen (**105**), TCO-ketoprofen (**114ax** and **114eq**), and the bioorthogonal reactant pair (**114** and **90**) were assessed (**Figure 28**). Based on these results, a concentration of 10 µM was chosen for further experiments.

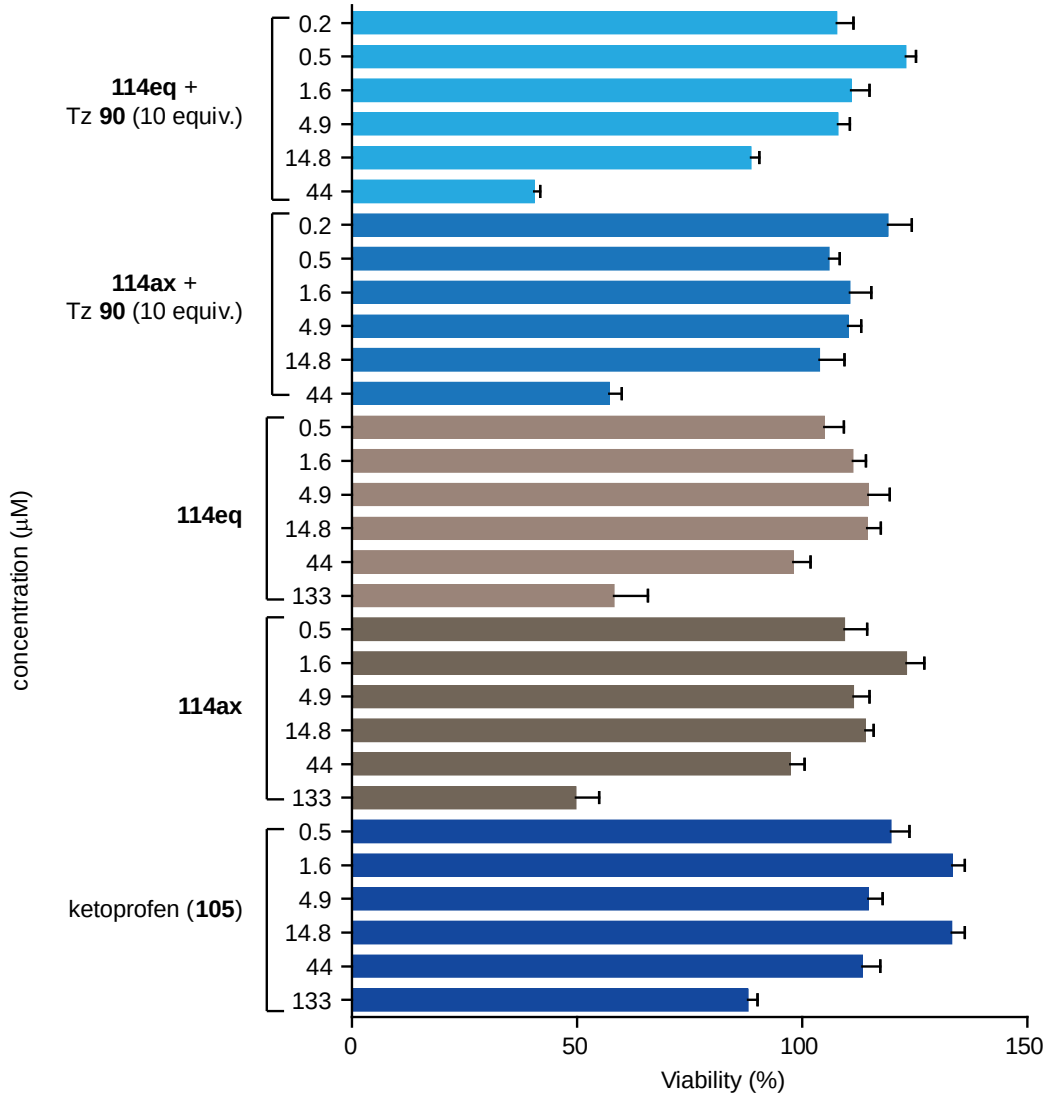

Figure 28. Representative toxicity data in RAW264.7 cells (ATCC® T1B-71) for ketoprofen (**105**), equatorial-TCO-ketoprofen (**114eq**), axial-TCO-ketoprofen (**114ax**), **114ax** + **90**, **114eq** + **90**. Compounds were dissolved in DMSO and added to cells in technical triplicates. Final concentration of DMSO in each well was < 0.5%. The experiment was performed 3 independent times and similar results were obtained each time.

Next, the amount of lipopolysaccharide (LPS) required to induce inflammation was determined. An inflammatory response results in an increased level of nitric oxide (NO) which has a half-life of 6 s. Nitrite (NO_2^-) is a stable, non-volatile, primary degradation product of NO. Therefore, NO production can be quantified by detection of nitrite using the Griess assay. This colorimetric assay utilises a mixture of reagents (**115**, **117**) that, in the presence of nitrite, can form an azo dye (**118**), resulting in an increase in absorbance at 540 nm (**Scheme 72**).[10]

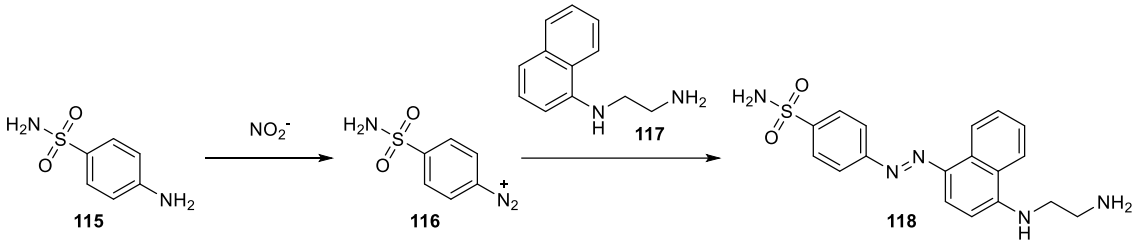

Scheme 72. Griess assay for the detection of nitrite ions.

After assessing both cell viability (**Figure 29**) and concentration of NO produced using the Griess assay, (**Figure 30**), it was found that the optimal concentration of LPS was 0.5 µg/mL. This was the least toxic concentration that could be used whilst still achieving the maximum inflammatory effect.

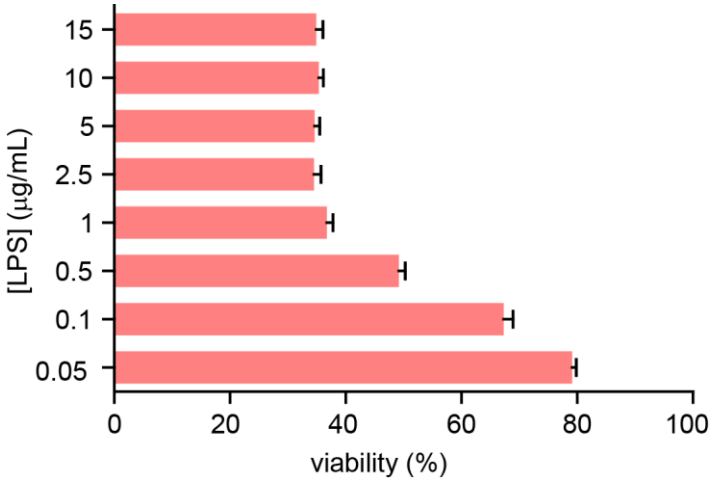

Figure 29. Representative toxicity data in RAW264.7 cells (ATCC® T1B-71) for LPS. The experiment was performed in technical triplicates (3 wells), 3 independent times and similar results were obtained each time.

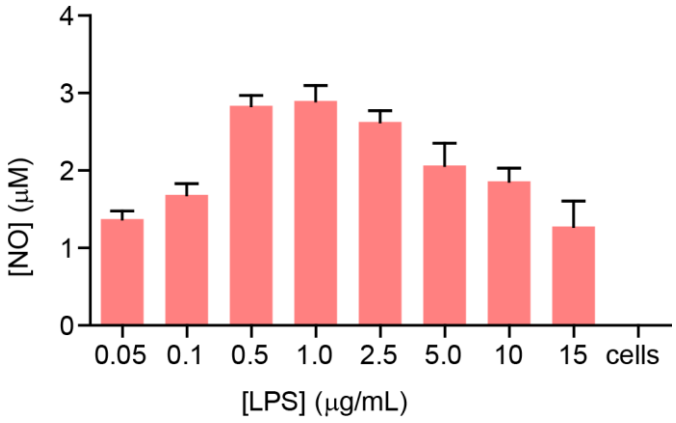

Figure 30. Representative concentration of NO produced in live macrophages upon addition of LPS. LPS was added to the cells in phenol red-free complete media. The optimal concentration of LPS was found to be 0.5 µg/mL. The experiment was performed in technical triplicates (3 wells), 3 independent times and similar results were obtained each time.

Next, the anti-inflammatory effect of tetrazine **90** was assessed using the Griess assay (**Figure 31**). Surprisingly, the anti-inflammatory effect of tetrazines and their reactivity with nitric oxide was observed as previously described.[11] However, a concentration of tetrazine **90** (50 µM) was chosen such that no anti-inflammatory activity was observed. In fact, it was observed that the NO concentration was higher for 50 µM tetrazine **90** than the LPS control. This may be due to endotoxin contamination as this difference was not observed in later experiments (**Figure 33** and **Figure 37**).

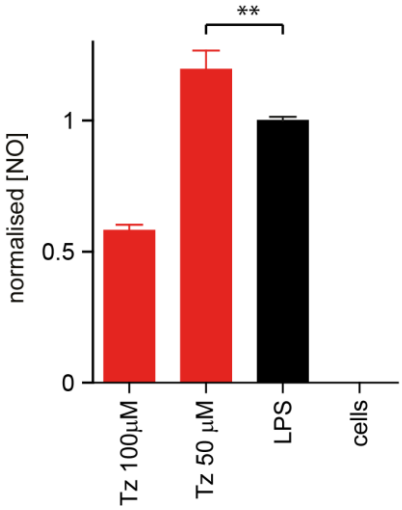

Figure 31. Optimisation of the concentration of tetrazine **90** using the Griess assay. 50 µM of tetrazine was chosen for further studies as no anti-inflammatory activity was observed at this concentration. The experiment was performed in technical triplicates (3 wells), 3 independent times and similar results were obtained each time. Representative data from 1 experiment is shown.

After the optimal concentration of LPS and tetrazine **90** were found, the anti-inflammatory effect of the bioorthogonal pair (**114ax/eq** + **90**) was assessed (**Figure 32**). RAW 264.7 cells were treated with LPS to induce an inflammatory response, then the compounds were added at non-toxic concentrations and the level of inflammation was assessed after 11 h. By using the Griess reagent to monitor the concentration of NO (**Figure 33**), we verified that when TCO-ketoprofen (**114**) was reacted with tetrazine **90** on LPS-stimulated macrophages a significantly enhanced anti-inflammatory effect was observed after 11 h ($p < 0.001$ for equatorial, $p < 0.01$ for axial). This reduction in inflammation corresponds to the successful cleavage of the TCO-ester bond from the caged drug leading to the release of ketoprofen.

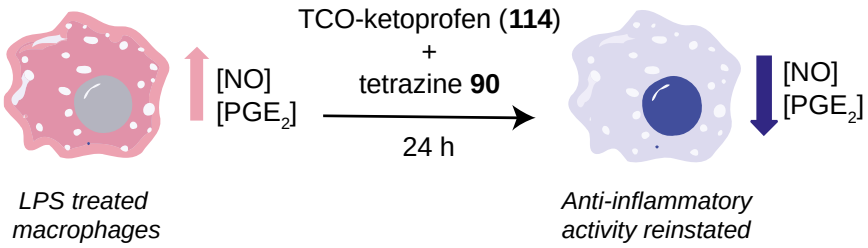

Figure 32. Tetrazine-mediated prodrug activation in live cells.

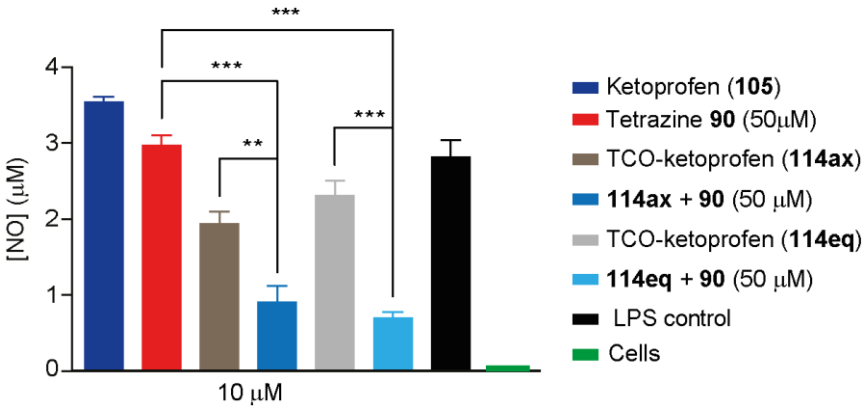

Figure 33. Griess assay used to determine the concentration of nitric oxide in the supernatant after incubation with compounds and LPS (0.5 μg/mL) for 11 h. Decaging of TCO-ketoprofen (**114**) resulted in decreased NO concentrations. The experiment was performed in technical triplicates (3 wells), 3 independent times and similar results were obtained each time. Representative data from 1 experiment is shown. ** ($P \leq 0.01$), *** ($P \leq 0.001$).

During our studies, we also observed that ketoprofen itself failed to reduce the NO levels, whereas TCO-ketoprofen (**114**) has a moderate effect on reducing NO levels (**Figure 33**). This is likely due to the poor membrane permeability of ketoprofen when compared to the caged drug. When protected as the TCO-ester, the cell permeability of ketoprofen was greatly improved, leading to a higher concentration of free drug in the cell as assessed by HPLC (**Figure 34**). Briefly, this study involved incubation of cells for 24 h with either the prodrug (**114**) or free drug (**105**). Subsequent HPLC analysis of the extracellular media revealed that almost no prodrug was detected, whereas a significant amount of ketoprofen was still observed. This experiment was performed by Luxi Qiao.

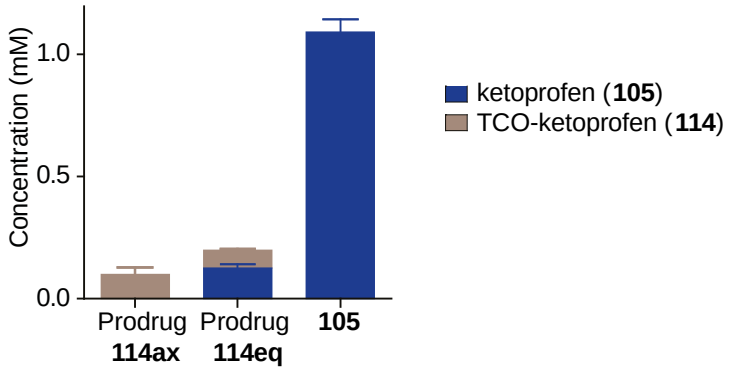

Figure 34. Concentration of TCO-ketoprofen (**114**) and ketoprofen (**105**) present in the media after 24 h after incubation of RAW264.7 cells with 1 mM of either **114ax**, **114eq** or **105**. The high presence of ketoprofen that remains in the media confirms the relatively poor membrane permeability of ketoprofen (**105**). Results are expressed as an average of three independent experiments. Experiment performed by Luxi Qiao.

The incubation time before analysis of the supernatant using the Griess reagent was shown to be important. Compounds and LPS (0.5 μg/mL) were added to the cells and plates were incubated for either 5h, 11h or 24h before analysis. After 5 h (**Figure 35**) the concentration of NO in all wells was below or too close to the detection limit of the Griess assay (0.5 μM).

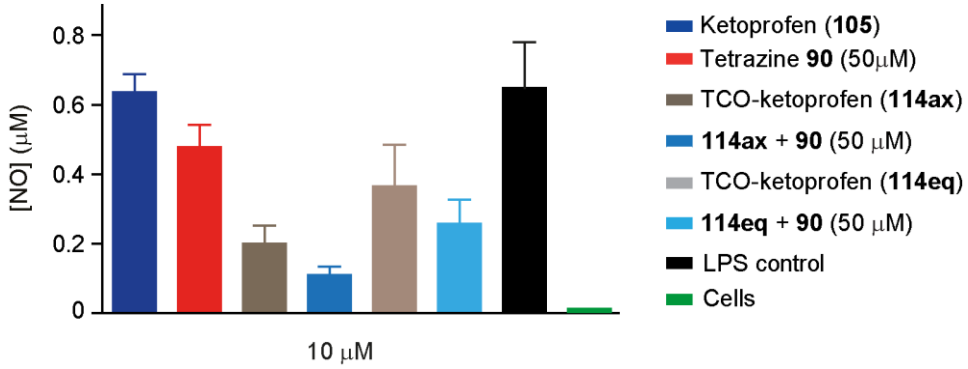

Figure 35. Griess assay used to determine the concentration of NO in the supernatant after incubation with compounds and LPS (0.5 μg/mL) for 5 h. Final concentration of DMSO in each well was ≤ 0.125%. Results were below (or too close to) the detection limit of the Griess assay.

After 11 h, a statistically significant reduction in NO was observed for the bioorthogonal pair compared to both the prodrug and tetrazine alone (**Figure 33**). However, after 24 h, the level of NO from the prodrug alone was the same as the bioorthogonal pair (**Figure 36**). While we expected the caged drug to show very little anti-inflammatory activity, this result suggested that activation might also happen without the tetrazine trigger.

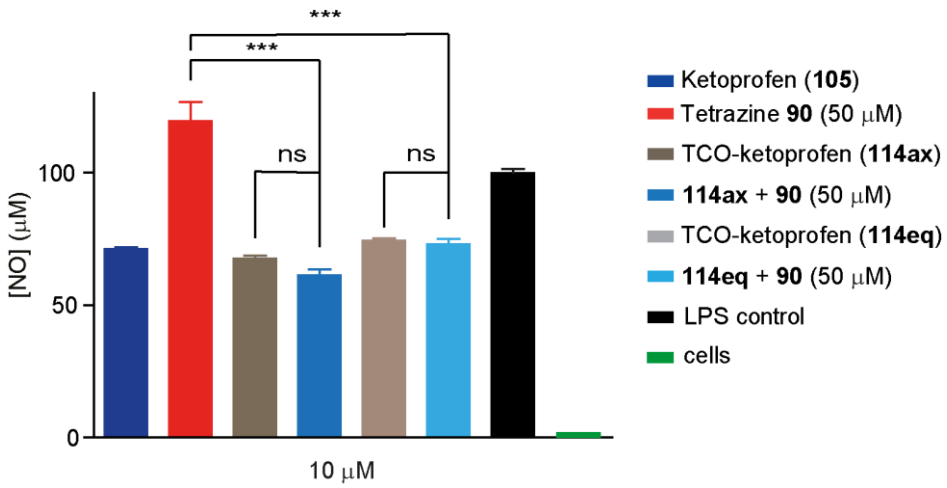

Figure 36. Griess assay used to determine the concentration of NO in the supernatant after incubation with compounds and LPS (0.5 μg/mL) for 24 h. Final concentration of DMSO in each well was ≤ 0.125%. The difference between prodrug **114** and the bioorthogonal pair (**114** + **90**) was not statistically significant. *** (P ≤ 0.001).

As previously mentioned, the ester bond was shown to be fully stable in complete cell culture media for 24 h at 37 °C. Therefore, this observation may be due to the hydrolytic enzymes inside the cell, which was confirmed by a reaction carried out with TCO-ketoprofen (**114**) and esterase from porcine liver (**Scheme 73**). This experiment was performed by Luxi Qiao. After 4 h, a small amount of ketoprofen was already released, and the amount increased over the next 20 hours to a yield of 71% for the axial isomer and 14% for the equatorial isomer. The release of carboxylic acids from ester prodrugs via intracellular esterases has been widely reported.[12–14]

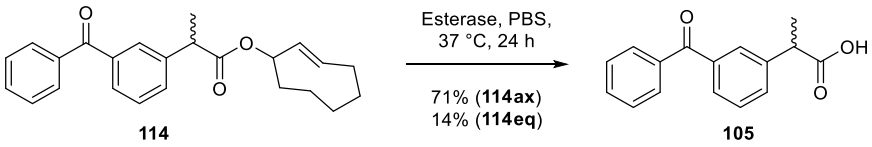

Scheme 73. Reaction of esterase from porcine liver with either the axial or equatorial isomer of TCO-ketoprofen (**114**). Yields were found by HPLC analysis. Experiment performed by Luxi Qiao.

The levels of inflammation were then assessed using an enzyme-linked immunosorbent assay (ELISA) to monitor the levels of prostaglandin E2 (PGE2), which has been shown to be overexpressed in this cell line when inflammation is stimulated by LPS.[15] Briefly, this assay uses a monoclonal antibody that competitively binds both PGE2 in the samples and PGE2-alkaline phosphatase molecules. The alkaline phosphatase produces a chromogenic signal upon the addition of *p*-nitrophenyl phosphate. Therefore, the concentration of PGE2 present in a sample (**Figure 37**) is inversely proportional to the absorbance produced by the bound enzyme. Cells with only LPS showed the highest level of PGE2 (4060 pg/mL), which confirmed that inflammation was successfully stimulated (**Figure 37**). A similarly high

concentration (4010 pg/mL) was observed with the tetrazine, confirming that the tetrazine alone does not have an anti-inflammatory effect. Despite the poor cell permeability of ketoprofen, cells incubated with ketoprofen (**105**) showed the lowest level of PGE2 (215 pg/mL). The anti-inflammatory effect of ketoprofen can be seen using this assay as the ELISA has a higher sensitivity than the Griess assay (detection limit 0.5 μM). TCO-ketoprofen (**114**) also showed lower levels of PGE2 than the LPS control (**114ax**: 686 pg/mL, **114eq**: 486 pg/mL). The bioorthogonal pair resulted in a statistically significant reduction in PGE2 concentration compared to the prodrug alone (**114ax** + **90**: 193 pg/mL, **114eq** + **90**: 200 pg/mL) ($p < 0.001$ for axial, $p < 0.01$ for equatorial). It was observed that the concentration of PGE2 was the same for the bioorthogonal pair as for free ketoprofen, therefore confirming that the anti-inflammatory activity was successfully reinstated upon decaging in live macrophages.

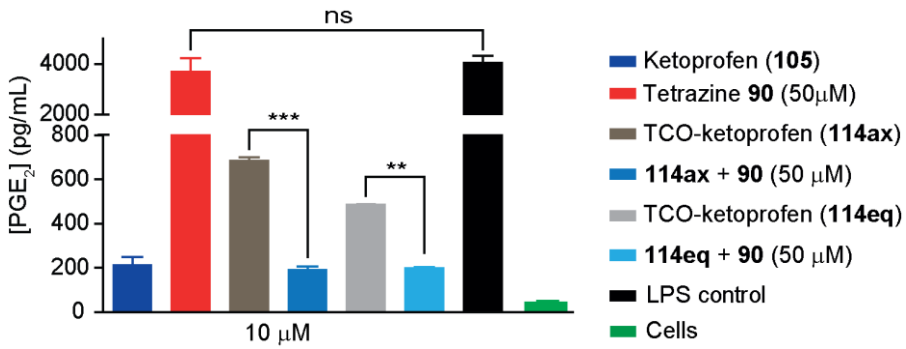

Figure 37. ELISA used to determine the concentration of PGE2. Results expressed as the concentration of PGE2 in the sample. Decaging of TCO-ketoprofen (**114**) resulted in decreased concentrations of PGE2. The experiment was performed in technical triplicates (3 wells), 2 independent times and similar results were obtained each time. Representative data from 1 experiment is shown. ** ($P \leq 0.01$), *** ($P \leq 0.001$).

2.4 Conclusion and future directions

In summary, we have expanded the application of bioorthogonal cleavage reactions to the carboxylic acid functional group. Both vinyl and TCO handles were investigated for masking carboxylic acid groups and their cleavage by tetrazines via the IEDDA reaction was studied. Due to the unstrained nature of the vinyl handle, the reaction with tetrazine proved to be slow (complete after > 11h). In addition, vinyl-protected ketoprofen proved unstable in biological media, limiting the application of this reaction. On the other hand, TCO-protected ketoprofen proved highly stable, likely due to the increased steric protection around the ester bond. In addition, the reaction with tetrazines proved rapid (complete within 2 minutes) showing that this reaction may be suitable for *in vivo* applications. During the synthesis, we also demonstrated that it is possible to use chiral HPLC to separate the desired axial *trans*-isomer from a mixture containing the less reactive *cis*- and equatorial *trans*-

isomers. This strategy is important as, under many reaction conditions, the *trans* double bond readily isomerises to form a mixture of diastereomers.

By extending the IEDDA reaction to the release of carboxylic acids and demonstrating the application on anti-inflammatory drugs, we have expanded the bioorthogonal prodrug activation strategy to encompass a wider range of drugs and diseases. A stable TCO-protected NSAID was successfully decaged in live macrophages, enabling the reinstatement of the anti-inflammatory activity. Near spontaneous release of the active drug after administration of the tetrazine trigger suggests that this strategy may hold *in vivo* potential.

We anticipate that antibodies could be used to target the bioorthogonal handles to extracellular receptors expressed on macrophages (e.g. CD204).[16] For example, an antibody-tetrazine conjugate could be used as the targeting agent. However, this would still result in off-target drug release due to the high cell permeability and non-specific intracellular enzymatic cleavage of the prodrug. In addition, the TCO prodrug would likely be unstable *in vivo* due to isomerisation of the *trans* double bond by Cu ions.[17] On the other hand, these problems could be avoided by conjugating the antibody to the prodrug. An ADC containing a bifunctional TCO linker[18] would prevent isomerisation of TCO (due to increased steric hindrance around the double bond) and stop the prodrug from entering cells. In a pretargeting strategy, after administration and localisation of the ADC at the target site, injection of the tetrazine trigger would result in extracellular drug release, which could then be internalised by target cells (**Scheme 74**). This approach would allow the fast and local delivery of ketoprofen at sites of inflammation.

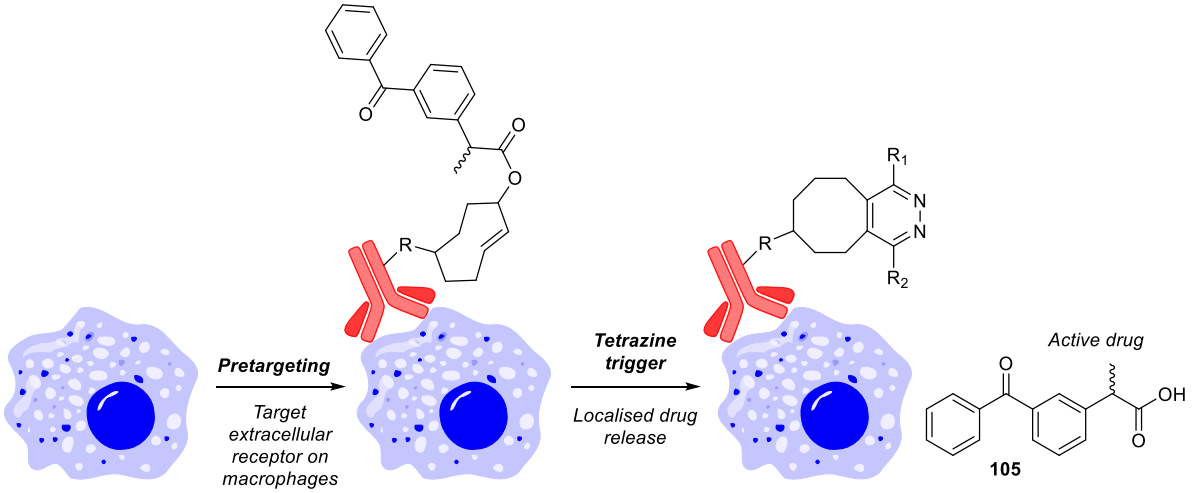

Scheme 74. Localised drug release at sites of inflammation through a pretargeting strategy.

2.5 References for Chapter 2

[1] R. M. Versteegen, W. ten Hoeve, R. Rossin, M. A. de Geus, H. M. Janssen, M. S. Robillard, *Angew. Chem. Int. Ed.* **2018**, *57*, 10494–10499.

[2] J. Krejzová, P. Šimon, E. Vavříková, K. Slámová, H. Pelantová, S. Riva, V. Spiwok, V. Křen, *J. Mol. Catal. B Enzym.* **2013**, *87*, 128–134.

[3] E. Jiménez-Moreno, Z. Guo, B. L. Oliveira, I. S. Albuquerque, A. Kitowski, A. Guerreiro, O. Boutureira, T. Rodrigues, G. Jiménez-Osés, G. J. L. Bernardes, *Angew. Chem Int. Ed.* **2017**, *56*, 243–247.

[4] X. Fan, Y. Ge, F. Lin, Y. Yang, G. Zhang, W. S. C. Ngai, Z. Lin, S. Zheng, J. Wang, J. Zhao, *et al.*, *Angew. Chem. Int. Ed.* **2016**, *55*, 14046–14050.

[5] P. Ghezzi, G. Melillo, C. Meazza, S. Sacco, L. Pellegrini, C. Asti, S. Porzio, A. Marullo, V. Sabbatini, G. Caselli, *et al.*, *J. Pharmacol. Exp. Ther.* **1998**, *287*, 969–974.

[6] H. Wu, S. C. Alexander, S. Jin, N. K. Devaraj, *J. Am. Chem. Soc.* **2016**, *138*, 11429–11432.

[7] M. Royzen, G. P. A. Yap, J. M. Fox, *J. Am. Chem. Soc.* **2008**, *130*, 3760–3761.

[8] G. Dormán, H. Nakamura, A. Pulsipher, G. D. Prestwick, *Chem. Rev.* **2016**, *116*, 15284–15398.

[9] F. Thalhammer, U. Wallfahrer, J. Sauer, *Tetrahedron Lett.* **1990**, *31*, 6851–6854.

[10] M. B. Grisham, G. G. Johnson, J. R. Lancaster, *Methods Enzymol.* **1996**, *268*, 237–246.

[11] M. Al-Omair, A. Sayed, M. Youssef, *Molecules* **2015**, *20*, 2591–2610.

[12] L. D. Lavis, *ACS Chem. Biol.* **2008**, *3*, 203–206.

[13] V. J. Stella, R. Borchardt, M. Hageman, R. Oliyai, H. Maag, J. Tilley, *Prodrugs : Challenges and Rewards*, Springer, **2007**.

[14] B. Testa, J. M. Mayer, in *Hydrolys. Drug Prodrug Metab.*, Verlag Helvetica Chimica Acta, Zürich, **2006**, pp. 419–534.

[15] F. Guan, H. Wang, Y. Shan, Y. Chen, M. Wang, Q. Wang, M. Yin, Y. Zhao, X. Feng, J. Zhang, *Biomed. reports* **2014**, *2*, 760–764.

[16] M. L. Fitzgerald, K. J. Moore, M. W. Freeman, G. L. Reed, *J. Immunol.* **2000**, *164*, 2692–2700.

[17] R. Rossin, S. M. Van Den Bosch, W. Ten Hoeve, M. Carvelli, R. M. Versteegen, J. Lub, M. S. Robillard, *Bioconjug. Chem.* **2013**, *24*, 1210–1217.

[18] R. Rossin, S. M. J. Van Duijnhoven, W. Ten Hoeve, H. M. Janssen, L. H. J. Kleijn, F. J. M. Hoeben, R. M. Versteegen, M. S. Robillard, *Bioconjug. Chem.* **2016**, *27*, 1697–1706.

Chapter 3

Development of a self-immolative linker for the release of alcohols

This chapter is based on the following publication and all figures are adapted from the published manuscript:

Development of a self-immolative linker for tetrazine-triggered release of alcohols in cells. **Sarah Davies**, Bruno L. Oliveira, and Gonçalo J. L. Bernardes. *Org. Biomol. Chem.*, **2019**, *17*, 5725-5730.

3.1 Introduction

Despite the large number of drugs that contain a hydroxyl group,[1] few bioorthogonal decaging reactions for the release of alcohols have been reported. Therefore, methods for fast decaging of protected alcohols would greatly expand the scope of drugs that can be used for *in vivo* prodrug activation. The aim of this chapter was to develop rapid decaging methods to release alcohols through the use of the tetrazine-TCO reaction. Since TCO is a highly reactive, strained alkene, we envisaged that TCO-protected alcohols would exhibit faster alcohol release than the previously reported vinyl ethers and would, therefore, provide a more useful strategy for *in vivo* applications. Here we describe the design, synthesis and decaging studies of several TCO-based linkers for masking alcohol functionality: TCO-carbonates, TCO-ethers and TCO-carbamate benzyl ethers (**Scheme 75**).

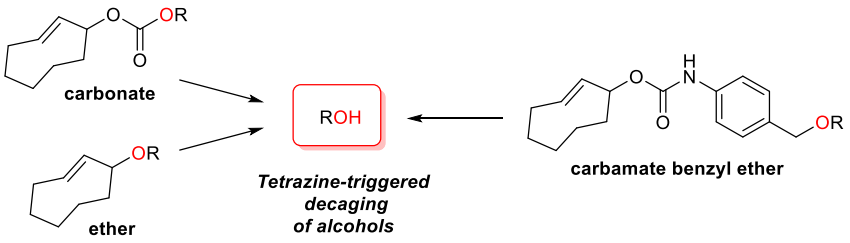

Scheme 75. Project aims: tetrazine-triggered release of alcohol-containing molecules from TCO-carbonates, TCO-ethers and TCO-carbamate benzyl ethers.

In the course of this work, additional methods for alcohol release from isonitrile[2] and TCO[3] based protecting groups were reported. Robillard reported that the TCO handle could be cleaved from

carbonates and ethers to release alcohol-containing molecules (**Scheme 76**).[3] The reported approach requires synthesis of the *cis*-cyclooctene ether followed by photochemical isomerisation to the *trans*-isomer. This final isomerisation step is very low yielding (3–12% after 1.3–7 days under flow) and requires a specialised flow set-up. Although this route is achievable on the reported model compounds, it is not always feasible to obtain such a large quantity of *cis*-product, particularly if this reaction is to gain more widespread use in the area of drug activation. In addition, the synthesis of the ether bond is challenging and attempts to form the ether bond from TCO-OH resulted in isomerisation to the *cis*-form.[3]

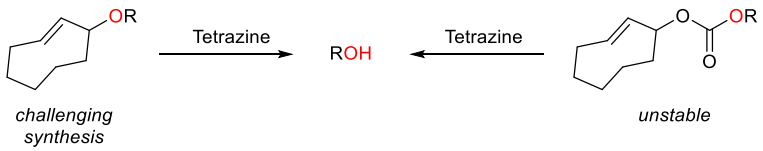

Scheme 76. Tetrazine-triggered release of alcohols from TCO-ethers and TCO-carbonates that were reported by the group of Robillard in the course of this work.[3]

3.2 Carbonate linker

Initially, taking inspiration from the reported TCO-carbamate linker, we proposed an analogous carbonate linker for the release of alcohols. Fluorescent compound 7-hydroxycoumarin (**122**) was chosen as the molecule of interest to enable both the kinetics of release and the stability of the linker to be easily assessed by fluorescence. Model compound **123** was synthesised by activation of TCO-OH (**119**) with *para*-nitrochloroformate (**120**) followed by reaction with 7-hydroxycoumarin (7-HC, **122**, **Scheme 77**).

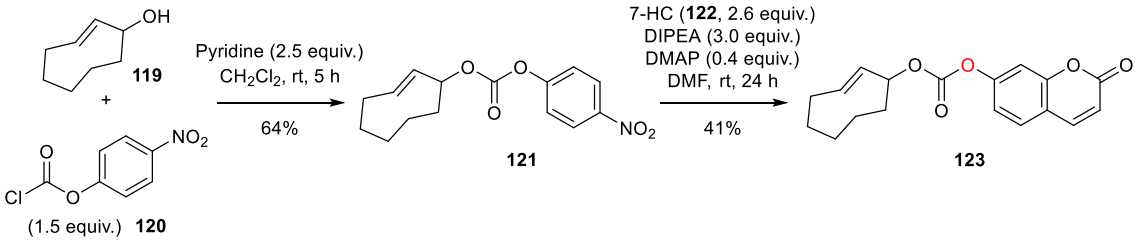

Scheme 77. Synthesis of carbonate **123**.

Next, the reaction of model compound **123** with tetrazine **58** in 50% DMSO/H_2O at 30 °C was studied under second-order conditions by measuring the fluorescence intensity (FI, λ_{ex} = 325 nm, λ_{em} = 460 nm, **Scheme 78**). Tetrazine **58** was chosen for this study as it gave the fastest rate of decaging in cells with the analogous TCO-carbamate.[4]

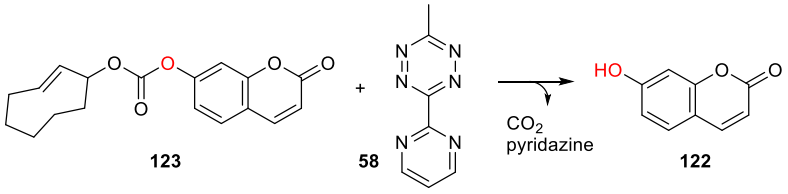

Scheme 78. Tetrazine-triggered release of 7-hydroxycoumarin (**122**) from carbonate **123**.

The increase in coumarin fluorescence was complete within 90 minutes ($t_{1/2}$ = 19 min, **Figure 38**). This rate of release is a similar order of magnitude to, but slower than, the release of doxorubicin from the carbamate linker (complete within 16 min).[5] Importantly it was significantly faster than the previously reported vinyl ether decaging [with 350-fold excess of vinyl ether, the fastest tetrazine had a pseudo first-order rate constant (k_{obs}) of approximately 2 x 10^{-4} s^{-1} that corresponds to a half-life of 58 min].[1]

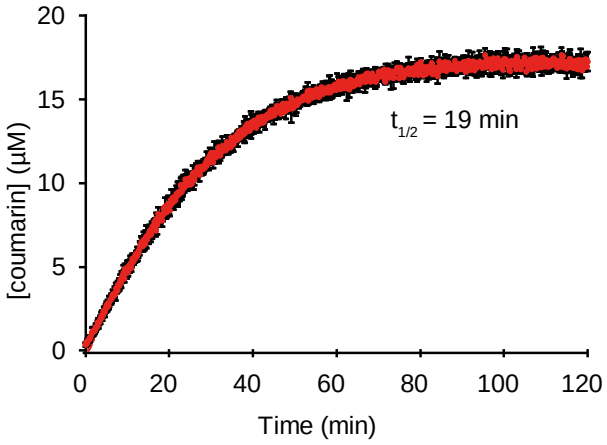

Figure 38. Release of 7-hydroxycoumarin (**122**) in 50% H_2O/DMSO at 30 °C monitored by following the increase in fluorescence (λ_{ex} = 325, λ_{em} = 460 nm).

However, carbonate **123** proved to be highly unstable in 20% human plasma ($t_{1/2}$ = 5 min) and cell media (DMEM + 10% FBS, $t_{1/2}$ = 45 min) and presented moderate stability in PBS ($t_{1/2}$ = 193 min, **Figure 39**), which prevents its application in biological systems. This result was consistent with the work of Robillard who recently reported a TCO-carbonate linker and showed that it underwent 100% fragmentation after 5 h in 50% mouse serum at 37 °C.[3]

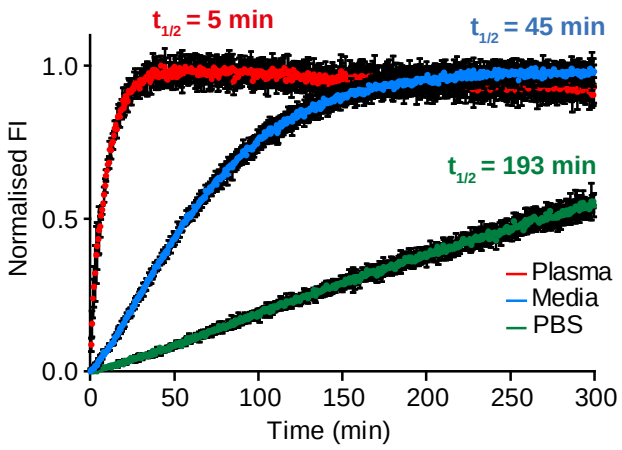

Figure 39. Stability of carbonate **123** in PBS, complete cell culture media (DMEM + 10% FBS) and 20% human plasma/PBS, followed by the increase in fluorescence (λ_{ex} = 325, λ_{em} = 460 nm). Data points and error bars shown.

Importantly, carbonate **123** was shown to be stable in 50% H_2O/DMSO over the time period of the decaging reaction (**Figure 40**).

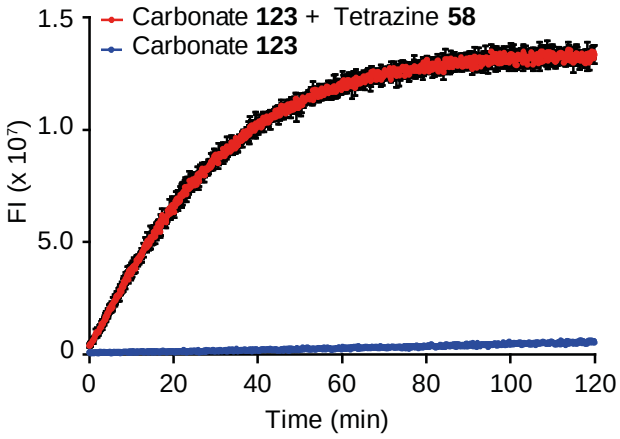

Figure 40. Stability of carbonate **123** in 50% H_2O/DMSO at 30 °C monitored by following the increase in fluorescence (λ_{ex} = 325, λ_{em} = 460 nm) at the same time as the decaging reaction of **123** + **58**.

3.3 Ether linker

Due to the limited stability of the carbonate linker, a new TCO-ether linker was proposed that was expected to be more stable. The envisaged decaging mechanism for this reaction is depicted in **Scheme 79**.[6]

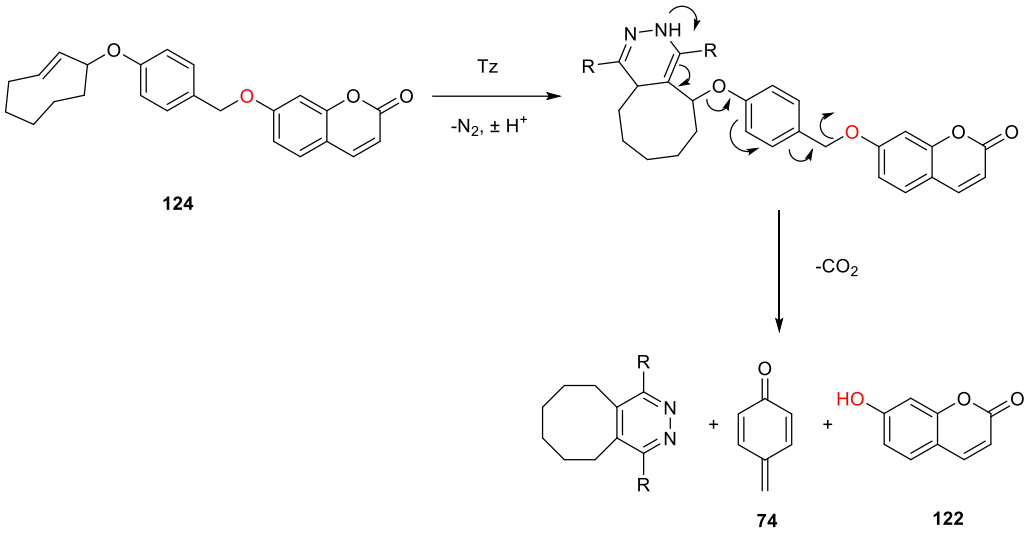

Scheme 79. Proposed mechanism of decaging of the TCO-ether linker.

We decided to use *cis*-cycloocten-1-ol (**111**) to establish a synthetic route to the TCO-ether linker. Not only does this avoid using the more expensive *trans*-isomer, it also allows us to assess whether late stage isomerisation to the *trans*-isomer is possible. Originally we planned to form the ether bond by converting *cis*-cyclooct-2-en-1-ol (**111**) into either mesylate **125** or tosylate **126** and reacting this with 4-hydroxybenzaldehyde (**Scheme 80**). We envisaged that either an S_N2 or S_N2' reaction could occur and both would result in desired product **127**. However, both the mesylation and tosylation were unsuccessful and no reaction occurred after 24 h in either case.

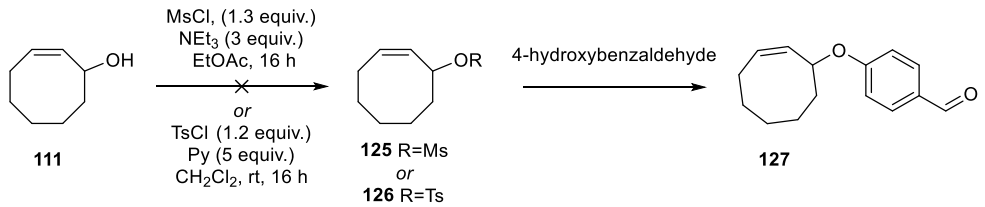

Scheme 80. Attempts to form the mesylate (**125**) or tosylate (**126**) of *cis*-cycloocten-1-ol (**111**) were unsuccessful.

A second route was then proposed, in which we planned to introduce the ether bond via a mitsunobu reaction with 4-hydroxybenzaldehyde (**128**, **Scheme 81**). The desired ether product **127** was obtained in 44% yield (50 mg) on a 0.5 mmol scale. However, the reaction is not scalable as only 2% yield was

obtained when the reaction was repeated on a 1.9 mmol scale. This step was then followed by reduction of the aldehyde with $NaBH_4$ which resulted in **129** in 50% yield. After this, attempts were made to convert the hydroxyl group into a suitable leaving group. However, attempts to form the tosylate and bromide proved unsuccessful. Formation of chloride **130** was achieved using methanesulfonyl chloride and this was then reacted with 7-hydroxycoumarin (**122**) to give **131** in 8% yield over 2 steps. Isomerisation of *cis*-compound **131** was then attempted, however this resulted in loss of alkene peaks in the ^{1}H NMR spectrum, indicating that this compound is unstable to the UV radiation that is required for isomerisation. The final 3 steps of this synthesis were carried out by Dr Bruno Oliveira.

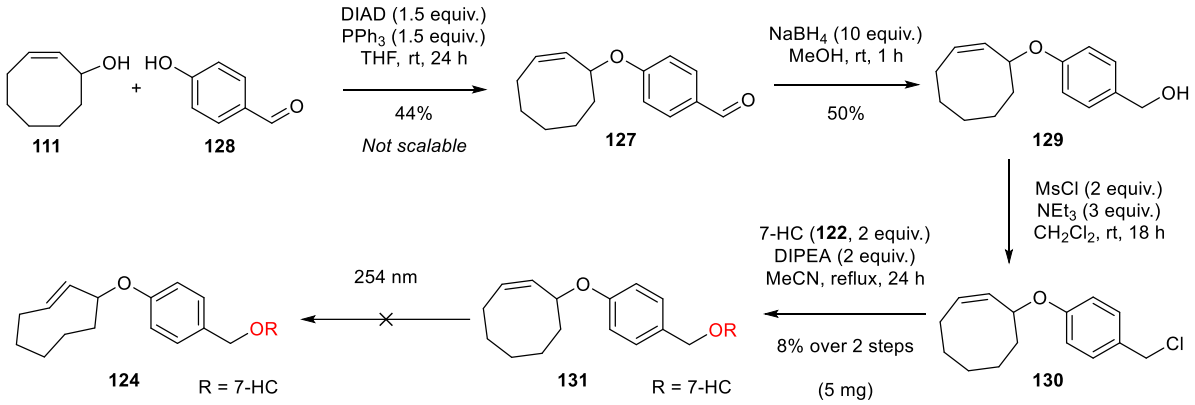

Scheme 81. Synthetic route to ether linker **124**.

Since it was not possible to isomerise the double bond in the last step, we decided to try isomerisation of the different intermediates. The stability of both alcohol **129** and chloride **130** to UV radiation was assessed in deuterated chloroform in a quartz cuvette using 2 penray lamps. ^{1}H NMR analysis showed that no alkene peaks were present after irradiation for 2 h (**Table 4**, **Entries 1 and 2**). Originally deuterated chloroform was chosen as the solvent in order to facilitate monitoring the reaction by ^{1}H NMR. However, it is possible that irradiation of $CDCl_3$ results in chloride radicals which can react with the double bond. Therefore, in a second attempt, alcohol **129** was irradiated in 50% ether/hexane and alkene peaks were still present by ^{1}H NMR after 2 h (**Table 4**, **Entry 3**). Alcohol **129** was expected to be more stable to UV irradiation than **130** since chloride is a better leaving group than hydroxide.

Table 4. Assessing the stability of intermediates **129** and **130** after irradiation at 254 nm for 2 h by observing whether the alkene is still present by ^{1}H NMR.

Entry	Compound	Solvent	Alkene peaks present by ^{1}H NMR
1	**129**	$CDCl_3$	No
2	**130**	$CDCl_3$	No
3	**129**	Et_2O/hexane	yes

The promising stability of the alkene in **129** to UV radiation prompted us to attempt the isomerisation of **129**. Alcohol **129** was irradiated for 6 h at 254 nm and every 30 min the reaction mixture was passed through a column of silver nitrate coated silica, which should selectively bind the *trans*-isomer[7] (**Scheme 82**). The silica was then dried and extracted with ammonium hydroxide, however, no *trans*-product was isolated. 15% of the *cis*-starting material was recovered from the washings of the column.

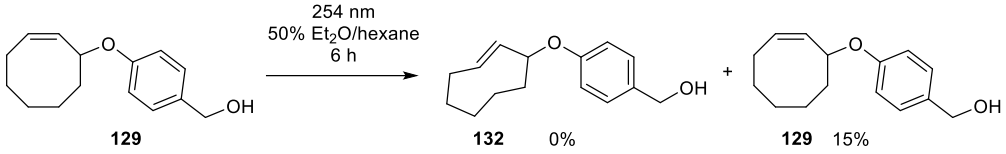

Scheme 82. Attempted isomerisation of **129**.

The isomerisation of *cis*-cyclooctenol (**111**) is low yielding and it seems it is even less efficient if the alcohol is functionalised. Indeed, Robillard required 5.5 grams of starting material **133** to give 144 mg (2.6%) of *trans*-product **134** after 7 days of isomerisation under flow (**Scheme 83**).[3]

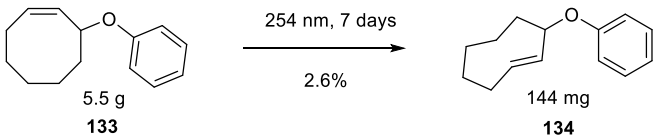

Scheme 83. Reported isomerisation of ether **133** required grams of starting material and resulted in very low yields of product **134**.[3]

Since the first step of this synthetic route is an unscalable mitsunobu reaction, it would be impractical to obtain gram quantities of the *cis*-ether. Therefore, we decided it was best to start with the *trans*-isomer of TCO-OH. However, unfortunately the mitsunobu reaction with TCO-OH (**119**) only resulted in the *cis*-isomer of the product (**127**, **Scheme 84**).

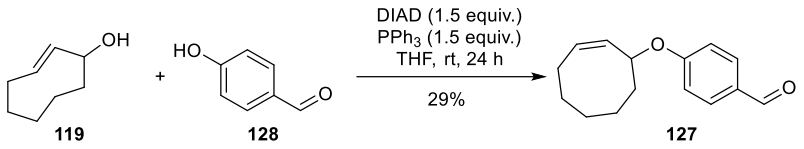

Scheme 84. Repeating the mitsunobu reaction with TCO-OH (**119**) resulted in complete isomerisation to the *cis*-product **127.**

Since the *trans* double bond in TCO is unstable to mitsunobu conditions and the late stage isomerisation of the *cis* double bond is not feasible, we decided not to pursue this route. An alternative linker was proposed which does not contain the synthetically challenging TCO-ether bond.

3.4 Carbamate benzyl ether linker

Next, we designed an alternative linker in which TCO is connected to a self-immolative benzyl ether linker through a carbamate (**Scheme 85**). This carbamate was expected to eliminate CO_2 and the free amine of the self-immolative linker, which can then undergo 1,6-elimination to release the free alcohol. In addition, use of the proposed TCO-carbamate benzyl ether linker for decaging should address the instability of the carbonate linker.

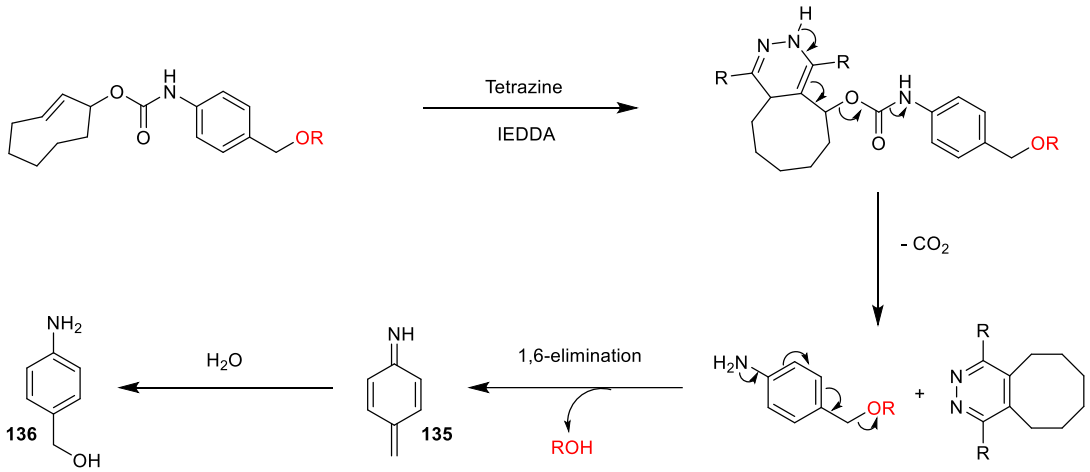

Scheme 85. Proposed mechanism of alcohol release from the TCO-carbamate benzyl ether linker.

Initially, we proposed a synthetic route which involved attaching the molecule of interest in the final step (**Scheme 86**). This minimises the amount of payload required, which is an important consideration when the molecule of interest is an expensive drug. Another reason we chose to attach the payload in the final step is that drugs often contain other functional groups that are incompatible with further synthetic steps. First, 4-aminobenzyl alcohol (**136**) was reacted with *tert*-butyl dimethylsilyl chloride (TBSCl) to give **137** in 77% yield. This was followed by reaction with triphosgene to generate isocyanate

138 and then reaction with TCO-OH to give desired carbamate **139** (10% yield over 2 steps). This yield is comparable to the previously reported one-step reaction of TCO-OH with commercial benzyl isocyanate, which gave yields of 21–37% with reaction times of ≥ 3 days.[5,8]

After this, TBS deprotection resulted in **140** with no observable isomerisation of the double bond. However, in the following bromination step with PBr_3, the double bond isomerised to give bromide **141** as 70% *cis*-isomer. Isomerisation occurred after 5 min at 0 °C and no further isomerisation occurred after the reaction was left for 12 h. This highlights the difficulty of synthesis involving TCO because the double bond is highly unstable and readily isomerises. This behaviour interferes with the decaging kinetics because the *cis*-isomer is 7 orders of magnitude less reactive towards tetrazines than the *trans*-isomer.[9] It was not possible to separate the *cis*- and *trans*-isomers of the bromide (owing to its instability on silica), so the mixture of isomers was used in the subsequent step.

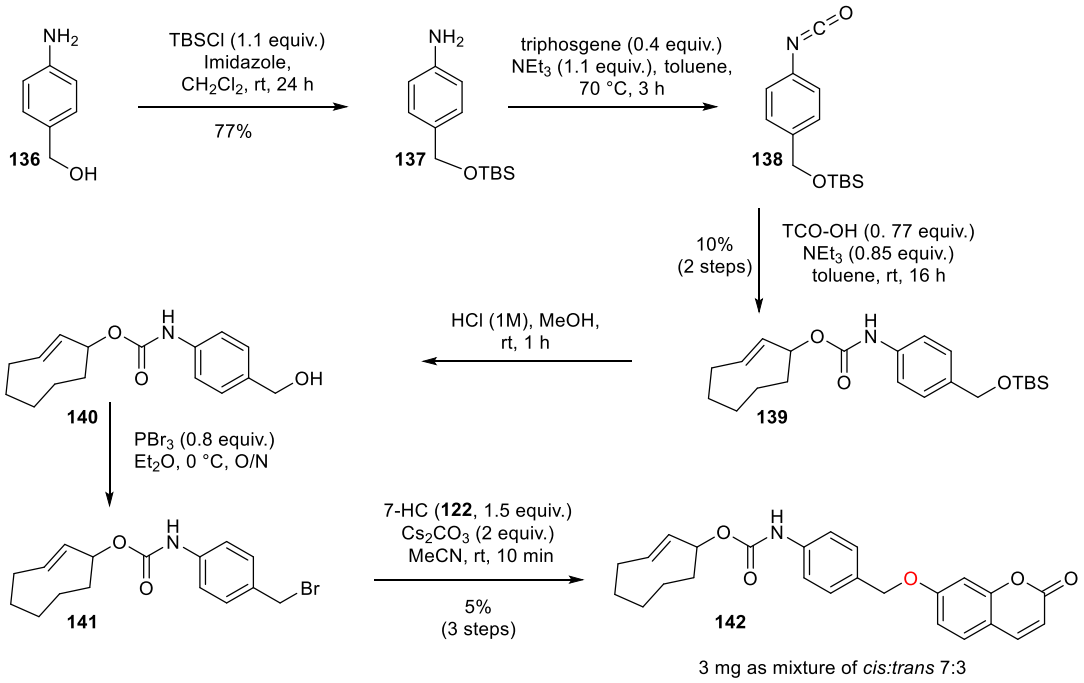

Scheme 86. First synthetic route to the synthesis of TCO-coumarin (**142**), in which the molecule of interest is attached in the final step. The product was obtained as a 7:3 mixture of *cis*:*trans*-isomers.

Reaction with 7-hydroxycoumarin (**122**) and caesium carbonate gave 3 mg of final product **142** as a 7:3 mixture of *cis*:*trans*-isomers. This corresponds to a yield of 5% over 3 steps. It has been reported that the *trans*-isomer selectively binds to $AgNO_3$-impregnated silica and this is used to separate the *trans*-isomer during the photochemical synthesis of TCO-OH.[10] However, attempts to separate the isomers of **142** by trapping onto $AgNO_3$-coated silica were unsuccessful. Interestingly, the product mixture is stable to further isomerisation for 3 weeks in $CDCl_3$ at room temperature (**Figure 41**).

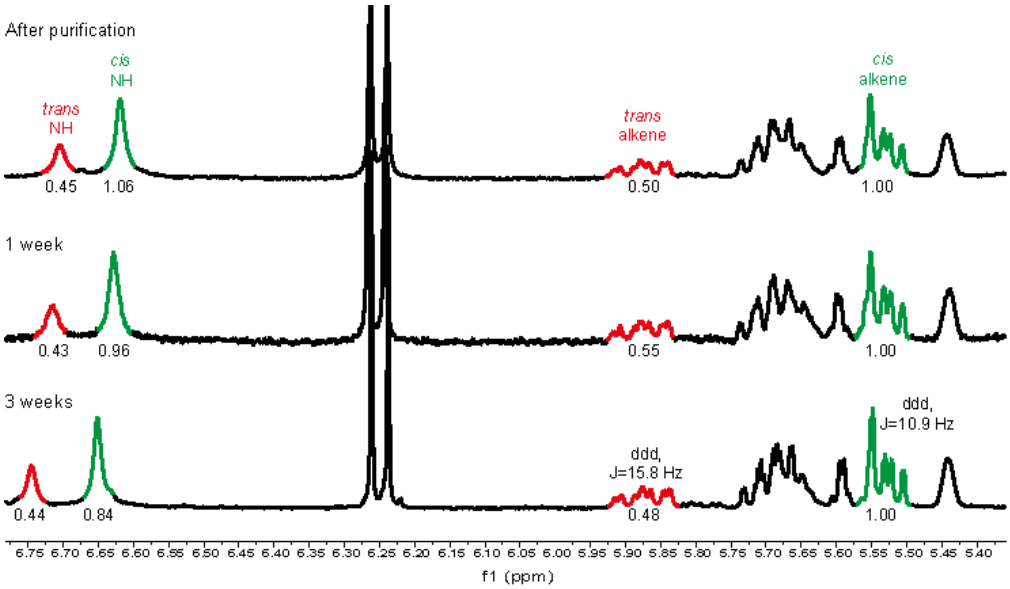

Figure 41. Alkene region of the ^{1}H NMR spectra of product **142** obtained as a 7:3 mixture of *cis*:*trans*-isomers. The NMR sample was left in $CDCl_3$ in light at rt and no further isomerisation occurred after 3 weeks.

With these results in hand we decided that this route was not synthetically useful since it required the use of a large amount of expensive TCO-OH to give the final compound in low yield, predominantly as the less active *cis*-isomer, which would then require separation by chiral HPLC.[11]

Therefore, we next attempted to attach TCO-OH in the final step. In this route, 4-aminobenzyl alcohol (**136**) was first protected with a *tert*-butyloxycarbonyl (Boc) group to give **143** in 96% yield (**Scheme 87**). Reaction with PBr_3 resulted in bromide **144**, which was subsequently reacted with 7-hydroxycoumarin (**122**) and caesium carbonate to give **145** in 20% yield over 2 steps. Next, Boc deprotection was attempted using bromotrimethylsilane (TMSBr), which is known to be compatible with coumarins.[12] We were worried that stronger acidic conditions would hydrolyse the coumarin lactone bond. Unfortunately, after removal of the Boc group, the self-immolative linker can undergo 1,6-elimination and although complete consumption of **145** occurred, no free aniline **146** was detected and coumarin **122** was observed by ^{1}H NMR.

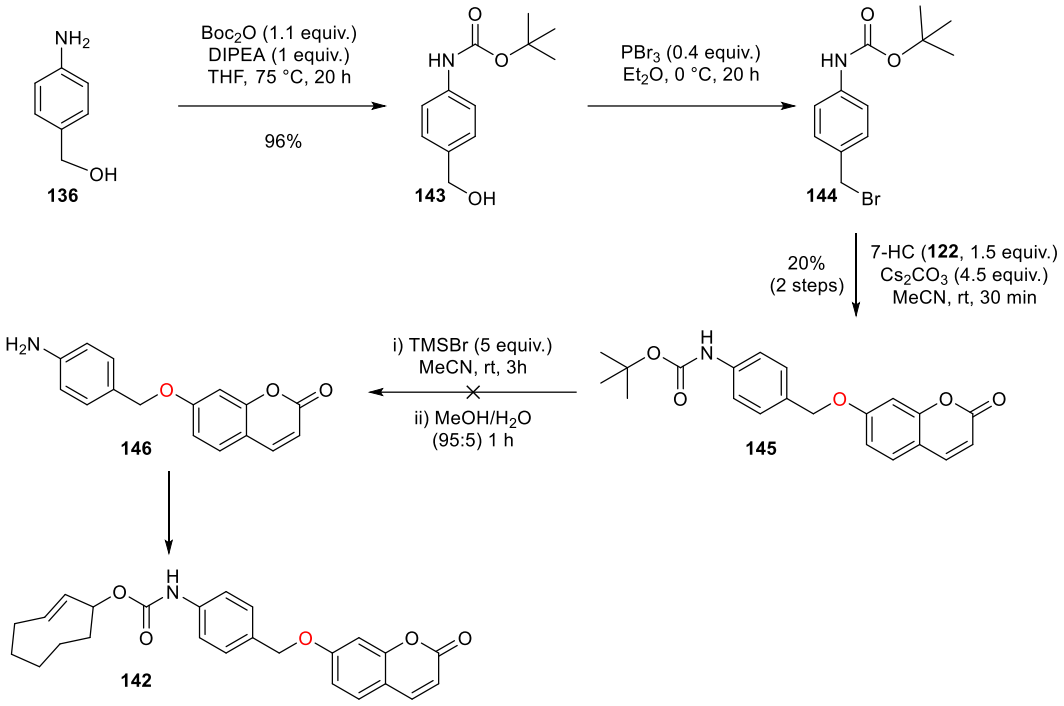

Scheme 87. Second synthetic route to the synthesis of TCO-coumarin (**142**), in which TCO is attached in the final step. Removal of the Boc protecting group resulted in an unstable aniline intermediate.

Next, an attempt was made to generate isocyanate **147** directly from **145** without isolating the free aniline intermediate **146** (**Scheme 88**). However, reaction with 2-chloropyridine and trifluoromethane sulfonic anhydride following the method by Spyropoulos *et al.*[13] proved unsuccessful. In another attempt, **145** was heated in a solution of triphosgene. It was proposed that the Boc group was thermally unstable and that, due to the high reactivity of triphosgene, aniline **146** would react rapidly before elimination could occur. However, no reaction occurred.

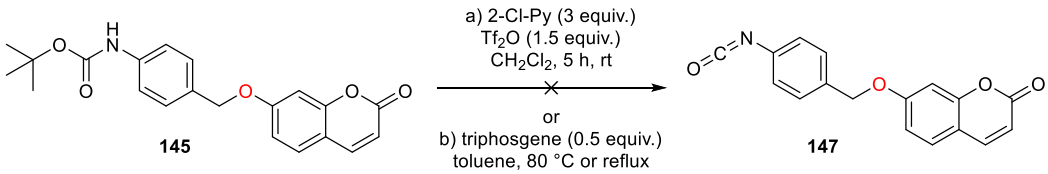

Scheme 88. Attempts to form isocyanate **147** directly from Boc protected **145**.

It was then found that isocyanates can be formed directly from anilinium chloride salts.[14] Therefore, the deprotection of **145** was then carried out using HCl (4 M in dioxane, **Scheme 89**). Upon completion of the reaction, removal of the solvent resulted in the anilinium chloride salt **148**, which was then reacted with triphosgene to give isocyanate **147**.[14] The formation of the anilinium chloride salt proved crucial to prevent elimination and generate the isocyanate from the Boc-protected amine, which may be a useful strategy in self-immolative linker synthesis.

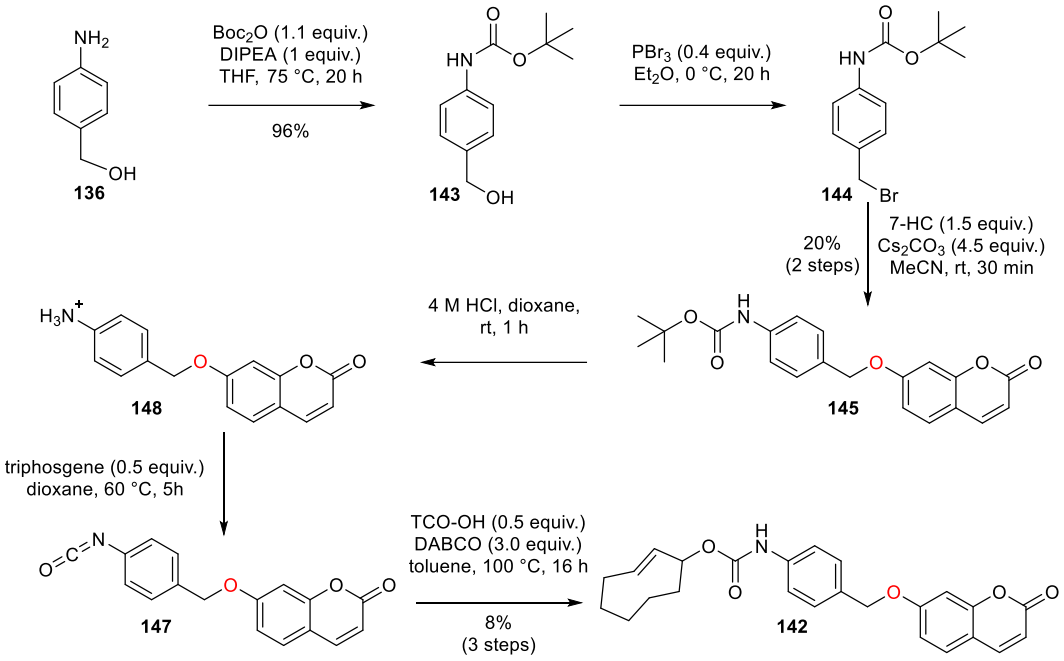

Scheme 89. Final synthetic route to the synthesis of TCO-coumarin (**142**), in which TCO is attached in the final step. Formation of isocyanate **147** from Boc protected **145** via the anilinium chloride salt **148** proved crucial to prevent elimination.

Finally, isocyanate **147** was reacted with TCO-OH. Dibutyltin dilaurate, a catalyst commonly used for isocyanate reactions, caused isomerisation of TCO (observed by TLC). However, by using 1,4-diazabicyclo[2.2.2]octane (DABCO) as a catalyst, final compound **142** was obtained in 8% yield over 3 steps. Again, although this yield is fairly low, it is similar to previous reactions of TCO-OH with isocyanates[5,8] and is an improvement on the one-step photochemical isomerisation (3–12% after 1.3–7 days under flow).[3] In addition, it does not require the alcohol in gram-scale, which is essential when working with expensive drug payloads. Importantly, the product was obtained entirely as the axial, *trans*-isomer.

3.5 Prodrug synthesis

Next, the developed route was applied to the synthesis of prodrugs. As previously mentioned, drugs often contain several reactive functional groups and, for this reason, it is common to attach the drug in the final synthetic step. However, in our optimised synthetic route it was essential to attach TCO in the final step in order to avoid isomerisation. This meant that it was necessary to attach the drug at an earlier stage. Therefore, we selected alcohol-containing drugs with little other functionality, in order to minimise problems of functional group tolerance during the synthesis: triclosan (TCS, **149**, an

antibacterial drug) and camptothecin (**81**, an anticancer, topoisomerase I inhibitor, **Figure 42**). Attempts to conjugate more structurally complex drugs to TCO were unsuccessful, as the presence of additional functional groups in the drug made it incompatible with the final steps of the synthesis.

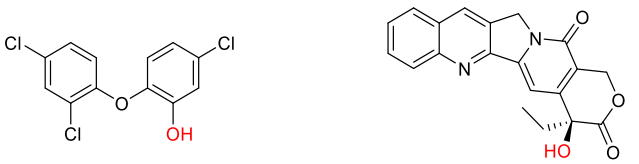

149 triclosan **81** (S) – (+) – Camptothecin

Figure 42. Alcohol-containing drugs triclosan (**149**) and camptothecin (**81**) were selected for prodrug synthesis due to their lack of other reactive functional groups.

Prodrug **153** was synthesised according to the previously reported protocol (**Scheme 90**). Reaction of bromide **144** with triclosan (**149**) gave **150** in 56% yield and conversion of **150** to **153** in the final 3 steps was achieved in 18% yield. Again, the product was obtained as 100% the axial, *trans*-isomer.

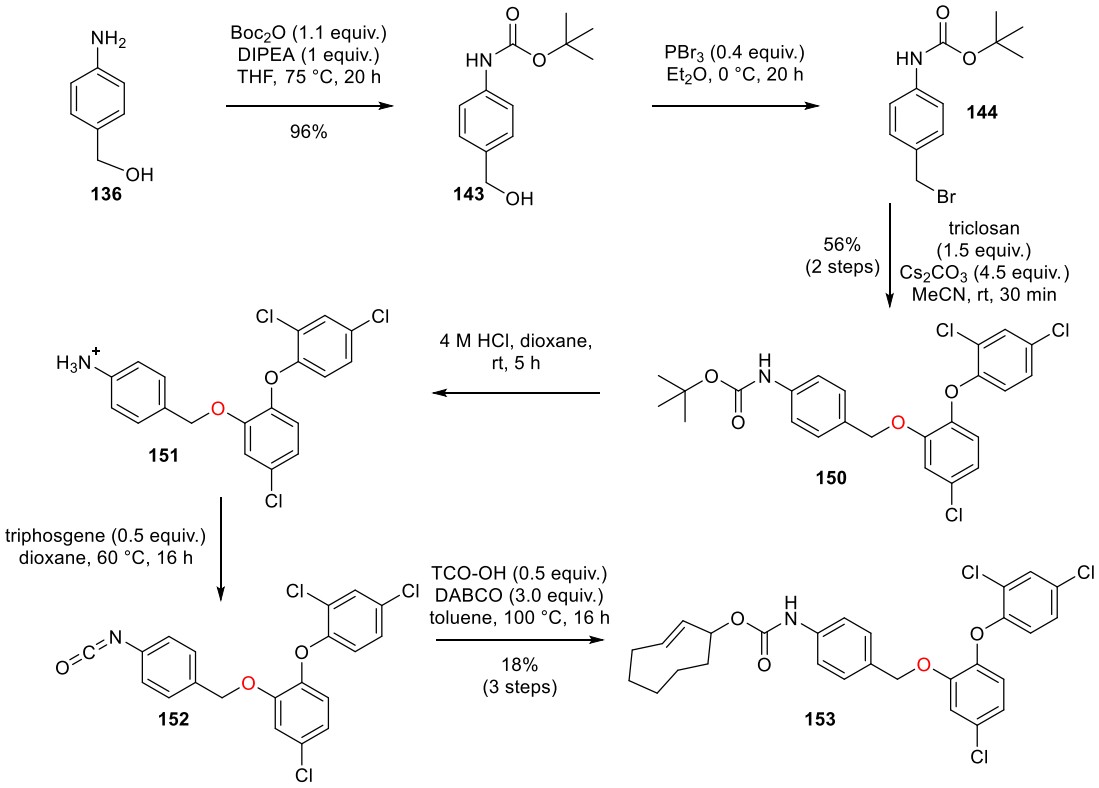

Scheme 90. Synthesis of TCO-protected triclosan (**153**).

Finally, the synthetic route was attempted using camptothecin. Reaction of camptothecin (**81**) with bromide **144** resulted in 49% of desired product **154** (**Scheme 91**).

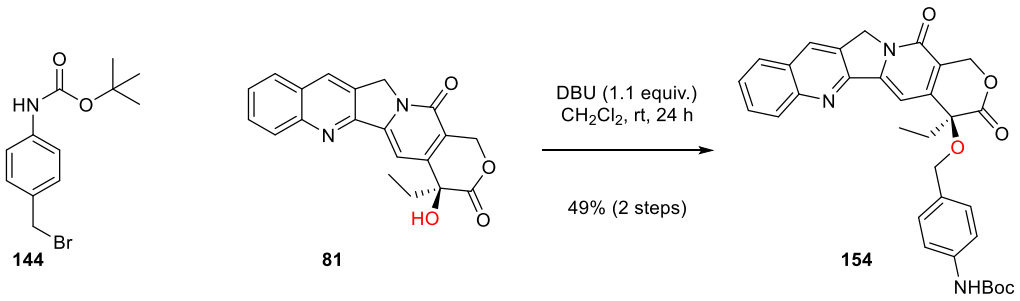

Scheme 91. Conjugation of camptothecin (**81**) with bromide **144**.

However, **154** proved highly unstable and after storage at -20 °C overnight, a significant reduction in the intensity of peaks corresponding to the linker (4.65 ppm: C*H*$_2$, 6.48 ppm: N*H*, 7.33 ppm: Ar-*H*) was observed by ^{1}H NMR (**Figure 43**). Therefore, this route was not viable for this compound.

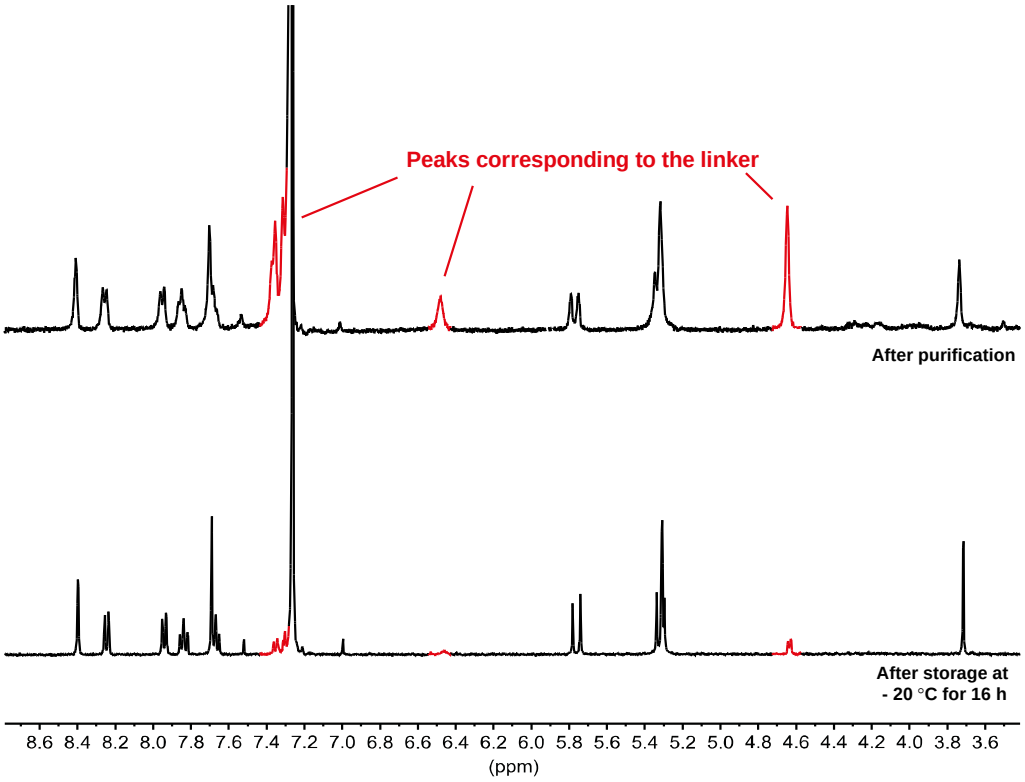

Figure 43. Section of the ^{1}H NMR spectra of **154** immediately after purification compared to after storage overnight at -20 °C. After storage, the peaks corresponding to the linker showed a significant reduction in intensity (4.65 ppm: C*H*$_2$, 6.48 ppm: N*H*, 7.33 ppm: Ar-*H*) and the remaining peaks correspond to camptothecin (**81**).

3.6 Kinetic and stability studies

The kinetics and stability of the TCO-carbamate benzyl ether linker were then assessed using model coumarin compound **142**. The stability of **142** was evaluated by monitoring the fluorescence intensity (λ_{ex} = 325 nm, λ_{em} = 460 nm) over 15 h. The compound proved to be stable for 15 h in PBS, complete cell culture media (DMEM + 10% FBS), Lysogeny broth (LB) media and 20% human plasma/H_2O, with no increase in fluorescence observed (**Figure 44**).

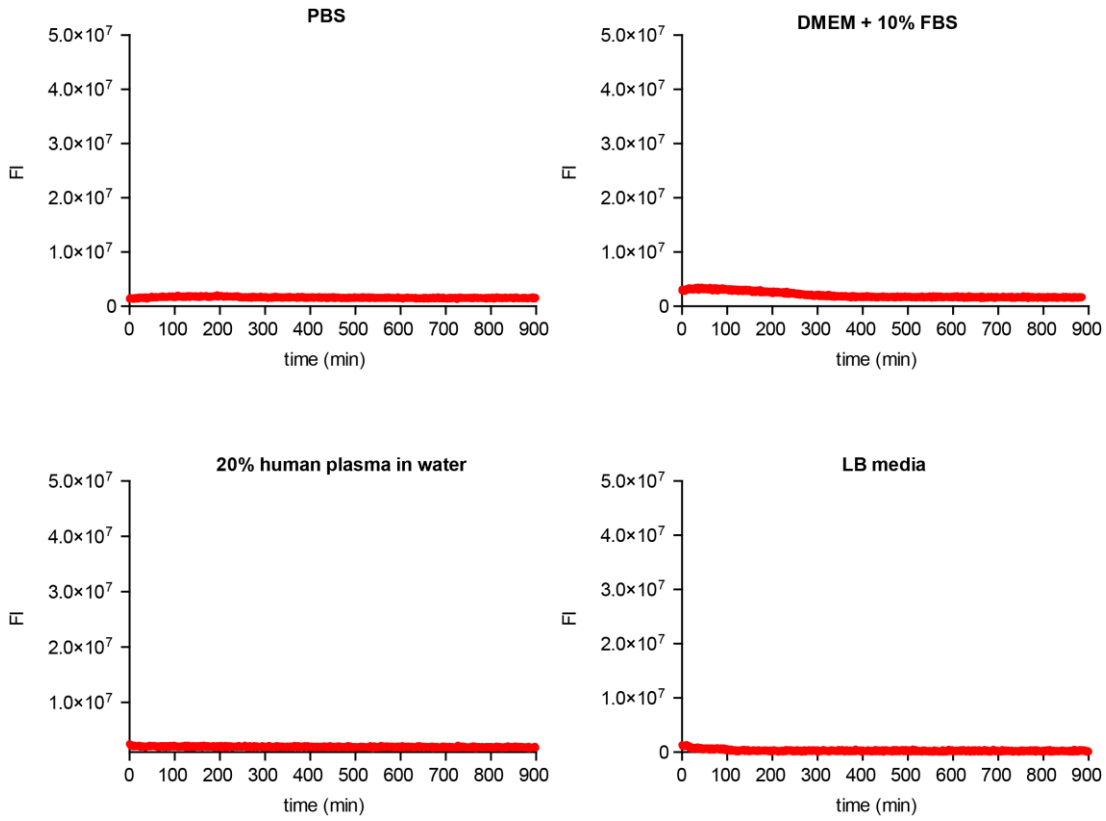

Figure 44. Stability of TCO-coumarin (**142**) in PBS, complete cell culture media (DMEM + 10% FBS), LB media and 20% human plasma/H_2O. Assessed by monitoring the fluorescence intensity (λ_{ex} = 325 nm, λ_{em} = 460 nm) over 15 h.

Before studying the reaction of **142** with tetrazines, quantitative NMR (qNMR) with benzoic acid as an external standard was used to accurately determine the concentration of stock solutions of each reagent (**Figure 45**). Briefly, a sealed capillary tube containing 10 mM benzoic acid in DMSO-D_6 was calibrated against stock solutions of 7-hydroxycoumarin (**122**) at known concentrations (26.5–5.4 mM prepared by accurate dilution based on solvent weight). The ^{1}H NMR spectra was recorded twice for each sample and the integration ratio of coumarin:benzoic acid was plotted against concentration. Importantly the relationship between concentration and integration ratio was shown to be solvent dependent. After calibration of the external standard, the capillary was added to NMR tubes

containing stock solutions of compounds and the ratio of integration (compound:benzoic acid standard) was measured. This was then converted to concentration using the fitting on the appropriate graph. This method was essential as < 10 mg of model compound **142** was synthesised and therefore, the mass balance error would be high. It is important to know accurate reagent concentrations for the determination of reaction rates using second-order kinetics, in which the reagents must be equimolar. qNMR can also be used to determine the concentration of saturated solutions, which is useful for compounds of low solubility (eg. tetrazine **15**).

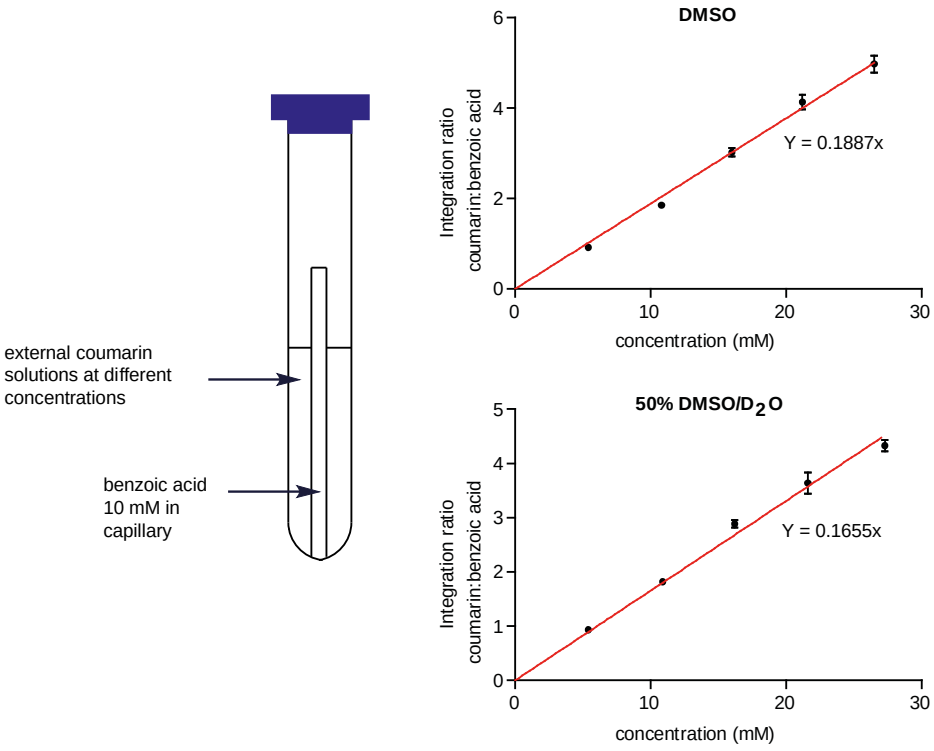

Figure 45. Quantitative NMR (qNMR) with benzoic acid as an external standard was used in order to accurately determine the concentration of stock solutions of each reagent. Calibration graphs of ^{1}H NMR integration ratios of coumarin:benzoic acid peaks *vs* coumarin concentration were plotted in two different solvent systems.

With exact concentrations of the stock solutions determined, we next studied the reaction of model compound **142** with tetrazines **15**, **58**, **89**, **90**, **91**, **155** (**Scheme 92**). In addition to the tetrazines studied in chapter 2, tetrazine **155**, bearing an amine group, was chosen (**Figure 46**).

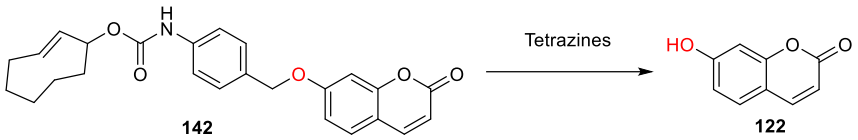

Scheme 92. Reaction of model compound **142** with tetrazines **15, 58, 89, 90, 91, 155**.

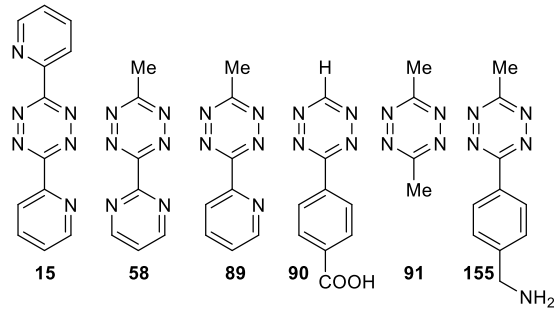

Figure 46. Structures of tetrazines chosen for studies with TCO-coumarin (**142**).

The reactants were mixed in a 1:1 ratio in 50% H_2O/DMSO and the reaction mixture was analysed after 24 h by HPLC. Concentration of the released coumarin was determined using a calibration curve with known concentrations of coumarin and internal standard (**Figure 47**). Briefly, mixtures of **122** at known concentrations (0.2–0.83 mM) and internal standard benzoic acid (0.67 mM) were analysed by HPLC/UV and the ratio of areas of the UV peaks at 220 nm were plotted against concentration of **122**.

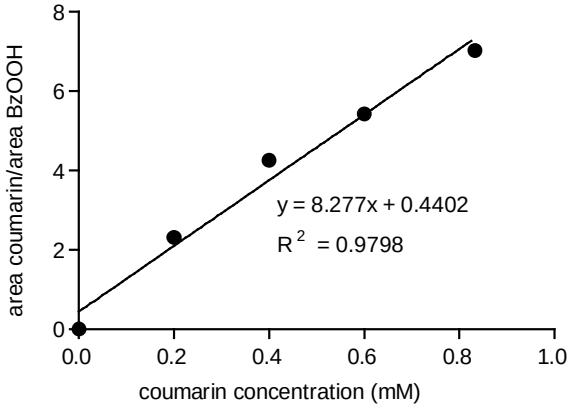

Figure 47. Calibration curve for the detection of 7-hydroxycoumarin (**122**) by HPLC.

The highest decaging yield (39%) was observed with tetrazine **90**. **15** and **155** showed particularly low yields (< 10%) whereas **91**, **89** and **58** resulted in yields of 22%, 25% and 32%, respectively (**Figure 48**).

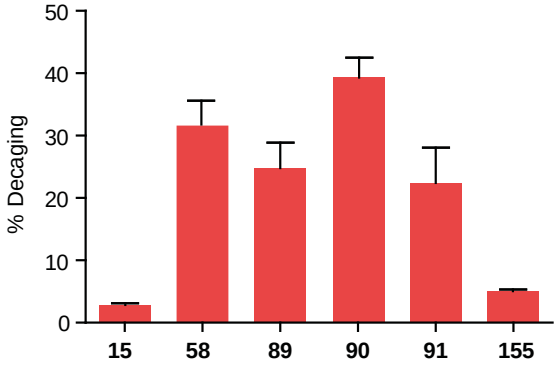

Figure 48. Decaging yield of the reaction of TCO-coumarin (**142**) with tetrazines after 24 h, assessed by HPLC/UV.

For this reason, along with its higher stability relative to other tetrazines (**Figure 49**), tetrazine **90** was chosen for subsequent studies.

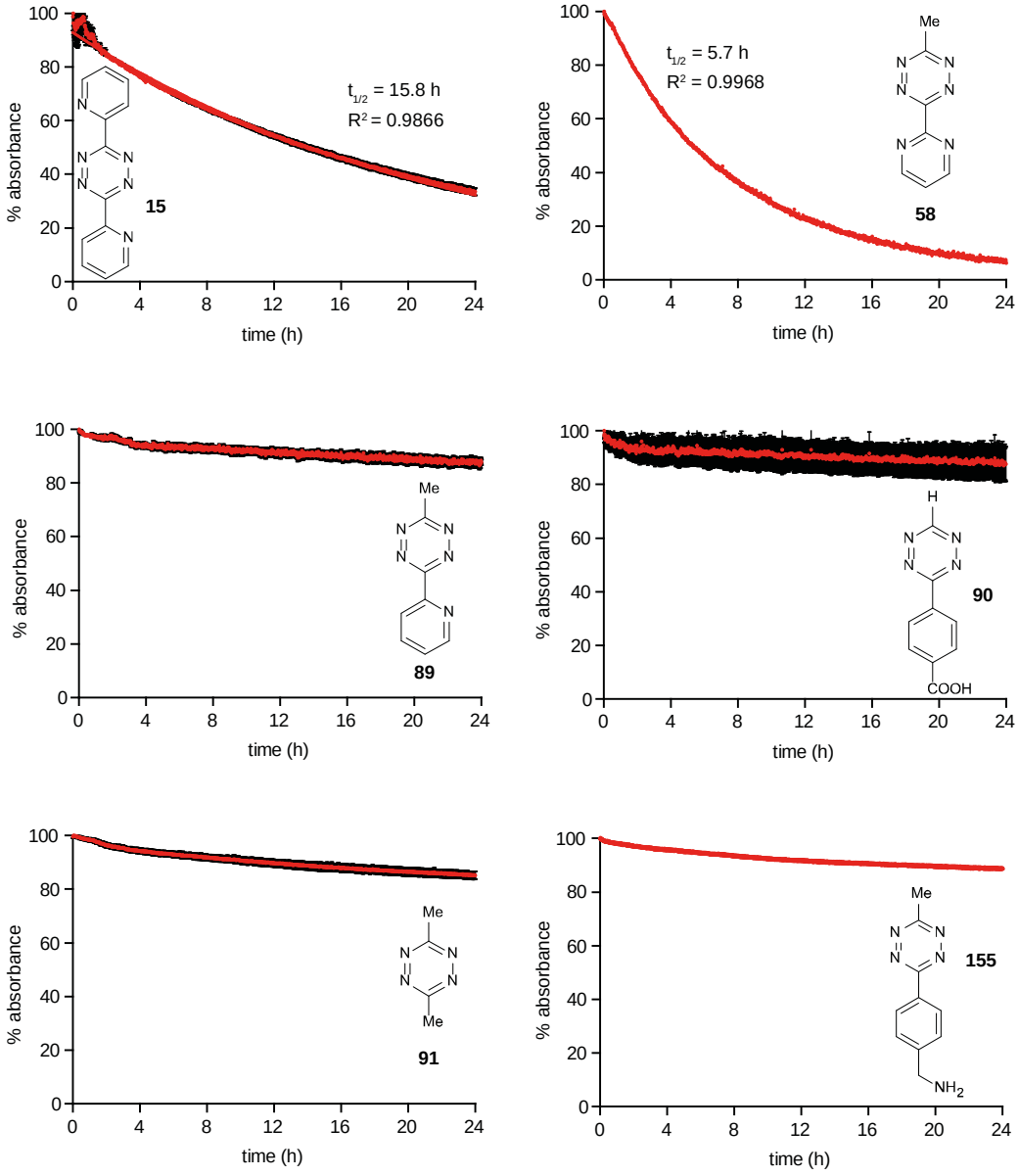

Figure 49. Stability of tetrazines **15**, **58**, **89**, **90**, **91**, **155** in 50% H_2O/DMSO assessed by monitoring the absorbance at 530 nm. Data for tetrazines **15**, **58**, **89**, **90**, **91** was previously shown in Chapter 2.

It should be mentioned that decaging yields are often obtained from monitoring the fluorescence intensity and comparing it to the maximum obtained after complete decaging of the protected fluorophore.[4] However, in our case we found that the reaction mixture can quench the coumarin fluorescence and therefore obtaining a yield by this method is unreliable. Briefly, an aliquot of the reaction mixture of TCO-coumarin (**142**) + tetrazine **90** was added to a sample of 7-hydroxycoumarin

(**122**) at various time points and the fluorescence intensity was recorded and compared to the fluorescence intensity of **122** alone (**Figure 50**).

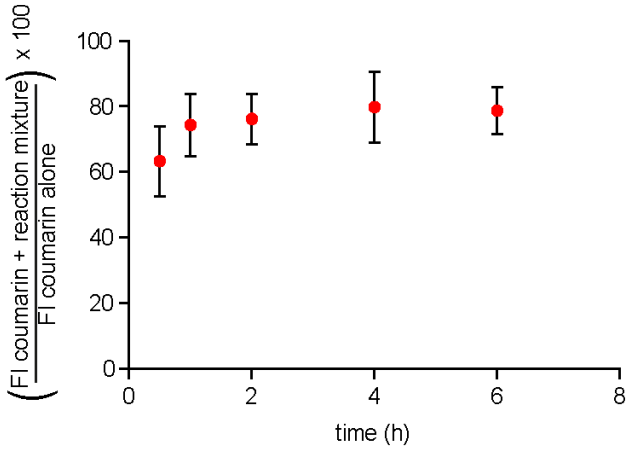

Figure 50. Quenching effect of the reaction mixture on the fluorescence of **122** in 50% H_2O/DMSO.

The kinetics of the reaction of **142** with tetrazine **90** (addition step) were then assessed by monitoring the decrease of the tetrazine absorbance at 530 nm using stopped-flow spectrometry. A calibration graph was obtained by plotting the absorbance at 530 nm for known concentrations of tetrazine **90** (0.15–1 mM) against concentration (**Figure 51**).

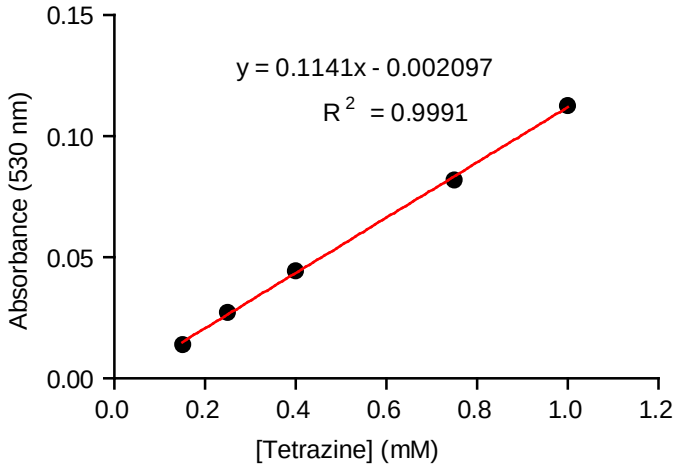

Figure 51. Stopped-flow calibration curve of tetrazine **90**.

142 and tetrazine **90** were then mixed in a 1:1 ratio and the absorbance at 530 nm was monitored and converted into concentration using the calibration graph. The second-order rate constant was found to be 96.4 ± 12.3 $M^{-1}s^{-1}$ ($t_{1/2}$ = 7 s) in DMSO (**Figure 52**).

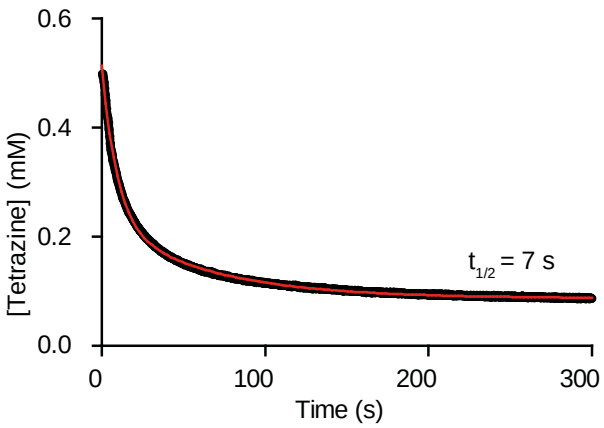

Figure 52. Rate of consumption of tetrazine upon reaction of **142** with **90**, determined by following the decrease in absorbance (λ = 530 nm) by stopped-flow.

In addition, the rate of decaging was determined by following the increase in fluorescence over time (**Figure 53**). These studies revealed that the release of coumarin **122** was complete within 120 minutes ($t_{1/2}$ = 27 min), which is faster than the previously reported vinyl ether[1] and similar to the release from the TCO-ether reported by Robillard (initial release is complete within 30 min and an additional 10% release occurs after 20 h).[3]

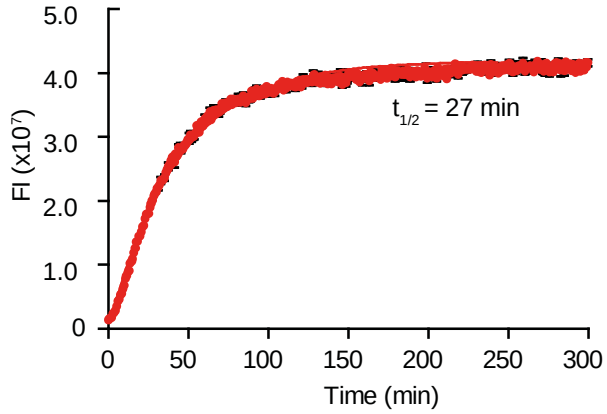

Figure 53. Rate of release of **122** upon reaction of **142** with **90** (final concentration 100 µM) in 50% H_2O/DMSO, determined by following the increase in fluorescence (λ_{ex} = 325, λ_{em} = 460 nm).

Importantly, the reaction was also shown to be compatible with cell media. The fluorescence intensity was measured over 5 h at 37 °C and the release of coumarin **122** was observed in 50% DMSO/LB media ($t_{1/2}$ = 120 min, **Figure 54**).

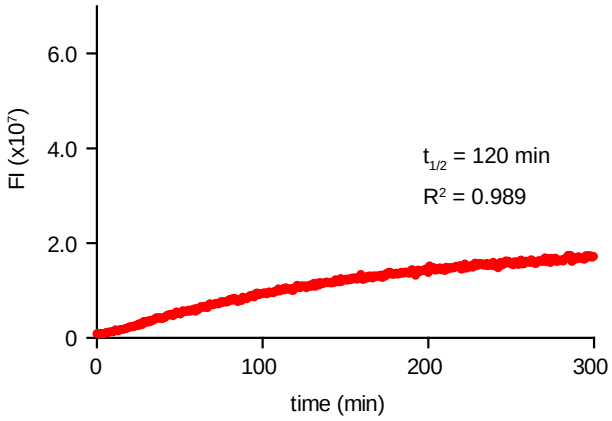

Figure 54. Rate of release of **122** upon reaction of **142** with **90** (final concentration 100 µM) in 50% DMSO/LB media determined by following the increase in fluorescence (λ_{ex} = 325, λ_{em} = 460 nm).

The release of coumarin **122** was also monitored by HPLC coupled to a fluorescence detector (**Figure 55**). The reaction was analysed at the following times: 5 min, 1 h, 2 h, 3 h, 4 h, 24 h.

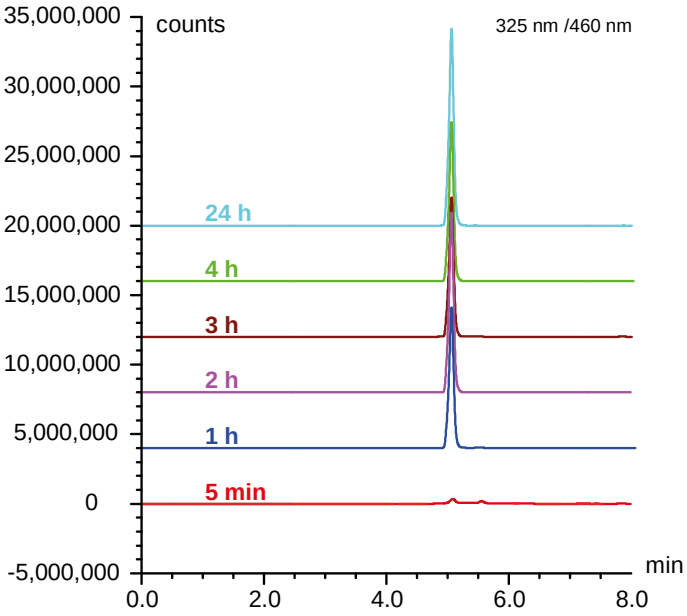

Figure 55. Following the reaction of TCO-coumarin (**142**) with **90** by HPLC/FLD (λ_{ex} = 325 nm, λ_{em} = 460 nm).

Finally, the yield of the reaction after 24 h was assessed under different conditions by HPLC analysis. The yield was shown to be highest in 50% H_2O/DMSO, although there was no clear correlation between water content and yield (**Figure 56**). It should be noted that it was not possible to study the reaction in > 50% H_2O owing to the limited solubility of **142**. The reaction was also shown to be pH dependent; similar yields (25–30%) were obtained for pH 4–7.4, however no reaction occurs at pH 9, which is consistent with previous reports.[15]

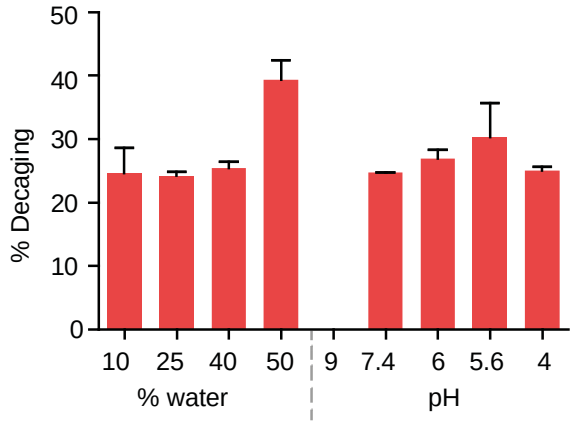

Figure 56. Decaging yield of the reaction of TCO-coumarin (**142**) with **90** determined by HPLC under different conditions after reaction for 24h. The conditions pH 9, 7.4, 6, 5.6, 4 refer to 50% DMSO/corresponding buffer (sodium phosphate (NaPi) pH 9, PBS pH 7.4, NaPi pH 6, acetate pH 5.6, acetate pH 4).

After studying the reaction of model compound **142** with tetrazines, the reaction of prodrug **153** with tetrazine **90** was then studied by HPLC. First, a calibration graph was obtained. Mixtures of triclosan (**149**) at known concentrations (0.2–1.2 mM) and internal standard benzoic acid (0.67 mM) were analysed by HPLC/UV and the ratio of areas of the UV peaks at 220 nm were plotted against concentration of **149** (**Figure 57**).

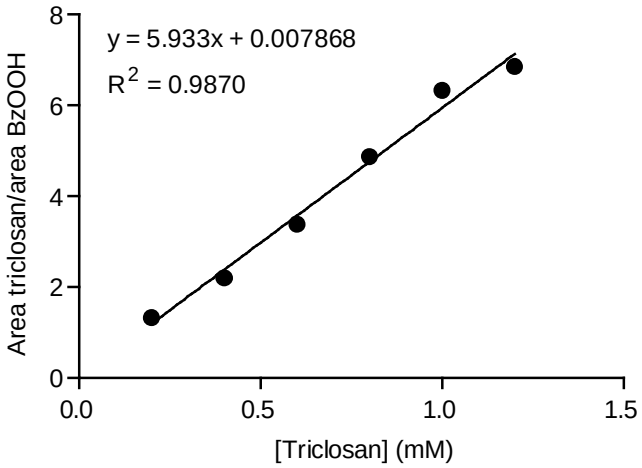

Figure 57. Calibration curve for detection of triclosan (**149**) by HPLC/UV

Next, the reaction of **153** and **90** was monitored by HPLC/UV at various timepoints (10 min, 30 min, 1 h, 2 h, 4 h, 24 h). The measured ratio of UV peaks was converted to concentration using the calibration graph and a decaging yield of 22% was observed (**Figure 58**).

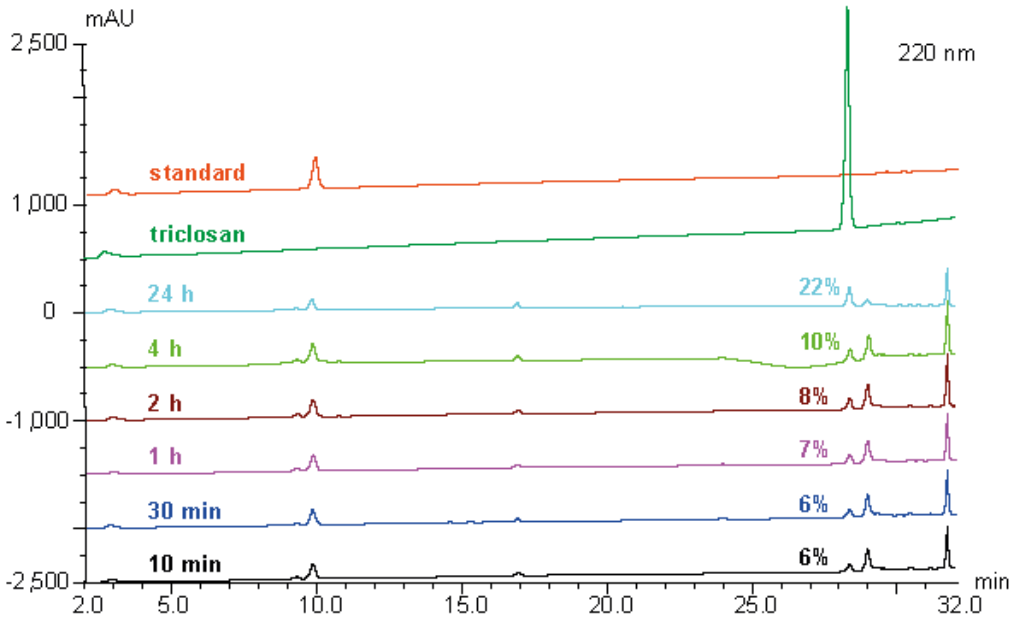

Figure 58. Decaging yield for the reaction of TCO-triclosan (**153**) with tetrazine **90** by HPLC analysis with an internal standard (benzoic acid).

In addition, detection of intermediate peaks by LC-MS analysis confirmed our proposed mechanism of decaging (**Figure 59**).

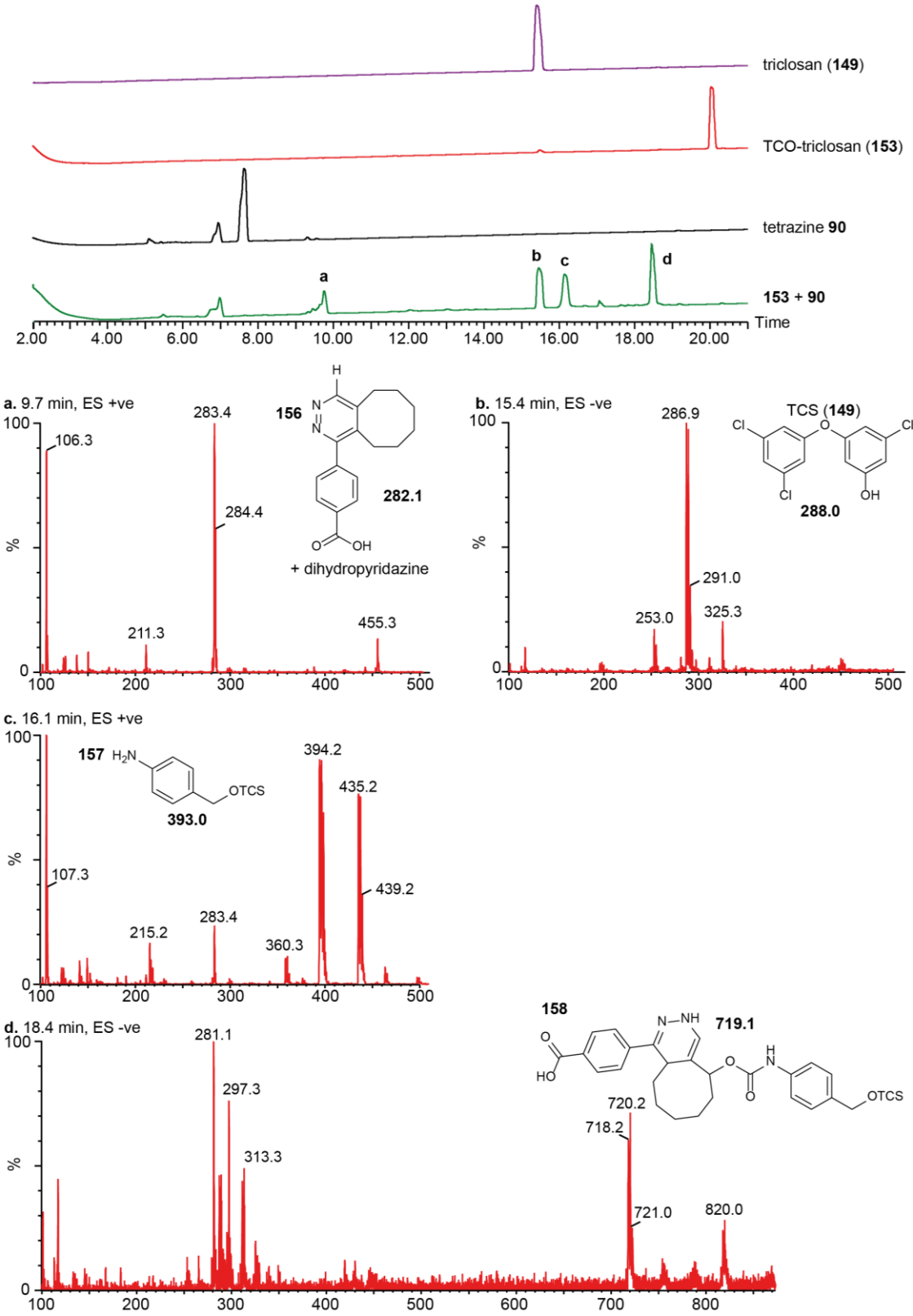

Figure 59. LC-MS analysis of reaction mixture of TCO-triclosan (**153**) and tetrazine **90** after 24 h.

3.7 Cell studies

Finally, the decaging reaction was carried out in the presence of live bacteria (*E. Coli* BL21(DE3), **Scheme 93**). Triclosan is a biocide that is found in many commercial products, for example toothpaste, soap and detergents. Its mechanism of action is inhibition of the enol-acyl carrier protein reductase (ENR) which is an essential enzyme for fatty acid synthesis.[16] This causes cell membranes to weaken, leading to cell death.

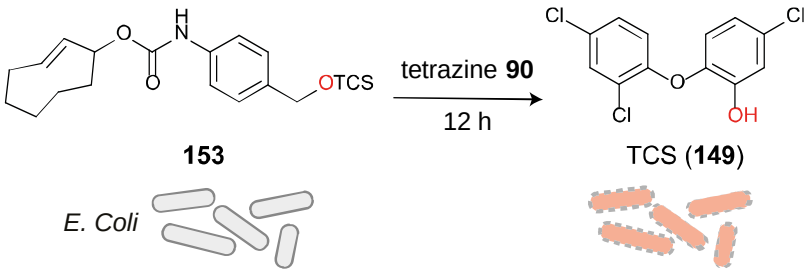

Scheme 93. Tetrazine-triggered prodrug activation in the presence of live cells.

First, the bactericidal activities of triclosan (**149**), prodrug **153** and **153** + **90** were determined by assessing the cell viability at concentrations of 50 nM–1 µM (**Figure 60**). The bioorthogonal reactant pair, TCO-triclosan (**153**) + tetrazine **90** (10 equiv.), was shown to be ≈ 3 times less active (IC_{50} = 298 ± 20 nM) than triclosan (**149**) alone (IC_{50} = 122 ± 10 nM). This lower activity is due to the non-quantitative decaging yield. Importantly, both the prodrug TCO-triclosan (**153**) and tetrazine **90** were shown to be non-toxic at all concentrations tested.

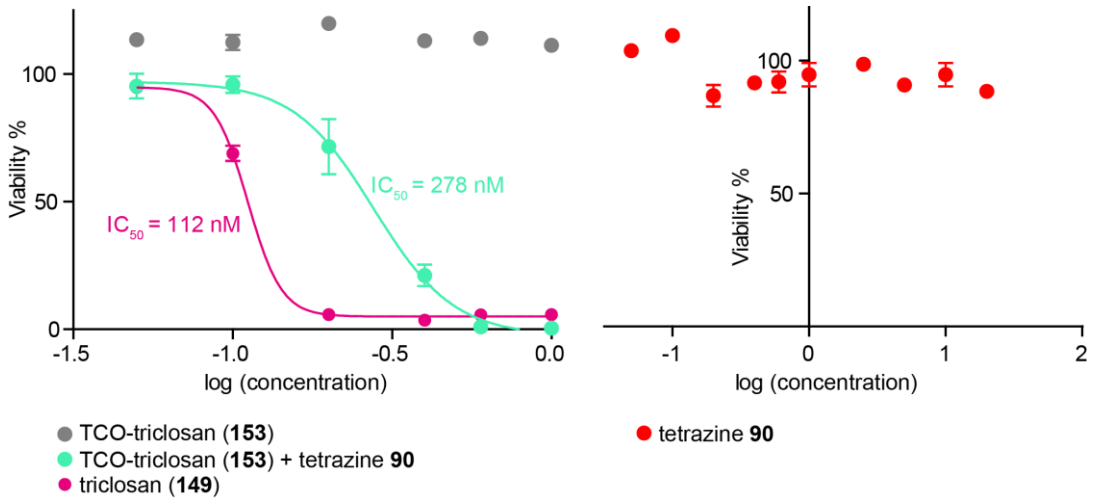

Figure 60. Representative IC_{50} curves. Toxicity assessed by the CellTiter-Blue assay. Tetrazine **90** and TCO-triclosan (**153**) proved to be non-toxic at all concentrations tested (0.05–1 µM for **153**, 0.5–10 µM for **90**). The experiment was performed in technical triplicates (3 wells), 3 independent times and similar results were obtained each time. Average IC_{50} values were found to be 122 ± 10 nM (**149**) and 298 ± 20 nM (**153** + **90**).

After the initial assessment of toxicity, the decaging reaction was then carried out at a concentration of 1 μM. Compounds were added to the cells and the viability was assessed after 12 h by the CellTiter-Blue cell viability assay (**Figure 61**). Tetrazine **90** and prodrug **153** alone have no effect on the viability, but together they result in 100% cell death, as expected from release of an antibacterial drug. Complete cell death was also observed when cells were treated with the free drug **149**. This confirms that the prodrug is activated in the presence of live cells.

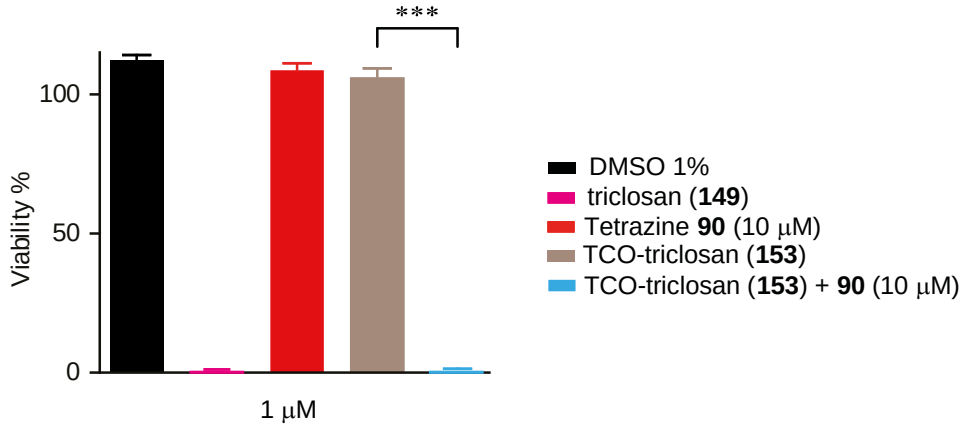

Figure 61. Representative cell viability data after treatment of *E. Coli* with either **149**, **90**, **153**, **153** + **90** assessed by the CellTiter-Blue assay. Treatment with bioorthogonal reactant pair **153** + **90** resulted in complete cell killing. The experiment was performed in technical triplicates (3 wells), 3 independent times and similar results were obtained each time. *** ($P \leq 0.001$).

In addition, the viability was also assessed by measuring the optical density at 600 nm (OD_{600}) (**Figure 62**) and the results were consistent with those obtained from the CellTiter-Blue cell viability assay. Again, it was observed that the OD_{600} was significantly reduced when cells were treated with **153** + **90** compared to **153** alone. Therefore, the reinstation of the bactericidal activity of triclosan (**149**) was achieved upon decaging of **153** in the presence of live cells.

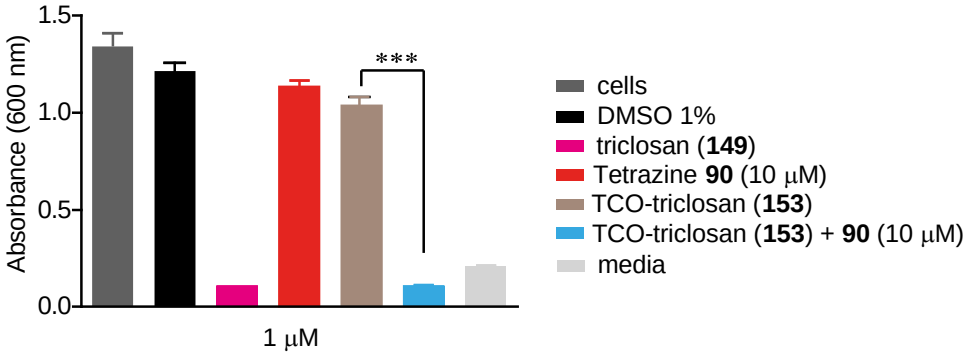

Figure 62. Representative cytotoxicity data of **149**, **90**, **153**, **153** + **90** assessed by measuring the OD_{600}. The experiment was performed in technical triplicates (3 wells), 3 independent times and similar results were obtained each time *** ($P \leq 0.001$).

3.8 Conclusion and future directions

We have explored TCO based protecting groups for masking alcohol functionality. Initially a TCO-carbonate linker was proposed and alcohol release occurred rapidly upon reaction of the carbonate with a tetrazine. However, this handle was limited by the instability of the carbonate under biological conditions. Therefore, we next designed an ether linker which was predicted to be more stable than the carbonate. However, the synthesis of the TCO-ether bond proved to be synthetically challenging. Finally, we successfully developed a TCO-carbamate benzyl ether linker for the controlled release of alcohol-containing drugs and fluorophores upon reaction with a tetrazine trigger.

A synthetic route was developed that enabled generation of TCO-carbamate benzyl ethers **142** and **153** as 100% the axial, *trans*-isomer by direct modification of *trans*-cyclooct-2-en-1-ol. The synthesis does not require a late stage photochemical isomerisation under flow, which is typically very low yielding and requires a specialised setup. The benzyl ether linker proved to be highly stable and can rapidly liberate alcohols under physiological conditions upon reaction with tetrazines. The mechanism and decaging yield were systematically examined by fluorescence and HPLC analysis by using a fluorogenic TCO-benzyl ether-coumarin probe (**142**) and different 3,6-substituted tetrazine derivatives. This study revealed that decaging occurs rapidly ($t_{1/2}$ = 27 min) and the cycloaddition step happens within seconds ($t_{1/2}$ = 7 secs) with reaction rates of ≈ 100 $M^{-1}s^{-1}$. In addition, observation of the intermediates confirmed the proposed 1,6-elimination mechanism from the aniline benzyl-ether derivative.

Importantly, the reaction was shown to be compatible with living organisms as demonstrated by the decaging of a prodrug of the antibacterial compound triclosan in the presence of live *E. Coli*, that resulted in complete cell killing by action of the released "OH-active drug". Overall, this work describes a new linker for masking alcohol functionality that can be rapidly reinstated through tetrazine-triggered decaging. The significant improvement in kinetics from the previous vinyl ether handle[1] suggests this reaction may hold potential for *in vivo* prodrug activation.

We envisage that this methodology could be used in a pretargeting strategy (as described in chapter 2), to deliver the TCO prodrug to the target site. Site selective drug release could then be achieved upon administration of the tetrazine trigger (**Scheme 94**). One of the challenges of this approach is achieving a homogeneous distribution of the antibody in the tumour, which in necessary in order to kill all cancer cells and prevent tumour relapse.[7] This may be addressed by using antibody fragments, such as antigen-binding fragments (Fabs), single-chain variable fragments (scFvs) and nanobodies, which result in faster tumour accumulation and homogeneous distribution at the tumour due to their

smaller size. In addition, since they have shorter circulation half-lives than full IgG antibodies, they result in higher tumour-to-background ratios.

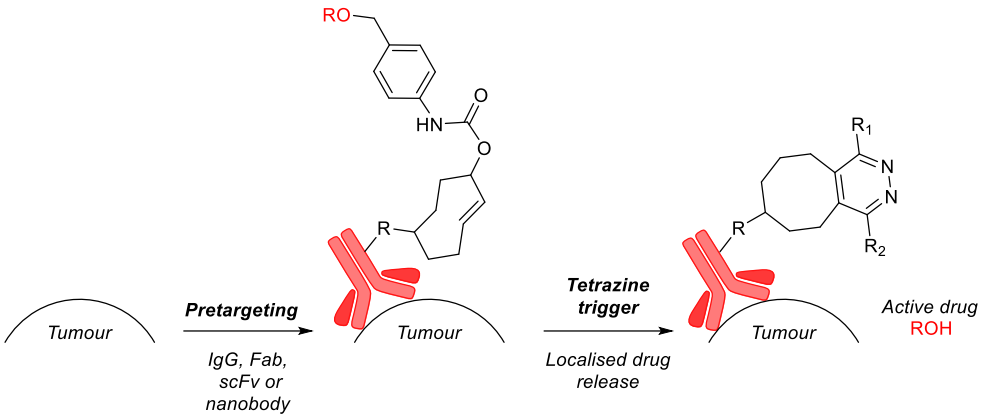

Scheme 94. A pretargeting strategy to achieve tumour-specific drug release. The use of smaller antibody fragments instead of full IgGs can lead to increased tumour penetration of the therapeutic agent.

A drawback of this work is that the drug must be attached at an early stage in the synthesis, as it is necessary to attach TCO in the final step in order to avoid isomerisation. Therefore, this restricts the range of drugs that can be used to those containing little or no other functionality, as other functional groups may not be compatible with later synthetic steps. However, the previously reported methodology involving UV isomerisation to the *trans*-isomer in the final step is also only applicable to a limited scope of drugs. For example, the presence of aromatic rings may interfere with the UV absorption of the compound and hinder isomerisation. Therefore, further work is required in order to develop alternative linkers and robust synthetic routes that can be tolerated by a wide range of alcohol-containing drugs.

3.9 References for Chapter 3

[1] E. Jiménez-Moreno, Z. Guo, B. L. Oliveira, I. S. Albuquerque, A. Kitowski, A. Guerreiro, O. Boutureira, T. Rodrigues, G. Jiménez-Osés, G. J. L. Bernardes, *Angew. Chem Int. Ed.* **2017**, *56*, 243–247.

[2] J. Tu, M. Xu, S. Parvez, R. T. Peterson, R. M. Franzini, *J. Am. Chem. Soc.* **2018**, *140*, 8410–8414.

[3] R. M. Versteegen, W. ten Hoeve, R. Rossin, M. A. de Geus, H. M. Janssen, M. S. Robillard, *Angew. Chem, Int. Ed.* **2018**, *57*, 10494–10499.

[4] X. Fan, Y. Ge, F. Lin, Y. Yang, G. Zhang, W. S. C. Ngai, Z. Lin, S. Zheng, J. Wang, J. Zhao, *et al.*, *Angew. Chem. Int. Ed.* **2016**, *55*, 14046–14050.

[5] R. M. Versteegen, R. Rossin, W. ten Hoeve, H. M. Janssen, M. S. Robillard, *Angew. Chem. Int. Ed.* **2013**, *52*, 14112–14116.

[6] S. S. Matikonda, D. L. Orsi, V. Staudacher, I. A. Jenkins, F. Fiedler, J. Chen, A. B. Gamble, *Chem. Sci.* **2015**, *6*, 1212–1218.

[7] M. Royzen, G. P. A. Yap, J. M. Fox, *J. Am. Chem. Soc.* **2008**, *130*, 3760–3761.

[8] M. S. Robillard, H. M. Janssen, W. ten Hoeve, R. M. Versteegen, R. Rossin, *Bio-Orthogonal Drug Activation*, **2016**, US2016/106859.

[9] F. Thalhammer, U. Wallfahrer, J. Sauer, *Tetrahedron Lett.* **1990**, *31*, 6851–6854.

[10] M. L. Blackman, M. Royzen, J. M. Fox, *J. Am. Chem. Soc.* **2008**, *130*, 13518–13519.

[11] S. Davies, L. Qiao, B. Oliveira, C. Navo, G. Jiménez-Osés, G. J. L. Bernardes, *ChemBioChem* **2019**, *20*, 1541–1546.

[12] P. Sanllehí, M. Casasampere, J. L. Abad, G. Fabriàs, O. López, J. Bujons, J. Casas, A. Delgado, *Chem. Commun.* **2017**, *53*, 5441–5444.

[13] C. Spyropoulos, C. G. Kokotos, *J. Org. Chem.* **2014**, *79*, 4477–4483.

[14] K. Kurita, T. Matsumura, Y. Iwakura, *J. Org. Chem.* **1976**, *41*, 2070–2071.

[15] J. C. T. Carlson, H. Mikula, R. Weissleder, *J. Am. Chem. Soc.* **2018**, *140*, 3603–3612.

[16] L. M. McMurry, M. Oethinger, S. B. Levy, *Nature* **1998**, *394*, 531–532.

Chapter 4

Experimental

4.1 General experimental

Solvents and reagents: All non-aqueous reactions were performed in oven-dried glassware under argon atmosphere unless otherwise stated. Argon gas was pre-dried via passage through calcium chloride. Reaction vessels were heated using thermostatically controlled dry-syn blocks with the liquid level of the flask below that of the heating block. Reaction temperatures refer to the thermostat set point. All reagents were purchased from commercial sources and used without further purification unless otherwise stated. *Trans*-cyclooct-2-en-1-ol (TCO-OH) was purchased as the axial isomer from Sirius Fine Chemicals. CH_2Cl_2, THF and Et_2O were purified either according to the method of Grubbs and Pangborn[1] or by distillation under an inert atmosphere (CH_2Cl_2, MeOH, toluene and MeCN were distilled from calcium hydride. THF and Et_2O were pre-dried over sodium wire then distilled from calcium hydride and lithium aluminium hydride). *N*,*N*-diisopropylethylamine (DIPEA) was purified by distillation over calcium hydride and stored over 4 Å molecular sieves. Petroleum ether and EtOAc were distilled on site. 'Petrol' refers to the distillate of petroleum ether collected between 40–60 °C unless otherwise stated. Water used experimentally was deionised and prepared on site. Flash column chromatography was performed using silica gel 60 Å (40–63 μm) from Material Harvest and preparative TLC was performed on Merck PLC 60 F254 plates. Analytical thin layer chromatography was performed using Merck Silica 42 gel 60 F254 1 mm glass plates and visualised by UV (254 nm) and/or by staining with potassium permanganate ($KMnO_4$).

Characterisation: NMR spectra were recorded on Bruker 400-Avance III HD, Avance DPX-400, 400-QNP Cryoprobe or 500-DCH Cryoprobe spectrometers. Chemical shifts are reported in parts per million (ppm) and the residual solvent peaks were used as an internal reference for chemical shift (^{1}H NMR $CDCl_3$ δ 7.26 ppm, MeOD δ 3.31 ppm, DMSO-*D_6* δ 2.50 ppm; ^{13}C NMR $CDCl_3$ δ 77.2 ppm, MeOD δ 49.0 ppm, DMSO-*D_6* δ 39.5 ppm). Multiplicities are described as s (singlet), d (doublet), t (triplet), q

(quartet), m (multiplet), dd (double doublet) and so on. Coupling constants (*J*) are reported in hertz (Hz) to 1 decimal place using MestreNova for signal processing. The centre of each peak is reported except for multiplet signals where a range of ppm values is given. Structural assignments are made with the aid of COSY, HSQC, and HMBC experiments, performed by the NMR Spectrometry Service, University of Cambridge. High-resolution mass spectra were performed by the Mass Spectrometry Service, Department of Chemistry, University of Cambridge using a Waters LCT Premier or a Waters Xevo G2-S spectrometer and ionised by ESI or ASAP.

4.2 Experimental procedures for Chapter 2

4.2.1 Synthetic procedures

bis(pyridin-2'-yl)-1,2,4,5-tetrazine (15) was purchased from Sigma-Aldrich.

3-Methyl-6-(pyrimidin-2'-yl)-1,2,4,5-tetrazine (**58**)

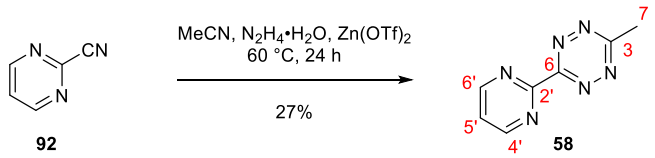

According to the procedure by Fan *et al.*,[2] 2-pyrimidinecarbonitrile (**92**, 0.53 g, 5.0 mmol, 1.0 equiv.), MeCN (1.30 mL, 25 mmol, 5.0 equiv.), zinc trifluoromethane sulfonate (91 mg, 0.25 mmol, 5 mol%) and hydrazine monohydrate (1.20 mL, 25 mmol, 5.0 equiv.) were added to a Schlenk tube under a positive argon gas stream. The reaction mixture was stirred at 60 °C for 24 h under argon. The reaction was cooled to rt then sodium nitrite $_{(aq)}$ (1 M, 50 mL) was added. HCl (1 M) was added until the reaction mixture was pH 3. The layers were separated and the aqueous phase was extracted with CH_2Cl_2 (3 x 100 mL). The combined organic layers were washed with brine (20 mL), dried over anhydrous Na_2SO_4 and concentrated *in vacuo*. Purification via flash column chromatography (2–4% MeOH/CH_2Cl_2) followed by another flash column chromatography (10–16% acetone/CH_2Cl_2) yielded **58** as a pink solid (0.237 g, 1.36 mmol, 27%). The NMR data were in accordance with literature data.[2]

R_f 0.25 (10% acetone/CH_2Cl_2).

^{1}H NMR (400 MHz, $CDCl_3$) δ 9.10 (d, *J* = 4.9 Hz, 2H, H4', H6'), 7.57 (td, *J* = 4.8, 1.0 Hz, 1H, H5'), 3.20 (d, *J* = 1.0 Hz, 3H, H7).

^{13}C NMR (101 MHz, $CDCl_3$) δ 168.7 (C3), 163.3 (C6), 159.6 (C2'), 158.4 (C4', C6'), 122.5 (C5'), 21.5 (C7).

Ethenyl 3-phenylpropanoate (87)

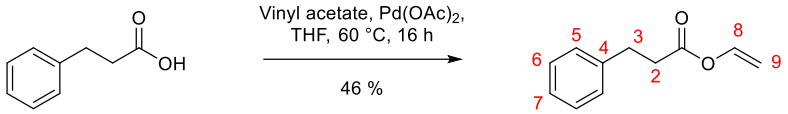

86 **87**

According to the procedure by Krejzová *et al.*,[3] palladium (II) acetate (22 mg, 0.098 mmol, 1 mol%) and vinyl acetate (10.1 mL, 110 mmol, 11.0 equiv.) were added to a solution of 3-phenylpropionic acid (**86**, 1.5 g, 10.0 mmol, 1.0 equiv.) in anhydrous, degassed THF (1 mL). The mixture was stirred at 60 °C for 16 h and then cooled to rt. Silica was added and all volatiles were removed *in vacuo*. Purification via flash column chromatography (5% EtOAc/Petrol) yielded **87** as a pale yellow oil (0.80 g, 4.6 mmol, 46%). The NMR data were in accordance with literature data.[3]

R_f 0.58 (5% EtOAc/Petrol).

^{1}H NMR (400 MHz, $CDCl_3$) δ 7.35 – 7.28 (m, 3H, H6, H8), 7.26 – 7.21 (m, 3H, H5, H7), 4.91 (dd, *J* = 14.0, 1.7 Hz, 1H, $H9_Z$), 4.60 (dd, *J* = 6.3, 1.6 Hz, 1H, $H9_E$), 3.02 (t, *J* = 7.8 Hz, 2H, H3), 2.75 (t, *J* = 7.8 Hz, 2H, H2).

^{13}C NMR (101 MHz, $CDCl_3$) δ 169.9 (C1), 141.1 (C8), 140.1 (C4), 128.6 (C6), 128.3 (C5), 126.4 (C7), 97.8 (C9), 35.6 (C2), 30.6 (C3).

3-Phenylpropionic acid (86) and **3,6-Bis(pyridin-2'-yl)pyridazine (88)**

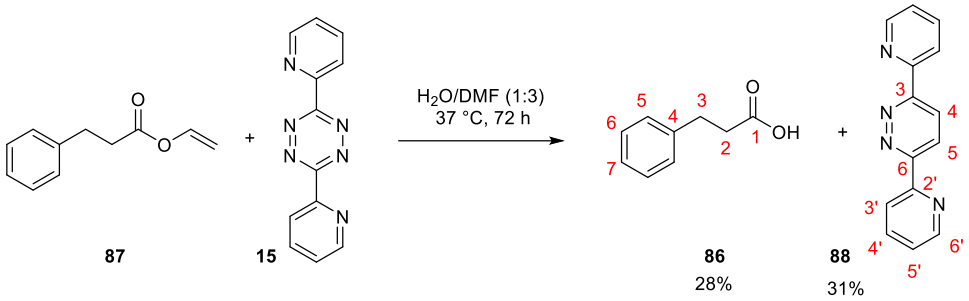

Ethynyl-3-phenylpropanoate (**87**, 34 mg, 0.193 mmol, 1.0 equiv.) and 2,6-di-2-pyridyl-1,2,4,5-tetrazine (**15**, 91 mg, 0.386 mmol, 2.0 equiv.) were suspended in 25% H_2O/DMF (16 mL) and stirred at 37 °C for 3 days. The reaction was cooled to rt and H_2O (40 mL) was added. The mixture was extracted with EtOAc (4 x 40 mL) and the combined organic layers were washed with 10% $LiCl_{(aq)}$ (4 x 40 mL) and brine (40 mL) then dried over anhydrous $MgSO_4$, filtered and concentrated *in vacuo.* Purification via flash column chromatography (50% EtOAc/Petrol) yielded 3-phenylpropionic acid (**86**) as a white solid (8 mg, 0.05 mmol, 28%) and 3,6-bis(pyridine-2-yl)pyridazine (**88**) as a yellow solid (14 mg, 0.06 mmol, 31%). The NMR data were in accordance with literature data.[4,5]

3-phenylpropionic acid (86)

R_f 0.23 (50% EtOAc/Petrol).

^{1}H NMR (400 MHz, $CDCl_3$) δ 7.33 – 7.27 (m, 2H, H6), 7.24 – 7.16 (m, 3H, H5, H7), 2.97 (t, *J* = 7.8 Hz, 2H, H3), 2.69 (t, *J* = 7.8 Hz, 2H, H2).

3,6-Bis(pyridin-2'-yl)pyridazine (88)

R_f 0.35 (50% EtOAc/Petrol).

^{1}H NMR (400 MHz, $CDCl_3$) δ 8.83 – 8.74 (m, 4H, H6', H3'), 8.71 (s, 2H, H4, H5), 7.93 (td, *J* = 7.8, 1.9 Hz, 2H, H4'), 7.43 (ddd, *J* = 7.5, 4.8, 1.2 Hz, 2H, H5').

^{13}C NMR (101 MHz, $CDCl_3$) δ 158.2 (C3, C6), 153.5 (C2'), 149.5 (C6'), 137.2 (C4'), 125.2 (C4, C5), 124.8 (C5'), 121.7 (C3').

3-Methyl-6-(pyridin-2'-yl)-1,2,4,5-tetrazine (89)

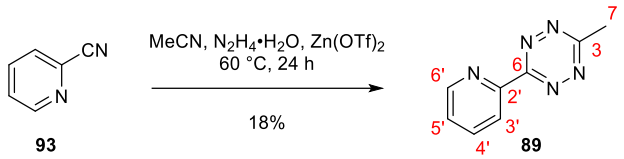

According to the procedure by Fan *et al.*,[2] 2-pyridinecarbonitrile (**93**, 0.104 g, 1.0 mmol, 1.0 equiv.), MeCN (0.26 mL, 5.0 mmol, 5.0 equiv.), zinc trifluoromethane sulfonate (18 mg, 0.05 mmol, 5 mol%) and hydrazine monohydrate (0.24 mL, 5.0 mmol, 5.0 equiv.) were added to a Schlenk tube under a positive argon gas stream. The reaction mixture was stirred at 60 °C for 24 h under argon. The reaction was cooled to rt then sodium nitrite $_{(aq)}$ (1 M, 10 mL) was added. HCl (1 M) was added until the reaction mixture was pH 3. The layers were separated and the aqueous phase was extracted with CH_2Cl_2 (3 x 50 mL). The combined organic layers were washed with brine (20 mL), dried over anhydrous Na_2SO_4 and concentrated *in vacuo*. Purification via flash column chromatography (10% acetone/CH_2Cl_2) yielded **89** as a pink solid (31 mg, 0.177 mmol, 18%). The NMR data were in accordance with literature data.[2]

R_f 0.41 (10% acetone/CH_2Cl_2).

^{1}H NMR (400 MHz, $CDCl_3$) δ 8.95 (ddd, *J* = 4.8, 1.8, 0.9 Hz, 1H, H6'), 8.64 (dt, *J* = 7.9, 1.1 Hz, 1H, H3'), 7.98 (td, *J* = 7.8, 1.7 Hz, 1H, H4'), 7.55 (ddd, *J* = 7.7, 4.8, 1.2 Hz, 1H, H5'), 3.16 (d, *J* = 0.8 Hz, 3H, H7).

^{13}C NMR (101 MHz, $CDCl_3$) δ 168.1 (C3), 163.6 (C6), 150.9 (C6'), 150.3 (C2'), 137.4 (C4'), 126.3 (C5'), 123.9 (C3'), 21.4 (C7).

4'-(1,2,4,5-tetrazin-3-yl)benzoic acid (90) was prepared by Ester Jiménez-Moreno (Bernardes group).[5]

dimethyl-1,2,4,5-tetrazine (91) was prepared by Russel Guo (Bernardes group)

Ethenyl 2-oxochromene-3-carboxylate (96)

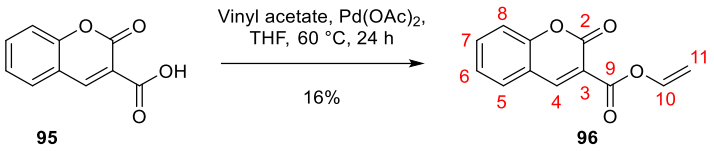

According to the procedure by Krejzová *et al.*,[3] palladium (II) acetate (3 mg, 0.013 mmol, 1 mol%) and vinyl acetate (1.07 mL, 11.6 mmol, 11 equiv.) were added to a solution of coumarin-3-carboxylic acid (**95**, 0.200 g, 1.05 mmol, 1.0 equiv.) in anhydrous, degassed THF (3 mL). The mixture was stirred at 60 °C for 24 h and then cooled to rt. Further portions of palladium (II) acetate (3 mg, 0.013 mmol, 1 mol%) were added after 16 h and 19 h. Silica was added and all volatiles were removed *in vacuo*. Purification of the dry residue directly via flash column chromatography (20–50% EtOAc/Petrol) gave **96** as a white solid (0.036 g, 0.167 mmol, 16%).

R_f 0.29 (50% EtOAc/Petrol).

Mp 124–126 °C.

^{1}H NMR (400 MHz, $CDCl_3$) δ 8.66 (s, 1H, H4), 7.76 – 7.64 (m, 2H, H5, H7), 7.50 (dd, *J* = 13.9, 6.2 Hz, 1H, H10), 7.44 – 7.34 (m, 2H, H6, H8), 5.16 (dd, *J* = 13.9, 1.9 Hz, 1H, $H11_Z$), 4.79 (dd, *J* = 6.2, 1.9 Hz, 1H, $H11_E$).

^{13}C NMR (101 MHz, $CDCl_3$) δ 159.9 (C9), 156.2 (C8a), 155.4 (C2), 149.8 (C4), 141.1 (C10), 134.9 (C7), 129.7 (C5), 125.0 (C6), 117.7 (C4a), 116.9 (C8), 116.8 (C3), 99.4 (C11).

IR (thin film, ν_{max}/cm^{-1}) 3063w, 1760s, 1643w, 1609m, 1567m, 1488w, 1452m, 1377m, 1300m, 1241m, 1211s, 1138s, 1012m, 963m.

HRMS (ESI^+): *m/z* calc. for $C_{12}H_8O_4$ $[M+H]^+$ 217.0501, found 217.0492, Δ -4.1 ppm.

Ethyl 7-hydroxy-2-oxochromene-3-carboxylate (99)

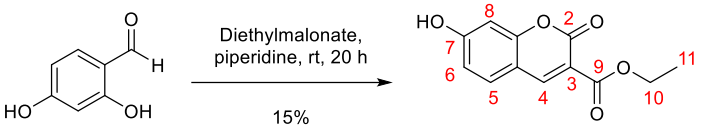

97 **99**

According to the procedure by Vieira *et al.*,[6] piperidine (0.12 mL, 1.21 mmol, 0.33 equiv.) was added to a solution of 2,4-dihydroxybenzaldehyde (**97**, 0.511 g, 3.70 mmol, 1.0 equiv.) in diethylmalonate (1.20 mL, 7.90 mmol, 2.1 equiv.). The reaction mixture was stirred at rt for 20 h then acidified using HCl (3M, 5 mL). The precipitate was filtered and washed with ice-cold water (10 mL). Purification via flash column chromatography (70% CH_2Cl_2/EtOAc) yielded **99** as a white solid (0.133 g, 0.568 mmol, 15%). The NMR data were in accordance with literature data.[6]

R_f 0.25 (70% CH_2Cl_2/EtOAc).

^{1}H NMR (400 MHz, DMSO-D_6) δ 8.67 (s, 1H, H4), 7.75 (d, *J* = 8.6 Hz, 1H, H5), 6.84 (dd, *J* = 8.6, 2.3 Hz, 1H, H6), 6.72 (d, *J* = 2.2 Hz, 1H, H8), 4.25 (q, *J* = 7.1 Hz, 2H, H10), 1.29 (t, *J* = 7.1 Hz, 3H, H11).

^{13}C NMR (101 MHz, DMSO-D_6) 164.5 (C7), 163.4 (C9), 157.6 (C8a), 156.9 (C2), 149.9 (C4), 132.6 (C5), 114.5 (C6), 112.5 (C3), 110.9 (C4a), 102.2 (C8), 61.3 (C10), 14.6 (C11).

7-Hydroxy-2-oxochromene-3-carboxylic acid (100)

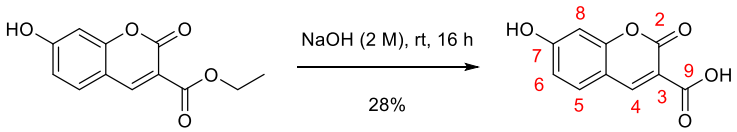

99 **100**

According to the procedure by Zhang *et al.*,[7] ethyl 7-hydroxy-2-oxochromene-3-carboxylate (**99**, 0.133 g, 0.568 mmol) was dissolved in $NaOH_{(aq)}$ (2M, 2.5 mL) and the reaction was stirred at rt for 16 h. The reaction was acidified with $HCl_{(aq)}$ (2M) until pH 2. The precipitate was washed with water followed by acetonitrile and then dried *in vacuo* to give **100** as a white solid (0.033 g, 0.160 mmol, 28%). The NMR data were in accordance with literature data.[7]

^{1}H NMR (400 MHz, DMSO-D_6) δ 8.68 (d, *J* = 1.6 Hz, 1H, H4), 7.75 (dd, *J* = 8.6, 1.5 Hz, 1H, H5), 6.85 (dt, *J* = 8.5, 1.9 Hz, 1H, H6), 6.74 (d, *J* = 2.3 Hz, 1H, H8).

Ethenyl 7-(ethenyloxy)-2-oxochromene-3-carboxylate (101)

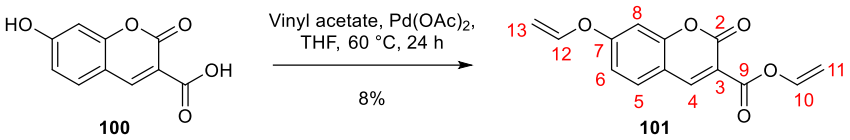

According to the procedure by Krejzová *et al.*,[3] palladium (II) acetate (3 mg, 0.013 mmol, 1 mol%) and vinyl acetate (0.98 mL, 10.7 mmol, 11 equiv.) were added to a solution of 7-hydroxycoumarin-3-carboxylic acid (**100**, 0.200 g, 0.970 mmol, 1.0 equiv.) in anhydrous, degassed THF (3 mL). The mixture was stirred at 60 °C for 24 h and then cooled to rt. Further portions of palladium (II) acetate (3 mg, 0.013 mmol, 1 mol%) were added after 16 h and 19 h. Silica was added and all volatiles were removed *in vacuo*. Purification of the dry residue directly via flash column chromatography (25% EtOAc/Petrol) yielded **101** as a white solid (20 mg, 0.077 mmol, 8%).

R_f 0.36 (25% EtOAc/Petrol).

Mp 94–97 °C.

^{1}H NMR (400 MHz, DMSO-D_6) δ 8.94 (d, J = 0.6 Hz, 1H, H4), 7.98 (d, J = 8.7 Hz, 1H, H5), 7.40 (dd, J = 13.9, 6.2 Hz, 1H, H10), 7.22 (d, J = 2.4 Hz, 1H, H8), 7.17 (dd, J = 8.7, 2.4 Hz, 1H, H6), 7.14 (dd, J = 13.4, 5.9 Hz, 1H, H12), 5.09 (dd, J = 13.9, 1.7 Hz, 1H, H11$_Z$), 4.99 (dd, J = 13.4, 1.9 Hz, 1H, H13$_Z$), 4.83 (dd, J = 6.2, 1.7 Hz, 1H, H11$_E$), 4.73 (dd, J = 5.9, 1.8 Hz, 1H, H13$_E$).

^{13}C NMR (101 MHz, DMSO-D_6) δ 161.5 (C7), 159.9 (C9), 156.9 (C8a), 155.9 (C2), 150.5 (C4), 146.5 (C12), 141.5 (C10), 132.6 (C5), 114.1 (C6), 113.2 (C4a), 112.9 (C3), 102.7 (C8), 99.5 (C11), 98.6 (C13).

IR (thin film, ν_{max}/cm^{-1}) 3045w, 1760s, 1715m, 1647m, 1608s, 1658m, 1498m, 1375m, 1292m, 1211m, 1122s, 940s.

HRMS (ASAP$^+$): *m/z* calc. for $C_{14}H_{11}O_5$ $[M+H]^+$ 259.0606, found 259.0601, Δ -1.9 ppm.

Ethenyl 7-hydroxy-2-oxochromene-3-carboxylate (102)

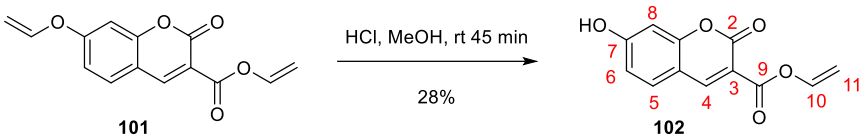

Ethenyl 7-(ethenyloxy)-2-oxochromene-3-carboxylate (**101**, 12 mg, 0.0465 mmol, 1.0 equiv.) was dissolved in MeOH (0.6 mL). HCl (0.3 mL, 12M, 3.6 mmol, 77 equiv.) was added and the reaction was stirred at rt for 45 min then concentrated *in vacuo*. CH_2Cl_2 (5 mL) was added and the solution was neutralised with $NaHCO_{3\,(aq)}$ (sat. soln.) at 0 °C. The layers were separated and the aqueous layer was extracted with CH_2Cl_2 (3 x 5 mL). The combined organic layers were washed with brine (10 mL), dried over anhydrous Na_2SO_4 and concentrated *in vacuo*. Purification via flash column chromatography (10–50% EtOAc/Petrol) yielded **102** as a peach solid (3 mg, 0.0129 mmol, 28%).

R_f 0.29 (50% EtOAc/Petrol).

Mp 188–192 °C.

^{1}H NMR (500 MHz, Methanol-d_4) δ 8.78 (d, *J* = 0.6 Hz, 1H, H4), 7.67 (d, *J* = 8.7 Hz, 1H, H5), 7.45 (dd, *J* = 13.9, 6.3 Hz, 1H, H10), 6.86 (dd, *J* = 8.7, 2.3 Hz, 1H, H6), 6.73 (d, *J* = 2.5 Hz, 1H, H8), 5.09 (dd, *J* = 14.0, 1.7 Hz, 1H, H11$_Z$), 4.73 (dd, *J* = 6.3, 1.7 Hz, 1H, H11$_E$).

^{13}C NMR (126 MHz, Methanol-d_4) δ 165.5 (C7), 160.3 (C9), 157.9 (C8a/C2), 157.8 (C8a/C2), 150.9 (C4), 140.9 (C10), 132.0 (C5), 114.3 (C6), 110.8 (C4a), 110.0 (C3), 101.7 (C8), 97.5 (C11).

IR (thin film, ν_{max}/cm^{-1}) 3558w, 3475w, 3058w, 2924w, 1741s, 1686m, 1617s, 1604s, 1452m, 1389m, 1214s, 1145s.

HRMS (ESI$^+$): *m/z* calc. for $C_{12}H_8O_5Na$ $[M+Na]^+$ 255.0264, found 255.0258, Δ -2.4 ppm.

2-(3-benzoylphenyl)propanoic acid (105)

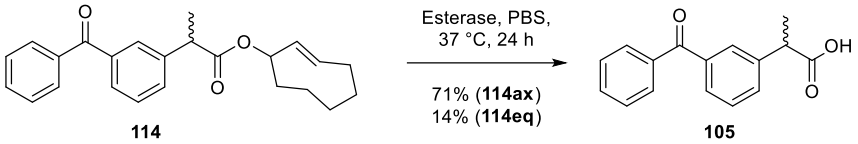

Esterase from porcine liver (0.125 units) and either the axial or equatorial isomer of TCO-ketoprofen (**114**, 0.5 µmol, 1.0 equiv.) were added to PBS buffer (1 mL, pH = 7.4) from a stock dissolved in DMSO (200 mM) and the mixture was shaken at 37 °C for 24 h. Analysis of the mixture by HPLC gave ketoprofen (**105**) in yields of 71% (axial isomer) and 14% (equatorial isomer). This experiment was performed by Luxi Qiao.

Vinyl 2-(3'-benzoylphenyl)propanoate (106)

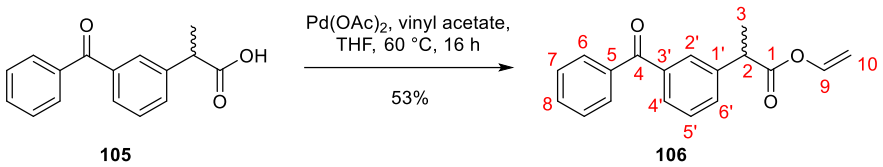

According to the procedure by Krejzova *et al.*,[3] palladium (II) acetate (13 mg, 0.06 mmol, 3 mol%) and vinyl acetate (2.0 mL, 21.6 mmol, 11.0 equiv.) were added to a solution of ketoprofen (**105**, 500 mg, 1.97 mmol, 1.0 equiv.) in anhydrous, degassed THF (5 mL). The mixture was stirred at 60 °C for 16 h, cooled to rt and then concentrated *in vacuo*. Purification via flash column chromatography (20–25% EtOAc/petrol) yielded **106** as a red oil (292 mg, 1.04 mmol, 53%). This experiment was performed by Luxi Qiao.

^{1}H NMR (400 MHz, $CDCl_3$) δ 7.81–7.73 (m, 3H, H2',H6), 7.69 (dt, *J* = 7.6, 1.5 Hz, 1H, H4'), 7.62–7.53 (m, 2H, H8, H6'), 7.50–7.42 (m, 3H, H5', H7), 7.30–7.21 (m, 1H, H9), 4.87 (dd, *J* = 14.0, 1.7 Hz, 1H, $H10_Z$), 4.58 (dd, *J* = 6.3, 1.7 Hz, 1H, $H10_E$), 3.86 (q, *J* = 7.2 Hz, 1H, H2), 1.57 (d, *J* = 7.2 Hz, 3H, H3).

^{13}C NMR (101 MHz, $CDCl_3$) δ 196.5 (C4), 171.3 (C1), 141.4 (C9), 140.1(C3'), 138.0 (C5), 137.6 (C1'), 132.7 (C6'), 131.6 (C8), 130.0 (C2'), 130.2 (C6), 129.4 (C4'), 128.8 (C5'), 128.5 (C7), 98.4 (C10), 45.3 (C2), 18.5 (C3).

IR (thin film, ν_{max}/cm^{-1}) 2980w, 2917w, 1747s, 1658s, 1645s, 1597m, 1579m, 1447m, 1379w, 1318m, 1281s, 1228w, 1201m, 1807br, 1076m, 947m, 876m, 821w, 789w, 768w, 704br.

HRMS (ESI$^+$): m/z calc. for $C_{18}H_{16}O_3{}^{23}Na$ $[M+Na]^+$ 303.0992, found 303.0978, Δ -4.3 ppm.

(2*Z*)-Cyclooct-2-en-1-ol (111)

110 **111**

According to the procedure by Becker *et al.*,[8] diphenyl diselenide (2.00 g, 6.41 mmol, 1.5 equiv.) was dissolved in CH_2Cl_2 (21 mL) and cooled to 0 °C under argon. Hydrogen peroxide solution (0.67 mL, 30% w/w in water, 6.51 mmol, 1.5 equiv.) was added dropwise and the reaction mixture was stirred vigorously for 30 min. Magnesium sulfate (1.07 g, 8.89 mmol, 2.1 equiv.) was added and the reaction was stirred for a further 30 min then allowed to warm to rt. Cyclooctene (**110**, 0.56 mL, 4.26 mmol, 1.0 equiv.) was added and the reaction was stirred at rt under argon for 20 h then cooled to 0 °C. *t*-butylhydroperoxide solution (4.56 mL, 5-6 M in decane, ≥ 22.8 mmol, ≥ 5.4 equiv.) was added slowly, the ice bath was removed and the reaction was stirred at rt for 20 h. The precipitate was filtered off and washed with diethyl ether. The filtrate was concentrated *in vacuo* and then redissolved in diethyl ether (30 mL) and washed sequentially with 5% $Na_2CO_{3(aq)}$ (17 mL, 9 mL), water (9 mL), 10% ferrous $sulfate_{(aq)}$ (17 mL, 9 mL), water (20 mL), $NaHCO_{3\ (aq)}$ (sat. soln., 20 mL), water (20 mL) and brine (20 mL). The organic layer was dried over anhydrous $MgSO_4$ for 24 h then concentrated *in vacuo*. Purification via flash column chromatography (20% Et_2O/Petrol) yielded **111** as a pale yellow oil (0.273 g, 2.16 mmol, 51%). The NMR data were in accordance with literature data.[9]

^{1}H NMR (400 MHz, $CDCl_3$) δ 5.63 (dddd, *J* = 10.4, 8.6, 7.0, 1.5 Hz, 1H, H3), 5.54 (ddd, *J* = 10.8, 6.6, 1.0 Hz, 1H, H2), 4.67 (ddd, *J* = 10.3, 6.3, 4.6 Hz, 1H, H1), 2.26 – 2.00 (2H, m, H4), 1.93 (1H, m, H8a), 1.75 – 1.34 (7H, m, H5-H7, H8b).

^{13}C NMR (101 MHz, $CDCl_3$) δ 135.0 (C2), 128.7 (C3), 69.5 (C1), 38.7 (C8), 29.1 (C5), 26.3 (C4), 25.9 (C6/C7), 23.7 (C6/C7).

(*Z*)-Cyclooct-2-en-1-yl 2'-(3''-benzoylphenyl)propanoate (113)

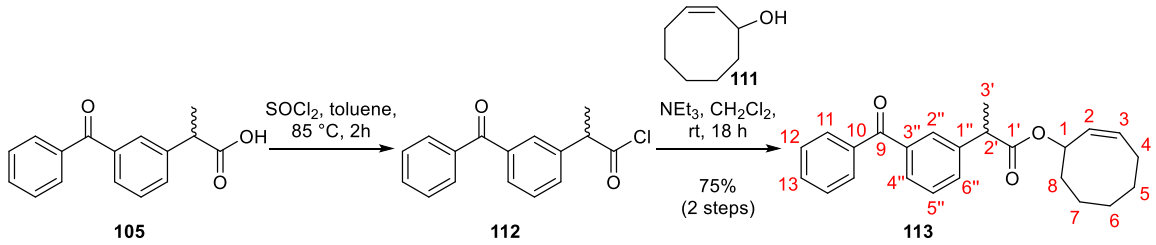

According to the procedure by Schlegel *et al.*,[10] a solution of ketoprofen (**105**, 40 mg, 0.157 mmol, 1.0 equiv.) and thionyl chloride (0.1 mL, 1.37 mmol, 8.7 equiv.) in toluene was stirred at 85 °C for 2 h. The reaction was cooled to rt then concentrated *in vacuo* to give acyl chloride **112** which was used directly in the subsequent step, assuming quantitative yield.

Triethylamine (0.1 mL, 0.72 mmol, 4.6 equiv.) was added to a solution of **112** (quantitative, 0.157 mmol) and *cis*-cycloocten-1-ol (**111**, 13 mg, 0.10 mmol, 0.6 equiv.) in CH_2Cl_2 (5 mL) and the mixture was stirred at rt for 18 h. The mixture was then concentrated *in vacuo*. Purification via flash column chromatography (20% EtOAc/petrol) yielded **113** as a yellow oil (28.1 mg, 0.08 mmol, 75%) as a mixture of diastereoisomers. This experiment was performed by Luxi Qiao.

^{1}H NMR (500 MHz, $CDCl_3$) δ 7.82–7.78 (m, 2H, H11), 7.75 (dt, *J* = 3.5, 1.9 Hz, 1H, H2''), 7.68 (dd, *J* = 7.6, 1.5 Hz, 1H, H4''), 7.61–7.57 (m, 1H, H13), 7.55 (ddt, *J* = 7.7, 4.5, 1.5 Hz, 1H, H6''), 7.50–7.41(m, 3H, H12, H5''), 5.69-5.58 (m, 2H, H2, H3), 5.45 (ddd, *J* = 10.8, 7.1, 1.3 Hz, 0.3 H, H1), 5.32 (ddd, *J* = 10.8, 7.0, 1.4 Hz, 0.7H, H1), 3.78 (q, *J* = 7.2 Hz, 1H, H2'), 2.27–2.17 (m, 1H, H4a), 2.13–2.02 (m, 1H, H4b), 1.92–1.83 (m, 0.7H, H8a), 1.81–1.72 (m, 0.3H, H8a), 1.67 (ddq, *J* = 12.8, 8.3, 4.1 Hz, 1H, H8b), 1.61–1.45 (m, 7H, H3', H5, H6), 1.44–1.36 (m, 1H, H7), 0.87 (qt, *J* = 8.6, 6.0 Hz, 1H, H7).

^{13}C NMR (126 MHz, $CDCl_3$) δ 196.7 (C9), 173.5 (C1'), 141.1 (C3''), 138.0 (C10), 137.7 (C1''), 132.6 (C6''), 131.7 (C2), 130.4(C13), 130.2 (C2''), 130.0 (C11), 129.4 (C3), 129.0 (C4''), 128.7 (C5''), 128.4 (C12), 73.0 (C1), 45.7 (C2'), 35.1 (C8), 28.9 (C4), 26.4 (C6), 25.9 (C5), 23.4 (C7), 18.6 (C3').

IR (thin film, ν_{max} /cm^{-1}) 2927s, 2855m, 1730s, 1660s, 1598w, 1448br, 1377w, 1318m, 1282s, 1205s, 1175br, 1077w, 1024br, 945br, 899br, 820w, 755m.

HRMS (ESI$^+$): m/z calc. for $C_{24}H_{26}O_3{}^{23}Na$ $[M+Na]^+$ 385.1774, found 385.1765, Δ -2.4 ppm.

(*E*)-Cyclooct-2-en-1-yl 2-(3-benzoylphenyl)propanoate (114)

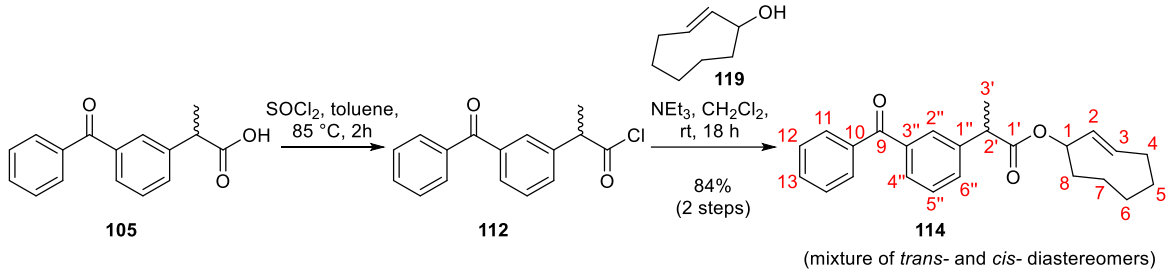

According to the procedure by Schlegel *et al*,[10] a solution of ketoprofen (**105**, 40 mg, 0.157 mmol, 1.0 equiv.) and thionyl chloride (0.1 mL, 1.37 mmol, 8.7 equiv.) in toluene was stirred at 85 °C for 2 h. The reaction was cooled to rt then concentrated *in vacuo* to give acyl chloride **112** which was used directly in the subsequent step, assuming quantitative yield.

Triethylamine (0.1 mL, 0.717 mmol, 4.6 equiv.) was added to a solution of **112** (quantitative, 0.157 mmol) and *trans*-cyclooct-2-en-1-ol (**119**, 13 mg, 0.10 mmol, 0.6 equiv.) in CH_2Cl_2 (5 mL) and the mixture was stirred at rt for 18 h. The mixture was then concentrated *in vacuo*. Purification via flash column chromatography (20% EtOAc/petrol) yielded **114** as a yellow oil as a mixture of 8 diastereomers (4 corresponding to the *cis*-isomer **113**) (33 mg, 0.09 mmol, 84%). This experiment was performed by Luxi Qiao.

Separation of chiral isomers using HPLC: The crude mixture was dissolved in 1% 2-propanol/hexane to a concentration of 5 mg/100 µL. 30 µL was injected each time, and the different peaks were collected in separate vials and concentrated *in vacuo*. The separation was performed on an Agilent 1100 series instrument with a YMC Chiralart Cellulose-SC column (250 x 4.6 mmI.D. s-3 µm). The mobile phase consisted of hexane and 2-propanol. The peaks were eluted with a step gradient (0–35 min 0.8% 2-propanol, 35–70 min 4% 2-propanol, 1 mL/min). This experiment was performed by Luxi Qiao.

IR (thin film, ν_{max} /cm^{-1}) 2924s, 2852m, 1733s, 1661s, 1598w, 1449m, 1378w, 1282s, 1205m, 1176br, 1122m, 1071m, 1023w, 989w, 952w, 932w, 907w, 818w, 719s.
HRMS (ESI^+): m/z calc. for $C_{24}H_{26}O_3{}^{23}Na$ $[M+Na]^+$ 385.1774, found 385.1760, Δ -3.7 ppm.

(R/S)-Axial:

^{1}H NMR (500 MHz, $CDCl_3$) δ 7.82–7.77 (m, 3H, H2”, H11), 7.68 (dt, *J* = 7.7, 1.4 Hz, 1H, H4”), 7.62–7.55 (m, 2H, H6”, H13), 7.51–7.42 (m, 3H, H5”, H12), 5.67 (dddd, *J* = 16.1, 11.1, 3.8, 1.0 Hz, 1H, H3), 5.49 (dd, *J* = 16.5, 2.4 Hz, 1H, H2), 5.39 (qq, *J* = 2.2, 1.1 Hz, 1H, H1), 3.86 (q, *J* = 7.2 Hz, 1H, H2’), 2.46–2.38 (m, 1H, H4a), 2.03–1.89 (m, 3H, H4b, H8), 1.86–1.77 (m, 1H, H7a), 1.64 (ddd, *J* = 13.0, 3.3, 1.7 Hz, 1H, H5a), 1.57 (d, *J* = 7.2 Hz, 3H, H3’), 1.53–1.47 (m, 1H, H5b), 1.41–1.36 (m, 1H, H6a), 0.85–0.80 (m, 1H, H6b), 0.79–0.68 (m, 1H, H7b).

^{13}C NMR (126 MHz, $CDCl_3$) δ 196.5 (C9), 173.0 (C1’), 141.0 (C3”), 137.9 (C10), 137.5 (C1”), 132.5 (C6”), 132.3 (C2), 131.6 (C13), 130.4 (C2”), 130.0 (C11), 129.3 (C3), 128.9 (C4”), 128.5 (C5”), 128.3 (C12), 73.9 (C1), 45.7 (C2’), 40.4 (C8), 35.9 (C4), 35.9 (C6), 29.0 (C5), 23.9 (C7), 18.2 (C3’).

(R/S)-Equatorial:

^{1}H NMR (500 MHz, $CDCl_3$) δ 7.82–7.76 (m, 3H, H2”, H11), 7.69 (dt, *J* = 7.7, 1.4 Hz, 1H, H4”), 7.62–7.55 (m, 2H, H6”, H13), 7.51–7.43 (m, 3H, H5”, H12), 5.46 (dd, *J* = 16.5, 2.3 Hz, 1H, H3), 5.40–5.33 (m, 2H, H1, H2), 3.85 (q, *J* = 7.2 Hz, 1H, H2’), 2.31 (dddd, *J* = 9.6, 4.9, 3.6, 1.5 Hz, 1H, H4a), 2.07–1.87 (m, 3H, H4b, H8), 1.82 (dddt, *J* = 14.9, 11.3, 5.1, 1.7 Hz, 1H, H7a), 1.70–1.51 (m, 2H, H5), 1.57 (d, *J* = 7.2 Hz, 3H, H3’), 1.39–1.32 (m, 1H, H6a), 1.00–0.92 (m, 1H, H6b), 0.79–0.69 (m, 1H, H7b).

^{13}C NMR (126 MHz, $CDCl_3$) δ 196.5 (C9), 172.9 (C1’), 140.9 (C3”), 137.9 (C10), 137.5 (C1”), 132.5 (C6”), 132.0 (C2), 131.6 (C13), 130.4 (C2”), 130.1 (C11), 129.4 (C3), 128.9 (C4”), 128.5 (C5”), 128.3 (C12), 73.9 (C1), 45.7 (C2’), 40.5 (C8), 35.9 (C4), 35.8 (C6), 29.0 (C5), 24.1 (C7), 18.1 (C3’).

4.2.2 Stability studies

***Vinyl-protected ketoprofen (106)*:** Stock solutions of **106** in MeCN (50 mM) were diluted in PBS, DMEM + 10% FBS or 10% human plasma in PBS to a final concentration of 1 mM. Acetophenone was used as an internal standard. A stock solution of acetophenone in MeCN (60 mM) was added to the samples to give a final concentration of 2.5 mM. The sample mixture was incubated at 37 °C and analysed at different times by HPLC/UV analysis (1 h, 2h, 4 h, 24 h). The HPLC/UV analysis was performed on a Dionex UltiMate 3000 UHPLC+ system (Thermo Scientific) with a Phenomenex Luna NH_2 Column (100 Å 5 µm, 250 mm x 4.6 mm). The mobile phase consisted of A: H_2O with 0.1% formic acid, and B: MeCN with 0.1% formic acid. The samples were eluted with a linear gradient (3–15 min 0–100% B, and 15–23 min 100% B, 0.50 mL/min. This experiment was performed by Luxi Qiao.

***Cis-cyclooctene-protected ketoprofen (113)*:** Stock solutions of **113** in MeCN (20 mM) were diluted in PBS, DMEM + 10% FBS or 10% human plasma in PBS to give a final concentration of 800 µM. Benzoic acid was used as an internal standard, and a stock solution of benzoic acid in MeCN (200 mM) was added to the samples to give a final concentration of 2 mM. The sample mixture was incubated at 37 °C and analysed at different times (1 h, 2 h, 4 h, 24 h, and 48 h) by HPLC/UV analysis. The HPLC/UV analysis was performed on an Agilent 1100 series instrument with a Phenomenex Luna NH_2 Column (100 Å 5 µm, 250 mm x 4.6 mm). The mobile phase consisted of A: H_2O with 0.1% TFA, and B: MeCN with 0.1% TFA. The samples were eluted with a linear gradient (3–20 min 0–100% B and 20–27 min 100% B, 0.50 mL/min). This experiment was performed by Luxi Qiao.

***Tetrazines 15, 58, 89, 90, 91*:** 60 µL of tetrazines **15**, **58**, **89**, **90**, **91** (2 mM, 50% DMSO/H_2O) was added to a 96 well plate (Greiner, black, clear bottomed) in technical triplicates and the absorbance was monitored over 24 h at 37 °C. For tetrazine **15**, which was not completely soluble at this concentration, the stock solution was centrifuged and the supernatant was used for the experiment. Readings were taken every minute using a SpectraMax i3x plate reader (λ_{max} = 530 nm). This assay was performed 3 independent times. Data were processed using GraphPad Prism (GraphPad Software, La Jolla, CA, USA).

Biological stability of tetrazine 90: A stock solution of tetrazine **90** in DMSO (400 mM) was diluted in PBS, DMEM + 10% FBS or 10% human plasma in PBS to give a final concentration of 10 mM. The sample mixtures were then filtered and the decay of the UV absorbance of the tetrazine at 530 nm was followed over 24 h at 37 °C with measurements taken at every 5 min with a Cary 100 instrument from Varian. This experiment was performed by Luxi Qiao.

4.2.3 Decaging studies

Kinetics of vinyl ester decaging: Rate constants were determined under pseudo-first order conditions. Stocks solutions in 30% H_2O/DMF were prepared for each tetrazine **15**, **58**, **89**, **90**, **91** (4 mM) and vinyl propionate (**103**, 300 to 700 mM). Mixing equal volumes of the stock solutions resulted in final concentrations of 2 mM for the tetrazine and 150–350 mM for vinyl propionate (**103**). The decay of the UV absorbance of the tetrazine at the corresponding wavelength was followed over time at 37 °C with a Cary 100 instrument from Varian and the data were fitted to an exponential one-phase decay equation $Y = (Y_0 – \text{Plateau})e^{(-kX)} + \text{Plateau}$. Each measurement was repeated three different times. The resulting values for k_{obs} were then plotted against the concentration of vinyl propionate and fitted to a linear equation to obtain the second-order rate constant k_2 from the slope. Data were processed using GraphPad Prism (GraphPad Software, La Jolla, CA, USA). This experiment was performed by Luxi Qiao.

Decaging of vinyl-protected ketoprofen (106): The caged compound **106** (1.25 mM) was mixed with tetrazine **90** (37.5 mM) in 43% MeOH in H_2O. The sample mixtures were incubated at 37 °C and analysed at different times (0 h, 24 h). The HPLC/UV analysis was performed on a Dionex UltiMate 3000 UHPLC+ system (Thermo Scientific) with a Phenomenex Luna NH_2 Column (100 Å 5 µm, 250 mm x 4.6 mm). The mobile phase consisted of A: H_2O with 0.1% formic acid, and B: MeCN with 0.1% formic acid. The samples were eluted with a linear gradient (3–10 min 0–100% B, and 10–17 min 100% B, 0.50 mL/min). This experiment was performed by Luxi Qiao.

***Decaging of TCO-protected ketoprofen (114)*:** TCO-ketoprofen (**114**) in DMF (23 µL, 11.4 mM), tetrazine **15**, **89**, **90** or **91** in DMF (23 µL, 11.4 mM) and the internal standard benzoic acid in MeCN (80 µL, 2 mM) were mixed to give final reactant concentrations of 2.1 mM (**114** and tetrazine **15**, **89**, **90** or **91**) and 1.3 mM (benzoic acid standard). For reactions in 25%, 50%, 75% water and 1% formic acid, the benzoic acid stock solution (and for 75% water, the tetrazine) was prepared in an appropriate solvent system (MeCN/H_2O) to ensure the correct final percentage of water in the reaction mixture. 25 µL of reactant mixture was quenched at different time points (10 s, 30 s, 2 min, 1 h, and 3 h) with an excess of TCO-OH (3.3 µL, 400 mM in MeCN). The sample was then diluted with 6.5 µL 50% MeCN/H_2O and injected into the LC-MS. The LC-MS analysis was performed on Waters SQD2 with Waters H-Class UPLC system with a Waters Acquity UPLC BEH C18 column (1.7µm, 2.1 x 50 mm). The mobile phase consisted of A: 10mM ammonium acetate with 0.1% formic acid, and B: 95% aqueous MeCN with 0.05% formic acid. The samples were eluted with a linear gradient (0.25–2 min 0–100% B, and 2–2.5 min 100% B, 0.80 mL/min).

4.2.4 Live cells studies

***Cell Culture*:** RAW264.7 (ATCC TIB-71) cells were routinely grown in a humidified incubator at 37 °C under 5% CO_2, and split before reaching confluence using a cell scraper. The cell line was grown on DMEM medium (catalogue number: 21063029) supplemented with 10% heat-inactivated FBS (Endotoxin level: ≤5 EU/mL, catalogue number: 10082147), 4 mM L-glutamine, 4500 mg/L glucose, 1 mM sodium pyruvate, 1500 mg/L sodium bicarbonate, and 100 units/mL penicillin. All reagents were bought from Gibco, Life Technologies (Thermo Fisher Scientific, UK), unless otherwise stated. Pipette tips were Pyrogen free and purchased from STARLAB, UK (catalogue number: S1126-7810).

***Cytotoxicity in RAW264.7 cells*:** Cytotoxicity of axial-TCO-ketoprofen (**114ax**), equatorial-TCO-ketoprofen (**114eq**), tetrazine **90**, ketoprofen (**105**) and LPS was assessed using a CellTiter-Blue Cell Viability Assay (ThermoFisher Scientific, USA). Briefly, cells were seeded at a concentration of 5,000 cells/well (200 µL) in flat-bottom 96-well plates and allowed to adhere and adapt to the plates for 24 h. At this point, increasing concentrations of each compound (dissolved in DMSO) were added in technical triplicates (for tetrazines: 440 µM, 148 µM, 49 µM, 16 µM, and 5.0 µM; for LPS: 15 µg/mL, 10 µg/mL, 5 µg/mL, 2.5 µg/mL, 1 µg/mL, 500 ng/mL, 100 ng/mL and 50 ng/mL); for other compounds: 133 µM, 44.4 µM, 14.8 µM, 4.9 µM, 1.6 µM, and 0.5 µM). Final concentration of DMSO in each well was < 0.5%. Plates were incubated for 3 days, at which time cell viability was assessed by the addition of CellTiter-Blue Reagent (dilution 1:10 from commercial stock) and incubation for a further 3 h, before analysis of fluorescence on a SpectraMax i3x plate reader (λ_{ex} = 570 nm, λ_{em} = 590 nm).

***Inhibition of nitric oxide production in LPS-stimulated RAW264.7 Cells*:** The anti-inflammatory effect of axial-TCO-ketoprofen (**114ax**), equatorial-TCO-ketoprofen (**114eq**), tetrazine **90**, ketoprofen (**105**), axial-TCO-ketoprofen (**114ax**) with tetrazine **90**, and equatorial-TCO-ketoprofen (**114eq**) with **90** was assessed using the Griess test, which detects nitric oxide (NO) levels by the production of a UV-active coloured azo compound. RAW264.7 cells were seeded at a density of 4 x 10^4 cells/well in 96-well plates and incubated for 24 h at 37 °C and 5% CO_2. At this point, the media was replaced with phenol red-free complete media (200 µL). Tetrazine **90** was added in technical triplicates by replacing the media with 200 µl of a 50 µM solution of tetrazine in phenol red-free complete media. Other compounds (dissolved in DMSO) were added in technical triplicates to give a concentration of 10 µM. LPS was then added to each well to give a concentration of 500 ng/mL. Final concentration of DMSO in each well was ≤ 0.125%. Plates were incubated for 11 h (5 h, 11 h, 24 h in optimisation experiments), at which time 100 µL of the supernatent was extracted and added to 100 µL of Griess reagent (Sigma-Aldrich) for 15 min before measurement of the absorbance on a SpectraMax i3x plate reader, (λ_{max} = 540 nm).

This assay was performed 3 independent times. Statistical analysis was performed on GraphPad Prism using a one-way analysis of variance (ANOVA).

***Cell permeability of TCO-ketoprofen and ketoprofen in RAW264.7 cells*:** The cell permeability of axial-TCO-ketoprofen (**114ax**), equatorial-TCO-ketoprofen (**114eq**), and ketoprofen (**105**) were evaluated by HPLC. Cells were seeded at a concentration of 125,000 cells/well (500 µL) in flat-bottom 24 well-plates and allowed to adhere and adapt to the plates for 24 h. At this point, media was replaced and LPS was added to each well in the concentration of 5 µg/mL and each compound was added (200 mM stock dissolved in DMSO) in technical triplicates for a final concentration of 1 mM. Final concentration of DMSO in each well was 0.5%. Plates were incubated for 24 h, at which time the media was collected, centrifuged, and the supernatant analyzed using HPLC. The HPLC/UV analysis was performed on a Dionex UltiMate 3000 UHPLC+ system (Thermo Scientific) with a Phenomenex Luna NH_2 Column (100 Å 5 µm, 250 mm x 4.6 mm). The mobile phase consisted of A: H_2O with 0.1% formic acid, and B: MeCN with 0.1% formic acid. The samples were eluted with a linear gradient (3−15 min 0−100% B, and 15−23 min 100% B, 0.50 mL/min).

***Inhibition of PGE2 expression in LPS-stimulated RAW264.7 Cells*:** The anti-inflammatory effect of axial-TCO-ketoprofen (**114ax**), equatorial-TCO-ketoprofen (**114eq**)**,** tetrazine **90**, ketoprofen (**105**), axial-TCO-ketoprofen (**114ax**) with tetrazine **90** and equatorial-TCO-ketoprofen (**114eq**) with tetrazine **90** was assessed using a competitive ELISA assay, which detects PGE_2 levels. RAW264.7 cells were seeded at a density of 4 x 10^4 cells/well in 96-well plates and incubated for 24 h at 37 °C and 5% CO_2. At this point, the media was replaced with phenol red-free complete media (200 µL). Tetrazine was added in technical triplicates by replacing the media with 200 µl of a 50 µM solution of tetrazine in phenol red-free complete media. Other compounds (dissolved in DMSO) were added in technical triplicates to give a concentration of 10 µM. LPS was then added to each well to give a concentration of 500 ng/mL. Final concentration of DMSO in each well was ≤ 0.125%. Plates were incubated for 11 h, at which time 100 µL of the content of each well was extracted. PGE_2 (R&D Systems, Minneapolis, USA) was measured according the manufacturer's directions. Statistical analysis was performed on GraphPad Prism using a one-way ANOVA.

Computational Studies were performed by Claudio Navo and Gonzalo Jiménez-Osés from the Universidad de la Rioja, Spain.[11]

4.3 Experimental procedures for Chapter 3

4.3.1 Synthetic procedures

(2*E*)-Cyclooct-2'-en-1'-yl 4-nitrophenyl carbonate (121)

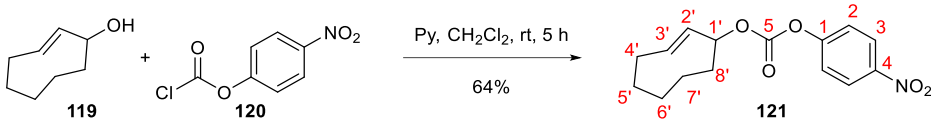

According to the procedure by Lemke *et al.*,[12] (2*E*)-cyclooct-2-en-1-ol (axial isomer) (**119**, 35 mg, 0.277 mmol, 1.0 equiv.) and pyridine (0.06 mL, 0.693 mmol, 2.5 equiv.) were dissolved in CH_2Cl_2 (3 mL). A solution of 4-nitrophenyl chloroformate (**120**, 84 mg, 0.416 mmol, 1.5 equiv.) in CH_2Cl_2 (3 mL) was added and the reaction was stirred at rt for 5 h. The reaction was stopped by addition of $NH_4Cl_{(aq)}$ (sat. soln., 5 mL) and the phases were separated. The aqueous phase was extracted with CH_2Cl_2 (2 x 10 mL) and the combined organic extracts were washed with brine (10 mL), dried over anhydrous Na_2SO_4 and concentrated *in vacuo*. Purification via flash column chromatography (5% EtOAc/Petrol) yielded **121** as a white solid (49 mg, 0.168 mmol, 61%). The NMR data were in accordance with the previously reported literature data.[12]

R_f 0.17 (5% EtOAc/Petrol).

^{1}H NMR (400 MHz, $CDCl_3$) δ 8.48 – 8.19 (m, 2H, H3), 7.42 (d, *J* = 9.2 Hz, 2H, H2), 6.00 (ddd, *J* = 16.2, 11.1, 3.8 Hz, 1H, H3'), 5.58 (dd, *J* = 16.2, 2.3 Hz, 1H, H2'), 5.51 – 5.35 (m, 1H, H1'), 2.55 (dd, *J* = 10.8, 4.3 Hz, 1H, H4a'), 2.30 – 2.17 (m, 1H, H8a'), 2.17 – 2.01 (m, 2H, H4b', H5a'), 1.99 – 1.87 (m, 1H, H6a'), 1.88 – 1.68 (m, 2H, H7a', H8b'), 1.63 – 1.50 (m, 1H, H5b'), 1.31 – 1.12 (m, 1H, H7b'), 0.86 (tdd, *J* = 12.9, 5.4, 3.2 Hz, 1H, H6b').

^{13}C NMR (101 MHz, $CDCl_3$) δ 155.6 (C1), 151.6 (C5), 145.3 (C4), 133.1 (C3'), 129.4 (C2'), 125.3 (C3), 121.8 (C2), 78.8 (C1'), 40.4 (C8'), 36.0 (C4'), 35.9 (C5'), 28.9 (C6'), 24.0 (C7').

(2*E*)-Cyclooct-2'-en-1'-yl 2-oxochromen-7-yl carbonate (123)

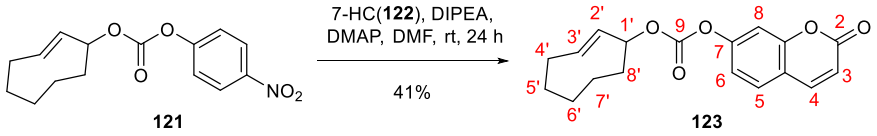

According to the modified procedure by Renslo *et al.,*[13] 7-hydroxycoumarin (**122**, 71 mg, 0.437 mmol, 2.6 equiv.), DIPEA (0.09 mL, 0.505 mmol, 3.0 equiv.) and 4-(*N*,*N*-dimethylamino)pyridine (DMAP, 8 mg, 0.067 mmol, 0.4 equiv.) were added to a solution of (2*E*)-cyclooct-2-en-1-yl 4-nitrophenyl carbonate (**121**, 49 mg, 0.168 mmol, 1.0 equiv.) in DMF (3 mL). The reaction mixture was stirred at rt for 24 h then an additional portion of 7-hydroxycoumarin (**122**, 30 mg, 0.185 mmol, 1.1 equiv.) and DIPEA (0.03 mL, 0.185 mmol, 1.1 equiv.) was added. The reaction was stirred for a further 3 h then diluted with Et_2O (30 mL), washed with HCl (1M, 10 mL), NaOH (1M, 5 x 10 mL), brine (20 mL), dried over anhydrous $MgSO_4$, filtered and concentrated *in vacuo*. Purification via flash column chromatography (20–25% EtOAc/Petrol) yielded **123** as a white solid (32 mg, 0.102 mmol, 61%).

R_f 0.30 (25% EtOAc/Petrol).

Mp 105–107 °C.

^{1}H NMR (400 MHz, $CDCl_3$**)** δ 7.69 (d, *J* = 9.5 Hz, 1H, H4), 7.49 (d, *J* = 8.5 Hz, 1H, H5), 7.23 (d, *J* = 2.3 Hz, 1H, H8), 7.16 (dd, *J* = 8.5, 2.3 Hz, 1H, H6), 6.40 (d, *J* = 9.5 Hz, 1H, H3), 5.98 (ddd, *J* = 16.2, 11.2, 3.8 Hz, 1H, H3'), 5.56 (dd, *J* = 16.2, 2.3 Hz, 1H, H2'), 5.46 – 5.40 (m, 1H, H1'), 2.53 (dd, *J* = 10.7, 4.3 Hz, 1H, H4a'), 2.27 – 2.16 (m, 1H, H8a'), 2.13 – 1.97 (m, 2H, H4b', H5a'), 1.92 (dddd, *J* = 15.1, 7.2, 3.5, 1.7 Hz, 1H, H6a'), 1.85 – 1.65 (m, 2H, H7a', H8b'), 1.65 – 1.46 (m, 1H, H5b'), 1.19 (dddd, *J* = 19.1, 15.0, 9.7, 1.7 Hz, 1H, H7b'), 0.92 – 0.72 (m, 1H, H6b').

^{13}C NMR (101 MHz, $CDCl_3$) δ 160.3 (C2), 154.7 (C8a), 153.5 (C7), 151.9 (C9), 142.8 (C4) , 133.1 (C3'), 129.5 (C2'), 128.6 (C5), 117.8 (C6), 116.7 (C4a), 116.2 (C3), 109.9 (C8), 78.6 (C1'), 40.5 (C8'), 36.0 (C4'), 35.9 (C5'), 29.0 (C6'), 24.0 (C7').

IR (thin film, ν_{max}/cm^{-1}) 2929m, 2852w, 1759s, 1726s, 1706m, 1619m, 1567w, 1503w, 1453w, 1401m, 1277m.

HRMS (ESI$^+$): *m/z* calc. for $C_{18}H_{18}O_5$ $[M+H]^+$ 315.1227, found 315.1220, Δ -2.1 ppm.

4-[(2'Z)-cyclooct-2'-en-1'-yloxy]benzaldehyde (127)

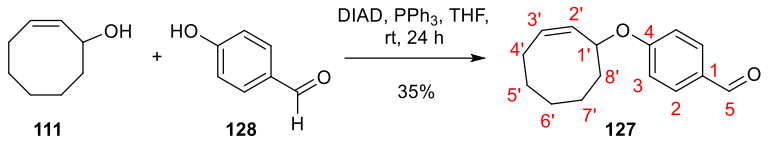

According to the modified procedure by Versteegen *et al.*[14] 4-hydrobenzaldehyde (**128**, 90 mg, 0.737 mmol, 1.5 equiv.) and triphenylphosphine (193 mg, 0.737 mmol, 1.5 equiv.) were added to a solution of *cis*-cyclooct-2-en-1-ol (**111**, 62 mg, 0.491 mmol, 1.0 equiv.) in THF (4 mL). The reaction mixture was cooled to 0 °C and diisopropyl azodicarboxylate (DIAD, 0.15 mL, 0.737 mmol, 1.5 equiv.) was added dropwise. The reaction was stirred in the dark at rt for 20 h. Silica was added and all volatiles were removed *in vacuo*. Purification of the dry residue directly via flash column chromatography (1–7% EtOAc/Petrol) gave **127** as a pale yellow oil (40 mg, 0.174 mmol, 35%).

R_f 0.34 (7% EtOAc/Petrol).

^{1}H NMR (500 MHz, $CDCl_3$) δ 9.86 (s, 1H, H5), 7.84 – 7.75 (m, 2H, H2), 6.99 – 6.92 (m, 2H, H3), 5.80 (dddd, *J* = 10.9, 9.1, 7.4, 1.6 Hz, 1H, H3'), 5.49 (ddd, *J* = 10.8, 7.1, 1.3 Hz, 1H, H2'), 5.17 (dddd, *J* = 8.6, 6.6, 4.6, 1.5 Hz, 1H, H1'), 2.38 – 2.19 (m, 2H, H4'), 2.11 (ddt, *J* = 13.0, 8.7, 4.4 Hz, 1H, H8a'), 1.87 – 1.36 (m, 6H, H5a', H6', H7', H8b'), 0.98 – 0.75 (m, 1H, H5b').

^{13}C NMR (126 MHz, $CDCl_3$) δ 190.8 (C5), 163.5 (C4), 132.0 (C3'), 131.9 (C2), 130.8 (C2'), 129.6 (C1), 115.7 (C3), 75.8 (C1'), 35.7 (C8'), 29.0 (C5'), 26.8 (C6'), 26.1 (C4'), 23.3(C7').

IR (thin film, ν_{max}/cm^{-1}) 2926m, 2854w, 1689s, 1597s, 1575m, 1506m, 1306m, 1246s, 1214m, 1157s.

HRMS (ASAP$^+$): *m/z* calc. for $C_{15}H_{18}O_2$ $[M]^+$ 230.1307, found 230.1302, Δ – 2.2 ppm.

{4-[(2Z)-cyclooct-2'-en-1'-yloxy]phenyl}methanol (129)

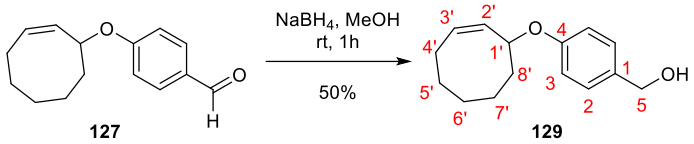

Aldehyde **127** (36 mg, 0.156 mmol, 1.0 equiv.) was dissolved in MeOH (2 mL) and cooled to 0 °C. Sodium borohydride (59 mg, 1.56 mmol, 10 equiv.) was added and the reaction was stirred at rt for 2 h. $NH_4Cl_{(aq)}$ (sat. soln., 2 mL) was added slowly and the reaction was stirred for 10 min. MeOH was removed *in vacuo* and the aqueous solution was extracted with EtOAc (3 x 5 mL). The organic layers were washed with brine (10 mL), dried over anhydrous Na_2SO_4 and concentrated *in vacuo.* Purification via flash column chromatography (20% EtOAc/PE) yielded **129** as a colourless oil (18 mg, 0.077 mmol, 50%).

R_f 0.20 (20% EtOAc/Petrol).

^{1}H NMR (500 MHz, MeOD) δ 7.26 – 7.16 (m, 2H, H2), 6.87 – 6.76 (m, 2H, H3), 5.74 (dddd, *J* = 10.8, 9.0, 7.2, 1.6 Hz, 1H, H3'), 5.45 (ddd, *J* = 10.9, 7.1, 1.4 Hz, 1H, H2'), 5.16 – 5.07 (m, 1H, H1'), 4.51 (s, 2H, H5), 2.41 – 2.29 (m, 1H, H4a'), 2.24 – 2.15 (m, 1H, H4b'), 2.11 – 2.00 (m, 1H, H8a'), 1.82 – 1.52 (m, 6H, H5a', H6', H7', H8b'), 1.46 (tdt, *J* = 12.6, 6.6, 3.4 Hz, 1H, H5b').

^{13}C NMR (126 MHz, MeOD) δ 157.5 (C4), 133.2 (C2'), 132.9 (C1), 129.6 (C3'), 128.1 (C2), 115.1 (C3), 74.8 (C1'), 63.6 (C5), 35.5 (C8'), 28.7 (C5'), 26.2 (C4'), 25.9 (C6'), 23.1(C7').

IR (thin film, ν_{max}/cm^{-1}) 3375m, 2927s, 2853m, 1611m, 1584w, 1509s, 1455w, 1241s, 1038m.

HRMS (ESI$^+$): *m/z* calc. for $C_{15}H_{20}O_2Na$ $[M+Na]^+$ 255.1356, found 255.1361, Δ 2.3 ppm.

(1'Z)-3'-[4-(chloromethyl)phenoxy]cyclooct-1'-ene (130)

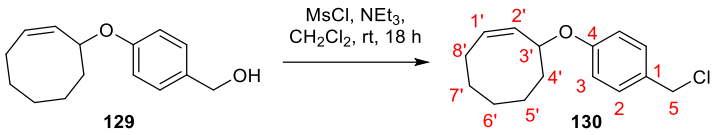

129 130

Triethylamine (78 µL, 0.516 mmol, 3.0 equiv.) was added to a solution of alcohol **129** (40 mg, 0.172 mmol, 1.0 equiv.) in CH_2Cl_2 (2 mL) and the solution was cooled to 0 °C. A solution of methanesulfonyl chloride (26 µL, 0.344 mmol, 2.0 equiv.) in CH_2Cl_2 (2 mL) was added dropwise and the reaction mixture was warmed to rt and stirred at rt for 18 h. The reaction mixture was concentrated *in vacuo* and filtered through silica (3% EtOAc/Petrol). This experiment was performed by Dr. Bruno Oliveira.

^{1}H NMR (400 MHz, $CDCl_3$) δ 7.29 (d, *J* = 5.7 Hz, 2H, H2), 6.93 – 6.77 (m, 2H, H3), 5.77 (dddd, *J* = 10.8, 9.0, 7.3, 1.6 Hz, 1H, H1'), 5.52 (ddd, *J* = 10.8, 7.1, 1.3 Hz, 1H, H2'), 5.10 (dddd, *J* = 11.5, 6.8, 4.7, 1.5 Hz, 1H, H3'), 4.57 (s, 2H, H5), 2.40 – 2.16 (m, 2H, H8'), 2.11 (ddt, *J* = 13.0, 8.9, 4.6 Hz, 1H, H4a'), 1.84 – 1.39 (m, 6H, H7a', H6', H5', H4b'), 0.96 – 0.79 (m, 1H, H7b').

7-({4''-[(2'Z)-cyclooct-2'-en-1'-yloxy]phenyl}methoxy)chromen-2-one (131)

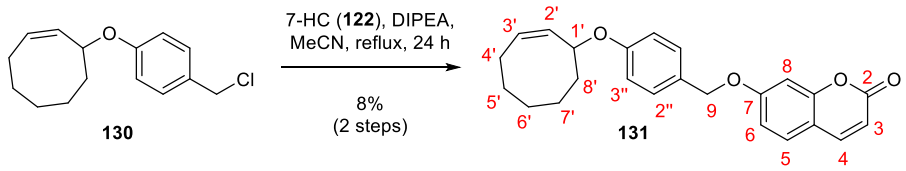

To a solution of chloride **130** (30 mg, 0.098 mmol, 1.0 equiv.) in MeCN (2 mL) was added a solution of 7-hydroxycoumarin (**122**, 31 mg, 0.193 mmol, 2.0 equiv.) and DIPEA (34 µL, 0.193 mmol, 2.0 equiv.) in MeCN (2 mL). The reaction mixture was refluxed for 24 h, then cooled to rt and concentrated *in vacuo*. Purification via flash column chromatography (0.5% MeOH/CH_2Cl_2) yielded **131** as a colourless oil (5 mg, 0.013 mmol, 8% over 2 steps). This experiment was performed by Dr. Bruno Oliveira.

^{1}H NMR (400 MHz, $CDCl_3$) δ 7.65 (d, *J* = 9.5 Hz, 1H, H4), 7.42 – 7.36 (m, 1H, H5), 7.36 – 7.30 (m, 2H, H6, H8), 6.97 – 6.88 (m, 4H, H2'', H3''), 6.27 (d, *J* = 9.5 Hz, 1H, H3), 5.78 (dddd, *J* = 10.8, 9.0, 7.2, 1.6 Hz, 1H, H3'), 5.53 (ddd, *J* = 10.9, 7.1, 1.3 Hz, 1H, H2'), 5.12 (dd, *J* = 11.4, 5.6 Hz, 1H, H1'), 5.06 (s, 2H, H9), 2.40 – 2.17 (m, 2H, H4'), 2.11 (ddt, *J* = 13.0, 8.8, 4.7 Hz, 1H, H8a'), 1.82 – 1.61 (m, 4H), 1.58 – 1.40 (m, 2H), 0.88 – 0.80 (m, 1H, H6').

4-{[(tert-butyldimethylsilyl)oxy]methyl}aniline (137)

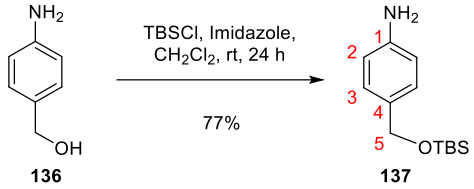

According to the procedure by Haynes *et al.*,[15] 4-aminobenzyl alcohol (**136**, 0.250 g, 2.03 mmol, 1.0 equiv.) and imidazole (0.152 g, 2.23 mmol, 1.1 equiv.) were dissolved in CH_2Cl_2 (5 mL). TBSCl (0.336 g, 2.23 mmol, 1.1 equiv.) was added and the reaction was stirred at rt for 24 h. The reaction was quenched with water (10 mL) and extracted with CH_2Cl_2 (4 x 10 mL). The combined organic layers were washed with brine (20 mL), dried over anhydrous Na_2SO_4 and concentrated *in vacuo*. Purification via flash column chromatography (40% EtOAc/Petrol) yielded **137** as a yellow liquid (0.373 g, 1.57 mmol, 77%). The NMR data were in accordance with reported data.[16]

R_f 0.76 (40% EtOAc/Petrol).

^{1}H NMR (400 MHz, $CDCl_3$) δ 7.18 – 7.06 (m, 2H, H3), 6.66 (d, *J* = 8.4 Hz, 2H, H2), 4.62 (s, 2H, H5), 3.61 (br s, 2H, NH_2), 0.92 (s, 9H, $OSi(CH_3)_2C(CH_3)_3$), 0.08 (s, 6H, $OSi(CH_3)_2C(CH_3)_3$).

tert-butyl[(4-isocyanatophenyl)methoxy]dimethylsilane (138)

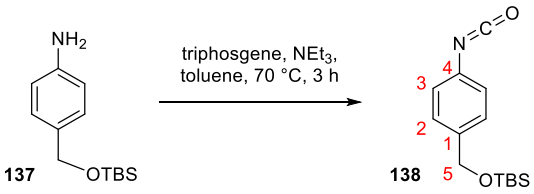

According to the procedure by Alaoui *et al.*,[17] amine **137** (50 mg, 0.211 mmol, 1.0 equiv.) was dissolved in toluene (5 mL). Triethylamine (0.03 mL, 0.232 mmol, 1.1 equiv.) and triphosgene (25 mg, 0.084 mmol, 0.4 equiv.) were added and the reaction mixture was heated to 70 °C for 3 h. The mixture was filtered, washed with toluene and concentrated *in vacuo* to give **138** as a colourless oil which was used directly in the next step assuming quantitative yield. The NMR data were in accordance with reported data.[17]

^{1}H NMR (400 MHz, $CDCl_3$) δ 7.31 – 7.24 (m, 2H, H2/3), 7.05 (dd, *J* = 8.5, 2.0 Hz, 2H, H2/3), 4.71 (s, 2H, H5), 0.95 (d, *J* = 1.6 Hz, 9H, $OSi(CH_3)_2C(CH_3)_3$), 0.10 (d, *J* = 1.6 Hz, 6H, $OSi(CH_3)_2C(CH_3)_3$).

(2*E*)-cyclooct-2-en-1-yl N-(4-{[(tert-butyldimethylsilyl)oxy]methyl}phenyl)carbamate (139)

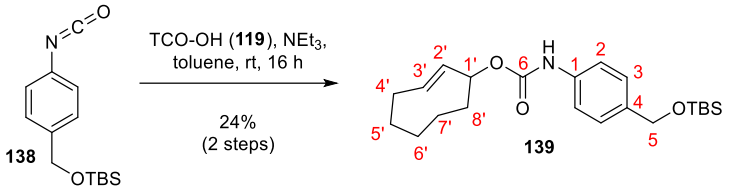

(2*E*)-Cyclooct-2-en-1-ol (**119**, axial isomer) (60 mg, 0.486 mmol, 1.0 equiv.) was dissolved in toluene (3 mL) and cooled to 0 °C. Triethylamine (0.07 mL, 0.535 mmol, 1.1 equiv.) was added followed by a solution of isocyanate **138** (166 mg, 0.632 mmol, 1.3 equiv.) in toluene (2 mL). The reaction was stirred at rt for 16 h then silica was added and all volatiles were removed *in vacuo*. Purification of the dry residue directly via flash column chromatography (2–10% EtOAc/Petrol) yielded **139** as a colourless oil (60 mg, 0.154 mmol, 24%).

R_f 0.26 (10% EtOAc/Petrol).

^{1}H NMR (500 MHz, $CDCl_3$) δ 7.36 (d, *J* = 8.2 Hz, 2H, H2), 7.25 (s, 1H, H3 (masked by $CDCl_3$ peak)), 5.88 (td, *J* = 13.2, 11.1, 3.6 Hz, 1H, H3'), 5.57 (dd, *J* = 16.4, 2.5 Hz, 1H, H2'), 5.44 (s, 1H, H1'), 4.69 (s, 2H, H5), 2.52 – 2.42 (m, 1H, H4a'), 2.20 – 2.10 (m, 1H, H8a'), 2.09 – 1.95 (m, 2H, H4b', H5a'), 1.89 (dddt, *J* = 12.8, 8.9, 5.2, 1.7 Hz, 1H, H6a'), 1.80 – 1.63 (m, 2H, H7a', H8b'), 1.53 – 1.43 (m, 1H, H5b'), 1.12 (ddt, *J* = 14.7, 12.7, 8.0 Hz, 1H, H7b'), 0.93 (s, 9H, $OSi(CH_3)_2C(CH_3)_3$), 0.89 – 0.77 (m, 1H, H6b'), 0.09 (s, 6H, $OSi(CH_3)_2C(CH_3)_3$).

^{13}C NMR (126 MHz, $CDCl_3$) δ 152.7 (C6), 136.7 (C4), 136.4 (C1), 132.1 (C3'), 131.0 (C2'), 126.9 (C3), 118.3 (C2), 74.4 (C1'), 64.7 (C5), 40.7 (C8'), 36.0 (C4'), 35.9 (C5'), 29.1 (C6'), 26.0 ($OSi(CH_3)_2C(CH_3)_3$), 24.2 (C7'), 18.4 ($OSi(CH_3)_2C(CH_3)_3$), -5.2 ($OSi(CH_3)_2C(CH_3)_3$).

HRMS (ESI$^+$): *m/z* calc. for $C_{22}H_{35}O_3NSiNa$ $[M+Na]^+$ 412.2278, found 412.2262, Δ –3.9 ppm.

(2''*E*)-cyclooct-2''-en-1''-yl N-(4-{[(2'-oxochromen-7'-yl)oxy]methyl}phenyl)carbamate (142) from route 1

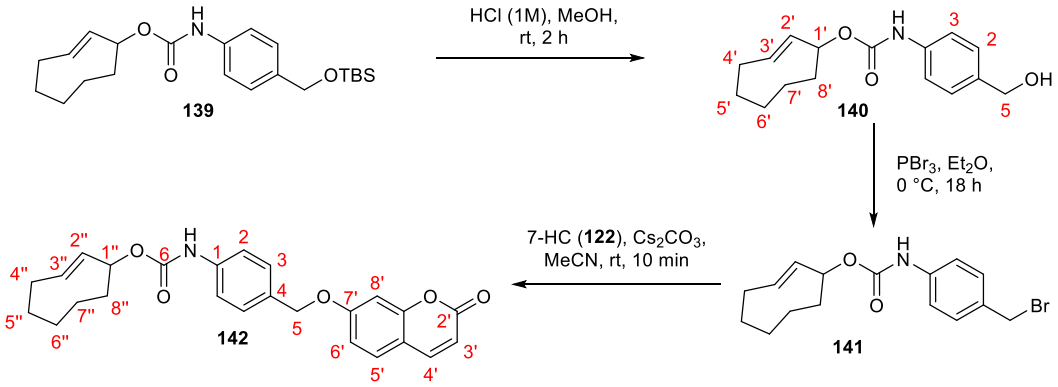

According to the procedure by Hay *et al.,*[18] **139** (60 mg, 0.154 mmol) was dissolved in MeOH (2 mL). HCl (1 M, 1 mL) was added and the reaction was stirred at rt for 1 h, until TLC showed complete consumption of the starting material. The reaction mixture was then poured into brine (5 mL) and extracted with EtOAc (3 x 10 mL). The combined organic layers were washed with water (10 mL), dried over anhydrous $MgSO_4$ and concentrated *in vacuo*. ^{1}H NMR showed that the reaction was not complete, so the crude mixture was redissolved in MeOH (2 mL) and HCl (1 M, 1 mL), stirred at rt for 1 h and then worked up as described above to give **140**, which was used crude in the following step assuming quantitative yield.

(2'*E*)-cyclooct-2'-en-1'-yl N-[4-(hydroxymethyl)phenyl]carbamate (140)

R$_f$ 0.11 (20% EtOAc/Petrol).

^{1}H NMR (400 MHz, $CDCl_3$) δ 7.40 (d, *J* = 8.0 Hz, 2H, H2), 7.33 – 7.28 (m, 2H, H3), 6.67 (s, 1H, N*H*), 5.88 (ddd, *J* = 15.8, 11.1, 3.7 Hz, 1H, H3'), 5.57 (dd, *J* = 16.4, 2.4 Hz, 1H, H2'), 5.44 (s, 1H, H1'), 4.64 (s, 2H, H5), 2.49 (dd, *J* = 10.5, 4.8 Hz, 1H, H4a'), 2.14 (dd, *J* = 14.3, 5.2 Hz, 1H, H8a'), 2.08 – 1.95 (m, 2H, H4b', H5a'), 1.95 – 1.83 (m, 1H, H6a'), 1.81 – 1.63 (m, 2H, H7a', H8b'), 1.58 (d, *J* = 4.8 Hz, 1H, H5b'), 1.10 (dd, *J* = 14.1, 6.1 Hz, 1H, H7b'), 0.83 (ddd, *J* = 16.6, 9.8, 4.3 Hz, 1H, H6b').

According to the procedure by Behnam *et al.*,[19] crude compound **140** was dissolved in Et_2O (5 mL) and cooled to 0 °C. PBr_3 (0.1 M in CH_2Cl_2, 0.12 mL, 0.8 equiv.) was added dropwise and the reaction was stirred at 0 °C for 18 h. The reaction mixture was then poured into $NaHCO_{3\,(aq)}$ (sat. soln., 10 mL) and extracted with Et_2O (3 x 10 mL). The combined organic layers were washed with water (20 mL), dried over anhydrous Na_2SO_4 and concentrated *in vacuo*. 2 products were observed by TLC and ^{1}H NMR which correspond to the *cis*- and *trans*-isomers. Compound **141** was used crude in the next step assuming quantitative yield.

(2'*E*)-cyclooct-2'-en-1'-yl N-[4-(bromomethyl)phenyl]carbamate (141)

R_f 0.61, 0.7 (20% EtOAc/Petrol).

^{1}H NMR (400 MHz, $CDCl_3$) δ 7.42 – 7.30 (m, 4H), 6.69 (s, 0.4H, N*H trans*), 6.61 (s, 0.6H, N*H cis*), 5.93 – 5.82 (m, 0.3H), 5.74 – 5.61 (m, 0.6H), 5.62 – 5.57 (m, 0.2H), 5.57 – 5.48 (m, 0.6H), 5.44 (s, 0.3H), 4.48 (d, *J* = 1.6 Hz, 2H), 2.52 – 2.41 (m, 1H), 2.34 – 2.21 (m, 1H), 2.19 – 2.09 (m, 1H), 2.08 – 1.96 (m, 1H), 1.94 – 1.82 (m, 0.3H), 1.81 – 1.47 (m, 4H), 1.19 – 1.02 (m, 0.5H), 0.94 – 0.73 (m, 1H). NMR not assigned due to mixture of isomers.

141 was dissolved in MeCN (2 mL) and added to a solution of 7-hydroxycoumarin (**122**, 19 mg, 0.116 mmol, 1.5 equiv.) and caesium carbonate (50 mg, 0.154 mmol, 2.0 equiv.) in MeCN (3 mL). The reaction mixture was stirred at rt for 10 min then the solvent was removed *in vacuo*. The residue was re-dissolved in CH_2Cl_2 (10 mL) and washed with water (5 mL), $NaHCO_{3\,(aq)}$ (sat. soln., 2 x 5 mL), water (5 mL), dried over anhydrous $MgSO_4$ and concentrated *in vacuo*. Purification via flash column chromatography (1% MeOH/CH_2Cl_2) yielded impure product **142** as a white powder (3 mg) as a 3:7 mixture of *trans:cis*. The product was not pure and ^{1}H NMR is only shown to confirm the mixture of isomers. Full characterisation was obtained on the pure *trans*-isomer of **142** that was obtained during route 2 (see below).

(2''*E*)-cyclooct-2''-en-1''-yl N-(4-{[(2'-oxochromen-7'-yl)oxy]methyl}phenyl)carbamate (142)

R_f 0.43 (1% MeOH/CH_2Cl_2).

^{1}H NMR (400 MHz, $CDCl_3$) δ 7.63 (d, *J* = 9.5 Hz, 1H, H4'), 7.44 (dd, *J* = 8.5, 6.8 Hz, 2H, H2), 7.36 (dt, *J* = 6.4, 2.3 Hz, 3H, H3, H5'), 6.92 – 6.84 (m, 2H, H6', H8'), 6.75 (s, 0.3H, N*H trans*), 6.65 (s, 0.7H, N*H cis*), 6.25 (d, *J* = 9.5 Hz, 1H, H3'), 5.88 (ddd, *J* = 15.8, 11.1, 3.7 Hz, 0.4H, H3'' *trans*), 5.71 (ddd, *J* = 10.9, 7.3, 1.8 Hz, 1.1H), 5.59 (t, *J* = 2.7 Hz, 0.2H), 5.53 (ddd, *J* = 10.9, 7.0, 1.3 Hz, 0.7H, H2'' or H3'' *cis*), 5.44 (s, 0.3H), 5.07 (d, *J* = 2.8 Hz, 2H, H5), 2.56 – 2.39 (m, 1H), 2.34 – 2.23 (m, 1H), 2.14 (ddt, *J* = 18.0, 7.7, 3.3 Hz, 1H), 2.02 (ddt, *J* = 14.6, 9.9, 4.8 Hz, 1H), 1.95 – 1.82 (m, 0.2H), 1.80 – 1.62 (m, 1H), 1.56 (q, *J* = 13.1, 11.8 Hz, 3H), 1.11 (td, *J* = 14.2, 6.0 Hz, 0.4H), 0.92 – 0.77 (m, 1H).

(2''*E*)-cyclooct-2''-en-1''-yl N-(4-{[(2'-oxochromen-7'-yl)oxy]methyl}phenyl)carbamate (142) from route 2

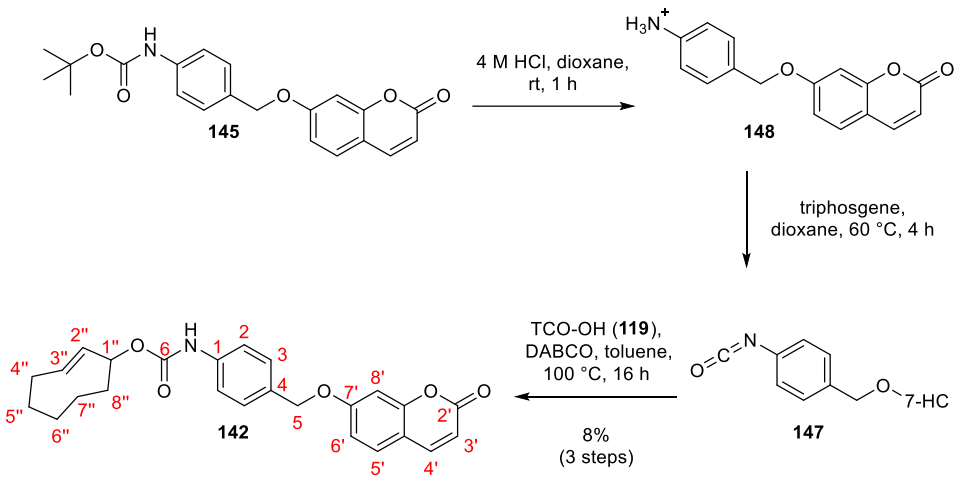

Boc protected aniline **145** (183 mg, 0.499 mmol, 1.0 equiv.) was dissolved in 4 M HCl in dioxane (8 mL) and the reaction was stirred at rt for 1 h. The solvent was evaporated, then the residue was redissolved in dioxane (8 mL). Triphosgene (74 mg, 0.249 mmol, 0.5 equiv.) was added and the reaction was heated to 60 °C for 4 h before the mixture was concentrated *in vacuo.* The residue was dissolved in toluene (20 mL) before the addition of DABCO (168 mg, 1.50 mmol, 3.0 equiv.) followed by TCO-OH (**119**, 31 mg, 0.250 mmol, 0.5 equiv.). The reaction was stirred at 100 °C for 16 h then cooled to rt. Purification via flash column chromatography (40% EtOAc/Petrol) then flash column chromatography (3% MeOH/CH_2Cl_2) yielded **142** as a white solid (8 mg, 0.019 mmol, 8%).

R_f 0.40 (40% EtOAc/Petrol).

$T_{decomp.}$ 139.7 °C.

^{1}H NMR (500 MHz, $CDCl_3$) δ 7.63 (dd, *J* = 9.5, 0.6 Hz, 1H, H4'), 7.45 (d, *J* = 8.3 Hz, 2H, H2), 7.39 – 7.34 (m, 3H, H3, H5'), 6.92 – 6.86 (m, 2H, H6', H8'), 6.75 – 6.70 (m, 1H, N*H*), 6.25 (d, *J* = 9.5 Hz, 1H, H3'), 5.88 (ddd, *J* = 15.8, 11.0, 3.6 Hz, 1H, H3''), 5.58 (dd, *J* = 16.4, 2.5 Hz, 1H, H2''), 5.44 (s, 1H, H1''), 5.07 (d, *J* = 3.5 Hz, 2H, H5), 2.49 (dd, *J* = 10.5, 5.1 Hz, 1H, H4a''), 2.22 – 2.10 (m, 1H, H8a''), 2.09 – 1.95 (m, 2H, H4b'', H5a''), 1.94 – 1.83 (m, 1H, H6a''), 1.80 – 1.64 (m, 2H, H7a'', H8b''), 1.56 – 1.42 (m, 1H, H5b''), 1.17 – 1.03 (m, 1H, H7b''), 0.91 – 0.75 (m, 1H, H6b'').

^{13}C NMR (126 MHz, $CDCl_3$) δ 162.0 (C7'), 161.3 (C2'), 156.0 (C8a'), 152.8 (C6), 143.5 (C4'), 138.3 (C1), 132.3 (C3''), 131.0 (C2''), 130.6 (C3), 128.9 (C5'), 128.8 (C4), 118.8 (C2), 113.4 (C6'), 113.4 (C3'), 112.9 (C4a'), 102.1 (C8'), 74.7 (C1''), 70.3 (C5), 40.8 (C8''), 36.2 (C4''), 36.1 (C5''), 29.2 (C6''), 24.4 (C7'').

IR (thin film, ν_{max}/cm^{-1}) 2981w, 2924w, 2855w, 1723m, 1612m, 1528m, 1463w, 1350w, 1277m, 1227m, 1059m, 801m, 734m, 618s.

HRMS (ESI$^+$): *m/z* calc. for $C_{25}H_{25}NO_5Na$ $[M+Na]^+$ 442.1625, found 442.1613, Δ –2.6 ppm.

tert-butyl N-[4-(hydroxymethyl)phenyl]carbamate (143)

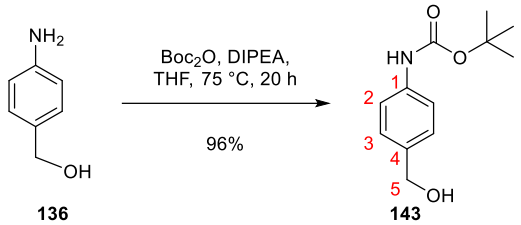

According to the procedure by Zhao *et al.,*[20] a solution of 4-aminobenzyl alcohol (**136**, 50 mg, 0.406 mmol, 1.0 equiv.), DIPEA (0.07 mL, 0.406 mmol, 1.0 equiv.) and Boc anhydride (89 mg, 0.408 mmol, 1.0 equiv.) in THF (4 mL) was heated to 75 °C for 20 h. The reaction was cooled to rt and the solvent was removed *in vacuo*. The residue was re-dissolved in EtOAc (10 mL), washed with HCl (0.1 M, 5 mL), dried over anhydrous $MgSO_4$ and concentrated *in vacuo*. Purification via flash column chromatography (50% EtOAc/Petrol) yielded **143** as white crystalline solid (87 mg, 0.390 mmol, 96%). The NMR data were in accordance with reported data.[20]

R_f 0.48 (50% EtOAc/Petrol).

$T_{decomp.}$ 81.6–82.4 °C.

^{1}H NMR (400 MHz, $CDCl_3$) δ 7.35 (d, *J* = 8.3 Hz, 2H, H2/3), 7.29 (d, *J* = 8.6 Hz, 2H, H2/3), 6.47 (s, 1H, N*H*), 4.63 (d, *J* = 5.2 Hz, 2H, H5), 1.52 (s, 7H, C(CH_3)$_3$).

tert-butyl N-[4-(bromomethyl)phenyl]carbamate (144)

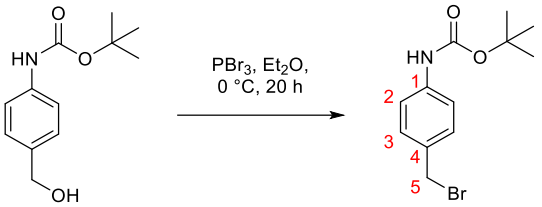

143 **144**

According to the procedure by Behnam *et al.*,[19] alcohol **143** (67 mg, 0.30 mmol, 1.0 equiv.) was dissolved in Et_2O (8 mL) and the solution was cooled to 0 °C. PBr_3 (1 M in CH_2Cl_2, 0.24 mL, 0.8 equiv.) was added dropwise and the reaction was stirred for 20 h at 0 °C. The reaction was poured into $NaHCO_{3\ (aq)}$ (sat. soln., 5 mL) and extracted with Et_2O (3 x 5 mL). The organic layers were washed with water (5 mL), dried over anhydrous Na_2SO_4 and concentrated *in vacuo*. This gave **144** as a white solid which was sufficiently pure by ^{1}H NMR to proceed to the next step. The NMR data were in accordance with reported data.[19]

R_f 0.85 (30% EtOAc/Petrol).

^{1}H NMR (400 MHz, $CDCl_3$) δ 7.33 (d, *J* = 2.2 Hz, 4H, H2, H3), 6.49 (s, 1H, N*H*), 4.48 (d, *J* = 1.9 Hz, 2H, H5), 1.52 (d, *J* = 1.9 Hz, 9H, C(CH_3)$_3$).

tert-butyl N-(4-{[(2'-oxochromen-7'-yl)oxy]methyl}phenyl)carbamate (145)

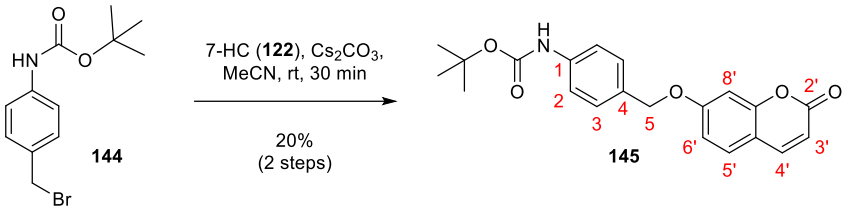

A solution of bromide **144** (0.30 mmol, 1.0 equiv., assuming quantitative yield) in MeCN (3 mL) was added to a solution of 7-hydroxycoumarin (**122**, 73 mg, 0.45 mmol, 1.5 equiv.) and caesium carbonate (195 mg, 0.60 mmol, 2.0 equiv.) in MeCN (5 mL). The reaction was stirred at rt for 30 min then the solvent was removed *in vacuo*. The residue was re-dissolved in CH_2Cl_2 (10 mL), washed with water (3 x 10 mL), dried over anhydrous $MgSO_4$ and concentrated *in vacuo*. Purification via flash column chromatography (30% EtOAc/Petrol) yielded **145** as a white solid (22 mg, 0.06 mmol, 20% over 2 steps).

R_f 0.28 (30% EtOAc/Petrol).

Mp 188 °C.

^{1}H NMR (500 MHz, $CDCl_3$) 7.63 (d, *J* = 9.5 Hz, 1H, H4'), 7.42 – 7.33 (m, 5H, H2, H3, H5'), 6.93 – 6.82 (m, 2H, H6', H8'), 6.50 (s, 1H, N*H*), 6.25 (d, *J* = 9.5 Hz, 1H, H3'), 5.07 (s, 2H, H5), 1.52 (s, 9H, C(CH_3)$_3$).

^{13}C NMR (126 MHz, $CDCl_3$) δ 161.9 (C7'), 161.2 (C2'), 155.8 (C8a'), 152.6 (*C*=O), 143.4 (C4'), 138.6 (C1), 130.1 (C4), 128.7 (C5'), 128.6 (C3), 118.6 (C2), 113.3 (C6'), 113.2 (C3'), 112.7 (C4a'), 101.9 (C8'), 80.8 (*C*(CH_3)$_3$), 70.2 (C5), 28.3 (C(CH_3)$_3$).

IR (thin film, ν_{max}/cm^{-1}) 3336m, 2987w, 1731m, 1699s, 1614s, 1598m, 1527s, 1453w, 1402m, 1385m, 1348m, 1315m, 1273m, 1228s, 1153s, 1002s, 815s.

HRMS (ESI$^+$): *m/z* calc. for $C_{21}H_{21}NO_5Na$ $[M+Na]^+$ 390.1312, found 390.1302, Δ −2.7 ppm.

tert-butyl N-{4''-[5-chloro-2-(2',4'-dichlorophenoxy)phenoxymethyl]phenyl}carbamate (150)

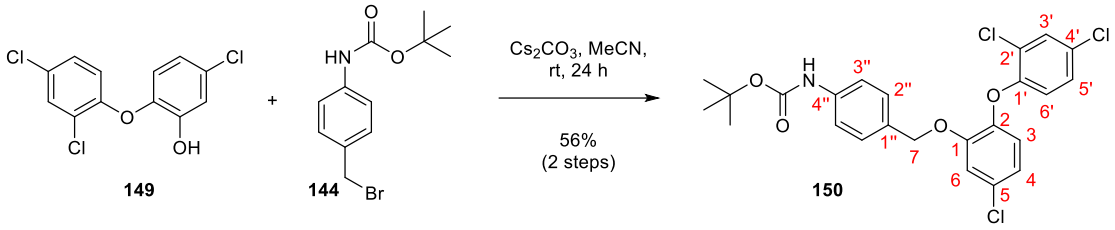

A solution of bromide **144** (0.560 mmol, 1.0 equiv., assuming quantitative yield) in MeCN (3 mL) was added to a solution of triclosan (**149**, 178 mg, 0.616 mmol, 1.1 equiv.) and caesium carbonate (365 mg, 1.12 mmol, 2.0 equiv.) in MeCN (2 mL). The reaction was stirred at rt for 24 h then the solvent was removed *in vacuo*. The residue was re-dissolved in CH_2Cl_2 (10 mL), washed with water (3 x 10 mL), dried over anhydrous $MgSO_4$ and concentrated *in vacuo*. Purification via flash column chromatography (10% EtOAc/Petrol) yielded **150** as a white solid (176 mg, 0.356 mmol, 63%).

R_f 0.18 (10% EtOAc/Petrol).

Mp 142–144 °C.

^{1}H NMR (400 MHz, $CDCl_3$) δ 7.40 (d, *J* = 2.5 Hz, 1H, H3'), 7.30 (d, *J* = 8.4 Hz, 2H, H3''), 7.11 (d, *J* = 8.5 Hz, 2H, H2''), 7.09 – 7.06 (m, 1H, H5'), 7.01 (d, *J* = 1.8 Hz, 1H, H6), 6.94 – 6.92 (m, 2H, H3, H4), 6.64 (d, *J* = 8.8 Hz, 1H, H6'), 6.51 (s, 1H, N*H*), 4.98 (s, 2H, H7), 1.52 (s, 9H, C(C*H*$_3$)$_3$).

^{13}C NMR (101 MHz, $CDCl_3$) δ 152.8 (*C*=O), 152.5 (C1'), 150.5 (C1), 143.6 (C2), 138.4 (C4''), 130.6 (C5), 130.4 (C4'), 130.3 (C3'), 128.2 (C2''), 128.1 (C1''), 127.7 (C5'), 124.7 (C2'), 122.2 (C3), 121.6 (C4), 118.5 (C3''), 118.2 (C6'), 115.9 (C6), 80.8 (*C*(CH$_3$)$_3$), 70.9 (C7), 28.5 (C(*C*H$_3$)$_3$).

IR (thin film, ν_{max}/cm^{-1}) 3360m, 1695s, 1599m, 1528s, 1498s, 1471s, 1406m, 1308m, 1366m, 1312m, 1270m, 1227s, 1163s, 1056s, 910m, 841s.

HRMS (ESI$^+$): *m/z* calc. for $C_{24}H_{22}NO_4{}^{35}Cl_3Na$ [M+Na]$^+$ 516.0507, found 516.0507, Δ 0.1 ppm.

(2'''*E*)-cyclooct-2'''-en-1-yl N-{4''-[5-chloro-2-(2,4'dichlorophenoxy)phenoxymethyl]phenyl} carbamate (153)

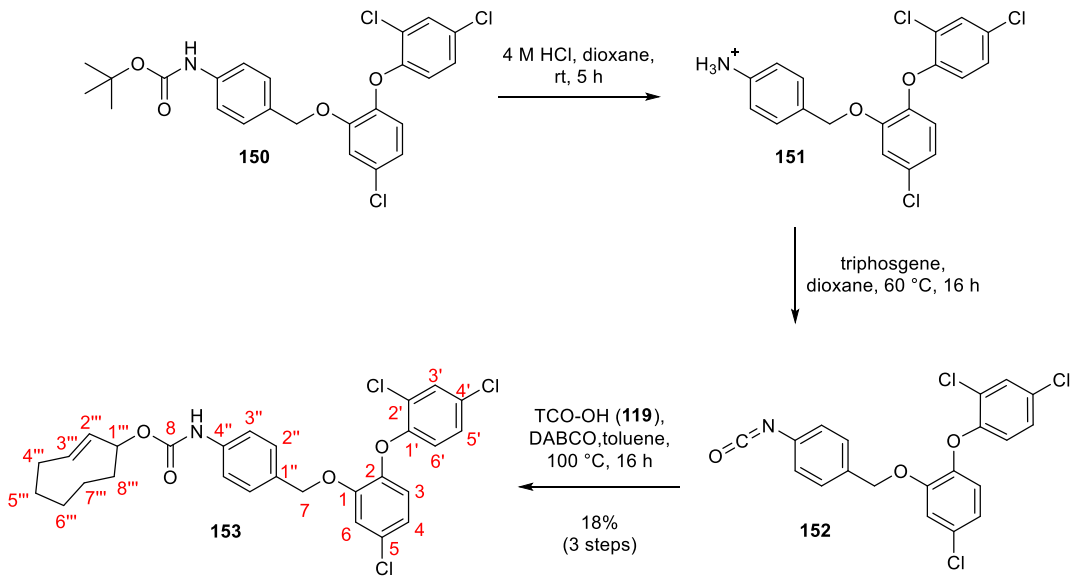

Boc protected aniline **150** (150 mg, 0.303 mmol, 1.0 equiv.) was dissolved in 4 M HCl in dioxane (5 mL) and the reaction was stirred at rt for 15 h. The solvent was evaporated then the residue was redissolved in dioxane (4 mL). Triphosgene (45 mg, 0.152 mmol, 0.5 equiv.) was added and the reaction was heated to 60 °C for 5 h. The mixture was concentrated *in vacuo.* The residue was dissolved in toluene (5 mL) then DABCO (102 mg, 0.909 mmol, 3.0 equiv.) was added followed by TCO-OH (**119**, 42 mg, 0.333 mmol, 1.1 equiv.) and the reaction was stirred at 100 °C for 19 h then cooled to rt. Purification via flash column chromatography (5% EtOAc/Petrol) then preparative TLC (70% CH_2Cl_2/petrol) yielded **153** as a white solid (9.7 mg, 0.0177 mmol, 18%).

R_f 0.45 (70% CH_2Cl_2/Petrol).

^{1}H NMR (400 MHz, $CDCl_3$) δ 7.41 (dd, *J* = 2.6, 0.6 Hz, 1H, H3'), 7.35 (d, *J* = 8.2 Hz, 2H, H3''), 7.12 (d, *J* = 8.4 Hz, 2H, H2''), 7.08 (ddd, *J* = 8.8, 2.5, 0.6 Hz, 1H, H5'), 7.01 (dd, *J* = 1.9, 0.9 Hz, 1H, H6), 6.94 (dd, *J* = 2.6, 0.7 Hz, 2H, H3, H4), 6.72 – 6.61 (m, 2H, H6', N*H*), 5.87 (ddd, *J* = 15.7, 11.0, 3.7 Hz, 1H, H3'''), 5.57 (dd, *J* = 16.4, 2.4 Hz, 1H, H2'''), 5.43 (s, 1H, H1'''), 4.99 (s, 2H, H7), 2.48 (td, *J* = 8.8, 7.3, 4.0 Hz, 1H, H4a'''), 2.19 – 2.10 (m, 1H, H8a'''), 2.07 – 1.94 (m, 2H, H4b''', H5a'''), 1.94 – 1.83 (m, 1H, H6a'''), 1.80 – 1.62 (m, 2H, H7a''', H8b'''), 1.48 (td, *J* = 12.6, 4.3 Hz, 1H, H5b'''), 1.17 – 1.04 (m, 1H, H7b'''), 0.91 – 0.76 (m, 1H, H6b''').

^{13}C NMR (101 MHz, $CDCl_3$) δ 152.6 (C8), 152.4 (C1'), 150.4 (C1), 143.5 (C2), 137.9 (C4''), 132.1 (C3'''), 130.9 (C2'''), 130.6 (C5), 130.4 (C4'), 130.2 (C3'), 128.1 (C2''), 128.0 (C1''), 127.6 (C5'), 124.6 (C2'), 122.0 (C3), 121.5 (C4), 118.5 (C3''), 118.0 (C6'), 115.8 (C6), 74.6 (C1'''), 70.8 (C7), 40.7 (C8'''), 36.0 (C4'''), 35.9 (C5'''), 29.1 (C6'''), 24.2 (C7''').

IR (thin film, ν_{max}/cm^{-1}) 2922m, 2853w, 1711m, 1599m, 1527m, 1494s, 1474s, 1407m, 1317m, 1227s, 1204m, 1075m.

HRMS (ESI): *m/z* calc. for $C_{28}H_{26}N_1O_4{}^{35}Cl_3Na$ $[M+Na]^+$ 568.0820, found 568.0810, Δ -1.7 ppm.

tert-butyl N-{4-[({19-ethyl-14,18-dioxo-17-oxa-3,13-diazapentacyclo [11.8.0.0^{2},^{11}.0^{4},^{9}.0^{15},^{20}] henicosa-1(21),2,4(9),5,7,10,15(20)-heptaen-19-yl} oxy)methyl]phenyl}carbamate (154)

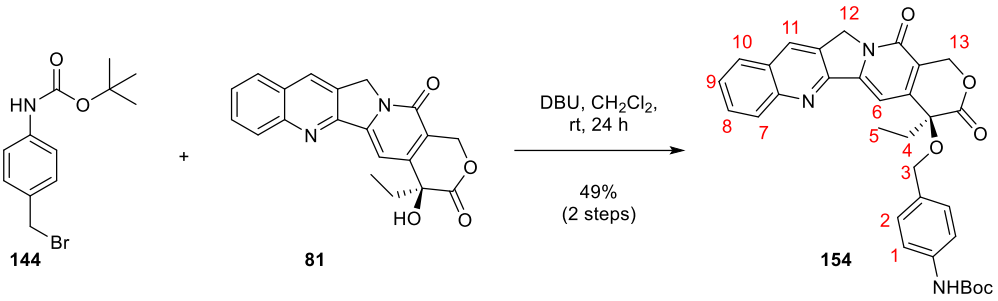

A solution of bromide **144** (0.403 mmol, 3.4 equiv., assuming quantitative yield) in CH_2Cl_2 (3 mL) was added to a solution of camptothecin (**81**, 41 mg, 0.118 mmol, 1 equiv.) and 1,8-diazabicyclo[5.4.0]undec-7-ene (DBU, 0.02 mL, 0.129 mmol, 1.1 equiv.) in CH_2Cl_2 (2 mL) at 0 °C. The reaction was stirred at 0 °C for 10 min and then rt for 24 h. The solvent was removed *in vacuo*. Purification of the dry residue directly via flash column chromatography (5–10% MeOH/CH_2Cl_2) yielded **154** as a white solid (32 mg, 0.058 mmol, 49%). The product decomposed after storage overnight at -20 °C, before full characterisation could be obtained.

R_f 0.15 (5% MeOH/CH_2Cl_2).

^{1}H NMR (400 MHz, $CDCl_3$) δ 8.41 (s, 1H, H11), 8.26 (d, *J* = 8.1 Hz, 1H, H7), 7.95 (d, *J* = 8.4 Hz, 1H, H10), 7.85 (s, 1H, H9), 7.69 (d, *J* = 8.7 Hz, 2H, H6, H8), 7.33 (d, *J* = 16.6 Hz, 4H, H1, H2), 6.48 (s, 1H, N*H*), 5.77 (d, *J* = 15.8 Hz, 1H, H13), 5.33 (d, *J* = 11.9 Hz, 3H, H12, H13), 4.65 (s, 2H, H3), 3.74 (s, 1H, O*H*), 1.97 (d, *J* = 43.5 Hz, 2H, H4), 1.27 (s, 8H, C(C*H*$_3$)$_3$), 1.07 (d, *J* = 7.5 Hz, 3H, H5).

4.3.2 Stability studies

TCO-carbonate (123) in 50% H_2O/DMSO: A solution of **123** (100 µM, 50% H_2O/DMSO) was added to a 96 well plate (Greiner, black, clear bottomed) in technical triplets. The fluorescence intensity was measured over 2 h at 37 °C, at the same time as measuring the fluorescence intensity of the reaction of **123** with tetrazine **58**. Readings were taken at 8 second intervals using a SpectraMax i3x plate reader (λ_{ex} = 325 nm, λ_{em} = 460 nm). This assay was performed 3 independent times. Data were processed using GraphPad Prism (GraphPad Software, La Jolla, CA, USA).

TCO-carbonate (123) in PBS, DMEM + 10% FBS and human plasma: 5 µL of **123** in DMSO (1 mM) was added to 95 µL PBS, DMEM + 10% FBS or 20% human plasma in PBS in a 96 well plate (Greiner, black, clear bottomed) in technical triplets. The fluorescence intensity was measured over 2 h at 37 °C. Readings were taken at 8 second intervals using a SpectraMax i3x plate reader (λ_{ex} = 325 nm, λ_{em} = 460 nm). This assay was performed 3 independent times. Data were processed and fitted to a one phase association using GraphPad Prism (GraphPad Software, La Jolla, CA, USA).

TCO-carbamate benzyl ether (142) in PBS, DMEM + 10% FBS and human plasma: 10 µL of **142** in DMSO (0.5 mM) was added to 90 µL PBS, DMEM + 10% FBS or 20% human plasma in H_2O or LB media in a 96 well plate (Greiner, black, clear bottomed) in technical triplets. The fluorescence intensity was measured over 15 h at 37 °C. Readings were taken at 30 second intervals using a SpectraMax i3x plate reader (λ_{ex} = 325 nm, λ_{em} = 460 nm). This assay was performed 3 independent times. Data were processed using GraphPad Prism (GraphPad Software, La Jolla, CA, USA).

Tetrazines 15, 58, 89, 90, 91, 155: 60 µL of tetrazines ***15, 58, 89, 90, 91, 155*** (2 mM, 50% DMSO/H_2O) was added to a 96 well plate (Greiner, black, clear bottomed) in technical triplicates and the absorbance was monitored over 24 h at 37 °C. For tetrazine **15**, which was not completely soluble at this concentration, the stock solution was centrifuged and the supernatant was used for the experiment. Readings were taken every minute using a SpectraMax i3x plate reader (λ_{max} = 530 nm). This assay was performed 3 independent times. Data were processed and fitted to a one phase decay using GraphPad Prism (GraphPad Software, La Jolla, CA, USA).

4.3.3 Decaging studies

Preparation and use of external NMR standard to determine accurate concentrations of stock solutions: A 100 mM solution of benzoic acid in DMSO was prepared in a volumetric flask. A sample of this solution was diluted in DMSO-D_6 to give a 10 mM solution which was then sealed inside a capillary tube. This external standard was then calibrated against stock solutions of 7-hydroxycoumarin at known concentrations (26.5–5.4 mM prepared by accurate dilution based on solvent weight). 7-hydroxycoumarin was chosen as the second reference compound as it contains peaks in the aromatic region of the ^{1}H NMR spectrum that do not overlap with the peaks from benzoic acid. Briefly, the coumarin sample and the capillary containing the external standard were placed in a medium-walled NMR tube (Wilmad, Precision, 400 MHz). The ^{1}H NMR spectra was recorded twice for each sample and the integration ratio of 7-hydroxycoumarin:benzoic acid was plotted against concentration.

The capillary was then added to NMR tubes containing stock solutions of compounds and the exact concentration of these stock solutions was determined by measuring the ratio of integration (compound:benzoic acid standard) and converting it to concentration using the fitting on the appropriate graph.

Decaging of 123 by monitoring the increase in fluorescence: Rate constants were determined under second order conditions. Stock solutions of **123** and **58** were prepared and the exact concentrations were determined by qNMR. Working solutions (200 µM in 50% H_2O/DMSO) were prepared by dilution. 40 µL these solutions were mixed together in a 96 well plate (Greiner, black, clear bottomed) in technical triplets to give a final reactant concentration of 100 µM. The fluorescence intensity was measured over 2 h at 37 °C with readings taken at 8 second intervals using a SpectraMax i3x plate reader (λ_{ex} = 325 nm, λ_{em} = 460 nm). An adhesive film (Bio-Rad) was used to prevent solvent evaporation. This assay was performed 3 independent times. Data were processed and fitted to a one phase association using GraphPad Prism (GraphPad Software, La Jolla, CA, USA).

Decaging of 142 by monitoring the increase in fluorescence: Rate constants were determined under second order conditions. Stock solutions of **142** and **90** were prepared and the exact concentrations were determined by qNMR. Working solutions (200 µM in 50% H_2O/DMSO) were prepared by dilution. 40 µL these solutions were mixed together in a 96 well plate (Greiner, black, clear bottomed) in technical triplets to give a final reactant concentration of 100 µM. The fluorescence intensity was measured over 5 h at 37 °C with readings taken at 8 second intervals using a SpectraMax i3x plate reader (λ_{ex} = 325 nm, λ_{em} = 460 nm). An adhesive film (Bio-Rad) was used to prevent solvent

evaporation. This assay was performed 3 independent times. Data were processed and fitted to a one phase association using GraphPad Prism (GraphPad Software, La Jolla, CA, USA).

Quenching effect of the reaction mixture on the coumarin fluorescence: TCO-coumarin (**142**) and tetrazine **90** were mixed to give a final concentration of 100 µM in 50% H_2O/DMSO for both reagents. The reaction was incubated at 37 °C for 6 h. At various timepoints (0.5, 1, 2, 4, 6 h) an aliquot was taken and added to a solution of 7-hydroxycoumarin (**122**) to give a final concentration of 50 µM in 50% H_2O/DMSO for 7-hydroxycoumarin (**122**), TCO-coumarin (**142**) and tetrazine **90**. The fluorescent intensity was measured and compared to that of a sample containing only coumarin **122** (50 µM, 50% H_2O/DMSO). Readings were taken using a SpectraMax i3x plate reader (λ_{ex} = 325 nm, λ_{em} = 460 nm) and the assay was performed 3 independent times. Data were processed using GraphPad Prism (GraphPad Software, La Jolla, CA, USA).

Yield of reaction of TCO-coumarin (142) with tetrazines 15, 58, 89, 91 by HPLC: TCO-coumarin (**142**), tetrazines ***15, 58, 89, 91*** and the internal standard benzoic acid were mixed to give final reactant concentrations of 0.83 mM (**142** and ***15, 58, 89, 91***) and 0.67 mM (benzoic acid standard) in 50% H_2O/DMSO. The sample mixtures were incubated at 37 °C and analysed after 24 h. The HPLC/UV analysis was performed on a Dionex UltiMate 3000 UHPLC+ system (Thermo Scientific) with a Phenomenex Kinetex C18 Column (100 Å 5 µm, 50 mm x 4.6 mm). The mobile phase consisted of A: H_2O with 0.1% formic acid, and B: MeCN with 0.1% formic acid. The samples were eluted with a linear gradient (1–10 min 0–50% B, and 10–14 min 50–100% B, 0.50 mL/min) and detected at 220 nm.

Yield of reaction of TCO-coumarin (142) with tetrazine 90 by HPLC: TCO-coumarin (**142**), tetrazine **90** and the internal standard benzoic acid were mixed to give final reactant concentrations of 0.83 mM (**142** and **90**) and 0.67 mM (benzoic acid standard) in the appropriate solvent system. The conditions pH 9, 7.4, 6, 5.6, 4 refer to 50% DMSO/corresponding buffer (NaPi pH 9, PBS pH 7.4, NaPi pH 6, acetate pH 5.6, acetate pH 4). A minimum of 50% DMSO was required for solubility of the reactants. The sample mixtures were incubated at 37 °C and analysed after 24 h. The HPLC/UV analysis was performed on a Dionex UltiMate 3000 UHPLC+ system (Thermo Scientific) with a Phenomenex Kinetex C18 Column (100 Å 5 µm, 50 mm x 4.6 mm). The mobile phase consisted of A: H_2O with 0.1% formic acid, and B: MeCN with 0.1% formic acid. The samples were eluted with a linear gradient (1–5 min 0–50% B and 5–8 min 50–100% B, 0.80 mL/min) and detected at 220 nm.

Yield of reaction of TCO-coumarin (142) with tetrazine 155 by HPLC: TCO-coumarin (**142**), tetrazine **155** and the internal standard benzoic acid were mixed to give final reactant concentrations of 0.83 mM (**142** and **155**) and 0.67 mM (benzoic acid standard) in 50% H_2O/DMSO. The sample mixtures

were incubated at 37 °C and analysed after 24 h. The HPLC/UV analysis was performed on a Dionex UltiMate 3000 UHPLC+ system (Thermo Scientific) with a Phenomenex Kinetex C18 Column (100 Å 5 µm, 50 mm x 4.6 mm). The mobile phase consisted of A: H_2O with 0.1% formic acid, and B: MeCN with 0.1% formic acid. The samples were eluted with a linear gradient (1–5 min 0–100% B, 0.80 mL/min) and detected at 220 nm.

Following reaction of TCO-coumarin (142) with tetrazine 90 by HPLC/FLD: TCO-coumarin (**142**) in DMSO (23 µL, 11.4 mM), tetrazine **90** in DMSO (23 µL, 11.4 mM) and the internal standard benzoic acid in MeCN (80 µL, 2 mM) were mixed to give final reactant concentrations of 0.83 mM (**142** and **90**) and 0.67 mM (benzoic acid standard). The reaction mixture was incubated at 37 °C and an aliquot was taken for analysis at 5 min, 1, 2, 3, 4 and 24 h. The HPLC/UV-FLD analysis was performed on a Dionex UltiMate 3000 UHPLC+ system (Thermo Scientific) coupled to a Dionex UltiMate 3000 fluorescence detector with a Phenomenex Kinetex C18 Column (100 Å 5 µm, 50 mm x 4.6 mm). The mobile phase consisted of A: H_2O with 0.1% formic acid, and B: MeCN with 0.1% formic acid. The samples were eluted with a linear gradient (1–5 min 0–50% B and 5–8 min 50–100% B, 0.80 mL/min) and detected at λ_{ex} = 325 nm, λ_{em} = 460 nm.

Second order rate constant of reaction of TCO-coumarin (142) with tetrazine 90: The second order rate constant was determined under second order conditions using stopped-flow spectrometry. Stock solutions of **142** and **90** were prepared and the exact concentrations were determined by qNMR. Working solutions (1 mM in DMSO) were prepared by dilution. The rate was calculated in 100% DMSO due to the poor solubility of **142** at this concentration. Both reactant solutions were injected simultaneously in a 1:1 ratio into the reaction vessel to give a final concentration of 0.5 mM. The decrease in absorbance at 530 nm was monitored for 6 minutes at 25 °C. A calibration curve was prepared for concentrations of tetrazine **90** of 0.15–1 mM and the absorbance values were converted into concentrations. The curve of concentration *vs* time was fitted to a two phase exponential decay using GraphPad Prism (GraphPad Software, La Jolla, CA, USA). This experiment was performed 3 independent times.

Decaging yield of TCO-triclosan (153) by HPLC: TCO-triclosan (**153**), tetrazine **90** and the internal standard benzoic acid were mixed to give final reactant concentrations of 0.83 mM (**153** and **90**) and 0.67 mM (benzoic acid standard) in 20% DMSO/MeCN. The reaction mixture was incubated at 37 °C and an aliquot was taken for analysis at 0.5, 1, 2, 4 and 24 h. The HPLC/UV analysis was performed on a Dionex UltiMate 3000 UHPLC+ system (Thermo Scientific) with a Phenomenex Kinetex C18 Column (100 Å 5 µm, 50 mm x 4.6 mm). The mobile phase consisted of A: H_2O with 0.1% formic acid, and B:

MeCN with 0.1% formic acid. The samples were eluted with a linear gradient (1–26 min 0–50% B, 26–29 min 50–70% B and 29–32 min 70–100% B, 0.80 mL/min) and detected at 220 nm.

Decaging of 153 by LC-MS: TCO-triclosan (**153**) and tetrazine **90** were mixed to give final reactant concentrations of 0.83 mM in 20% DMSO/MeCN. The reaction mixture was incubated at 37 °C and analysed after 24 h. The LC-MS analysis was performed on a Waters SQ Detector 2 with a Waters Acquity UPLC H-Class system and a Waters Acquity UPLC BEH C18 column (1.7µm, 2.1 x 50 mm). The mobile phase consisted of A: H_2O with 0.1% formic acid, and B: MeCN with 0.1% formic acid. The samples were eluted with a linear gradient (0–20 min 0–100% B, 0.20 mL/min).

4.3.4 Live cell studies

Cell Culture: *E. Coli* BL21(DE3) cells (ThermoFisher Scientific, USA) were cultured in Luria Bertani (LB) broth (MP Biomedicals). Overnight cultures were prepared by inoculating 20 mL of LB broth and incubating at 37 °C, shaken at 180 rpm.

Cytotoxicity in E. Coli BL21(DE3) cells: Cytotoxicity of triclosan (**149**), TCO-triclosan (**153**), tetrazine **90**, TCO-triclosan (**153**) + **90** was assessed using a CellTiter-Blue Cell Viability Assay (ThermoFisher Scientific, USA). Overnight cultures were diluted and added to flat-bottom 96-well plates to give a density of 0.002 OD_{600} units (200 µL). Compounds (dissolved in DMSO) were added to wells in 6 replicates to give final concentrations of 0.05 µM, 0.1 µM, 0.2 µM, 0.4 µM, 0.6 µM, 1.0 µM for **149** and **153** and 0.5 µM, 1 µM, 2 µM, 4 µM, 6 µM, 10 µM for tetrazine **90**. Final concentration of DMSO in each well was ≤ 1%. The plates were incubated at 37 °C for 12 h. 100 µL from each well was transferred to a new plate, for use in the cell density assay. Cell viability was assessed by the addition of 20 µL CellTiter-Blue Reagent to the remaining 100 µL in the initial plate. After incubation for a further 2 h without shaking, the fluorescence was measured on a SpectraMax i3x plate reader (λ_{ex} = 570 nm, λ_{em} = 590 nm). Statistical analysis was performed on GraphPad Prism using a one-way ANOVA.

Cell density assay in E. Coli BL21(DE3) cells: Cytotoxicity of triclosan (**149**), TCO-triclosan (**153**), tetrazine **90**, TCO-triclosan (**153**) + **90** was assessed by measuring the OD_{600}. Overnight cultures were diluted and added to flat-bottom 96-well plates to give a density of 0.002 OD_{600} units (200 µL). Compounds (dissolved in DMSO) were added to wells in 6 replicates to give a final concentration of 1 µM for **149** and **153** and 10 µM for tetrazine **90**. Final concentration of DMSO in each well was ≤ 1%. The plates were incubated at 37 °C for 12 h. 100 µL from each well was transferred to a new plate and the absorbance was measured on a SpectraMax i3x plate reader (λ = 600 nm). Statistical analysis was performed on GraphPad Prism using a one-way ANOVA.

4.4 References for Chapter 4

[1] A. B. Pangborn, M. A. Giardello, R. H. Grubbs, R. K. Rosen, F. J. Timmers, *Organometallics* **1996**, *15*, 1518–1520.

[2] X. Fan, Y. Ge, F. Lin, Y. Yang, G. Zhang, W. S. C. Ngai, Z. Lin, S. Zheng, J. Wang, J. Zhao, *et al.*, *Angew. Chem. Int. Ed.* **2016**, *55*, 14046–14050.

[3] J. Krejzová, P. Šimon, E. Vavříková, K. Slámová, H. Pelantová, S. Riva, V. Spiwok, V. Křen, *J. Mol. Catal. B Enzym.* **2013**, *87*, 128–134.

[4] T. Ohishi, L. Zhang, M. Nishiura, Z. Hou, *Angew. Chem. Int. Ed.* **2011**, *50*, 8114–8117.

[5] E. Jiménez-Moreno, Z. Guo, B. L. Oliveira, *et. al.*, *Angew. Chem. Int. Ed.* **2017**, *56*, 243–247.

[6] L. C. C. Vieira, M. W. Paixão, A. G. Corrêa, *Tetrahedron Lett.* **2012**, *53*, 2715–2718.

[7] W. Zhang, Z. Ma, W. Li, G. Li, L. Chen, Z. Liu, L. Du, M. Li, *ACS Med. Chem. Lett.* **2015**, *6*, 502–506.

[8] N. Becker, E. M. Carreira, *Org. Lett.* **2007**, *9*, 3857–3858.

[9] D. J. Mack, B. Guo, J. T. Njardarson, *Chem. Commun.* **2012**, *48*, 7844–7846.

[10] D. C. Schlegel, B. L. Zenitz, C. A. Fellows, S. C. Laskowski, D. C. Behn, D. K. Phillips, I. Botton, P. T. Speight, *J. Med. Chem.* **1984**, *27*, 1682–1690.

[11] S. Davies, L. Qiao, B. L. Oliveira, C. D. Navo, G. Jiménez-Osés, G. J. L. Bernardes, *ChemBioChem* **2019**, *20*, 1541–1546.

[12] E. Lemke, C. Schultz, T. Plass, I. Nikic, J.-E. Hoffmann, I. V. Aramburu, *Multiple Cycloaddition Reactions for Labeling of Molecules*, **2015**, US2016/0340297 A1.

[13] A. Renslo, E. Lauterwasser, S. Fontaine, B. Spangler, J. Wells, *Cyclic Peroxides as Prodrugs for Selective Delivery of Agents*, **2015**, WO2015/123595 A1.

[14] R. M. Versteegen, W. ten Hoeve, R. Rossin, M. A. de Geus, H. M. Janssen, M. S. Robillard, *Angew. Chem. Int. Ed.* **2018**, *57*, 10494–10499.

[15] K. M. Haynes, N. Abdali, V. Jhawar, H. I. Zgurskaya, J. M. Parks, A. T. Green, J. Baudry, V. V. Rybenkov, J. C. Smith, J. K. Walker, *J. Med. Chem.* **2017**, *60*, 6205–6219.

[16] Y. Shimizu, M. Noshita, Y. Mukai, H. Morimoto, T. Ohshima, *Chem. Commun.* **2014**, *50*, 12623–12625.

[17] A. El Alaoui, F. Schmidt, C. Monneret, J. C. Florent, *J. Org. Chem.* **2006**, *71*, 9628–9636.

[18] M. P. Hay, W. R. Wilson, W. A. Denny, *Bioorg. Med. Chem.* **2005**, *13*, 4043–4055.

[19] M. A. M. Behnam, D. Graf, R. Bartenschlager, D. P. Zlotos, C. D. Klein, *J. Med. Chem.* **2015**, *58*, 9354–9370.

[20] H. Zhao, P. Reddy, M. B. Rubio, *Targeted Polymeric Prodrugs Containing Multifunctional Linkers*, **2009**, US8367065B2.

Appendix (NMR spectra)

^{1}H NMR (400 MHz, $CDCl_3$) of 3-Methyl-6-(pyrimidin-2'-yl)-1,2,4,5-tetrazine (**58**)

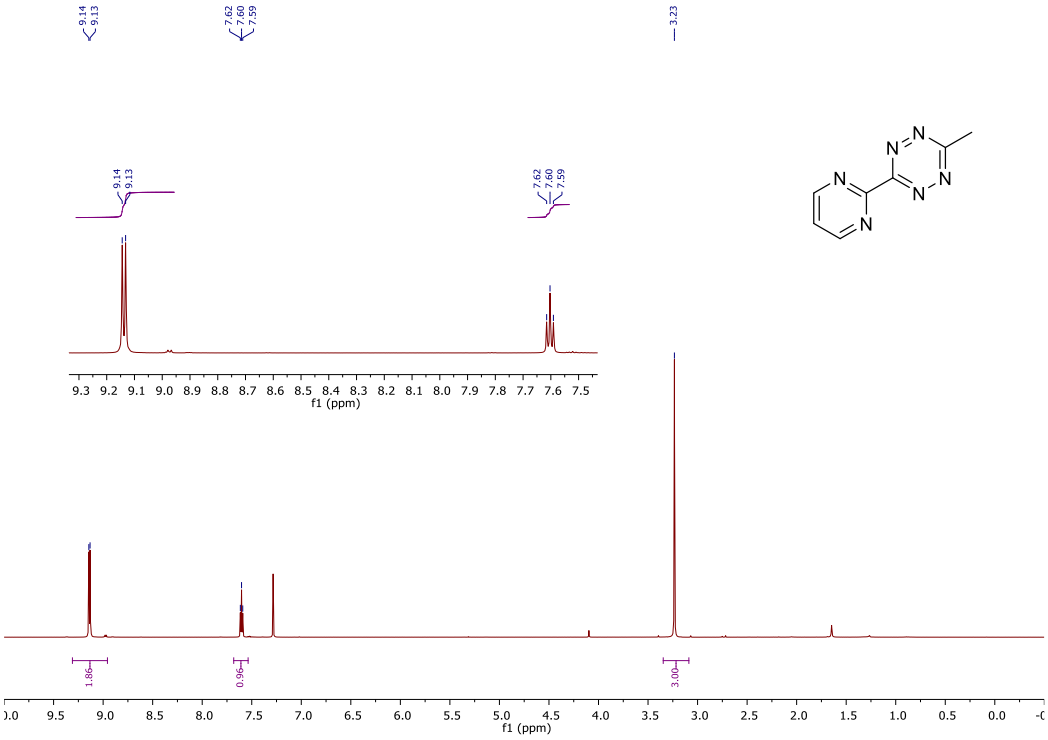

^{13}C NMR (101 MHz, $CDCl_3$) of 3-Methyl-6-(pyrimidin-2'-yl)-1,2,4,5-tetrazine (**58**)

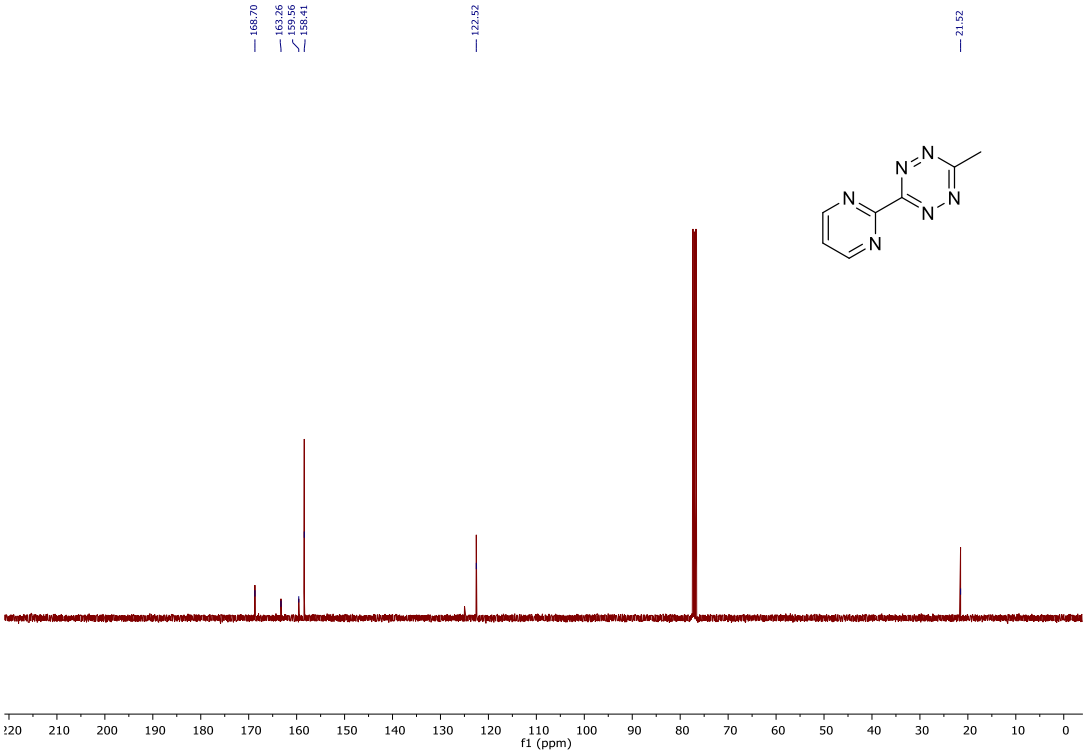

^{1}H NMR (400 MHz, $CDCl_3$) of 3-phenylpropionic acid (**86**)

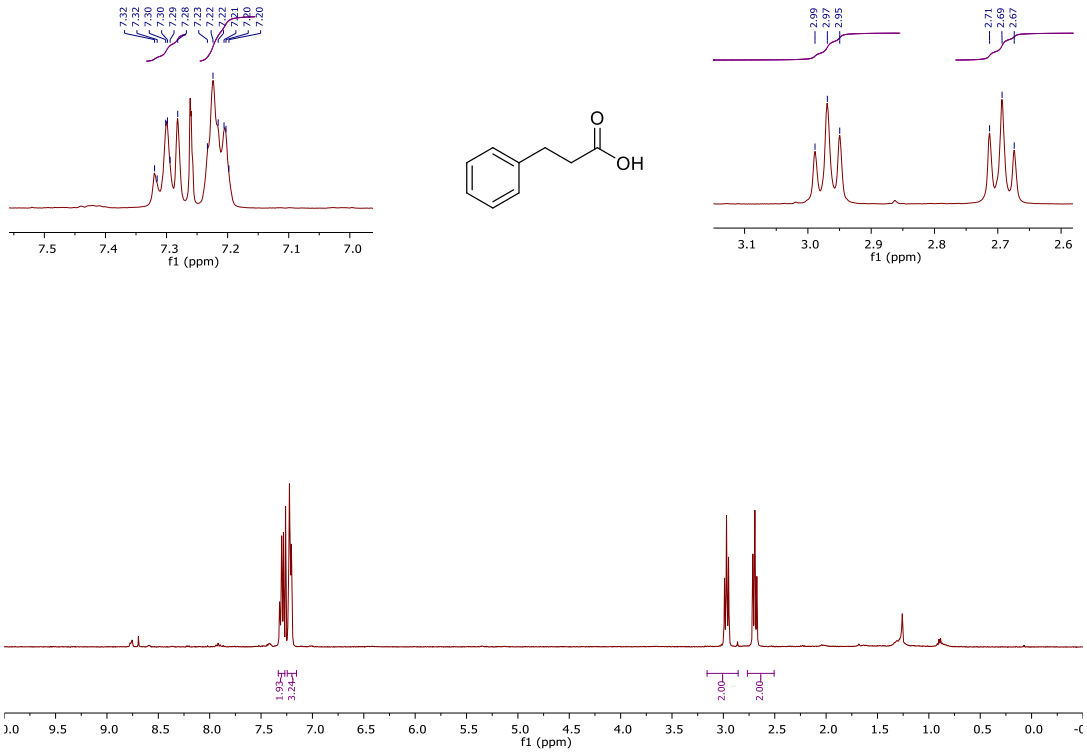

^{1}H NMR (400 MHz, $CDCl_3$) of Ethenyl 3-phenylpropanoate (**87**)

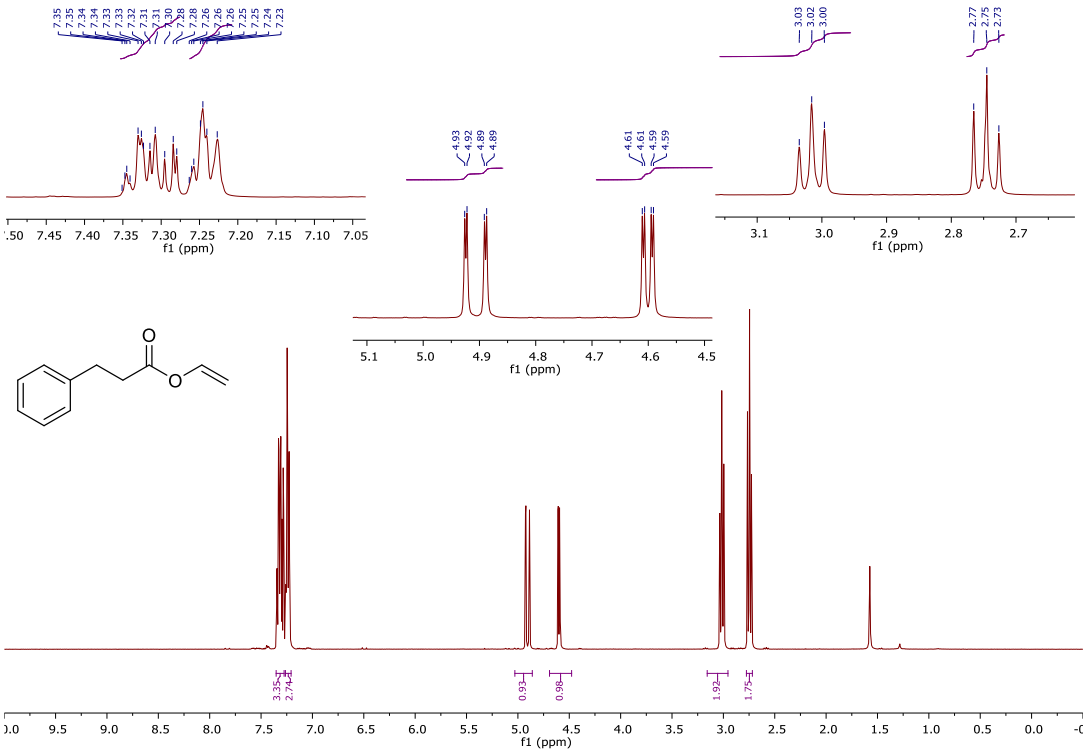

^{13}C NMR (101 MHz, $CDCl_3$) of Ethenyl 3-phenylpropanoate (**87**)

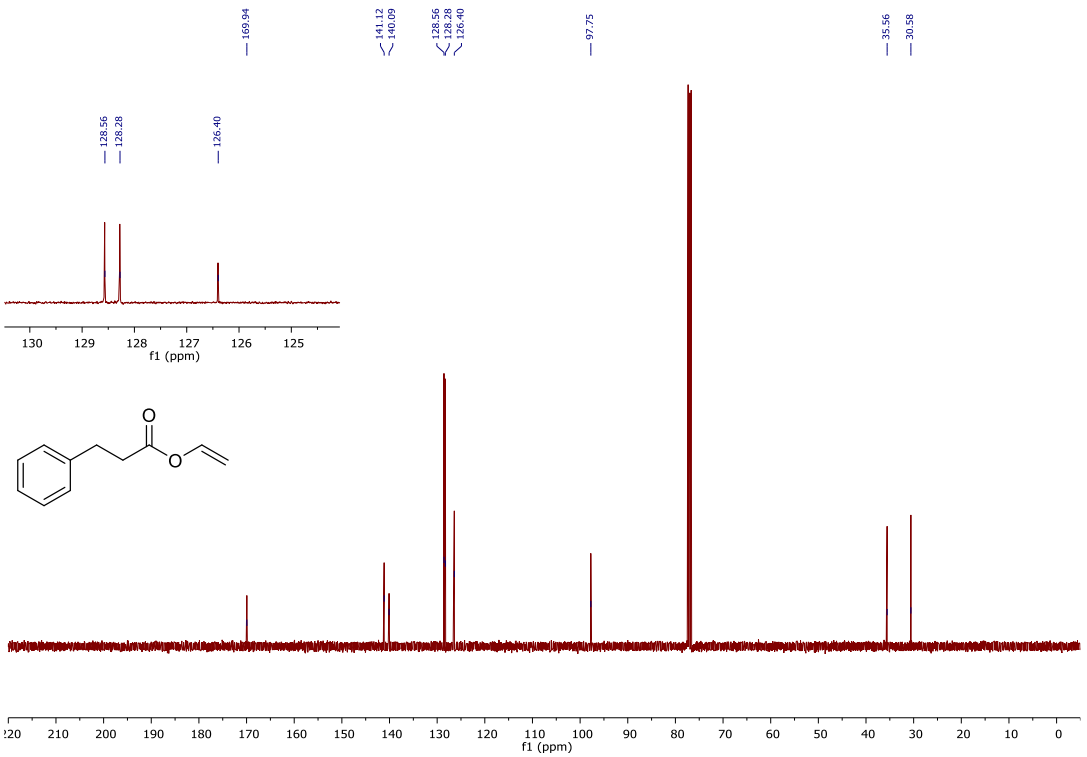

^{1}H NMR (400 MHz, $CDCl_3$) of 3,6-Bis(pyridin-2'-yl)pyridazine (**88**)

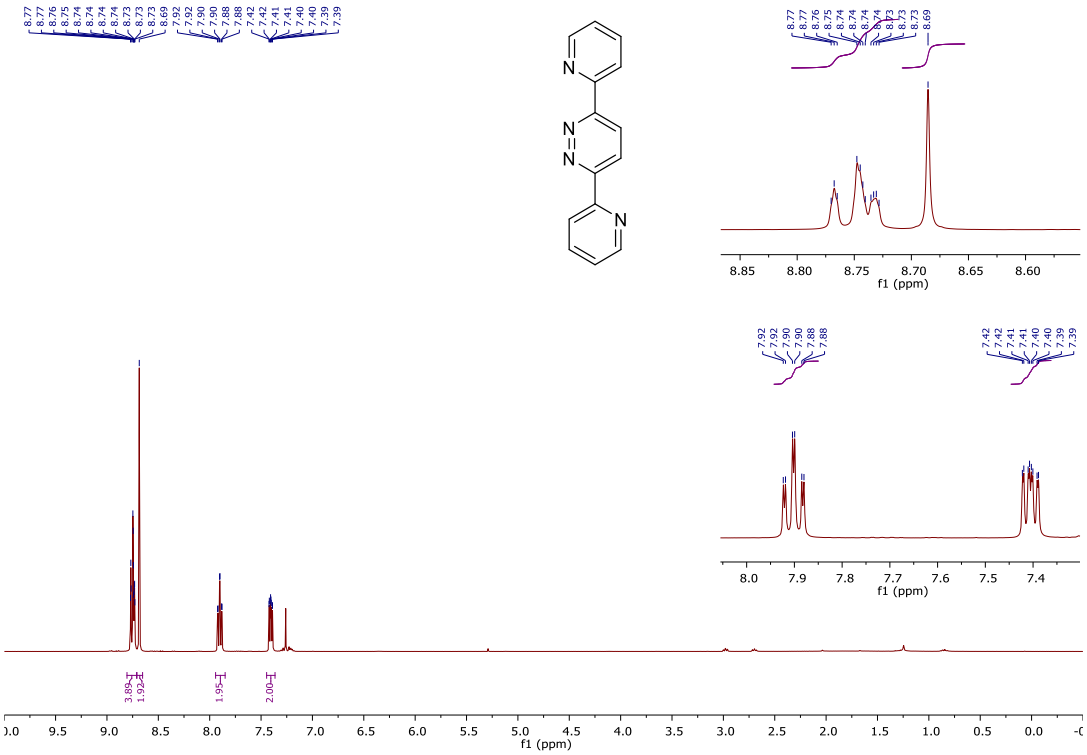

^{13}C NMR (101 MHz, $CDCl_3$) of 3,6-Bis(pyridin-2'-yl)pyridazine (**88**)

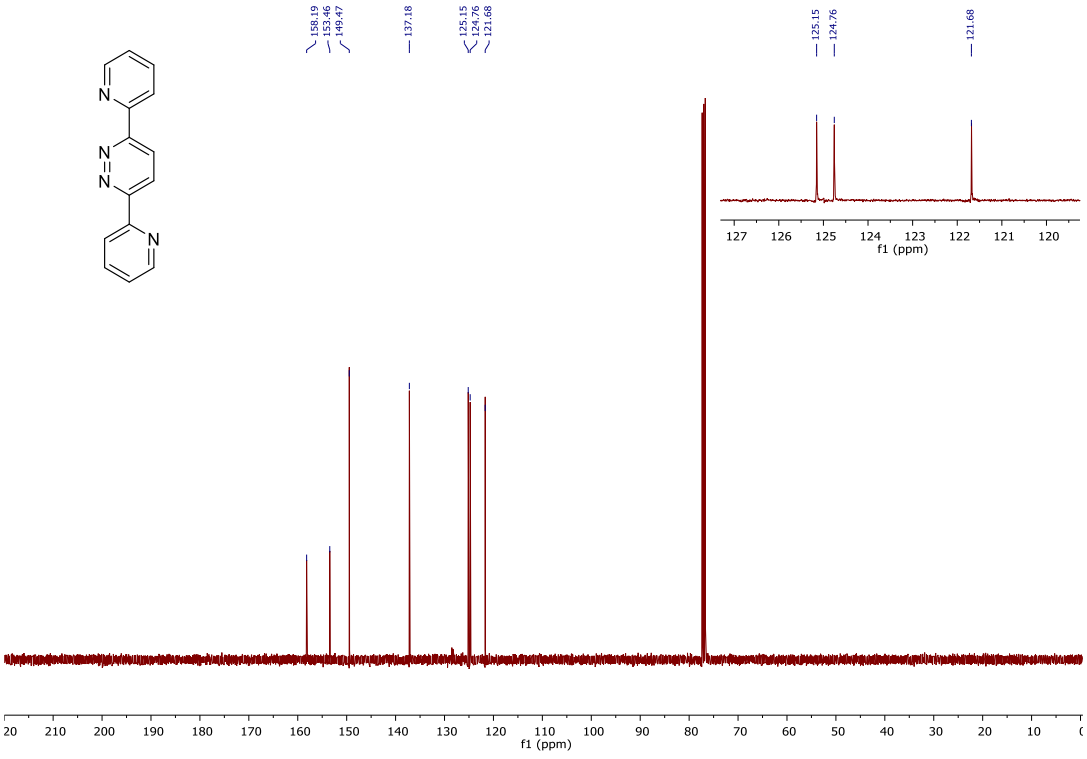

^{1}H NMR (400 MHz, $CDCl_3$) of 3-Methyl-6-(pyridin-2'-yl)-1,2,4,5-tetrazine (**89**)

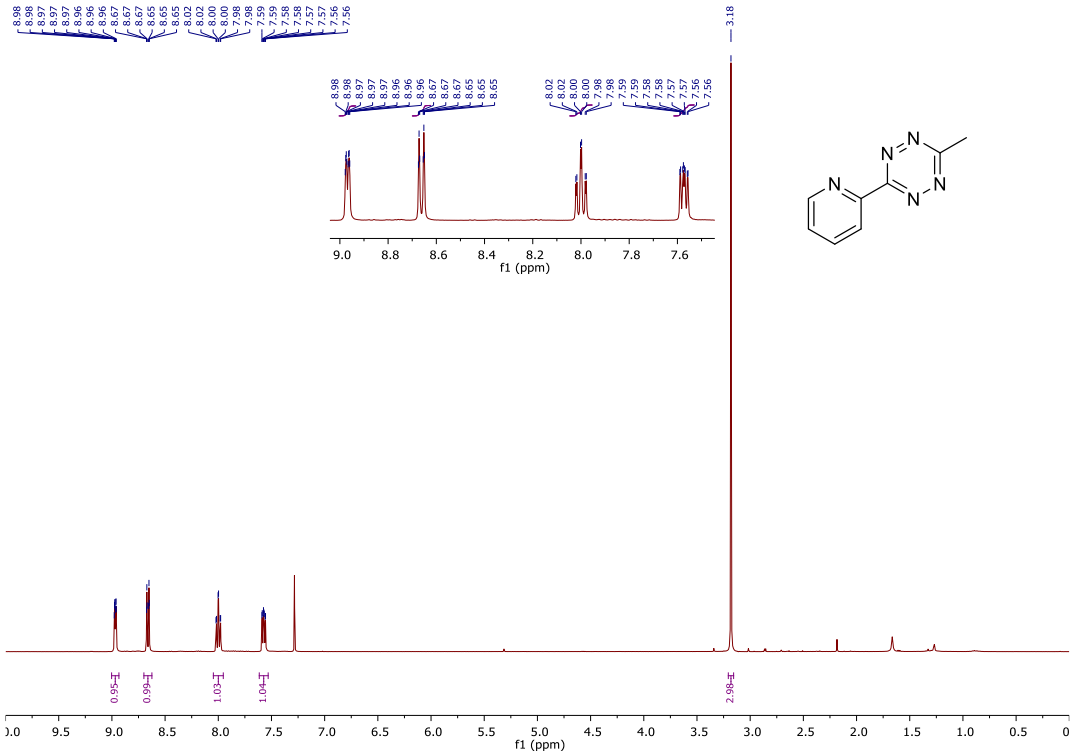

^{13}C NMR (101 MHz, $CDCl_3$) of 3-Methyl-6-(pyridin-2'-yl)-1,2,4,5-tetrazine (**89**)

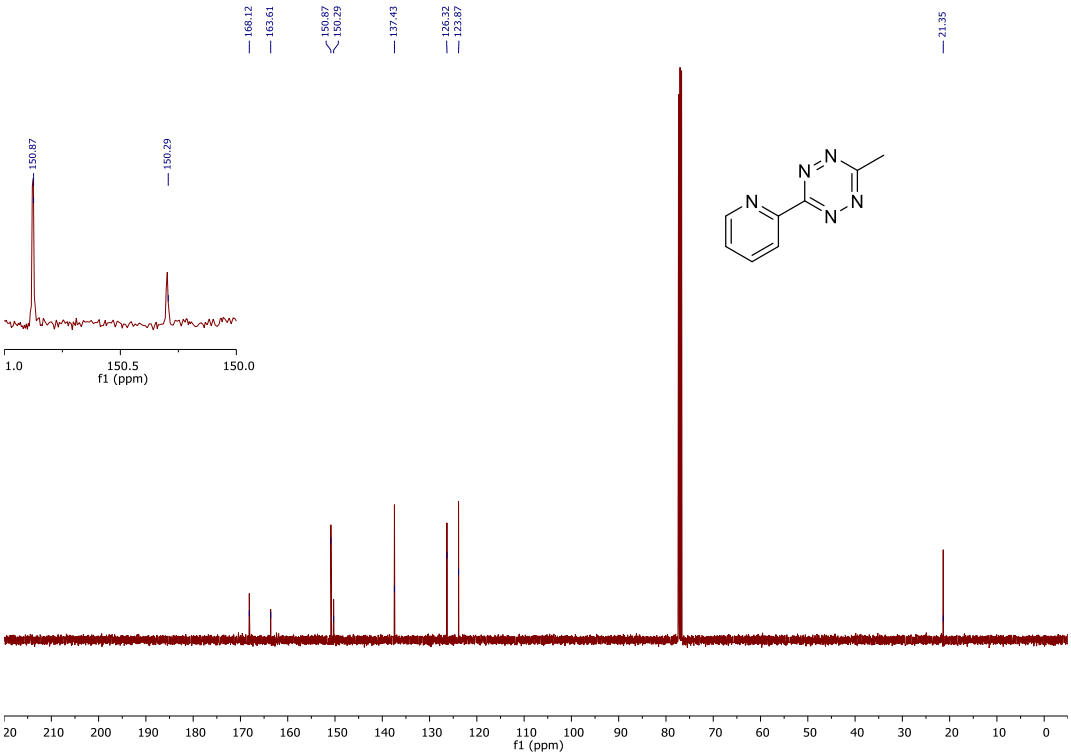

^{1}H NMR (400 MHz, $CDCl_3$) of Ethenyl 2-oxochromene-3-carboxylate (**96**)

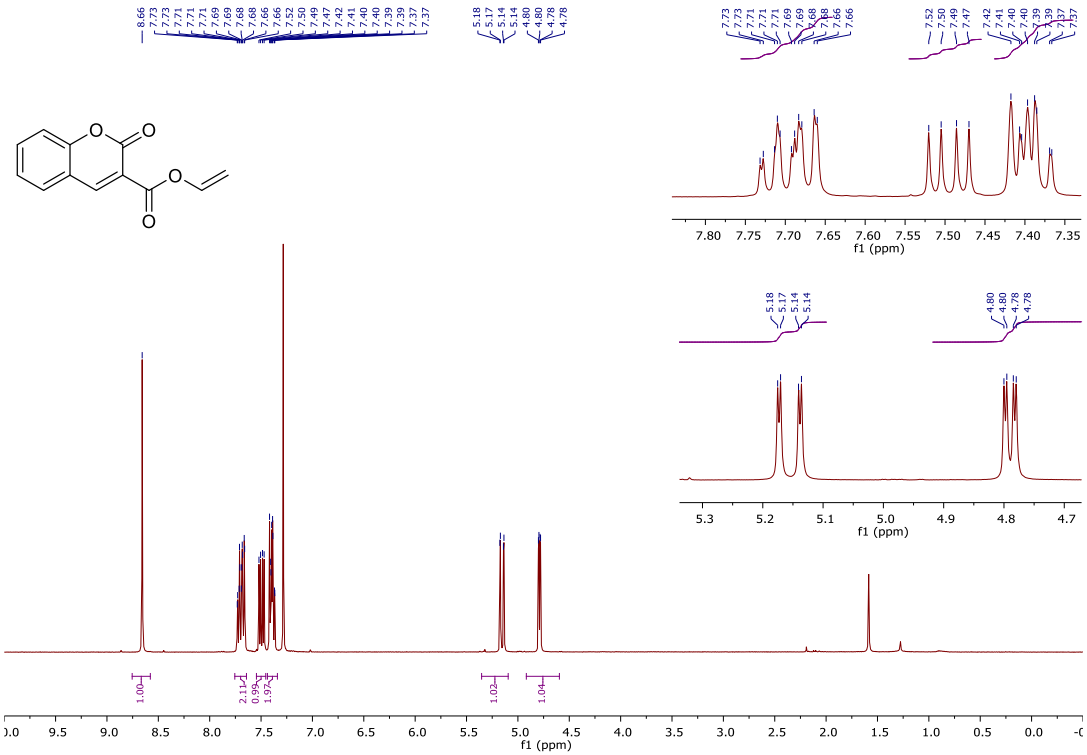

^{13}C NMR (101 MHz, $CDCl_3$) of Ethenyl 2-oxochromene-3-carboxylate (**96**)

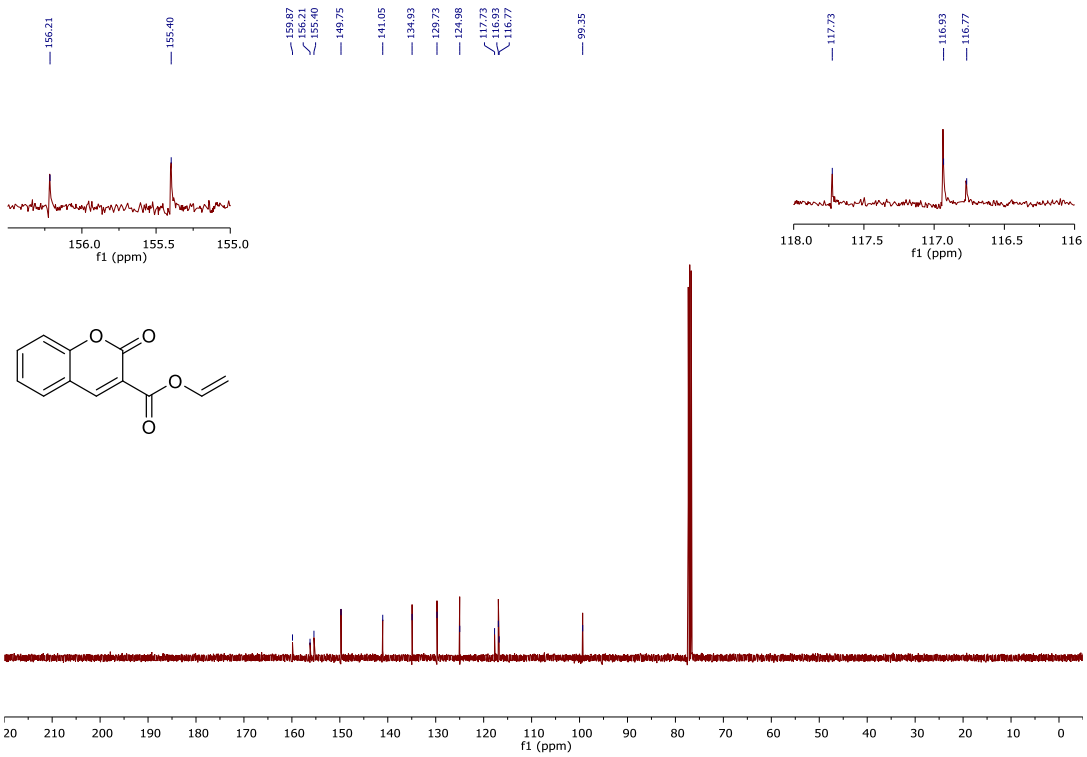

^{1}H NMR (400 MHz, DMSO-D_6) of Ethyl 7-hydroxy-2-oxochromene-3-carboxylate (**99**)

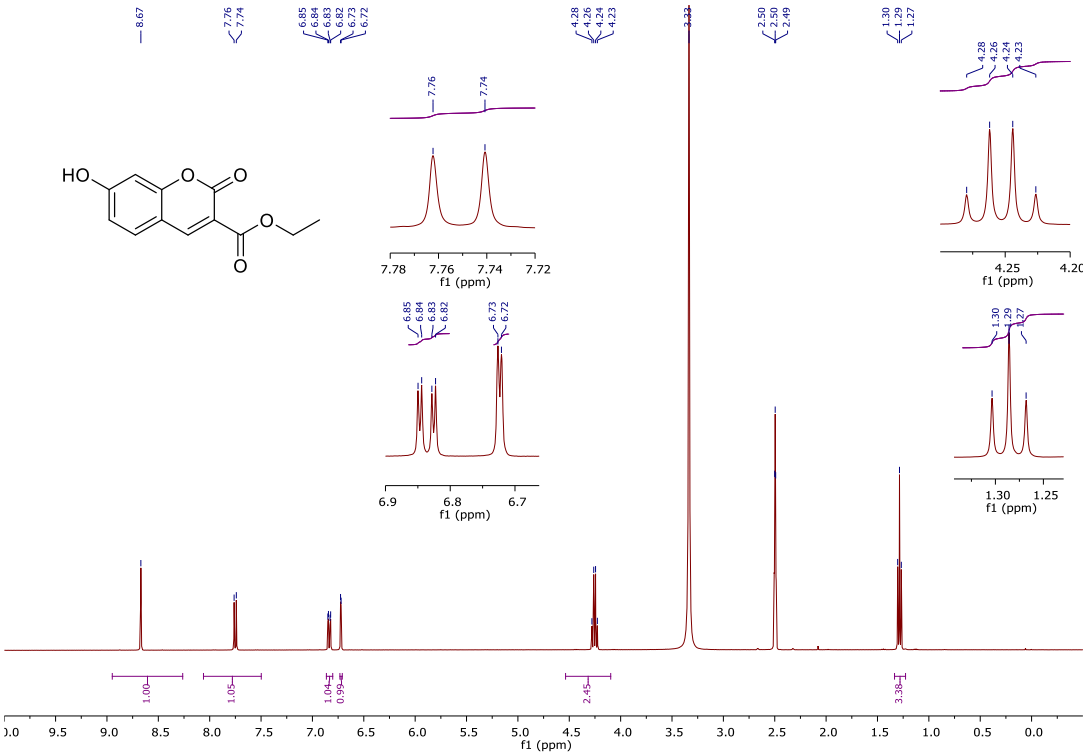

^{13}C NMR (101 MHz, DMSO-D_6) of Ethyl 7-hydroxy-2-oxochromene-3-carboxylate (**99**)

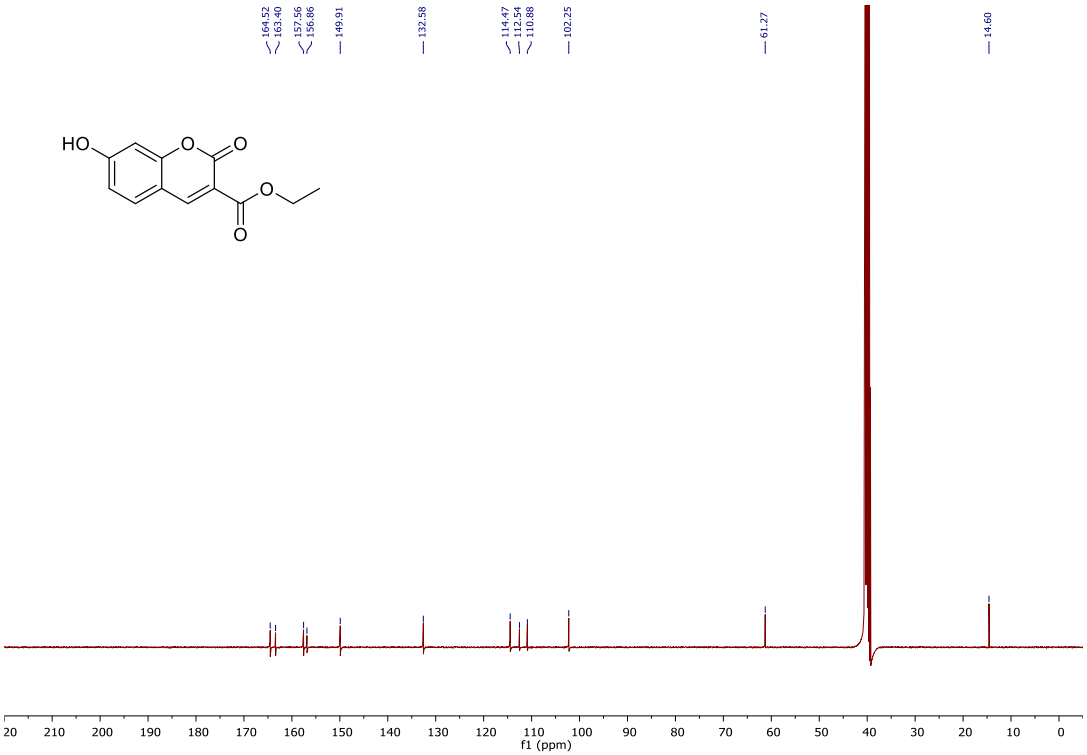

^{1}H NMR (400 MHz, DMSO-D_6) of 7-Hydroxy-2-oxochromene-3-carboxylic acid (**100**)

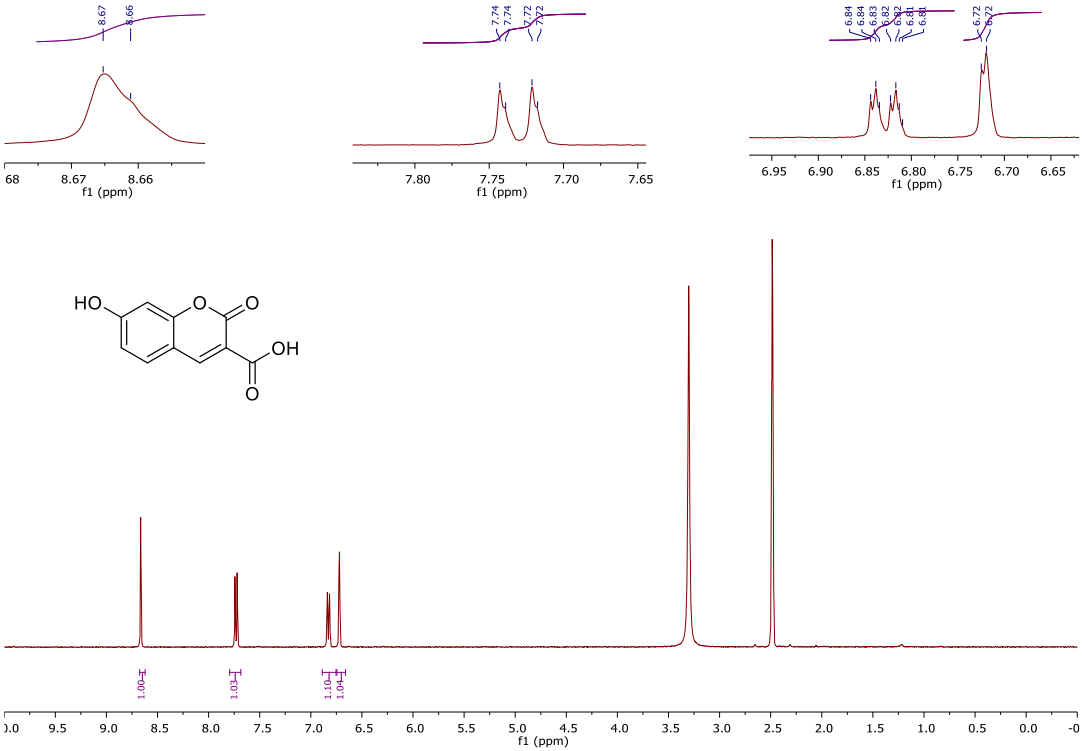

^{1}H NMR (400 MHz, DMSO-D_6) of Ethenyl 7-(ethenyloxy)-2-oxochromene-3-carboxylate (**101**)

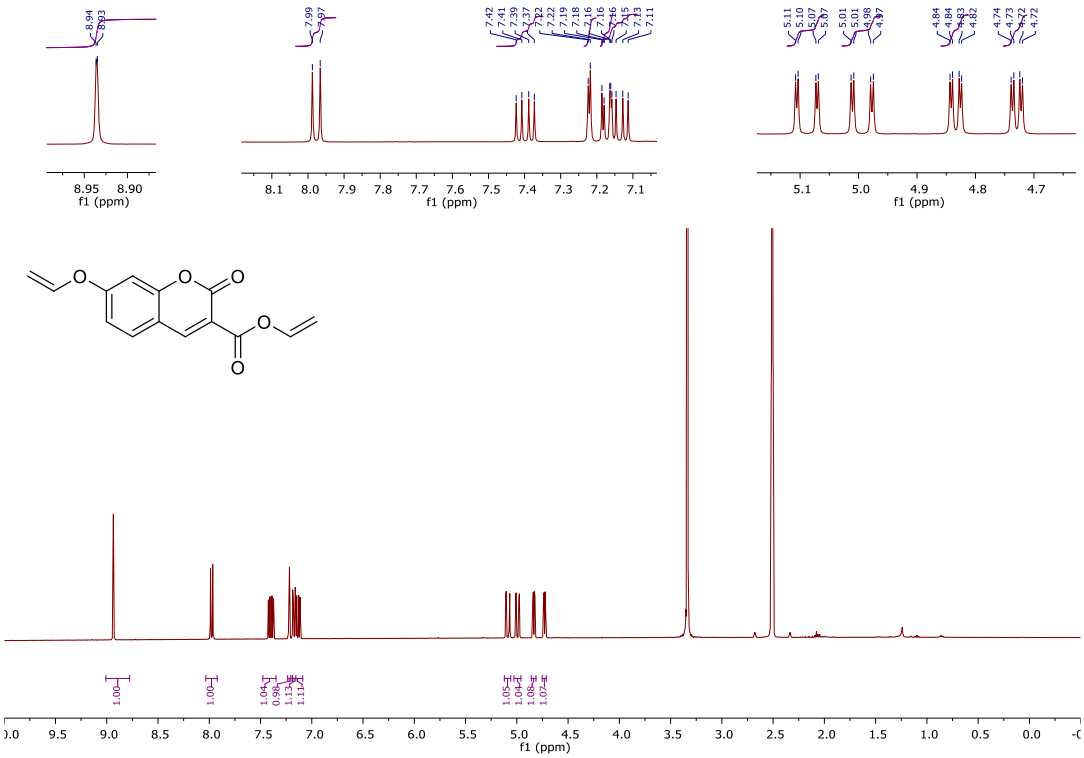

^{13}C NMR (101 MHz, DMSO-D_6) of Ethenyl 7-(ethenyloxy)-2-oxochromene-3-carboxylate (**101**)

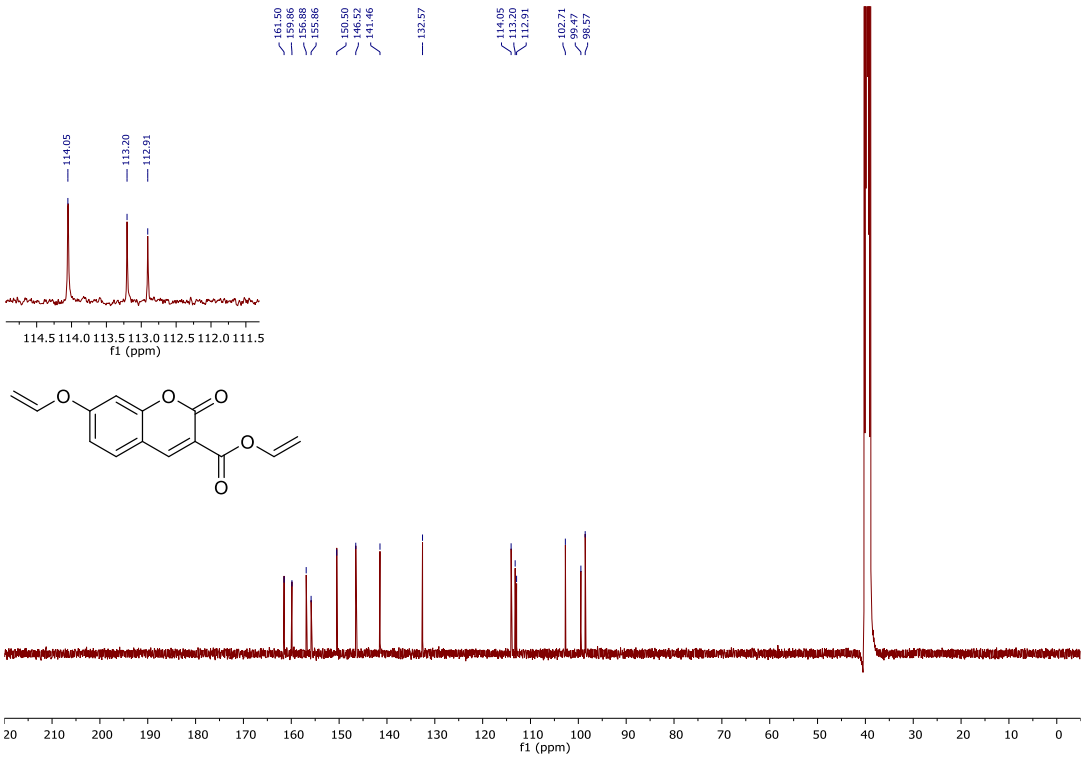

^{1}H NMR (500 MHz, Methanol-d_4) of Ethenyl 7-hydroxy-2-oxochromene-3-carboxylate (**102**)

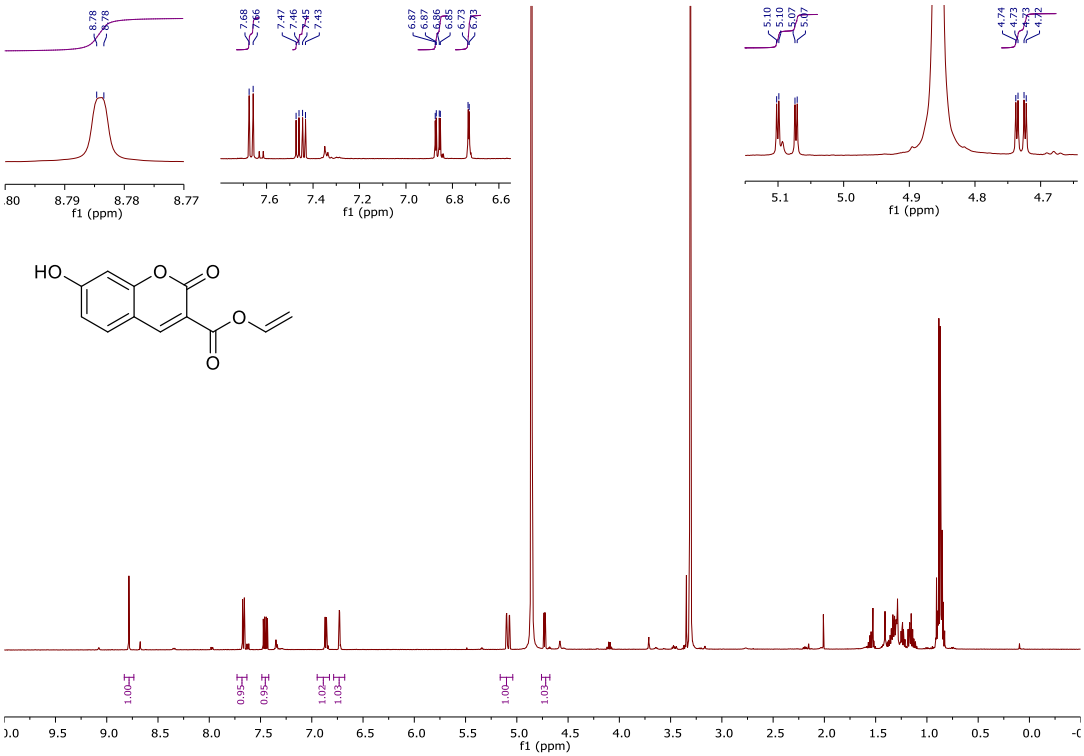

^{13}C NMR (126 MHz, Methanol-d_4) of Ethenyl 7-hydroxy-2-oxochromene-3-carboxylate (**102**)

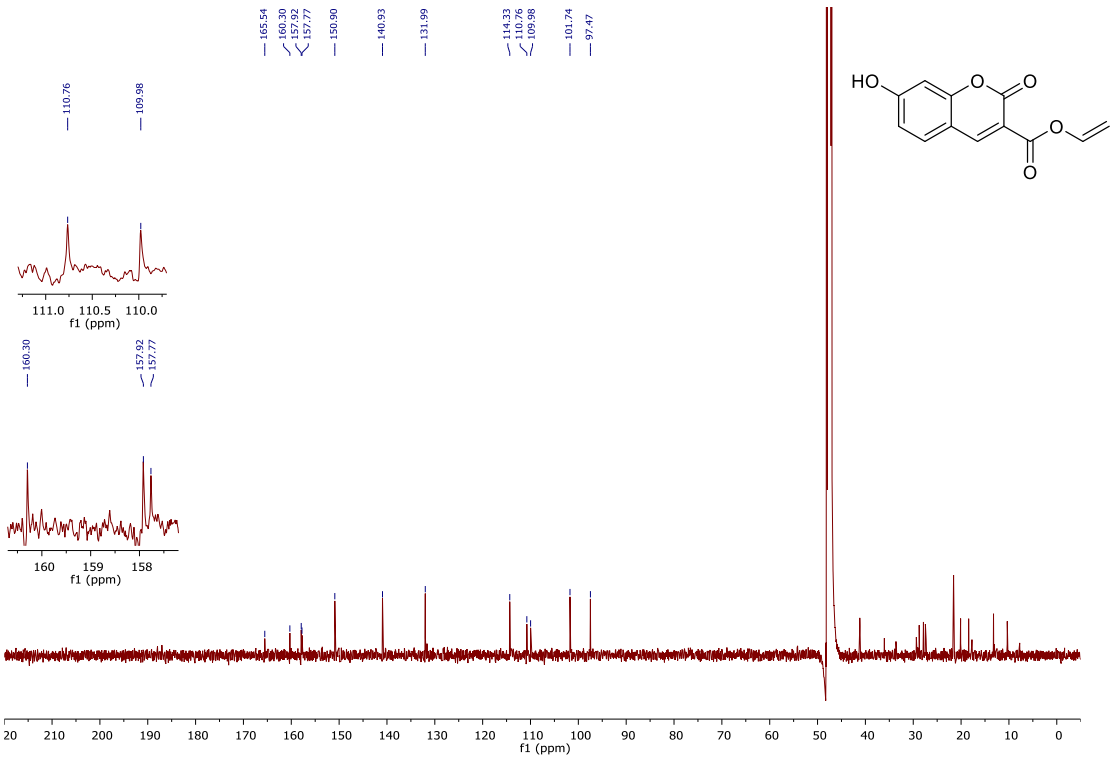

^{1}H NMR (400 MHz, $CDCl_3$) of vinyl 2-(3-benzoylphenyl)propanoate (**106**)

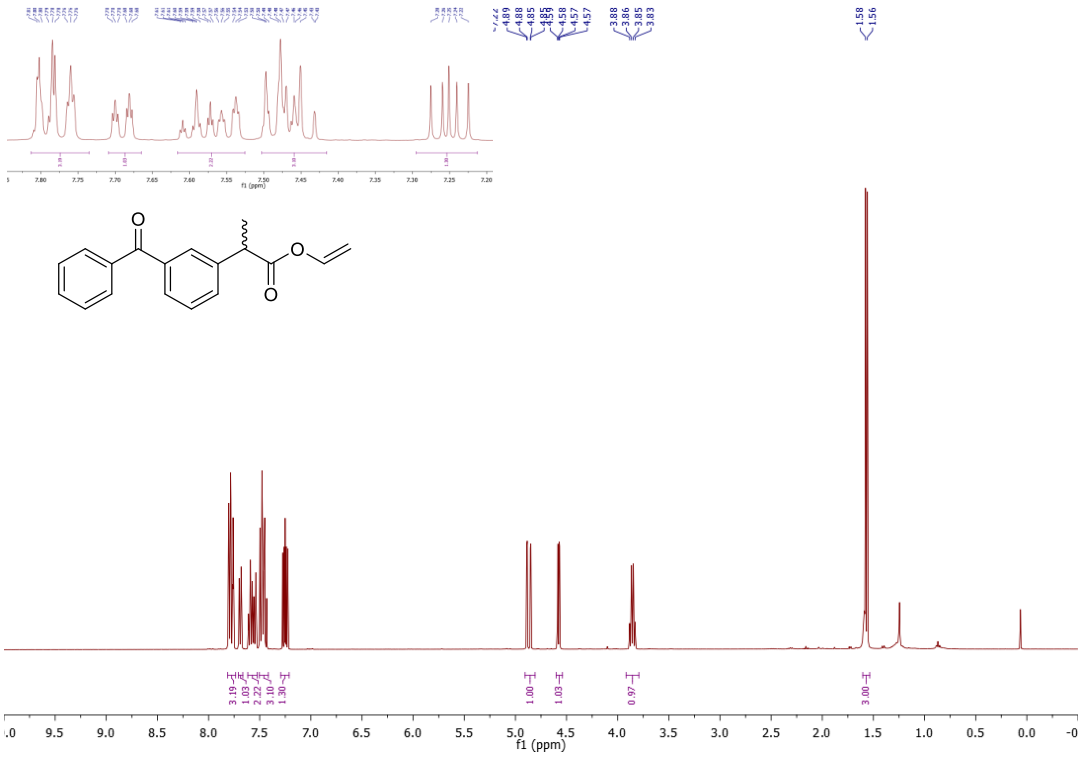

^{13}C NMR (101 MHz, $CDCl_3$) of vinyl 2-(3-benzoylphenyl)propanoate (**106**)

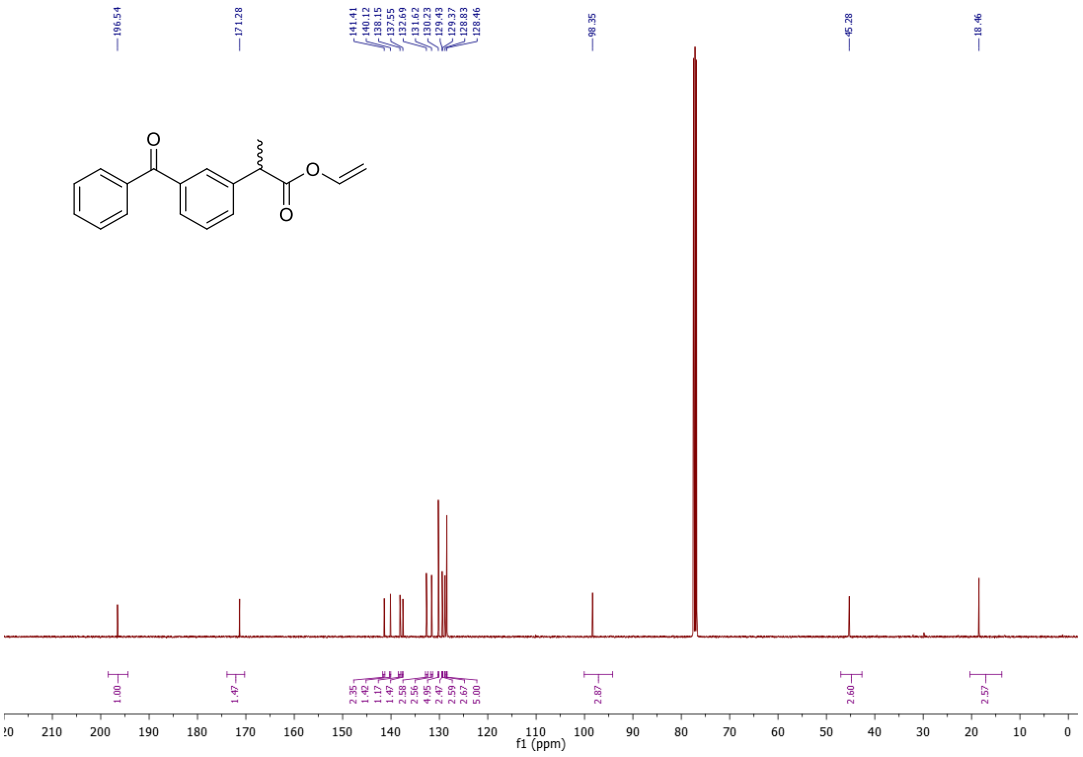

^{1}H NMR (400 MHz, $CDCl_3$) of (2*Z*)-Cyclooct-2-en-1-ol (**111**)

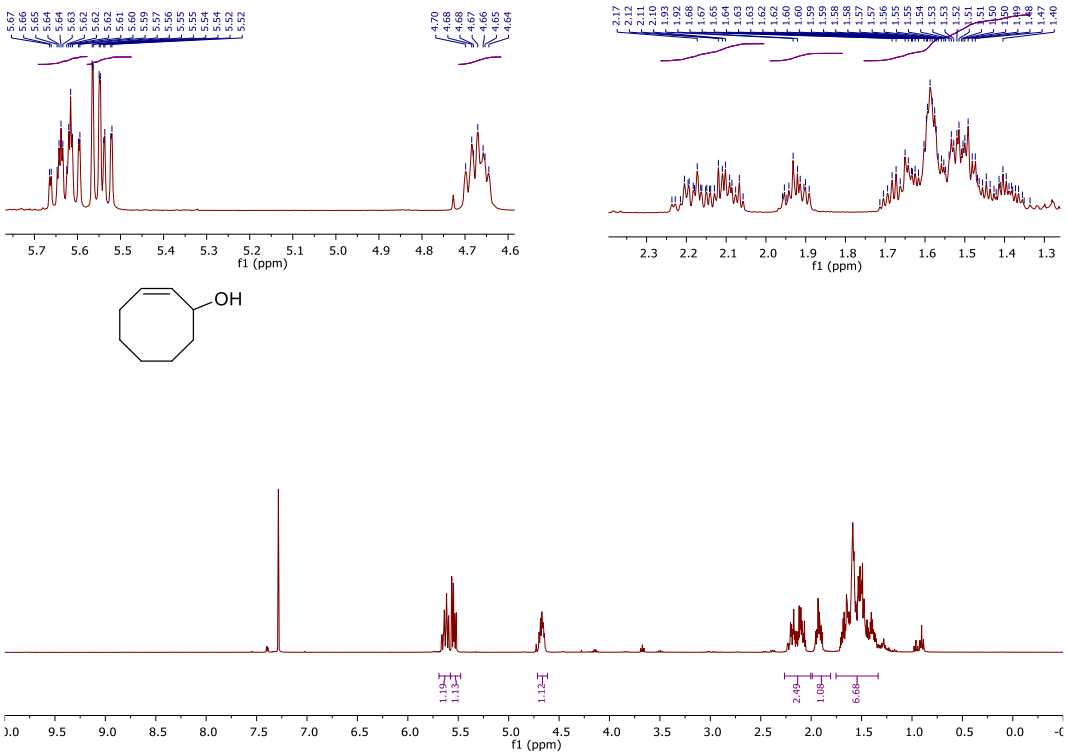

^{13}C NMR (101 MHz, $CDCl_3$) of (2*Z*)-Cyclooct-2-en-1-ol (**111**)

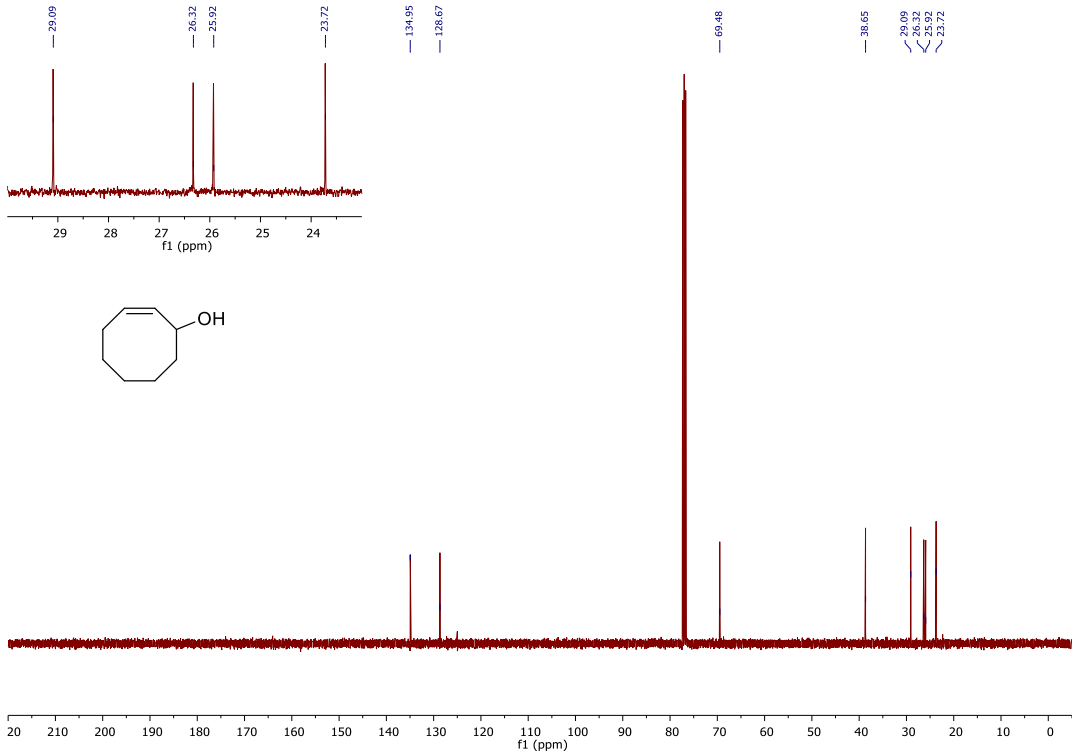

^{1}H NMR (500 MHz, $CDCl_3$) of (*Z*)-Cyclooct-2-en-1-yl 2-(3-benzoylphenyl)propanoate (**113**)

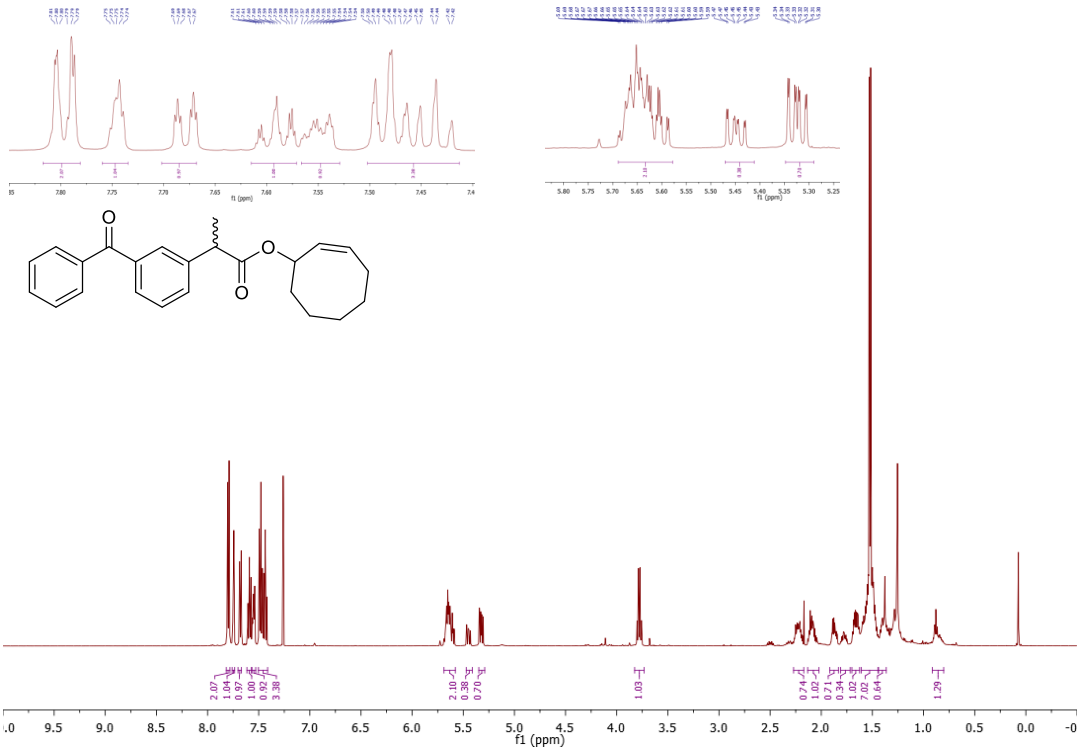

^{13}C NMR (126 MHz, $CDCl_3$) of (*Z*)-Cyclooct-2-en-1-yl 2-(3-benzoylphenyl)propanoate (**113**)

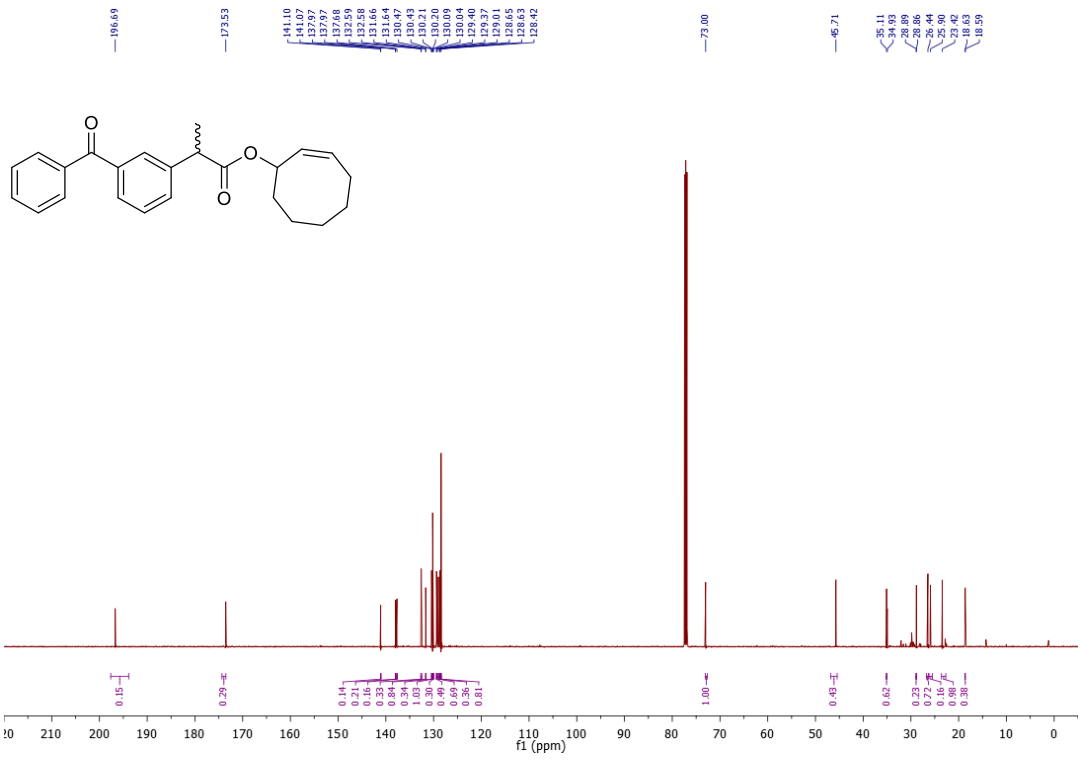

^{1}H NMR (500 MHz, $CDCl_3$) of (*E*)-Cyclooct-2-en-1-yl 2-(3-benzoylphenyl)propanoate (**114**)

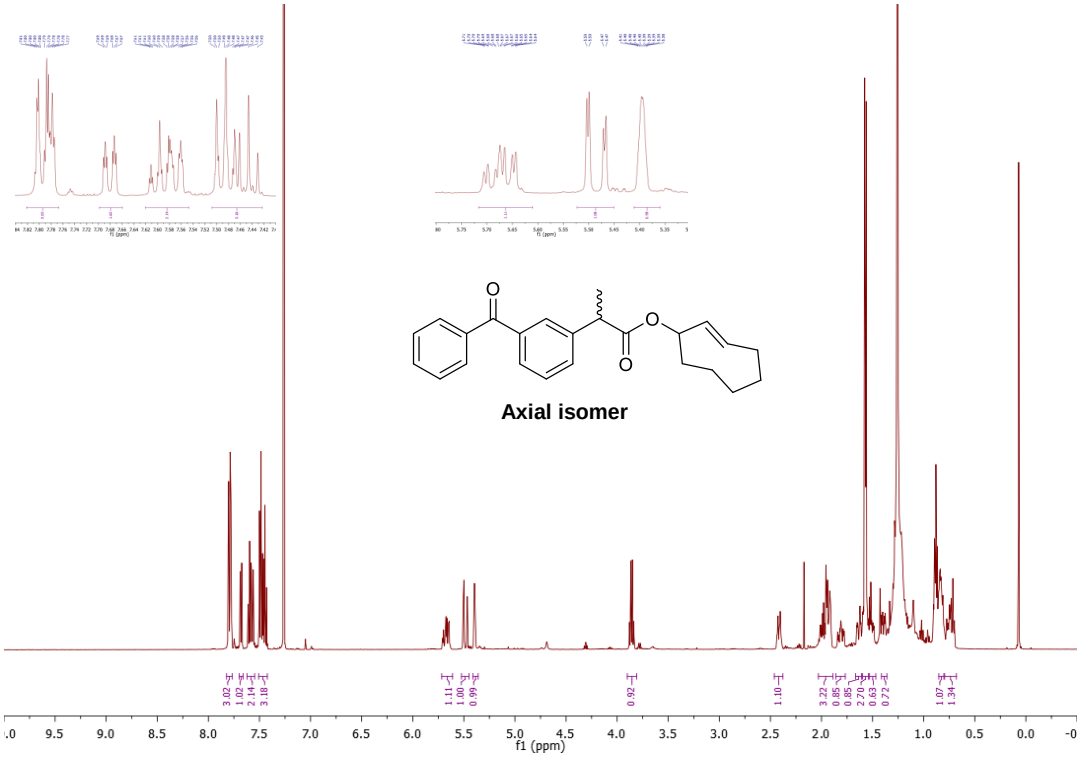

^{13}C NMR (126 MHz, $CDCl_3$) of (*E*)-Cyclooct-2-en-1-yl 2-(3-benzoylphenyl)propanoate (**114**)

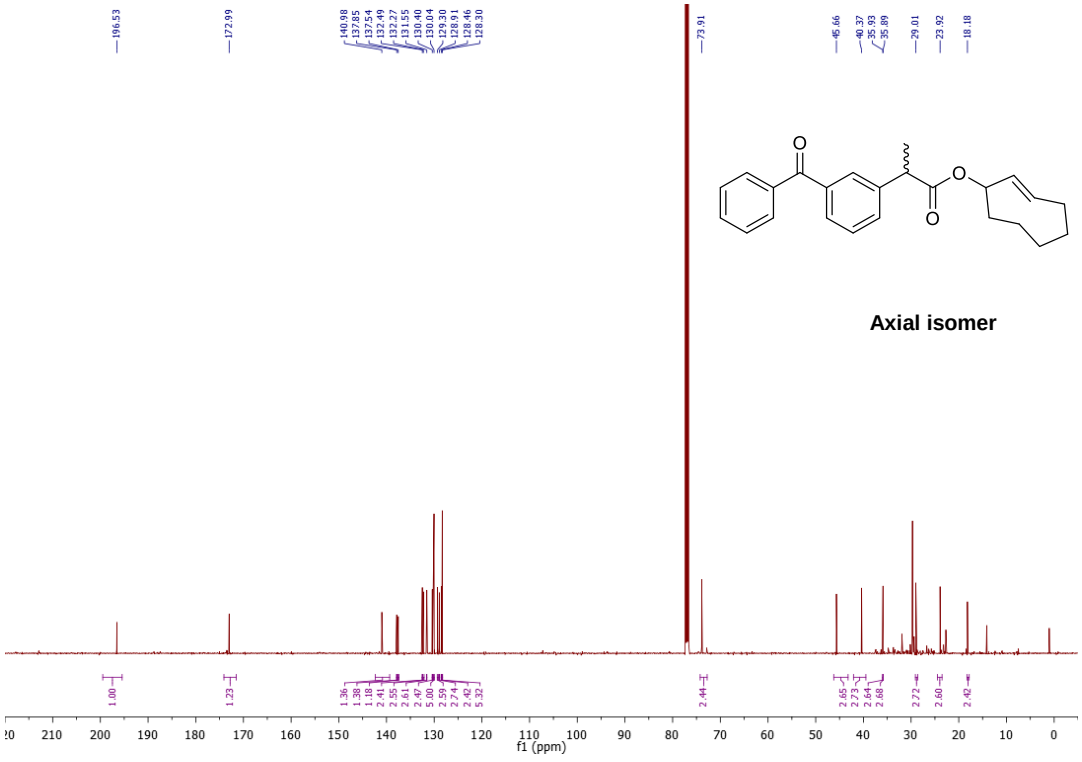

^{1}H NMR (500 MHz, $CDCl_3$) of (*E*)-Cyclooct-2-en-1-yl 2-(3-benzoylphenyl)propanoate (**114**)

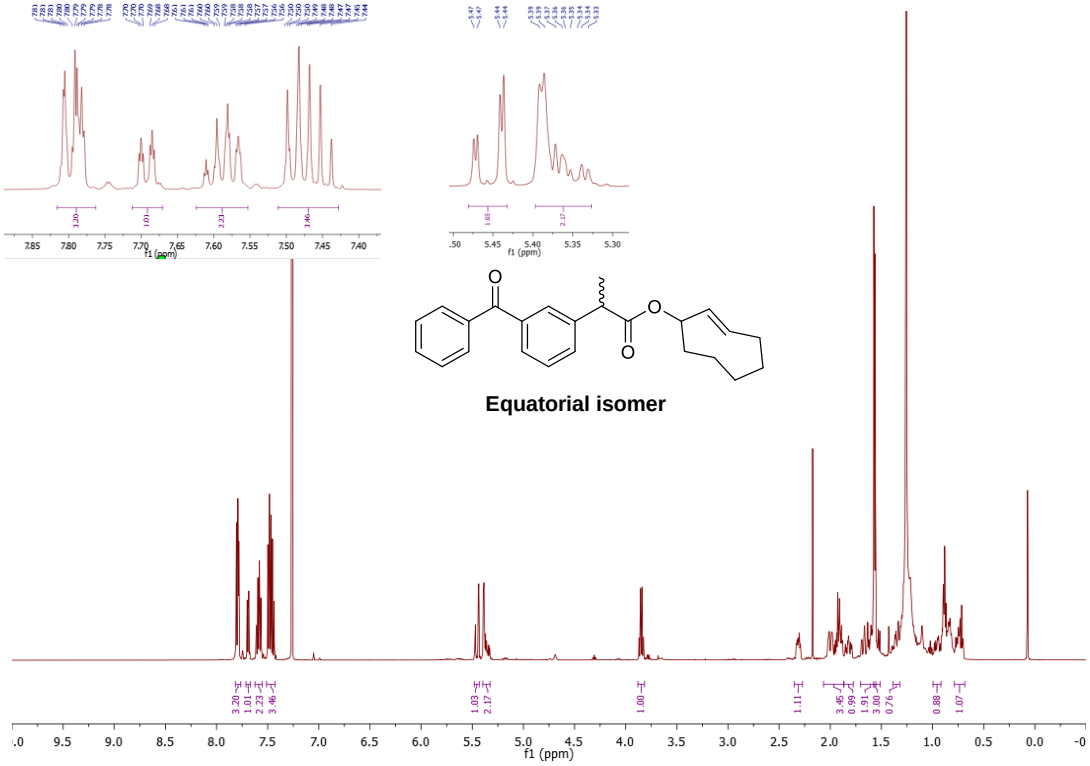

^{13}C NMR (126 MHz, $CDCl_3$) of (*E*)-Cyclooct-2-en-1-yl 2-(3-benzoylphenyl)propanoate (**114**)

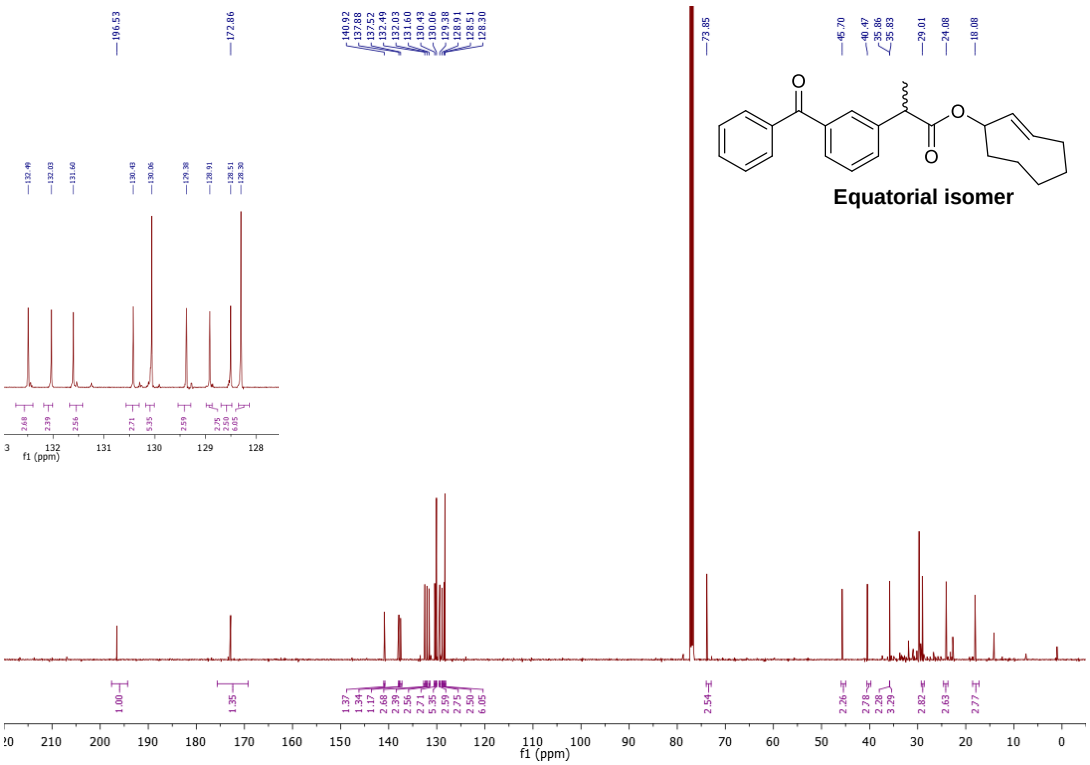

^{1}H NMR (400 MHz, $CDCl_3$) of (2*E*)-Cyclooct-2'-en-1'-yl 4-nitrophenyl carbonate (**121**)

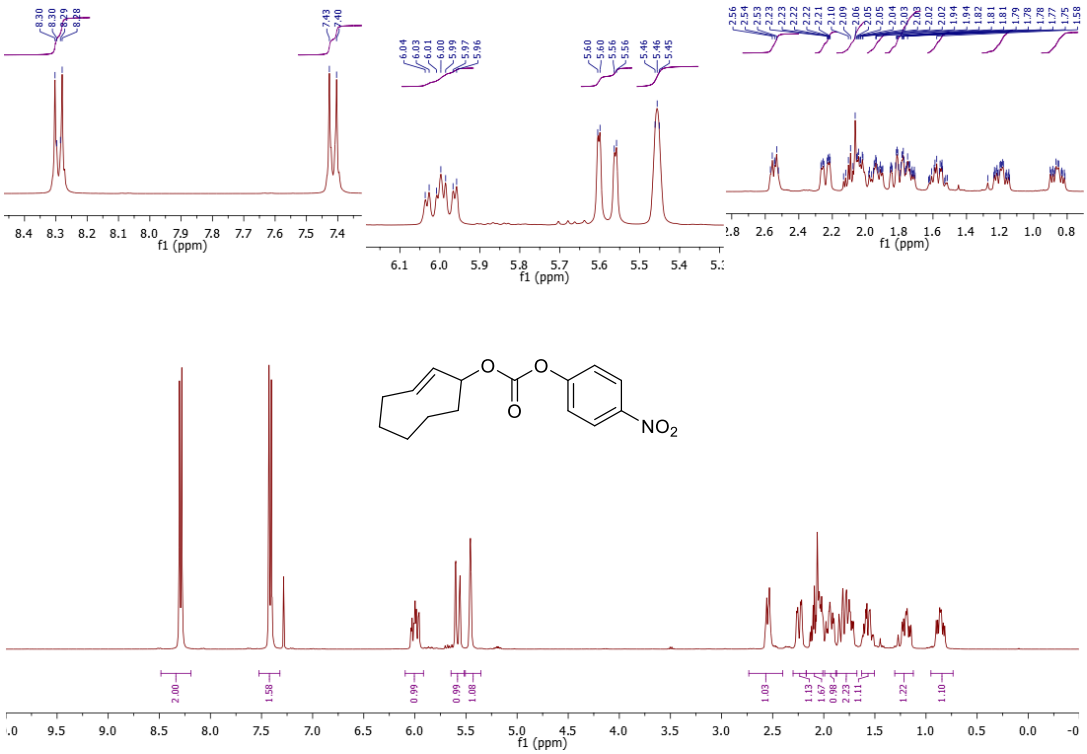

^{13}C NMR (101 MHz, $CDCl_3$) of (2*E*)-Cyclooct-2'-en-1'-yl 4-nitrophenyl carbonate (**121**)

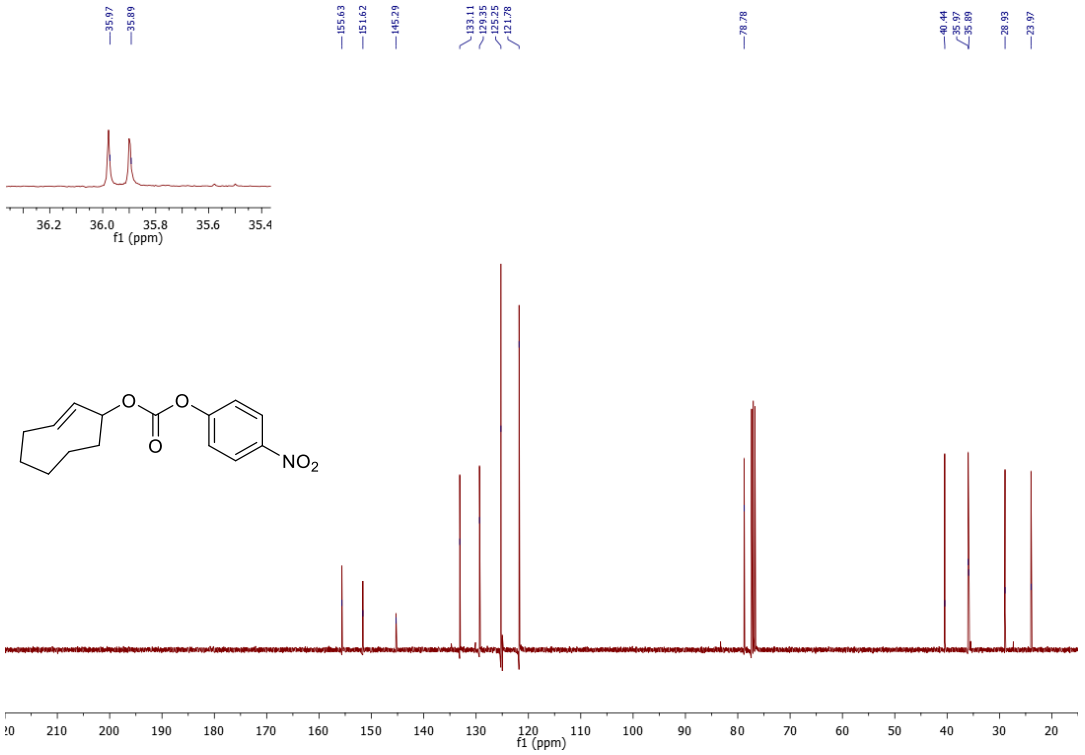

^{1}H NMR (400 MHz, $CDCl_3$) of (2*E*)-Cyclooct-2'-en-1'-yl 2-oxochromen-7-yl carbonate (**123**)

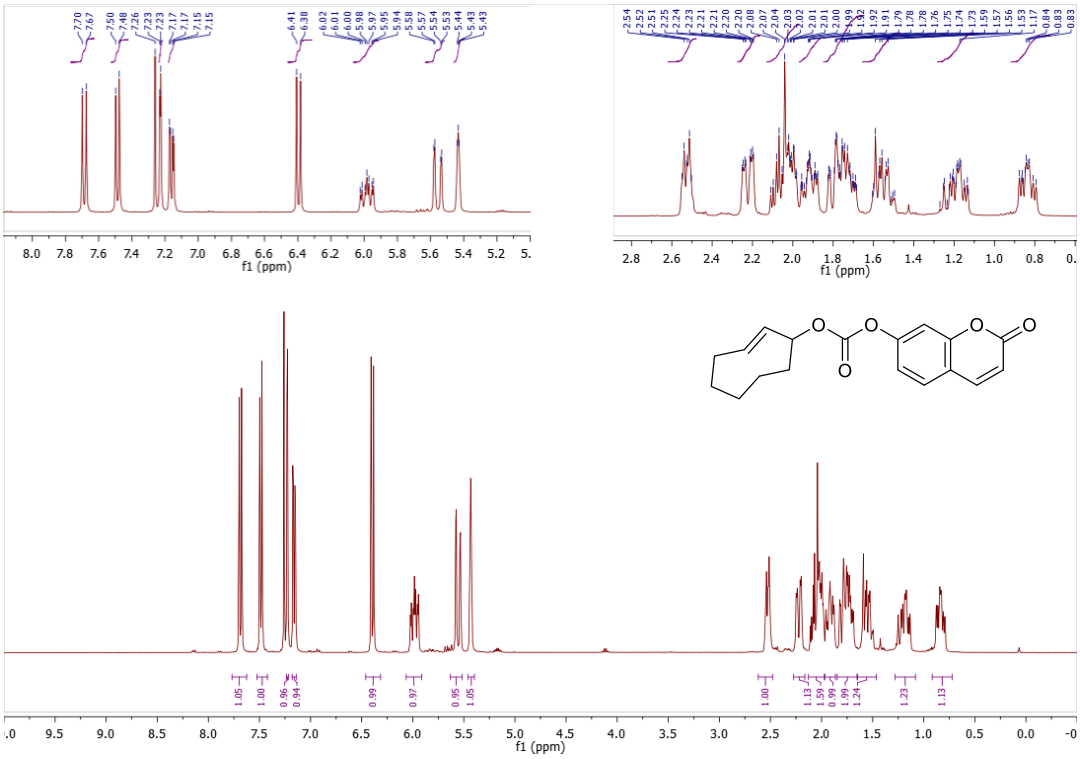

^{13}C NMR (101 MHz, $CDCl_3$) of (2*E*)-Cyclooct-2'-en-1'-yl 2-oxochromen-7-yl carbonate (**123**)

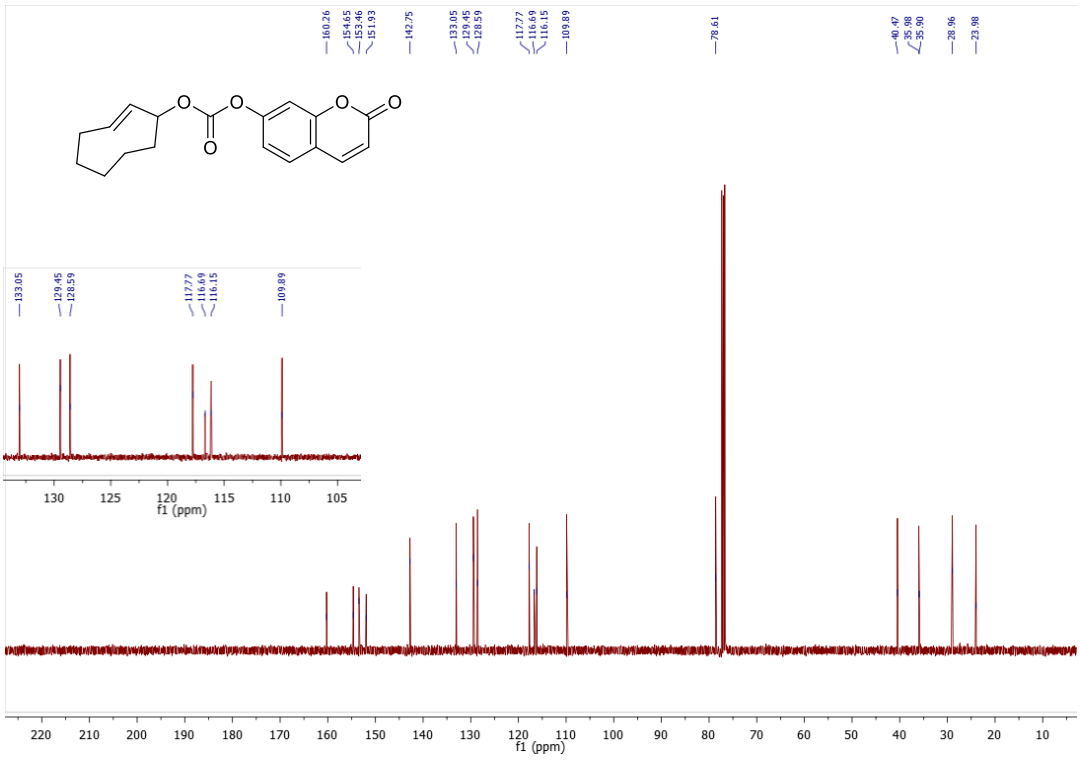

^{1}H NMR (500 MHz, $CDCl_3$) of 4-[(2'Z)-cyclooct-2'-en-1'-yloxy]benzaldehyde (**127**)

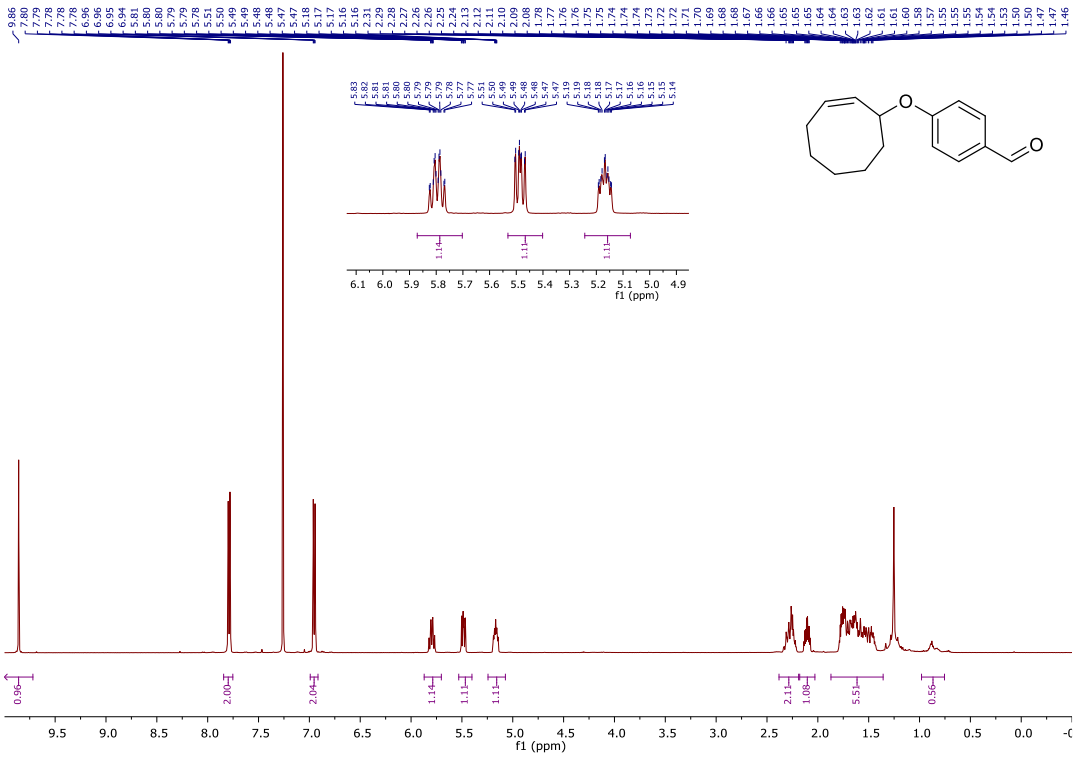

^{13}C NMR (126 MHz, $CDCl_3$) of 4-[(2'Z)-cyclooct-2'-en-1'-yloxy]benzaldehyde (**127**)

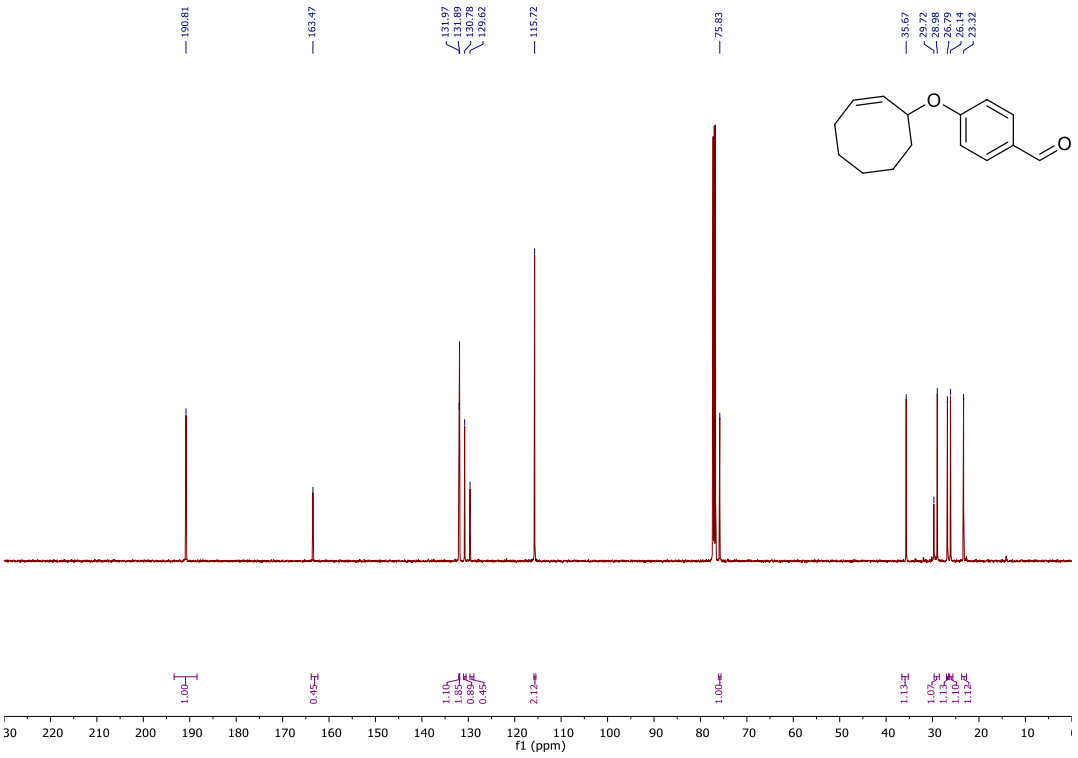

^{1}H NMR (500 MHz, Methanol-d_4) of {4-[(2Z)-cyclooct-2-en-1-yloxy]phenyl}methanol (**129**)

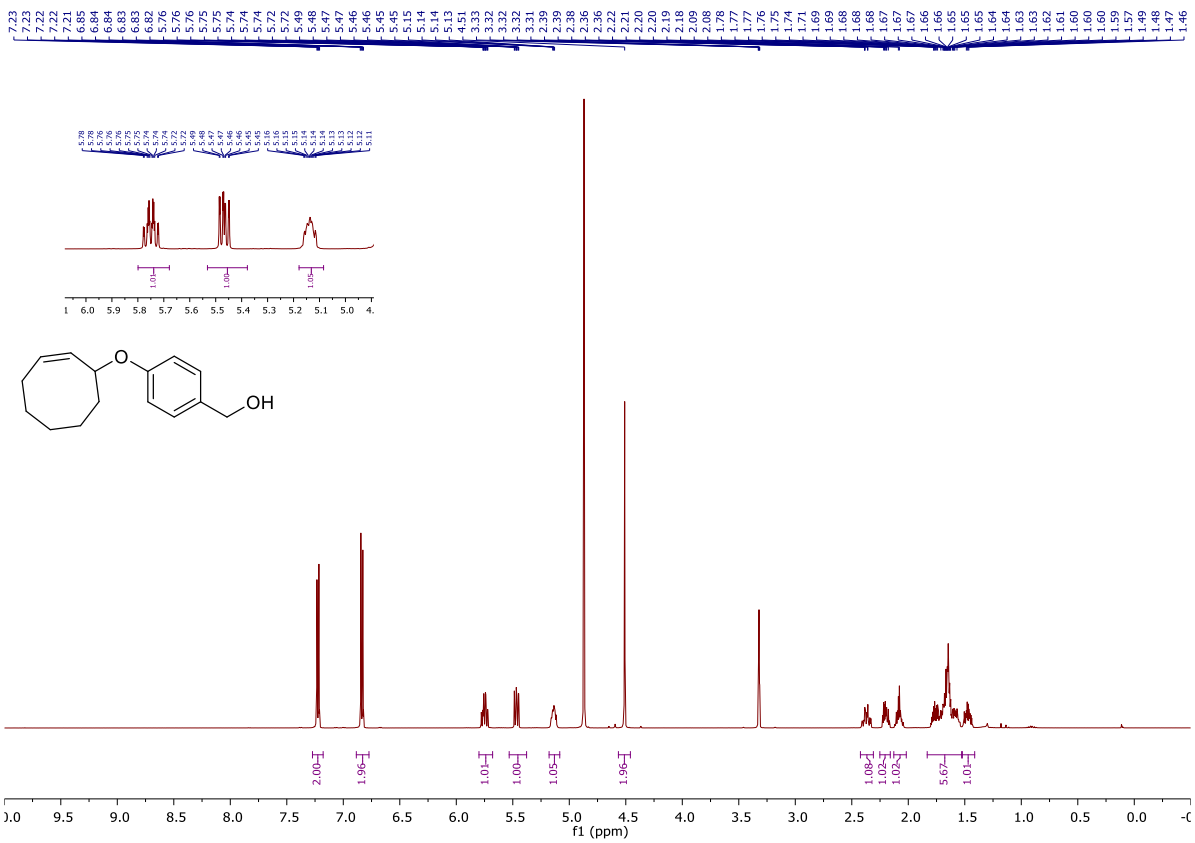

^{13}C NMR (126 MHz, Methanol-d_4) of {4-[(2Z)-cyclooct-2-en-1-yloxy]phenyl}methanol (**129**)

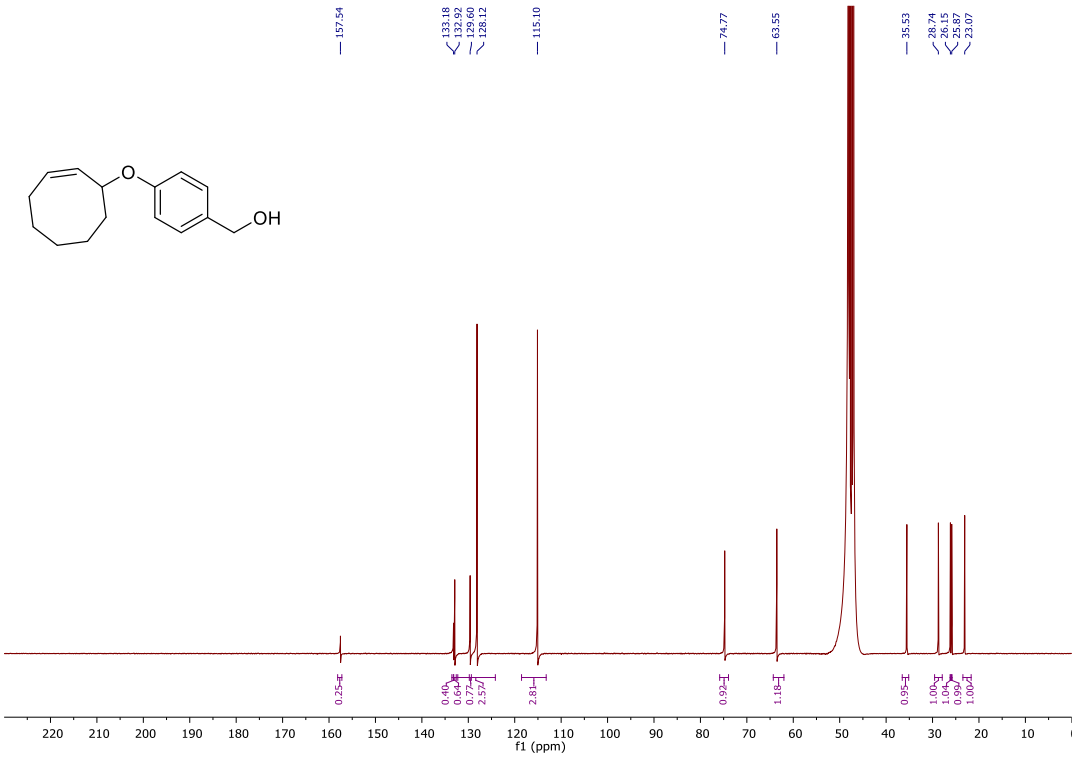

^{1}H NMR (400 MHz, $CDCl_3$) of (1'Z)-3'-[4-(chloromethyl)phenoxy]cyclooct-1'-ene (**130**)

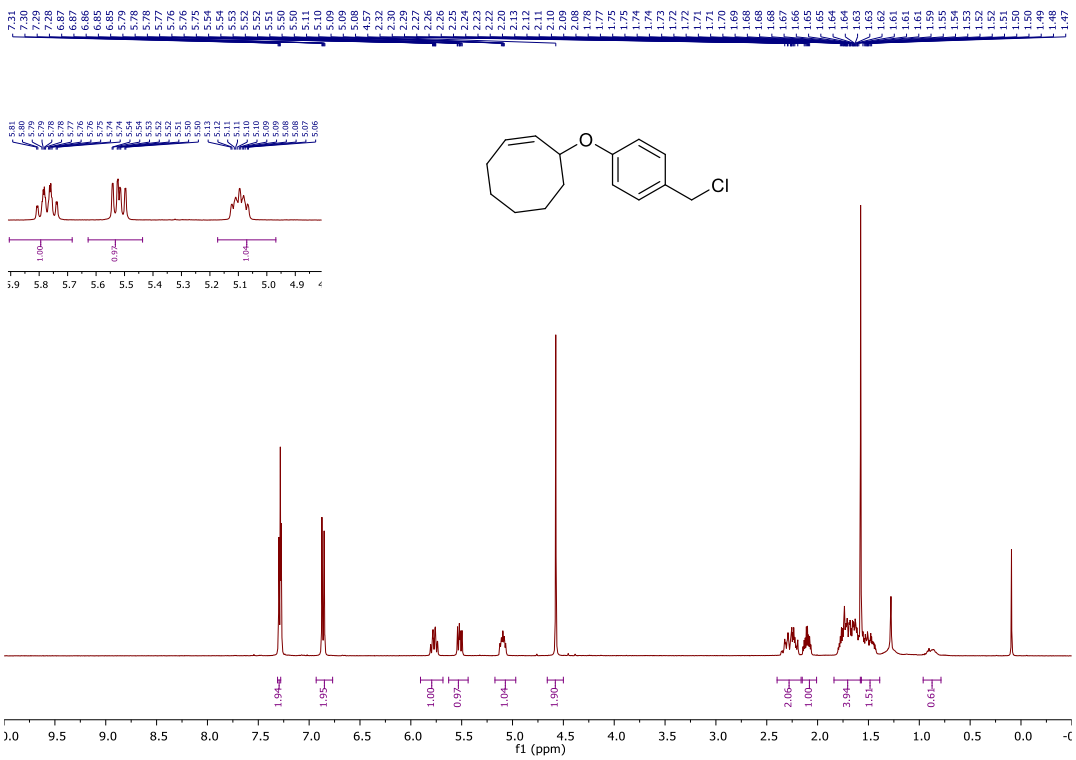

^{1}H NMR (400MHz, $CDCl_3$) of 7-({4''-[(2'Z)-cyclooct-2'-en-1'-yloxy]phenyl}methoxy)chromen-2-one (**131**)

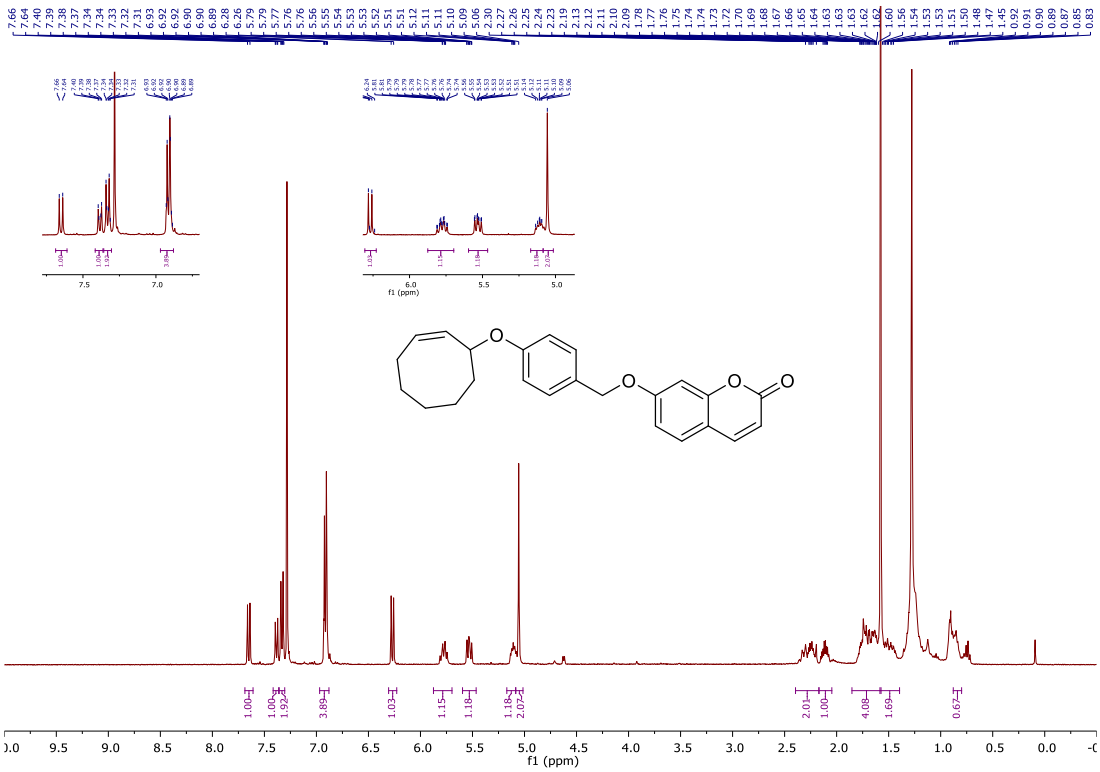

^{1}H NMR (400 MHz, $CDCl_3$) of 4-{[(tert-butyldimethylsilyl)oxy]methyl}aniline (**137**)

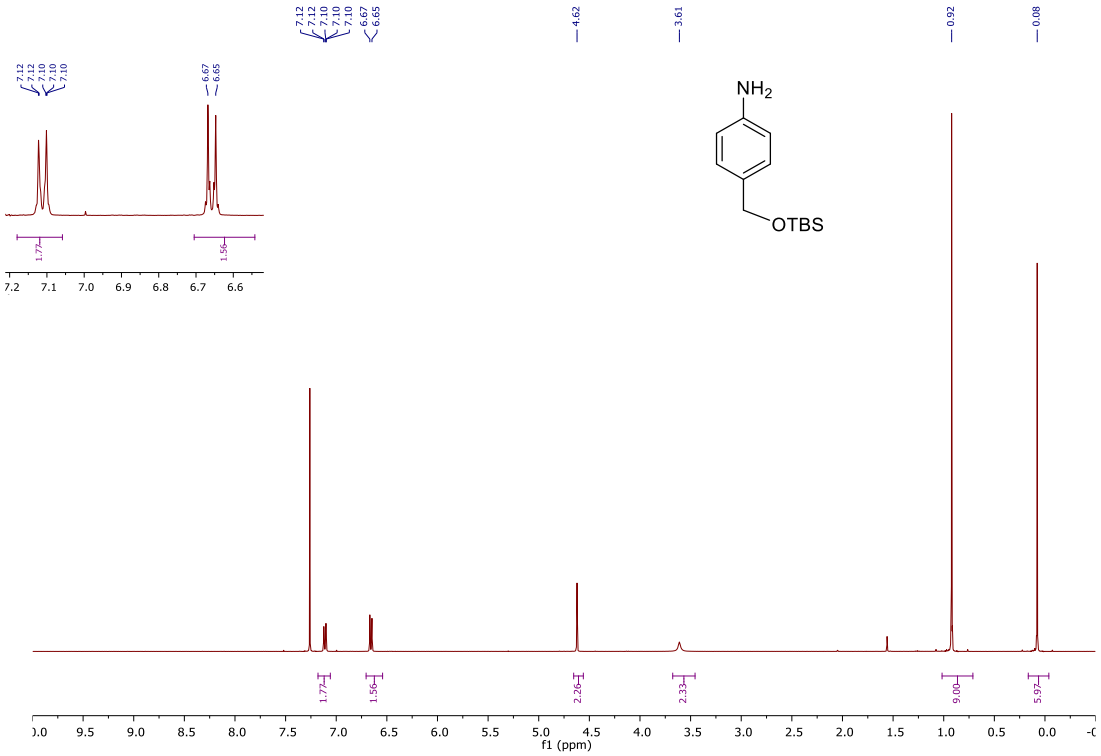

^{1}H NMR (400 MHz, $CDCl_3$) of tert-butyl[(4-isocyanatophenyl)methoxy]dimethylsilane (**138**)

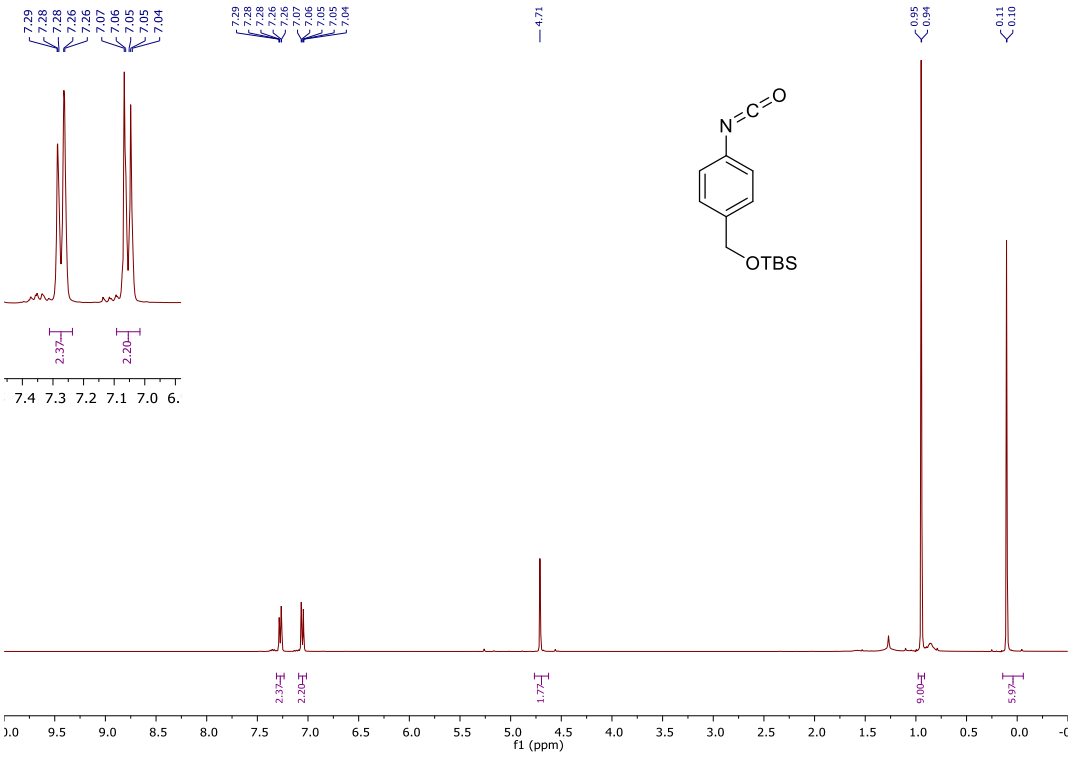

^{1}H NMR (500 MHz, $CDCl_3$) of (2*E*)-cyclooct-2-en-1-yl N-(4-{[(tert-butyldimethylsilyl)oxy]methyl}phenyl)carbamate (**139**)

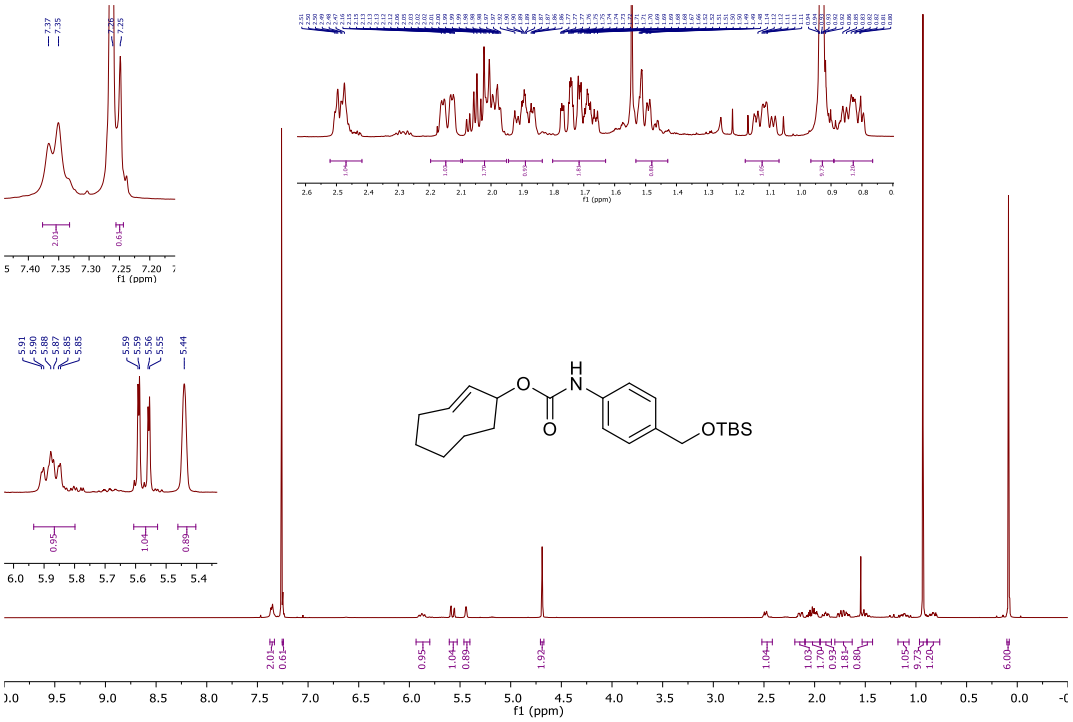

^{13}C NMR (126 MHz, $CDCl_3$) of (2*E*)-cyclooct-2-en-1-yl N-(4-{[(tert-butyldimethylsilyl)oxy]methyl}phenyl)carbamate (**139**)

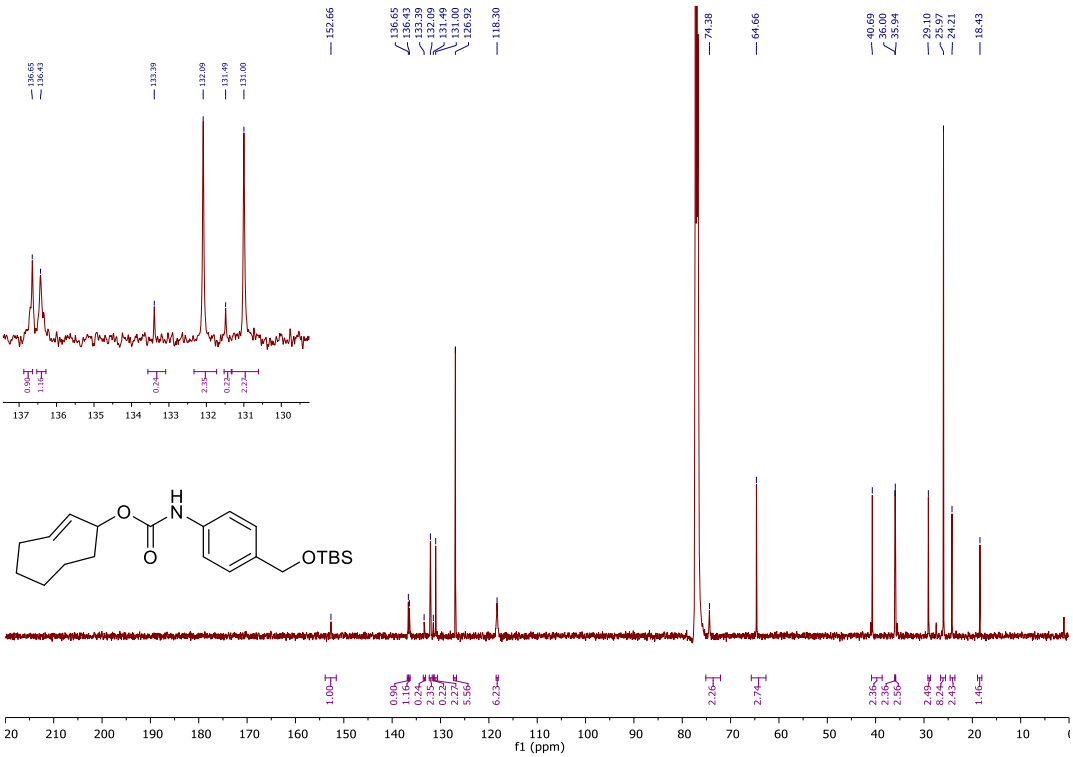

Crude ^{1}H NMR (400 MHz, $CDCl_3$) of (2'*E*)-cyclooct-2'-en-1'-yl N-[4-(hydroxymethyl)phenyl]carbamate (**140**)

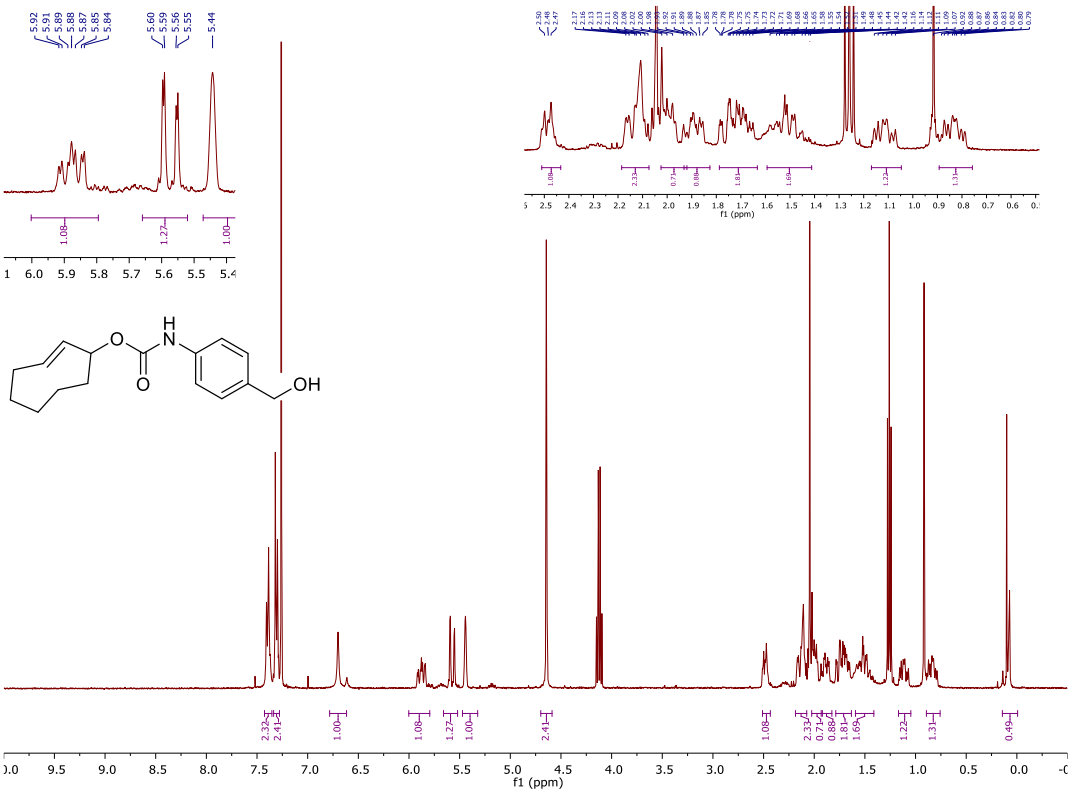

^{1}H NMR (400 MHz, $CDCl_3$) of (2'*E*)-cyclooct-2'-en-1'-yl N-[4-(bromomethyl)phenyl]carbamate (**141**)

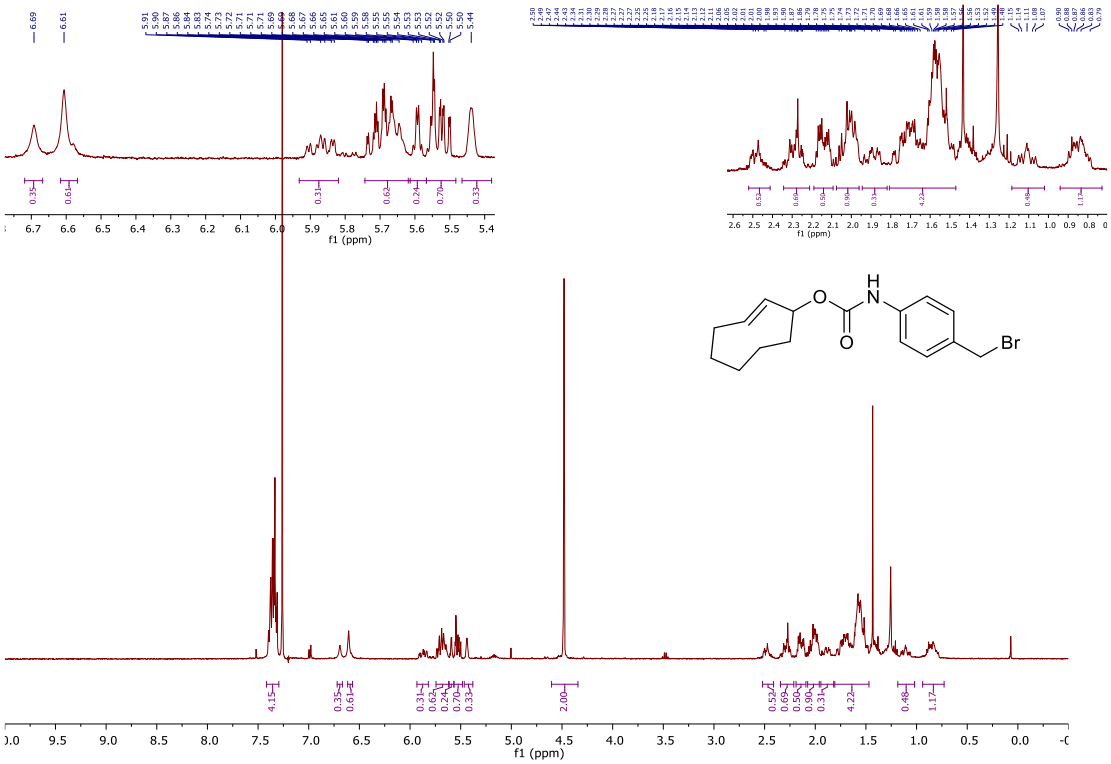

Crude ^{1}H NMR (400 MHz, $CDCl_3$) of (2''*E*)-cyclooct-2''-en-1''-yl N-(4-{[(2'-oxochromen-7'-yl)oxy]methyl}phenyl)carbamate (**142**) from route 1

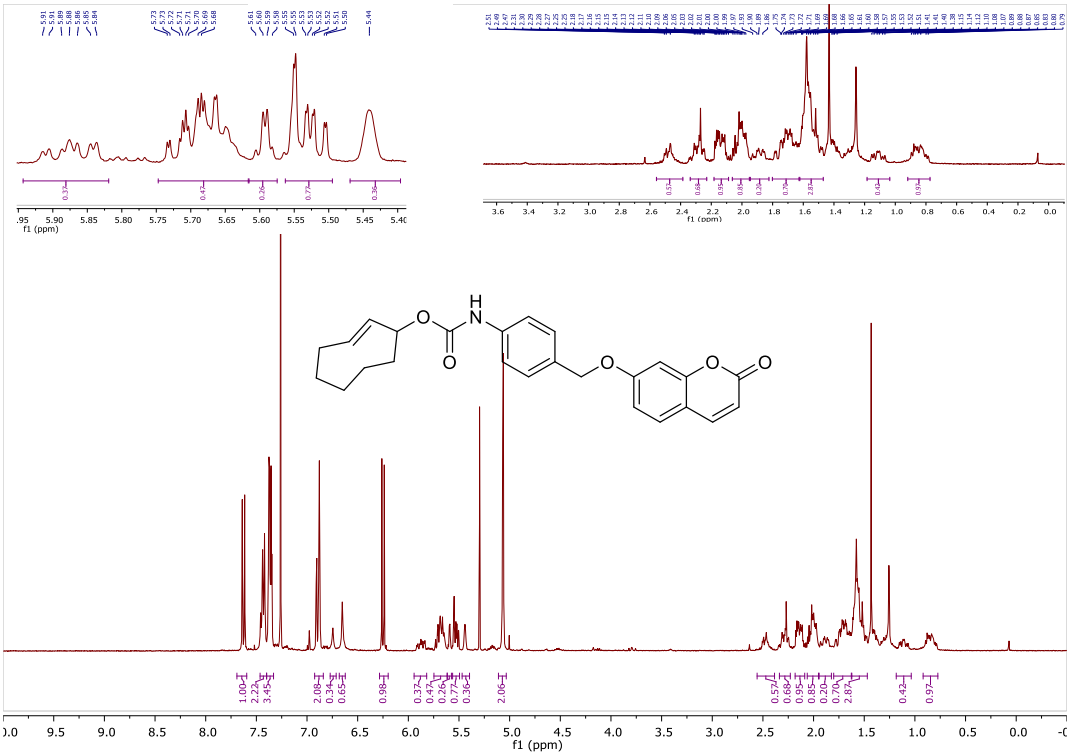

^{1}H NMR (500 MHz, $CDCl_3$) of (2''*E*)-cyclooct-2''-en-1''-yl N-(4-{[(2'-oxochromen-7'-yl)oxy]methyl}phenyl)carbamate (**142**) from route 2

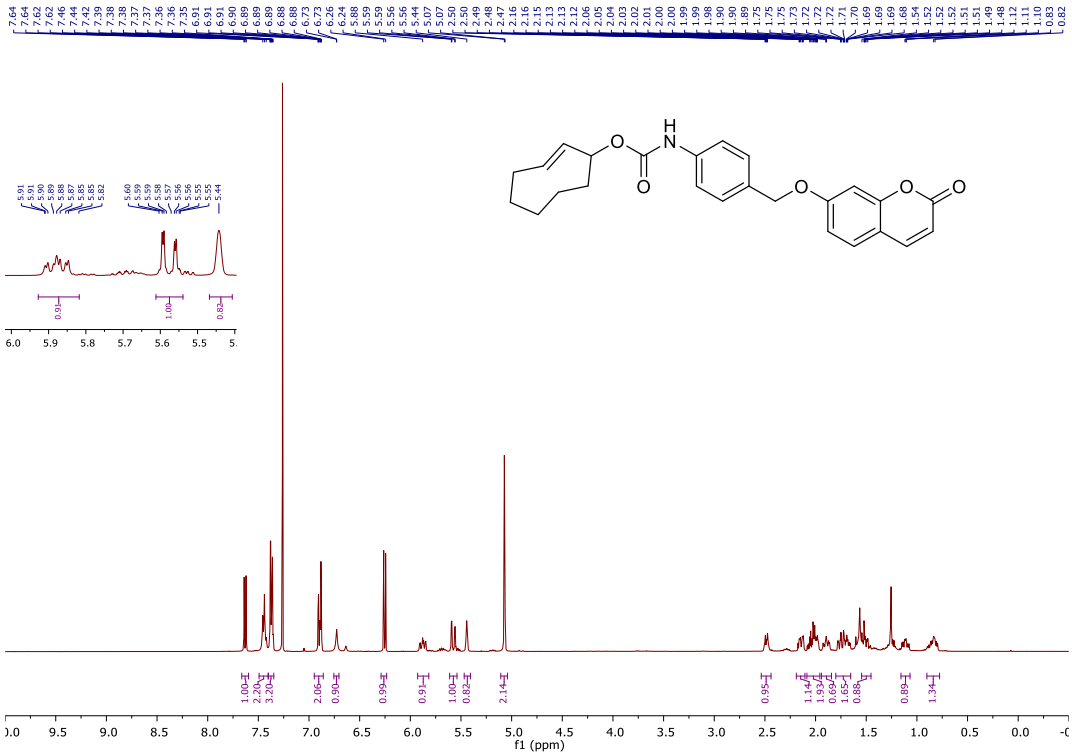

^{13}C NMR (126 MHz, $CDCl_3$) of (2''*E*)-cyclooct-2''-en-1''-yl N-(4-{[(2'-oxochromen-7'-yl)oxy]methyl}phenyl)carbamate (**142**) from route 2

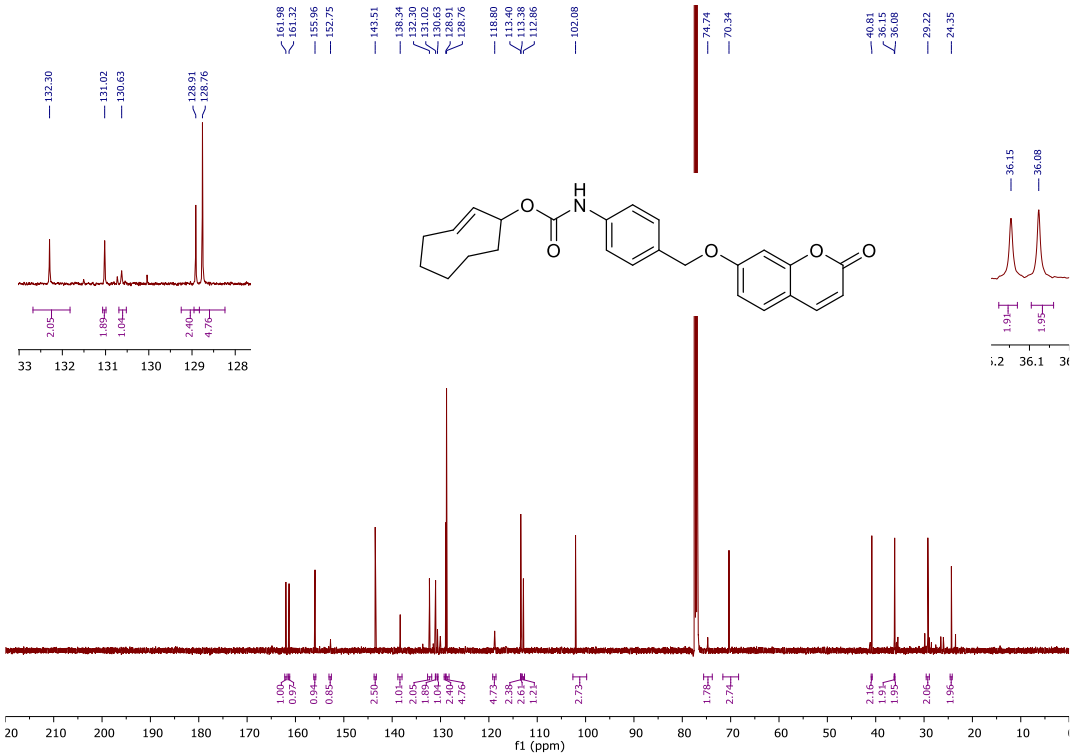

^{1}H NMR (400 MHz, $CDCl_3$) of tert-butyl N-[4-(hydroxymethyl)phenyl]carbamate (**143**)

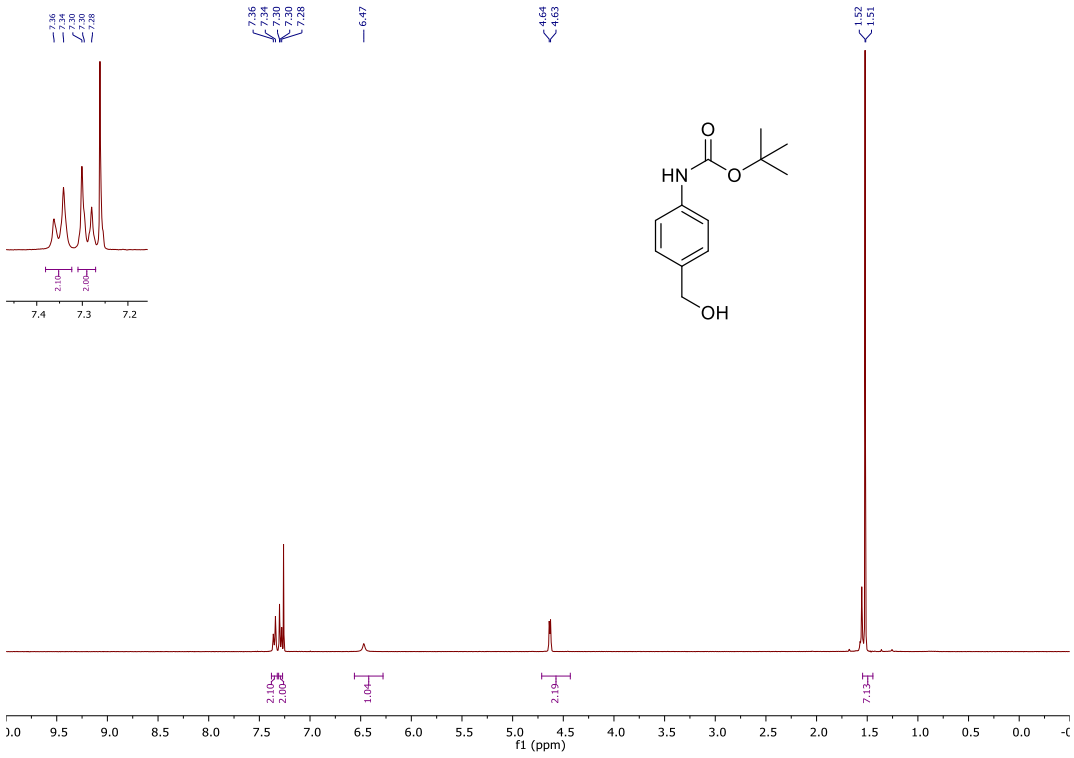

^{1}H NMR (400 MHz, $CDCl_3$) of tert-butyl N-[4-(bromomethyl)phenyl]carbamate (**144**)

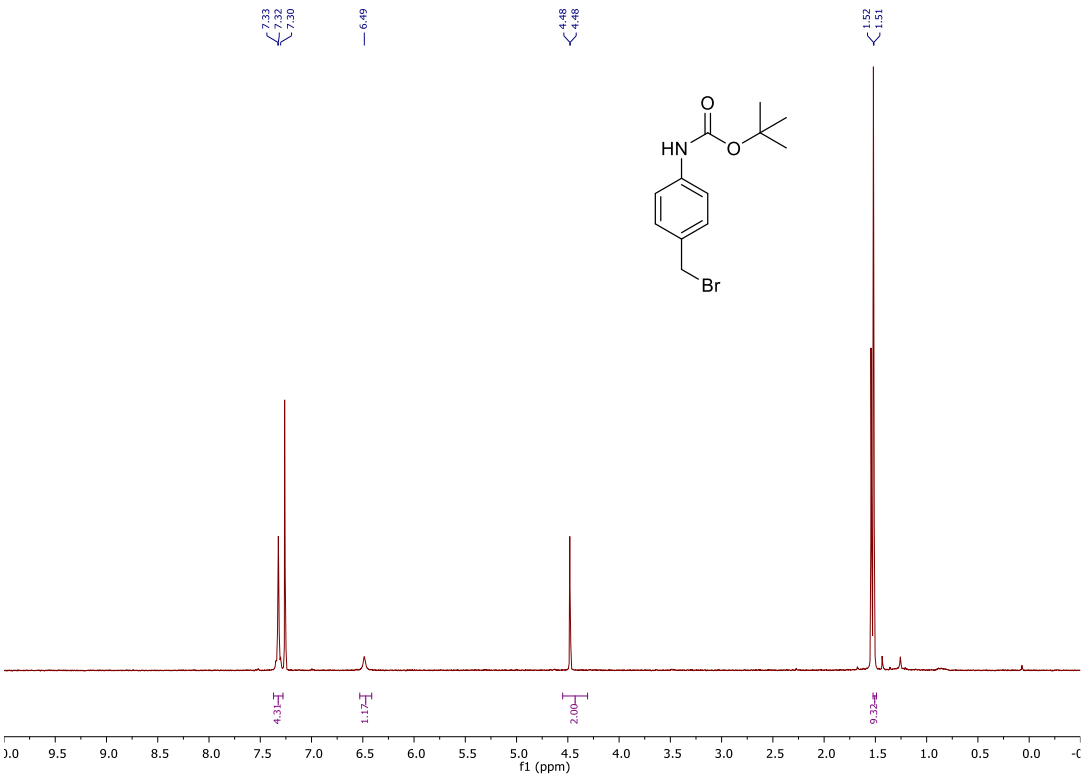

^{1}H NMR (500 MHz, $CDCl_3$) of tert-butyl N-(4-{[(2'-oxochromen-7'-yl)oxy]methyl}phenyl)carbamate (**145**)

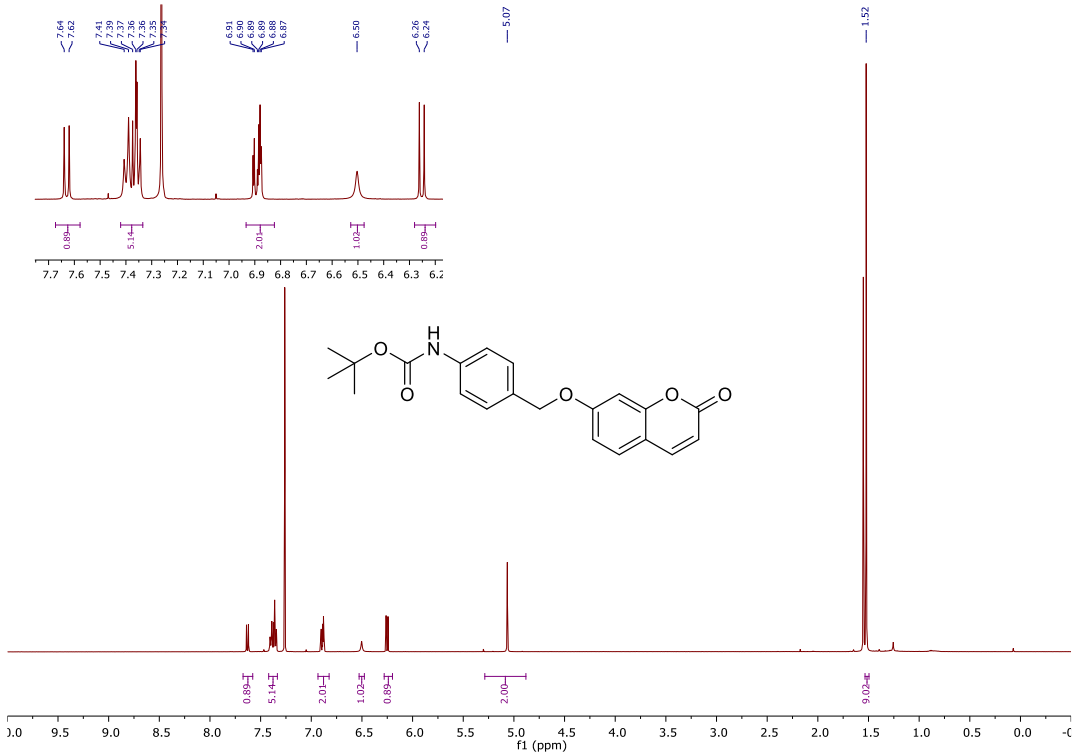

^{13}C NMR (126 MHz, $CDCl_3$) of tert-butyl N-(4-{[(2'-oxochromen-7'-yl)oxy]methyl}phenyl)carbamate (**145**)

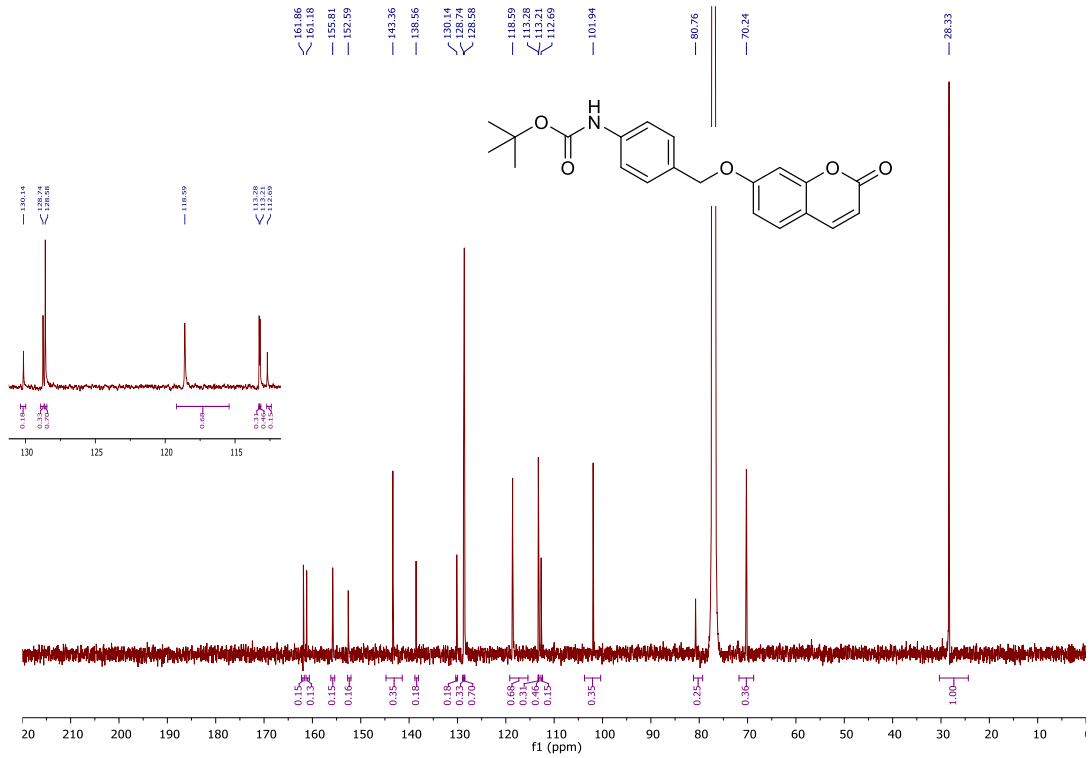

^{1}H NMR (400 MHz, $CDCl_3$) of tert-butyl N-{4''-[5-chloro-2-(2',4'-dichlorophenoxy)phenoxymethyl]phenyl}carbamate (**150**)

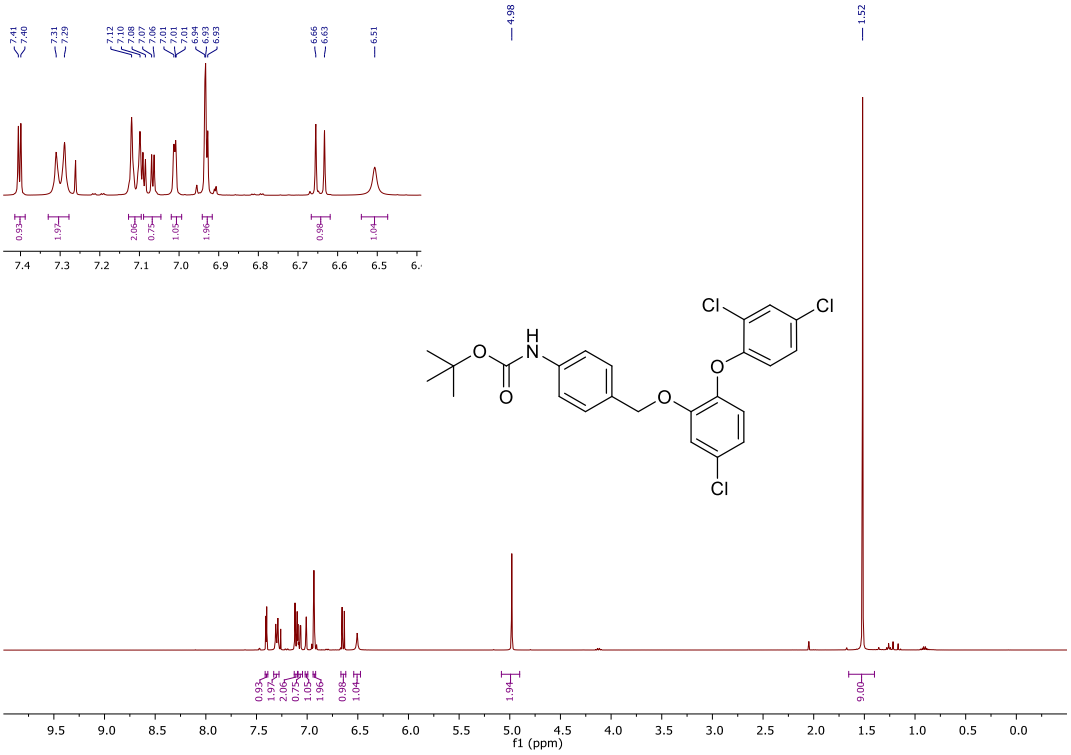

^{13}C NMR (101 MHz, $CDCl_3$) of tert-butyl N-{4''-[5-chloro-2-(2',4'-dichlorophenoxy)phenoxymethyl]phenyl}carbamate (**150**)

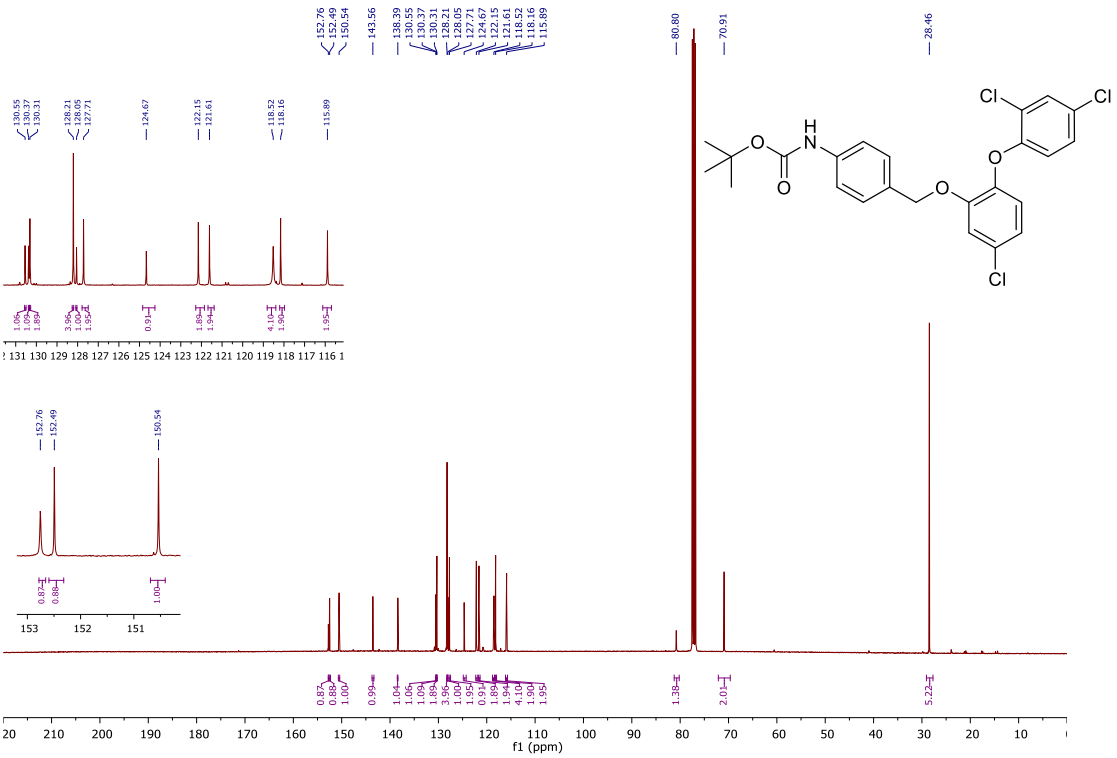

^{1}H NMR (400 MHz, $CDCl_3$) of
(2‴*E*)-cyclooct-2‴-en-1-yl N-{4″-[5-chloro-2-(2′,4′-dichlorophenoxy)phenoxymethyl]phenyl}carbamate (**153**)

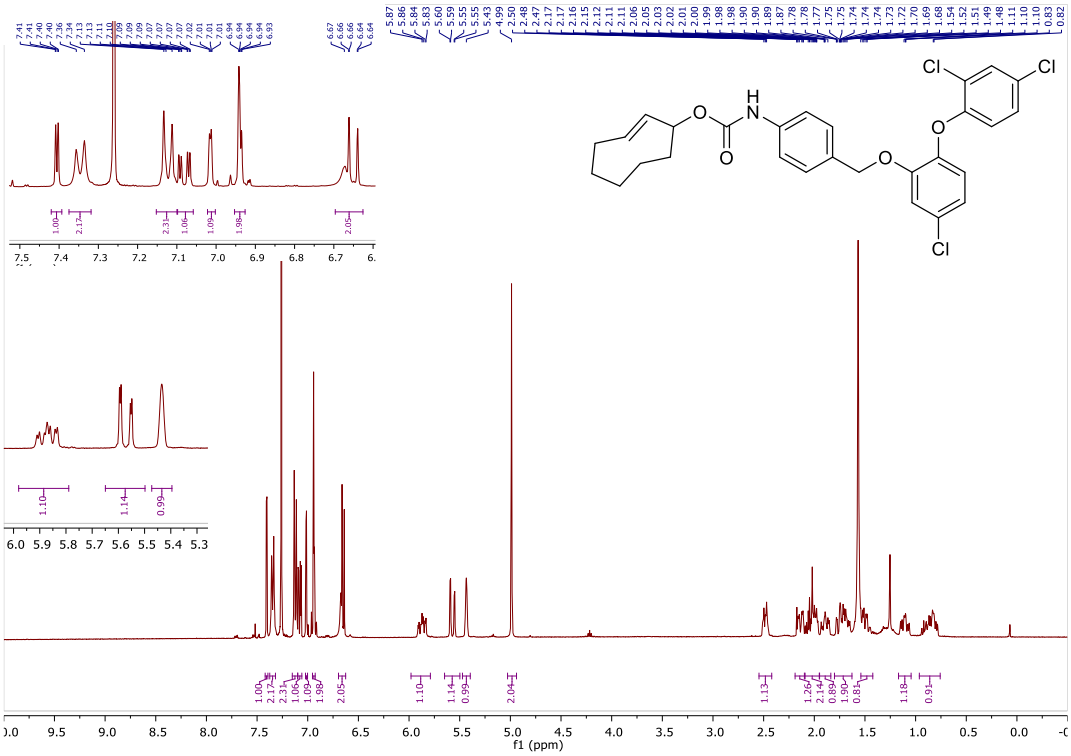

^{13}C NMR (101 MHz, $CDCl_3$) of
(2‴*E*)-cyclooct-2‴-en-1-yl N-{4″-[5-chloro-2-(2′,4′-dichlorophenoxy)phenoxymethyl]phenyl}carbamate (**153**)

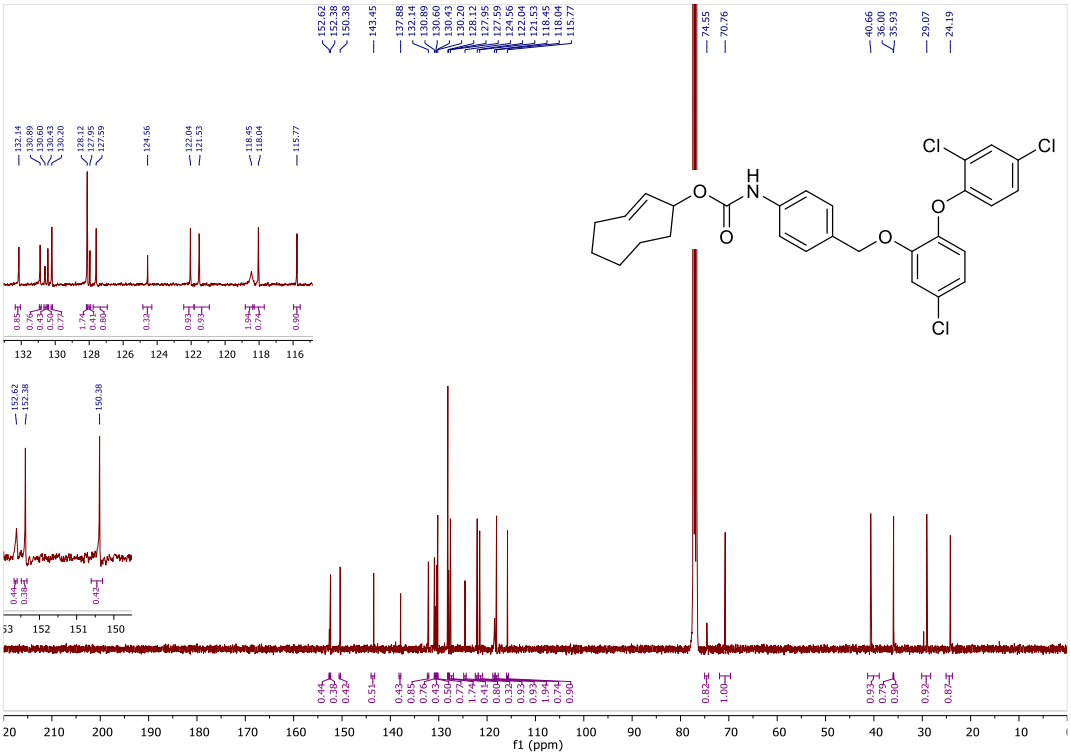

^{1}H NMR (400 MHz, $CDCl_3$) of tert-butyl N-{4-[({19-ethyl-14,18-dioxo-17-oxa-3,13-diazapentacyclo [11.8.0.0^{2,11}.0^{4,9}.0^{15,20}] henicosa-1(21),2,4(9),5,7,10,15(20)-heptaen-19-yl} oxy)methyl]phenyl}carbamate (**154**)